The White Book of ELI Nuclear Physics Bucharest-Magurele, Romania

The ELI-Nuclear Physics working groups

Contents

1 Foreword

This report contains a comprehensive description of the new international research infrastructure, the Extreme Light Infrastructure - Nuclear Physics facility (ELI-NP), emphasizing the physics which can be addressed with it. The report has been prepared from contributions by many people from various laboratories throughout the world. Their contributions have be merged by a group of editors. This report at the same time demonstrates that ELI-NP can count on a large international user community. Here the extreme light infrastructure consisting of two components: a very high intensity laser system (10-30 PW) and a very brilliant, intense γ beam of up to 19 MeV, 0.1 % band width and $10^{13}\gamma/s$. With this report we demonstrate our deep conviction that this infrastructure will create a new European laboratory with a broad range of science covering new nuclear physics, astrophysics, fundamental high field physics as well as applications in nuclear materials, radioactive waste management, material science and life sciences.

For the realization of ELI-NP we envisage the design of the facility to allow a flexible layout of the experiments and the possibility for further upgrading according to the available resources. The ELI-NP facility will be built in such a way to accommodate its future growth, for example:

- *to include after 2016 new experiments and to upgrade the laser power and gamma beam intensity and energy*
- *after 2020 to include the most ambitious and far reaching projects as well as the ones that are yet to be discovered. It may include an upgrade of the γ beam facility, using a superconducting energy recovery linac reaching to higher intensities of $10^{15}\gamma/s$ and improved bandwidth*

2 Executive Summary

2.1 Basic Objectives

ELI will be the only European and International Centre for high-level research on ultra-high intensity laser, laser-matter interaction and secondary sources with unparalleled possibilities. Its pulse peak power and briefness will go beyond the current state-of-the-art by several orders of magnitude. Because of its unique properties, this multidisciplinary facility will provide magnificent new opportunities to study the fundamental processes unfolded during light-matter interaction.
ELI will create a platform, where Extreme Light applications for the benefit of society will be dynamically promoted. In its mission ELI will practice a vigorous technology transfer to European SMEs and large firms. High on ELI agenda will be the training of aspiring scientists and engineers in the numerous disciplines associated with the Extreme Light.
The ELI project, a collaboration of 13 European countries, will comprise four pillars:

- High Energy Beam Science devoted to the development and usage of dedicated beam lines with ultra short pulses of high energy radiation and particles reaching almost the speed of light (100 GeV).
  This part of ELI will be realized in Prague (Czech Republic)

- Attosecond Laser Science designed to conduct temporal investigation of electron dynamics in atoms, molecules, plasmas and solids at attosecond scale (10^{-18}) sec.
  Szeged (Hungary) will host the short pulse pillar of ELI.

- Laser-based Nuclear Physics:
  The third site in Magurele (near Bucharest/Romania) will focus on laser-based nuclear physics. While atomic processes are well suited to the visible or near visible laser radiation, as a third pillar ELI-NP will generate radiation and particle beams of higher energy and with brilliance suited to studies of nuclear and fundamental processes.

- Ultra High Field Science that will explore relativistic laser-matter interaction in an energy range where totally new phenomena like radiation dominated interaction become dominant.
  The decision on the location of the technologically most challenging pillar will be taken in 2012 after validation of the technology.

For ELI-NP it is foreseen to install in the first stage (2011-2015) two arms of the APOLLON-type laser, each with a power of 10 PW. A highly brilliant γ beam will be generated via the laser interaction with a brilliant bunched electron beam. Thus ELI-NP will allow either combined experiments between the high-power laser and the γ beam or stand-alone experiments.
For the Extreme Light Infrastructure - Nuclear Physics facility (ELI-NP) two new central instruments are planned:

1. A very high intensity laser beam, where two 10 PW Apollon-type lasers are coherently added to the high intensity of $10^{23} - 10^{24}$W/cm^2 or electrical fields of $2 \cdot 10^{15}$V/m.

2. A very intense, brilliant, very low bandwidth, high-energy γ beam, which is obtained by incoherent Compton back scattering of a laser light on a very brilliant, intense, classical electron beam.

This infrastructure will create a new European laboratory with a broad range of science covering frontier fundamental physics, new nuclear physics and astrophysics as well as applications in nuclear materials, radioactive waste management, material science and life sciences.

2.2 The Scientific Case of ELI-Nuclear Physics

In this project we want to use a very high intensity laser and a very brilliant, intense γ beam to achieve major progress in nuclear physics and its associated fields like the element synthesis in astrophysics and many new applications or even to observe in fundamental physics the first catalysed pair creation from the quantum vacuum.

At the Extreme Light Infrastructure - Nuclear Physics facility will be possible to perform either combined experiments between the high-power laser and the γ beam or stand-alone experiments using each of these major instruments.

We should first place the laser developments into the right perspective. Typical nuclear excitation energies are of the order of 100 keV – 1 MeV and typical nuclear radii are below 10 fm. Thus relevant electrical field strengths in a nucleus, which change the dynamics, are of the order of 100 keV/(e·10 fm)=10^{19}V/m and as such much beyond the Sauter field strength for pair creation from the vacuum of $1.3 \cdot 10^{18}$V/m [5]. Since fields beyond the Sauter field cause cascades of e^+e^- pairs and limit the field to the Sauter field, it is impossible to reach laser fields which directly influence the internal dynamics of nuclei significantly. On the other hand, ion acceleration using high power laser allows to produce 10^{15} times more dense ion beams than achievable with classical acceleration. The cascaded fission-fusion reaction mechanism can then be used to produce very neutron-rich heavy nuclei for the first time. These nuclei allow to investigate the $N = 126$ waiting point of the r-process in nucleosynthesis. With this type of new laser acceleration mechanism very significant contributions to one of the fundamental problems of astrophysics, the production of the heavy elements beyond iron in the universe can be addressed. According to a recent report by the National Research Council of the National Academy of Science (USA), the origin of the heaviest elements remains one of the 11 greatest unanswered questions of modern physics [1].

The second instrument, the intense, brilliant γ beam, is envisaged to provide a photon flux of $I = 10^{13}/[\mathrm{s}\,(100\,\mu\mathrm{m})^2]$, or – introducing the maximum Breit-Wigner cross section λ^2/π for 5 MeV γ quanta of $(\approx 100$ fm$)^2$ – a flux of $10^{-5}/[\mathrm{s}\,(100\,\mathrm{fm})^2]$, thus demonstrating the limitations by the presently achievable photon flux, where e.g. pump-probe experiments will remain impossible. The reflecting relativistic mirror probably will work at larger wave length. However it is a high risk that the reflecting relativistic mirror with 10^{14} photons per shot and $(\mu\mathrm{m})^2$ will also be realized for MeV energies. If so, double excitation and pump-probe experiments in nuclear physics would become possible for the first time. The main achievements with the γ beam facility probably will occur with high resolution at higher nuclear excitation energies. Identifying the new neutron halo isomers closely below the neutron binding energy would open a new field of nuclear spectroscopy. Thus the nuclear physics experiments have to be carefully designed and it has to be considered that the success of lasers in atomic physics cannot simply be duplicated in nuclear physics due to the very different scales and dimensions.

The γ beam will have unique properties in world wide comparison and opens new possibilities for high resolution spectroscopy at higher nuclear excitation energies. They will lead to a better understanding of nuclear structure at higher excitation energies with many doorway states, their damping widths, and chaotic behaviour, but also new fluctuating properties in the time and energy domain. The detailed investigation of the pygmy dipole resonance above and below the particle threshold is very essential for nucleosynthesis in astrophysics. The γ beam also opens many new possibilities for applications. The γ beam itself can be used to map the isotope distributions of nuclear materials or radioactive waste remotely via Nuclear Resonance Fluorescence (NRF) measurements [6]. At lower energies around 100 keV the high resolution of the beam is very important for protein structural analysis. In addition we want to produce low energy, brilliant, intense neutron beams and low energy, brilliant, intense positron beams, which open new fields in material science and life sciences. The possibility to study the same target with these very different brilliant beams will be unique and advance science much faster.

The high power laser allows for intensities of up to 10^{24}W/cm^2. Here very interesting synergies are achievable with the γ beam and the brilliant high energy electron beam to study new fundamental processes in high field QED. When the γ beam is injected into the focus of the high intensity laser, which in this special case consists of a standing E-field of two focused lasers, the most recent non-perturbative QED calculations predict that one can observe already at 10^{24} W/cm^2 the catalytic pair creation from the vacuum [2–4]. If confirmed, this would constitute a very basic non-perturbative

Table 1: Overview of the main areas of the scientific case of ELI-NP

Science Case of ELI-NP	
Basic Science	**Applications**
Fundamental physics of perturbative and non-perturbative high-field QED: – pair creation, high energy γ rays, birefringence of the quantum vacuum	Developing nuclear resonance fluorescence (NRF) for nuclear materials and radioactive waste management: – ^{235}U,^{239}Pu, minor actinides, neutron poisson
High-resolution nuclear spectroscopy: (γ,γ'), (γ,n), (γ,p), (γ,α), (e,e'), $(e,e'\gamma)$, (γ,f) – neutron halo isomers, chaotic properties of nuclear states, nuclear potential landscape, parity-violating meson-nucleon coupling, pygmy dipole resonance	Brilliant γ, X, n, e^+, e^- micro beams in material science and life science: – (γ,n) reaction at threshold for low energy neutrons, (γ,e^+e^-) reaction at 2-3 MeV for cold positrons
Astrophysics of the r-, s-, p-processes in nucleosynthesis: – masses of waiting point nuclei, pygmy resonance	Developing techniques of laser acceleration and of a brilliant γ beam for nuclear physics: – relativistic mirrors

textbook QED result. Also the radiation damping theory could be tested very accurately with the very brilliant electron beam injected into the laser focus. Here reflected high-energy γ quanta and cascades of e^+e^- pairs could be studied as a function of the γ factor of the electron beam and the laser field strength. While the predictions for radiation damping will probably be correct in the perturbative regime, the different theoretical approximations can be tested very sensitively for nonlinear radiation damping. On the other hand, the central questions of high-field QED for the ultra-relativistic laser-plasma interaction with $I \geq 10^{24}$ W/cm^2 including all new corresponding applications will be subject of the 4th pillar of ELI on ultra-high fields.

Amongst other goals, the envisaged new nuclear physics spectroscopy aims at a much better understanding of highly excited chaotic nuclear resonances, while up to now nuclear physics – due to the facilities – focused more on various lower lying vibrational and rotational nuclear states with more collective nuclear motion. Also the transition from collective to chaotic motion is of large interest. Though the basic ideas of a compound nuclear state were already formulated by N. Bohr in 1936 [7], now we have a much more detailed theory of these states within the framework of random-matrix theory [8] and conceptual pictures like quantum chaos. Due to the new experimental possibilities within ELI-NP, new theoretical predictions for experiments are introduced [9]. One example: A nuclear state excited by a γ pulse below the particle threshold is predicted to decay exponentially in time via γ quanta, while a state above the particle threshold shows a different decay law resulting from folding an exponential function with a power law. To verify these new decay laws in the attosecond and zeptosecond time range will be quite an experimental challenge, however, at the same time it would constitute an essential confirmation of random matrix theory. In the energy domain other known properties of compound nuclear states like Ericson fluctuations [12] or long range energy correlations will be studied in a systematic way. If double excitations become possible with the relativistic mirror γ beam, the excited state can be treated with random-matrix theory similar to the double giant dipole excitation [10]. Here the new laser based measuring technologies will start a much better understanding of these high lying states and will lead to a reincarnation of nuclear physics, where the MeV photon pulses with much shorter wavelength and much shorter pulse duration will lead to an improved insight into compound nuclear states and quantum chaos.

In the field of basic nuclear physics, a better theoretical understanding of compound nuclear resonances in comparison with much improved experiments will also lead to better models for the element

synthesis in astrophysics.
On a deeper level nuclear physics is described by QCD and their effective theories like chiral symmetry breaking and the condensate structure of low-energy QCD [11]. Here close lying resonances or the newly planned parity violating experiments at high excitation energies are a typical example, where we want to determine the parity-violating effective couplings between Z_0 and π, ρ and ω mesons.
Compared to former γ facilities, the much improved bandwidth is decisive for the new γ beam facility. Several experiments, like the parity violation experiment, only become possible due to this much better bandwidth.The large majority of γ beam experiments will profit proportionally from the better bandwidth, because the widths of the studied nuclear levels are significantly smaller than the width of the beam. Thus the ratio of 'good' γ quanta within the nuclear linewidth compared to the 'bad' γ quanta outside, which undergo Compton scattering and cause background in the detectors, will be significantly improved.
Besides a wide range of fundamental physics projects, a variey of applied research will also be enabled at ELI-NP. Our compilation of these applied physics projects does not reflect a weighting of the political, socio-economical or scientific importance of the projects:
The project to develop techniques for remote characterization of nuclear materials or radioactive waste via NRF will gain large importance for society in Europe. The unsolved problems of long-term storage of radioactive waste from reactors, while having to deal with large amounts of old, insufficiently characterized radioactive waste requires a precise isotopic characterization in the first place. It may even turn out that a detailed in-situ characterization of partially used reactor fuel elements may result in producing more usable energy in reactors for the same amount of radioactive waste.
On the other hand the new production schemes of medical isotopes via the (γ,n) reactions might also reach socio-economical relevance. The new types of neutron and positron sources may reach large importance in material and life sciences; even more of the γ-facility will be upgraded in a further phase.

References

[1] E. Haseltine, http://discovermagazine.com/2002/feb/cover

[2] G. V. Dunne, H. Gies and R. Schützhold, Phys. Rev. D **80**, 111301 (2009) [arXiv:0908.0948 [hep-ph]].

[3] V. N. Baier and V. M. Katkov, "Pair creation by a photon in an electric field," arXiv:0912.5250 ;(2009).

[4] N.B. Narozhny, Zh. Eksp. Teo. Fiz. **54**, 676 (1968).

[5] F. Sauter, "Über das Verhalten eines Elektrons im homogenen elektrischen Feld nach der relativistischen Theorie Diracs," Z. Phys. **69**, 742 (1931).

[6] R. Hajima et al., NIM **A 608**, S57 (2009).

[7] N. Bohr, Nature **137**, 344 (1936).

[8] H.A. Weidenmüller and G.T. Mitchell, *Random marices and chaos in nuclear Physics:Nuclear structure*, Rev. Mod. Phys. **81**, 539 (2009).
G.E. Michell, A. Richter and H.A. Weidenmüller, *Random Matrices and Chaos in Nuclear Physics: Nuclear Reactions*, arXiv:1001.2411v1[nucl-th]14 jan 2010.

[9] H.A. Weidenmüller and B. Dietz, *Photonuclear Reactions induced by Intense Short Laser pulses*, to be published (2010).

[10] J.Z. Gu and H.A. Weidenmüller, Nucl. Phys. **A 690**, 382 (2001).

[11] P. Finelli etal., Nucl. Phys. **A 735**, 449 (2004).
N. Kaiser and W.Weise, Nucl. Phys. **836**, 256 (2010).

J.W. Holt et al., Phys. Rev. **C 81**, 024002 (2010).
N. Kaiser; arXiv 1003.1143 (2010).

[12] T. Ericson, Phys. Rev. Lett. **5**, 430 (1960).

[13] N. Bohr and J.A. Wheeler, Phys. Rev **56**, 426 (1939).
A. Feshbach, C.E. Porter and V.F. Weisskopf, Phys. Rev. **96**, 448 (1954).

Conceptual Design Report for the multi-PW laser system at ELI Nuclear Physics Facility, Bucharest-Măgurele, Romania

Editors:
Jean-Paul Chambaret[1], **Răzvan Dabu**[2], **Daniel Ursescu**[2]
[1]Institut de la Lumière Extrême, Palaiseau, France
[2]National Institute for Lasers, Plasma and Radiation Physics (INFLPR), Măgurele, Romania

3 Conceptual Design Report for the multi-PW laser system at ELI Nuclear Physics Facility

3.1 Introduction

ELI Nuclear Physics Facility, Bucharest, Romania

The ELI Nuclear Physics (ELI-NP) facility to be placed in Măgurele, near Bucharest, in Romania, will mainly focus on laser-based nuclear physics. The ELI-NP facility will generate γ and particle beams with high energies and brilliances suited to studies of nuclear and fundamental processes. The core of the facility is a multi-PW laser system. In order to perform cutting edge nuclear physics experiments, a complementary highly brilliant γ beam, with energies in the 15 MeV range, will be generated via the laser interaction with a brilliant bunched electron beam. Thus ELI-NP will allow either combined experiments between the high power laser and the γ beam or PW laser stand-alone experiments. The design of the facility is modular, reserving the space for further extension of the laser system and allowing the extension of the experimental area at a later moment in time, according to the needs.

A laser system consisting in a Ti:sapphire oscillator, OPCPA Front End and Ti:sapphire high-energy amplification at $\sim$0.8 μm wavelength is considered as the basic solution for the ELI-NP facility. A Front End based exclusively on a Ti:sapphire oscillator and amplifiers could be alternatively used. A laser system based on a Ti:sapphire or Nd:glass oscillator OPCPA pre-amplifier and high-energy amplification in mixed Nd:doped glasses at $\sim$1 μm wavelength represents a back-up solution for the ELI-NP laser facility.

The ELI-NP laser facility will have two Front Ends. They will temporally stretch and amplify initial ultrashort pulses with 800 nm central wavelength to the 100 mJ level, preserving the needed large bandwidth of the 15 fs laser pulses and the temporal contrast of the pulses in the range of 10^{-12}. Due to the complexity of such OPCPA system, the alignment and maintenance time for one Front End is long. To avoid such dead-times, only one Front End is planned to operate at a given time, the second one being used during the maintenance of the other Front End, significantly increasing the available beam-time of the laser facility.

After the Front End, the pulses are split and distributed to further laser amplifiers, reaching few Joules of energy at 10 Hz repetition rate and few tens of Joules at a repetition period of the order of few seconds. At these energy levels, the pulses can be extracted from the laser amplification chain and recompressed to shortest duration in vacuum compressors. Subsequently, they are distributed to the high repetition rate experimental areas.

Alternatively, the laser pulses are further amplified in the amplification chains to energies of the order of 200 J. The repetition rate of the pump lasers will restrict the repetition period of the high energy pulses to the minutes range. Adaptive optics and optical isolation of the pulses will be implemented before the optical compressors. The ultrashort pulses will be distributed to the high energy experimental areas, where stand-alone experiments or combined nuclear physics experiments using the highly brilliant γ beam will be performed.

Coherent combination of the high power ultrashort pulses with the ultraintense and ultrashort pulses from the parallel amplification chains is envisaged, in order to reach intensities of the order of 10^{23} W cm^{-2} and above. The operation of the experiments will take place in parallel, the laser pulses being delivered to different experimental areas on request.

The experimental program of the ELI-NP facility addresses both fundamental science research and application-oriented developments. Fundamental physics of perturbative and non-perturbative high-field QED, high resolution nuclear spectroscopy and astrophysics-related studies of r-, s-, and p-processes in nucleosynthesis are included in the basic scientific research. The emerging applications are related to the development of the nuclear resonance fluorescence (NRF) reactions for radioactive waste management, to the use of brilliant γ, X, n, e^+, e^- microbeams in material science and life science and to the development of techniques of laser acceleration and of brilliant γ beam for nuclear physics.

The risks associated with the achievement of the ELI-NP laser system specifications could be classified as follows:

1) final pulse duration

2) spatial and temporal contrast
3) high energy output in the range of 200 J/pulse and above
4) coherent combination of the pulses

With the back-up OPCPA-mixed glass solution, the final pulse duration would be longer, but the energy per pulse would be in the range of kJ/pulse, while the 20 PW level could be reached without coherent beam combintion.

3.2 Laser Architecture and Technical Layout

3.2.1 Current status

Based on CPA technology [1, 2], petawatt-level laser pulses make it possible to experimentally investigate highly nonlinear processes in atomic, molecular, plasma, and solid-state physics and to access previously unexplored states of matter.

The petawatt laser power was achieved as early as 1997 [3, 4], based on chirped-pulse amplification in Nd:glass. Until now, other laboratories have reported petawatt-level laser systems [5–9].

All devices and projects now available may be classified into three types, according to the gain medium they employ: (1) neodymium glass [3, 3–6, 9, 12, 14–16], (2) titanium-sapphire [7, 17], and (3) optical parametric amplifiers with KDP and DKDP crystals [11, 18, 22] (see Table 2). In all three types, energy (in the form of population inversion) is stored in neodymium ions in glass. In the first case, this energy is directly converted into the energy of a chirped pulse that is then compressed. In the second and third cases, the stored energy is converted into the energy of a narrowband nanosecond pulse, which, upon second-harmonic conversion, serves as the pump for chirped-pulse amplifiers. This pump either provides population inversion in a Ti:sapphire crystal or is parametrically converted into chirped pulses in the nonlinear crystal.

Peak power is determined by the duration and energy of the compressed pulses. Maximum energy is achieved in glass-based lasers, because energy that has been stored as population inversion is directly converted into a chirped pulse. However, the narrow bandwidth of Nd glasses typically restricts the compressed-pulse duration to about 500 fs. A 1.1 PW laser based on hybrid optical parametric chirped pulse amplification (OPCPA) and mixed Nd:glass amplifiers (silicate Nd:glass rod and phosphate Nd:glass disks) has been demonstrated. It produces ultra-short laser pulses of 186 J energy and 167 fs duration [9]. Ti:sapphire lasers have a large-gain bandwidth, allowing pulse compression down to 10–20 fs. Due to gain narrowing, up to now, the reported pulse duration of hundreds of TW and PW-class Ti:sapphire laser amplifiers was at least 30 fs [6, 7, 17, 19, 21].

1 PW femtosecond laser system based on Ti:Sapphire power amplifiers was recently reported [29]. A further increase to 10 PW or more is limited by several technological developments. Current crystal growth technologies can produce commercially available Ti:sapphire crystals with an aperture of no more than 10 cm. When attempting to overcome the petawatt energy level, such a small aperture will limit the chirped-pulse energy due to optical breakdown and self-focusing. Recently, 170 mm diameter Ti:sapphire crystals of good optical quality were obtained [22]. The perspective of getting in the near future laser crystals with more than 180 mm clear aperture is encouraging. The currently grown Ti:sapphire crystals allow to generate maximum 5 PW fs pulses, if parasitic lasing bottle neck is resolved.

Parametric amplifiers are free of the above disadvantages. Current nonlinear KDP and DKDP crystals have an aperture of 40 cm or more and the gain bandwidth of the DKDP corresponds to a 10–20 fs duration of the amplified pulse. At the same time, in parametric amplifiers, the energy conversion efficiency of a Nd laser mono-pulse at fundamental frequency into a chirped pulse is typically only at the level of 10%. Also, parametric amplifiers require very-short (about 1 ns) pump pulse. Similar or larger apertures of amplifying media are available in case of Nd:glass disks lasers.

Thus, in existing approaches to petawatt and multi-petawatt lasers, the peak power is mainly limited either by the bandwidth (neodymium ion lasers), the crystal aperture (Ti:sapphire lasers), or the efficiency of the energy conversion from a pump wave into a signal wave, and difficulties related to the development of high energy short pulse duration pump lasers (lasers with optical parametric amplifiers). For all these laser systems, the main challenges are the manufacturing of large diameter

mirrors (more than 30 cm diameter) for laser beam handling (steering, wave-front correction, focusing) and high energy/power laser beam characterization.
Due to existing technical bottlenecks, the design and building of a 10-PW class laser is a very difficult task. At present, the commercial femtosecond laser systems in operation reached the level of 200 TW. Few companies (Thales, Amplitude Technologies-France, National Energetics-USA) assert they are able now to build femtosecond laser systems generating up to 1 PW power. 10-PW laser projects, with deadlines in 2013-2015, are under development in United Kingdom (RAL) and France (ILE). The above mentioned companies consider also the possibility to reach the multi-PW level in the next few years.

3.2.2 Multi-PW laser approach implementation

The most appropriate approach to achieve the 10 PW laser power class could be determined by considering the following factors:

1. Ability to fulfill required specifications:
   a) Peak pulse power of the order of 10 PW or more per one amplifier chain
   b) Pulse-width of the re-compressed amplified pulse 25-160 fs
   c) Rep-rate 1/10 – 1/60 Hz
   d) Ns & ps contrast $>10^{12}$
   e) Focused laser intensity $\geq 10^{23}$ W/cm^2 (laser beam focused near the diffraction limit)
2. Existing techniques proved by the long term laser facilities operation (e.g. 200 TW Ti:sapphire CPA laser systems)
3. Existing laser components and devices necessary to reach 10 PW power class (e.g. 40 cm diameter DKDP crystals, large aperture Nd:glass disks)
4. Required laser components and devices that could be probably developed in the next years (20 cm diameter Ti:S rods; Nd:YAG, Yb:YAG, Nd:glass, diode pumped lasers; diffraction gratings, etc.)
5. Predicted technological development in the next 5 years.
6. Energy consumption/laser pulse.
7. Conditions of operation and expected laser system long-term stability.
8. Costs of the whole laser system.
9. Support from the expert groups.

Table 2: Comparison of known CPA petawatt laser projects. Symbols "+", "-" denote advantages and disadvantages of three concepts up to 1-PW power level.

Main characteristics	**1**		**2**		**3**	
Gain medium Stored energy medium	Ti:sapphire Nd:glass		DKDP Nd:glass		Mixed Nd:glasses Nd:glass	
Pump wavelength	2ω Nd	(−)	2ω Nd	(−)	*No additional*	(+)
Pump duration, ns	>10	(+)	1	(−)	*pump laser*	(+)
Amplifier aperture, cm	10	(−)	40	(+)	>40	(+)
Minimum duration, fs	25	(+)	15	(+)	150 fs	(−)
Efficiency (1ω Nd →fs), %	15	(−)	10	(−)	100	(+)
Repetition rate (determined by available pump lasers)	0.1 Hz	(+)	1 pulse/20 min	(−)	from 1 pulse/20 min up to 1 pulse/min	(−)
Number of PWs from a 1-kJ 1ω Nd	6		4		6	
Maximum power obtained, PW	0.85 [7]		0.56 [8]		1.10 [9]	

For OPCPA at high energy level, it is necessary to pump with a 1-2 ns pulse-duration, hundreds of Joules pulse energy. A very expensive and complex high energy pump laser is required. The

solution proposed in the 10 PW project of the Rutherford Appleton Laboratory, United Kingdom, is to use the already existing kJ energy Nd:glass VULCAN laser for pumping at low repetition rate (1-2 pulses/hour). Due to the absence of a similar laser system that could be used as high energy OPCPA pump laser, we consider that this solution is not suitable in the case of ELI-NP.
In case of laser systems based on direct amplification in mixed (silicate & phosphate) Nd:glasses, the actual pulse duration is 160 fs and could be reduced in the next future down to 100-120 fs. Considering the necessary laser energy to reach 1-PW power, the drawback of 4-5 times longer pulse duration compared to Ti:sapphire lasers is compensated by the absence of frequency doubling and energy transfer from the pump lasers to the gain media that host the laser radiation generating the femtosecond pulses. By amplification in Ti:sapphire, the predicted peak power that could be reached in the next 3-5 years is limited at about 10 PW. Next scaling would be possible only by coherent beam combination of several 10-PW Ti:sapphire femtosecond lasers. Laser systems based on direct amplification in glasses are scalable using the existing technology up to several tens of PW or even to above 100 PW in a single amplifier arm. Laser amplification in glasses at very high energy (few kJ per pulse) in a single laser amplification chain imposes a limitation of the repetition rate (1 pulse every 20-30 minutes) compared to the last amplifier of a 10-PW Ti:sapphire laser that could be pumped by a number of 4-8 frequency doubled Nd:glass lasers with an expected repetition rate of 1 pulse/min. Nevertheless, recent achievements in the cooling of high energy Nd:glass disk lasers predict a possible 1 pulse/minute repetition rate of a 10-PW CPA laser with mixed Nd-doped glasses.
For the above mentioned reasons, the following solutions could be considered as suitable for the ELI-NP multi-PW laser:

(1) **High energy amplification in Ti:sapphire (∼30 fs pulse duration)**

   a) Hybrid laser system that consists in a Front End based on a Ti:sapphire oscillator and OPCPA in BBO, LBO crystals, followed by high energy amplifiers with Ti:sapphire rods;

   b) Front End based on Ti-sapphire oscillator-amplifiers and high energy amplifiers with Ti:sapphire rods

(2) **High energy amplification in mixed Nd-doped glasses (100-150 fs pulse duration)**, as a back-up solution. Hybrid system that consists in a Front End based on OPCPA in BBO, YCOB crystals, followed by high energy amplification in mixed silicate and phosphate Nd:glass rods and disks. The specifications for the back-up solution: 2 kJ/pulse, 100 fs, 1 shot/min @ 1050 nm.

The basic solution for ELI-NP laser facility consists in an OPCPA Front End and Ti:Sapphire high-energy amplification stages. A Front End based exclusively on Ti:sapphire oscillator and amplifiers, with XPW for high intensity contrast, is considered as an alternative option.
A back-up solution is a laser system based on OPCPA Front End and high energy amplification in mixed Nd-doped glasses.
The existence of a back-up solution is very important for diminishing the risk of the project. The main Ti:Sapphire solution proposed for the laser Front End and the high energy amplifiers chain is described in the following sections.

3.2.3 Front End

Three types of Front End configurations could be considered for broadband PW-class CPA laser systems: all Ti:Sapphire, ultra-broadband OPCPA with optical synchronization of the seed and pump laser, and broadband OPCPA based on BBO crystals with electronic synchronization.

All Ti:Sapphire Front End
The schematic of the Front End is illustrated in Figure 1 [23]. The first module of the laser system is an ultra-broadband Ti:Sapphire oscillator using dispersive-mirror technology for broadband intracavity group delay dispersion compensation. The oscillator pulses are stretched to 20-ps after appropriate isolation. After a 10-Hz slicer Pockels cell, pulses are amplified to about 2-mJ pulse-energy in a

multi-pass Ti:Sa amplifier. The spectrum and spectral phase can be pre-shaped by a DAZZLER Acousto-Optic Programmable Dispersive Filter to optimize the amplifier output.
After recompression, the laser pulses are injected in a XPW filter in order to improve the temporal contrast. The filter is based on the generation of a cross polarized wave relative to the incoming one in two BaF_2 crystals placed between two crossed polarizers [24]. The contrast improvement is given by the extinction ratio of a pair of high quality polarizers. This filter enables also two others important functions: spatial filtering and pulse duration shortening by a factor of $\sqrt{3}$. After the XPW filter, the pulses are stretched to nearly 2-ns and then amplified in three multi-pass amplifiers to about 200-mJ. To compensate for the gain narrowing of the multi-pass amplifiers, a MAZZLER Acousto-Optic Programmable Gain Control Filter can be used. The Ti:Sa gain media of the multi-pass amplifiers are water-cooled. The Front End output is coupled to the 1-PW amplifiers chain by a Faraday isolator.
The required performances of the 1-PW Front End output are:

- Pulse energy: $E_{out} = 150-200$ mJ;
- Pulse duration: $\tau_{out} \approx 2$ nsec;
- Pulse bandwidth: > 40-nm;
- Temporal contrast (ps & ns): $\sim 10^{12}$;
- Pulse repetition rate: 10-Hz;
- Central wavelength: 800-nm;

:

Pump lasers:

- **PL1**: Diode-pumped single longitudinal mode CW laser, 5-W at 532-nm wavelength, 220 VAC, 1 KVA apparent power (integrated in the oscillator).
- **PL2**: Flash-pumped, electrooptically Q-switched Nd:YAG laser, 10-mJ output at 532-nm wavelength and 10-Hz repetition rate, supergaussian smooth spatial profile, 220 VAC, 1 KVA apparent power.
- **PL3**: Flash-pumped, electrooptically Q-switched Nd:YAG laser, 100-mJ output at 532-nm wavelength and 10-Hz repetition rate, supergaussian smooth spatial profile, 0.6 KW power consumption, 220 VAC, 2 KVA.
- **PL4**: Flash-pumped, electrooptically Q-switched Nd:YAG laser 1-J / 532-nm, 10-Hz, 4-6 ns, supergaussian smooth spatial profile, 220 VAC, single phase 20 A, 6 KVA, 6 liters/minute at 10-40 PSI pressure drop.

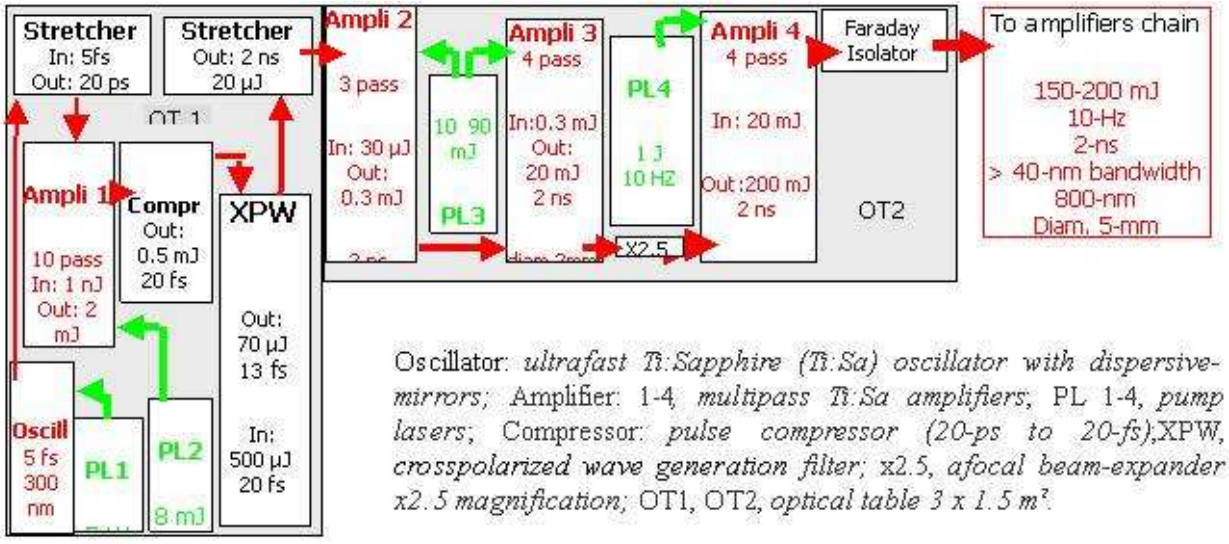

Figure 1: Schematic overview of the Ti:Sa 1-PW Front End [23]

Table 3: Front End requirements

Apparent power	11 KVA, 1 phase, 220 VAC
Power consumption	8 KW
Cooled Water	8 liters / min, 12 C degree
Clean room class	At least 50 000
Relative humidity	30 – 50 %
Clean room dimensions	5 x 6 m^2

Ultra-broadband OPCPA Front End

The goal of this configuration is very demanding: to provide energetic ultra-broadband laser pulses for Ti:Sa power-amplifiers chain. The main characteristics of the output pulse are: 800-nm central wavelength. 100-mJ energy, > 70-nm spectral bandwidth (that means after compression < 10-fs full width at half-maximum duration), 10-Hz repetition rate.
The schematic of the OPCPA Front End includes an 800-nm CPA signal chain and an 1030-nm CPA pump chain, as shown in Figure 2 [23]. The 800-nm chain begins with a commercial ultrashort Ti:Sapphire oscillator-amplifier system (25-fs pulse width, 2-mJ pulse-energy, > 30-nm bandwidth at 800-nm central wavelength and 1 kHz repetition rate). The output of the Ti:Sa amplifier is spectrally enlarged in an argon-filled hollow-fiber to obtain ultra-broadband laser pulses of less than 10-fs duration. Then the pulses are injected in a XPW filter in order to improve the temporal contrast. After XPW filter the pulse is back-reflection isolated and is chirped in a stretcher to 10 ps. The chirped pulse is then amplified in two ultra-broadband non-collinear OPCPA stages (NOPCPA) that use BBO or LBO nonlinear crystals. The NOPCPA stages are pumped with 515-nm nanosecond pulses provided by a part of the frequency-doubled pump chain output. This picosecond OPCPA process is mandatory to preserve at the same time high gain and broadbandwith.
It is critically important for efficient and stable operation of the OPCPA stages to accurately synchronize pump and signal pulses. An all-optical synchronization technique [26, 27] is used in this configuration. The pump and signal chains are injected with the same seed provided by the Ti:Sa oscillator and exact synchronization can be maintained while the pump pulses are boosted to high energies.
A very weak narrowband signal of 1030-nm extracted from the broadband output pulse of the Ti:Sa oscillator is used as a pump-seed. The energy of the seed pulse is further increased in an ytterbium doped fiber amplifier. The amplified seed is chirped and then is injected into a diode-pumped regenerative amplifier based on potassium gadolinium tungstate crystals doped with ytterbium (Yb:KGW). The output of the regenerative amplifier (2 mJ, 700 ps, 1 kHz, 1030 nm) is injected into a chain of diode-pumped multipass amplifiers based on different ytterbium- doped crystals (KGW, CaF_2, YAG) to reach after recompression and frequency doubling, 100 mJ unchirped energy. This picosecond pump is used to amplifiy the signal through an OPCPA preamplifier to 10-20 mJ. A 20 mJ remaining part of the pump beam will be then stretched again to ns pulse duration and amplified to finally infrared pulses of 2 J energy, 2 ns duration, possibly at 100 Hz repetition rate at 1030 nm wavelength.
After frequency doubling in nonlinear crystals the high-energy output (1 J pulse energy, 1.8 ns duration, 0.9 nm bandwidth, 10 Hz repetition rate, 515 nm wavelength) is used to pump the final NOPCPA amplifier stage. The signal exiting the picosecond OPCPA preamplifier is then stretched again to 1 ns. The losses induced in the secondary stretcher (30% throughput) will be compensated in this final NOPCPA stage. The largest issue will be to combine the chirp of the signal and the chirp of the pump beam to preserve the final compressibility of the PW pulse. The output of the first NOPCPA provides ultra-broadband pulses of 15-mJ energy, <70-nm bandwidth, 800-nm central wavelength at 100-Hz rate, that are further amplified in the final NOPCPA. During amplification, the repetition rate of the pump pulses is gradually reduced from 1-KHz at the regenerative amplifier to 10-Hz at the final NOPCPA stage.

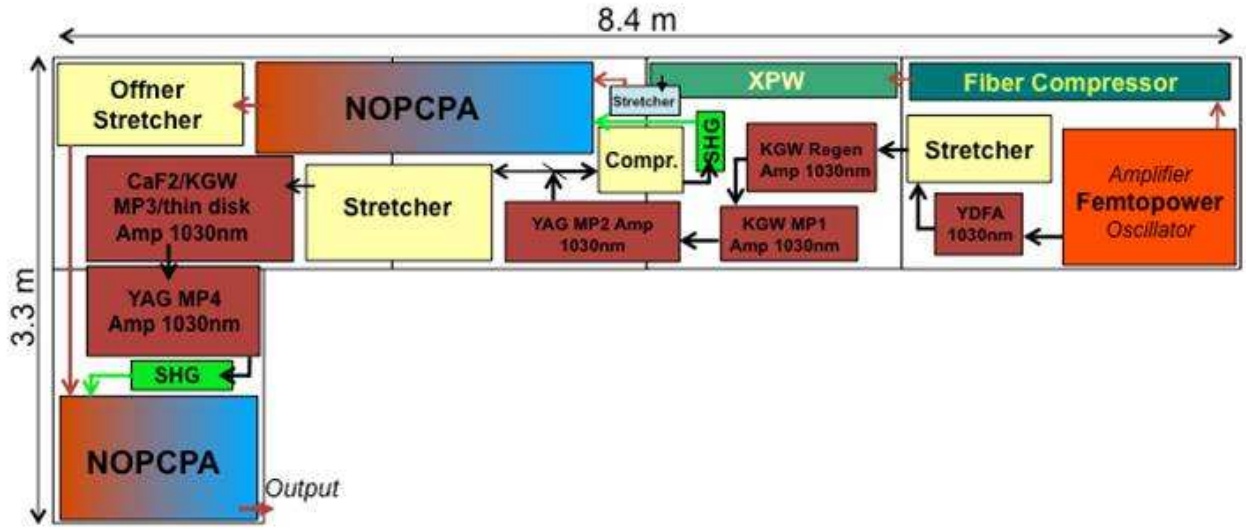

Figure 2: Schematic overview of the 1-PW Front End [23] YDFA, *ytterbium doped fiber amplifier*; MP1-MP4, *multipass amplifiers based on ytterbium- doped crystals (KGW, CaF_2, YAG);* XPW, *cross-polarized wave generation filter.* NOPCPA, *non-collinear optical parametric chirped pulse amplifiers*

An active control of the spectral phase by using DAZZLER dispersive filters will be necessary for both signal and pump pulses.

OPCPA critical design issues
• Very precise time/space synchronization of signal and pump pulses;
• High-intensity/ high-stability and high quality pump beams (not currently available);

OPCPA key features:
• High signal gain (>1000 in a single pass crystal);
• Broad bandwidth (ultrashort re-compressed pulses);
• Negligible thermal loading;
• High signal - noise contrast ratio;
• High energy pulses in available large non-linear crystals, no transversal lasing;

Table 4: OPCPA Front End requirements

Apparent power	9 KVA, 1 phase, 220 VAC
Power consumption	7 KW
Cooled Water	6 liters / min, 12 C degree
Clean room class	At least 50 000
Relative humidity	30 – 50 %
Clean room dimensions	5.5 x 10.5 m^2

Nanosecond OPCPA Front End
An alternative solution is a simple electronically synchronized OPCPA Front End. Seed pulses generated by a Ti:sapphire oscillator are stretched up to ns duration and are amplified in BBO crystals pumped by nanosecond laser pulses given by Nd:YAG lasers [9] up to few millijoule level. The majority of the system gain is achieved in 2-4 OPCPA stages, which use non-collinear optimized OPA geometries. A good intensity contrast of the amplified pulses is preserved. Unlike the OPCPA based on optical synchronization with BBO crystals seeded by spectrally broadened input pulses and pumped by picosecond pulses, the available gain bandwidth in this case is broad-enough to amplify pulses

re-compressible down to 25-30 fs, similar with the pulse duration obtained in Ti:sapphire amplifier systems.

3.2.4 High rep rate PW amplifiers

The stage of amplification consists of two multi-pass Ti:Sa amplifiers: a pre-amplifier and a power amplifier. The amplifiers chain has a gain of 120-140 to yield an output pulse-energy exceeding 30 J (Figure 3). The Front End pulses are spatially filtered and magnified to an appropriate diameter, and then are seeded into the preamplifier. After backreflection isolation, the 3-5 J output pulses of the preamplifier are again spatially filtered and magnified and then are injected into the power amplifier. The fluence of the laser beam is maintained down to 1.5 J/cm^2 and the local peaks should be below 2 J/cm^2 in the amplifier chain.
The preamplifier is pumped by two laser beams of 8 J pulse energy provided by four nanosecond Nd:YAG lasers of 4 J pulse-energy at 532 nm wavelength and 10 Hz repetition-rate. Two high-energy nanosecond Nd:Glass lasers of 50 J pulse-energy at 527 nm and 0.1-0.05 Hz repetition-rate are used to pump the power amplifier.
The required performances of the 1-PW Amplifiers Chain output are:

- Pulse energy: $E_{out} > 30$ J;
- Pulse duration; $\tau_{out} \approx 2$ nsec;
- Re-compressible down to 20 fs;
- Pulse repetition rate: 0.1-0.05 Hz;
- Central wavelength: 800 nm;

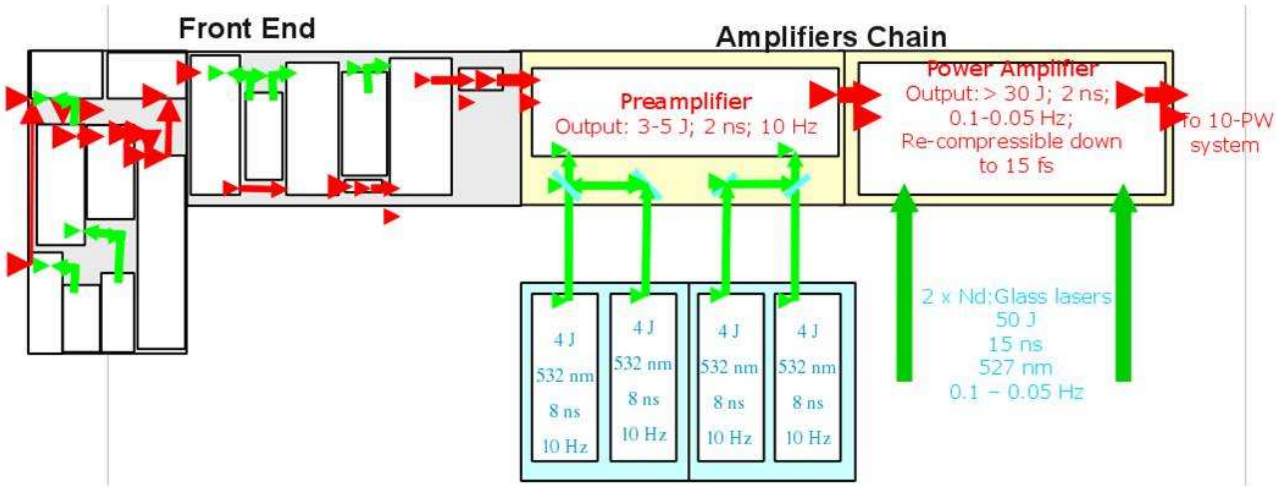

Figure 3: Schematic overview of the 1−Petawatt laser chain

Critical design issues of the Amplifiers Chain
As it is well known in femtosecond laser technology, the quality of the pump beams is a key parameter to achieve good beam quality of the amplified pulses and high efficiency. Two main factors are critical for the green pump beams:
• Smooth spatial profile with no hot spots, to avoid the generation of gain inhomogeneity, a very important parameter in multipass power amplifiers. Combining the beam homogenization technique based on diffractive optical elements with the double pass pumping technique, a high-quality optical pumping could be obtained if managing carefully the coherence properties of the pump laser itself. A compromise must be chosen between high spatial coherence leading to high SHG conversion efficiency but 100% energy modulations (fringes) on the pump crystal, and low spatial coherence necessary for efficient smoothing but reducing drastically the SHG efficiency. To overcome this difficulty and obtain efficient beam smoothing and high SHG sophisticated longitudinal mode beating must be implemented in the pump oscillator to suppress the temporal coherence [28].

• Low beam-quality parameter M^2 for easy focusing and long Rayleigh length to achieve a good overlap of pump and infrared beams in Ti:Sa crystals. As the pump repetition rate increases, the thermal optical power of the gain media increases proportionally and the pump waist must be reduced to maintain the gain at a high value and this is making the M^2 issue more critical.
• Ti:Sa cooling technique and the crystal mount design have to minimize the thermal effects induced in gain media and the transverse lasing, in order to preserve a high gain with a Strehl ratio near the diffraction limit. Cryogenically cooling of the preamplifier Ti:sapphire rod at 10 Hz repetition rate is considered.
• Accurate time positioning of the gain buildup curve could prevent the transverse lasing and also reduces ASE. This technique is based on the fine synchronization of the different pump lasers on the amplifiers chain. This technique could be efficient to reduce transverse parasitic lasing, but it must be combined with more efficient strategies consisting in careful management of the absorption coefficient of the TiSa crystal, and even more efficient, the management of the optical reflective (or scattering) properties of the crystal perimeter surfaces. Moreover for large pumping areas, the transverse ASE gain could be high enough to deplete the population inversion and reduce the amplification efficiency without any need of transverse oscillations. Transverse ASE management is one of the biggest issues at that level of amplification.
• Alternative solution of power supplies with closed loop water cooling and chillers instead of cooled water are considered. In this case the necessary water flow rate will be drastically diminished.

Table 5: The requirements for 1−PW Amplifier Chain

Apparent power	100 KVA, 1 phase, 220 VAC, 50 Hz, 20x25 A plugs
Power consumption	80 KW
Cooled Water	100 liters / min, 12-17 C degree
Clean room class	At least 50 000
Relative humidity	30 – 50 %
Clean room dimensions	12 x 6 m^2 (including the Front End)

3.2.5 High energy amplifiers

The output of the 1-PW system is injected in a high-energy amplifiers chain in order to finally increase the pulse energy to about 200 J while keeping the bandwidth broad enough for 15-30 fs pulses. The 10-PW class chain consists of two multi-pass high-energy Ti:Sa amplifiers: 80-J amplifier stage and the 200-J final amplifier stage operating at a repetition rate of 1 pulse per minute.
These high-performance parameters require an important technological effort to develop a new generation of laser components (laser mirrors, Ti:Sa crystals, pump lasers) with improved features regarding the size, optical quality, damage-threshold, pump-beam quality and pulse-energy.
Critical design issues of the 10-PW class chain
• High-quality Ti:Sapphire crystals of large sizes: 200-mm diameter [23];
• Large-size laser mirrors (300 mm diameter) having a high reflectivity in a bandwidth of 200-nm around the 800-nm central wavelength and also the control of group velocity dispersion (GVD) at 2.5 J/cm^2 working energy density [23];
• Laser mirrors with variable spectral reflectivity for each amplifier input in order to minimize the gain-narrowing effect in the Ti:Sa amplifiers [23];
• 100-400 J green pump-beams with homogenized smooth spatial profile without hot spots and low beam-quality parameter M^2 for easy focusing and long Rayleigh length to achieve a good overlap of pump and infrared beams in Ti:Sa crystals;
• Ti:Sa cooling technique and the crystal mount design in order to minimize the thermal effects induced in gain media;

• Accurate time positioning of the gain buildup curve to prevent the transverse lasing and also reduces ASE. This technique involves a fine synchronization of the different pump lasers on the amplifiers chain.
• Alternative solution of power supplies with closed loop water cooling and chillers instead of cooled water are considered. In this case the necessary water flow rate will be drastically diminished.

Table 6: The requiremens for the multi-PW Amplifier Chain

Apparent power	130 KVA, 1 phase, 220 VAC, 50 Hz, 30x25 A plugs
Power consumption	100 KW
Cooled Water	100 liters / min, 12-17 C degree
Clean room class	At least 50 000
Relative humidity	30 – 50 %
Clean room dimensions	10 x 5 m^2

3.2.6 ELI-NP multi-PW laser system conceptual design

The schematic drawing of the ELI-NP multi-PW laser system is shown in the figure 4. The design of the facility is modular, reserving the space for further extension of the laser system and allowing the extension of the experimental area later in time, according to the needs. Pump laser types are specified only for proving the feasibility.

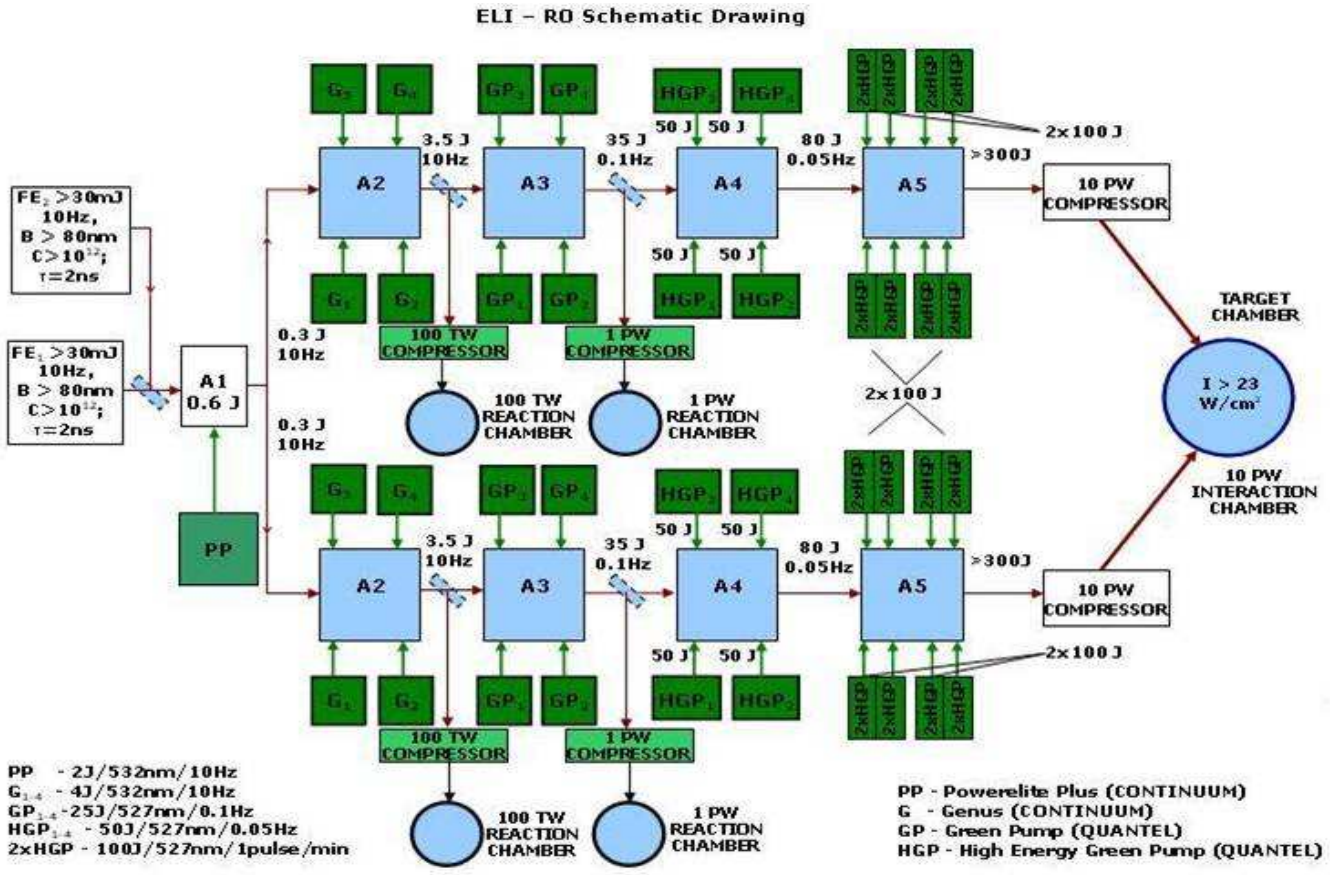

Figure 4: ELI-NP scheme. FE1, FE2 - Font-End based on OPCPA or Ti:sapphire amplification. A1-A5 - Ti:sapphire amplifiers.

The basic solution for ELI-NP laser facility consists in OPCPA technology at the Front End and Ti:Sapphire high-energy amplification stages. A Front End based exclusively on Ti:sapphire oscillator

and amplifiers, with XPW for high intensity contrast, is considered as an alternative option. The ELI-NP laser facility will have two Front Ends. They will temporally stretch and amplify initial ultrashort pulses with 800 nm central wavelength to the 30 mJ level, preserving the needed large bandwidth of the 15 fs laser pulses and the temporal contrast of the pulses in the range of 10^{-12}. Due to the complexity of such OPCPA system, the alignment and maintenance time for one Front End is long. To avoid such dead-times, one Front End is planned to operate at a time, the second one being used during the maintenance of the other Front End, significantly increasing the available beam-time of the laser facility.
The pulses of 2 ns at 10 Hz repetition rate generated by the Front End are amplified by A1 up to 600 mJ, splitted and distributed to further A2 laser amplifiers. A1 is pumped by a 2J green (532 nm) nanosecond Nd:YAG laser. After A2 laser pulses are amplified to 3.5 J at 10 Hz repetition rate. A2 is pumped by 4 X 4 J green lasers. The Ti:sappire rod of the A2 amplifier will be cryogenically cooled for 10 Hz operation. Using a flipper mirror these pulses can be sent to a temporal compressor and, after compression down to 25 fs, to a 100 TW reaction chamber. 35 J pulses at 0.1 Hz repetition rate are generated after amplifier A3, pumped by 4 x 25 J Nd:glass lasers. A secondary output is dedicated to experiments at 1 PW power level. At these energy levels, the laser pulses can be extracted from the laser amplification chain and recompressed to less than 25 fs pulse duration in a vacuum compressor. Subsequently, they are distributed to the 1 PW experiments room.
Alternatively, the laser pulses are further amplified in the amplification chain to energies of the order of 200 J in the last two power amplifiers A4 and A5 with a repetition rate of at least 1 pulse/min. A4, pumped by four high energy lasers (50 J/pulse at 35 ns pulse duration), raises the pulse energy up to 80 J with a repetition rate of 0.05 Hz. The last amplifier is pumped by 8 x 100 J green lasers coupled in 4 pairs of 200 J pump energy each. The output beam diameter of 180 mm is expanded to 400 mm before the 10-PW temporal compressor input. Adaptive optics and optical isolation of the pulses will be implemented before the optical compressor.
The ultrashort pulses will be distributed to the high energy experimental areas, where stand-alone experiments or combined nuclear physics experiments using the highly brilliant γ beam will be performed.
Coherent combination of the high power ultrashort pulses from the parallel amplification chains is envisaged, in order to reach intensities of the order of 10^{23} W cm^{-2} and above. The operation of the experiments will take place in parallel, the laser pulses being delivered to different experimental areas on request.
Besides the basic laser system architecture presented in the figure 4, a back-up solution for a single beamline 20-PW laser based on light energy amplification in mixed Nd-doped glasses is considered [9]. In this case, pulses generated by a Ti:Sappire or Nd:glass oscillator at 1 μm wavelength are stretched to 6-8 ns and amplified in a OPCPA pre-amplifier to a $\sim$1 J energy. Next, pulses would be amplified in Nd:glass amplifier stages. In the first stage, that consists in a double-pass 15 cm aperture disk amplifier, pulses would be amplified up to 200 J. Glass slabs at this stage would be a combination of mainly silicate and some phosphate Nd:glass flashlamp-pumped disks. Finally, pulses would be amplified in a chain of 31 cm aperture disks, constructed solely from phosphate glass, at 2,3-2,5 kJ. Compression would occur in a grating compressor constructed by tiling three multi-layer dielectric gratings. This would then yield recompressed pulse energy of 2-2,2 kJ in a pulse duration of 100-120 fs.

3.2.7 ELI-NP laser building sketch

The two arms of multi-PW ELI-NP laser system are placed in an area of approximate 42 x 34 m^2 (figures 5 and 6). A 50 x 50 m^2 area would be available for further extensions of the laser system and experimental rooms. The laser system is installed in a 10.000 class clean room, thermally stabilized within $\pm$ 0.5 K, and controlled humidity of 30-50%. The actual area of the laser clean room is about 820 m^2 with at least 3 m height.
Working conditions and radioprotection measures in each experimental room will be defined depending on proposed experiments. Big area experimental rooms allow a variable configuration of radioprotection walls.

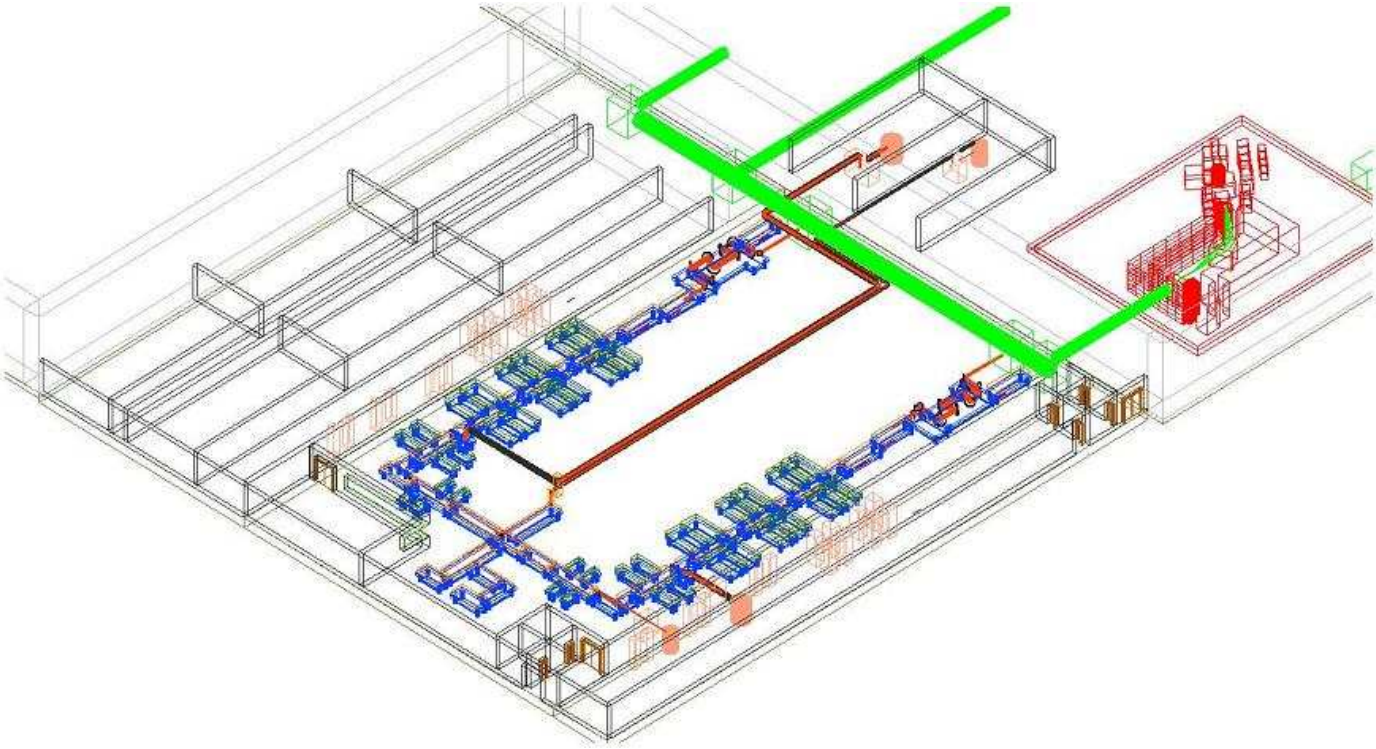

Figure 5: Possible layout of the ELI-NP facility

Ti:sapphire laser components and pump green laser heads are arranged inside the clean room on a network of rigid joint optical tables of 90 cm height from the floor, with at least 30 cm thickness of the tables. The level of optical axes of laser beams is about 150 mm up from the surface of optical tables in the Front End, A1, and A2 amplifiers and 250 mm in the A3-A5 amplifiers. Optical axes of input laser beams for 100 TW, 1 PW, and 10 PW vacuum compressors are raised up to 1.5 m from the floor by periscopes.
All power supplies are placed in two technical rooms of approximate 110 m^2 area and 3.5 m height each. In case of pump lasers with closed loop liquid cooling, all chillers will be installed out of the building. There are two experimental rooms for each laser arm, where femtosecond laser beams of 100 TW at 10 Hz and 1 PW at ≥ 0.1 Hz repetition rate are available for different laser-matter interactions. If we consider a laser system running at 10 Hz up to 100 TW power and at maximum 1 Hz up to 10 PW,the estimated electrical power consumption will be 2×200 kW = 400 kW for the whole laser system. The necessary of cooling water flow rate depends on the technical solution chosen by the producers for pump lasers and could be estimated as maximum 2×200 l/min = 400 l/min in case that all pump lasers will be cooled by running water (no closed loop chillers).

3.3 Pulse Compression

The compressor is a complementary device to the optical stretcher and compensates for the temporal stretching of the pulse. The main parameter for the temporal analysis is the group delay dispersion (GDD). In the case of the stretcher-compressor for the Apollon-type system, GDD is of 14.3 ps/nm [23]. The Offner type stretcher is presented in fig. 7. However, if the pulse bandwidth is less than the specified one, not only the pulse duration after compression is longer than the specified 15 fs but also the diffractive gratings in the compressor can be damaged for the same specified pulse energy. To compensate such an effect, the length of the compressor has to be increased, the beam pulse might be expanded or, alternatively, the output energy of the amplifiers has to be reduced.
The optical compressors are planned for each of the amplification arms as follows:
- at the end of the Front End a test compressor is needed for each Front End;
- at the output of the 10 Hz amplifier (100 TW class);
- at the output of the 0.1-1 Hz amplifier (1 PW class);

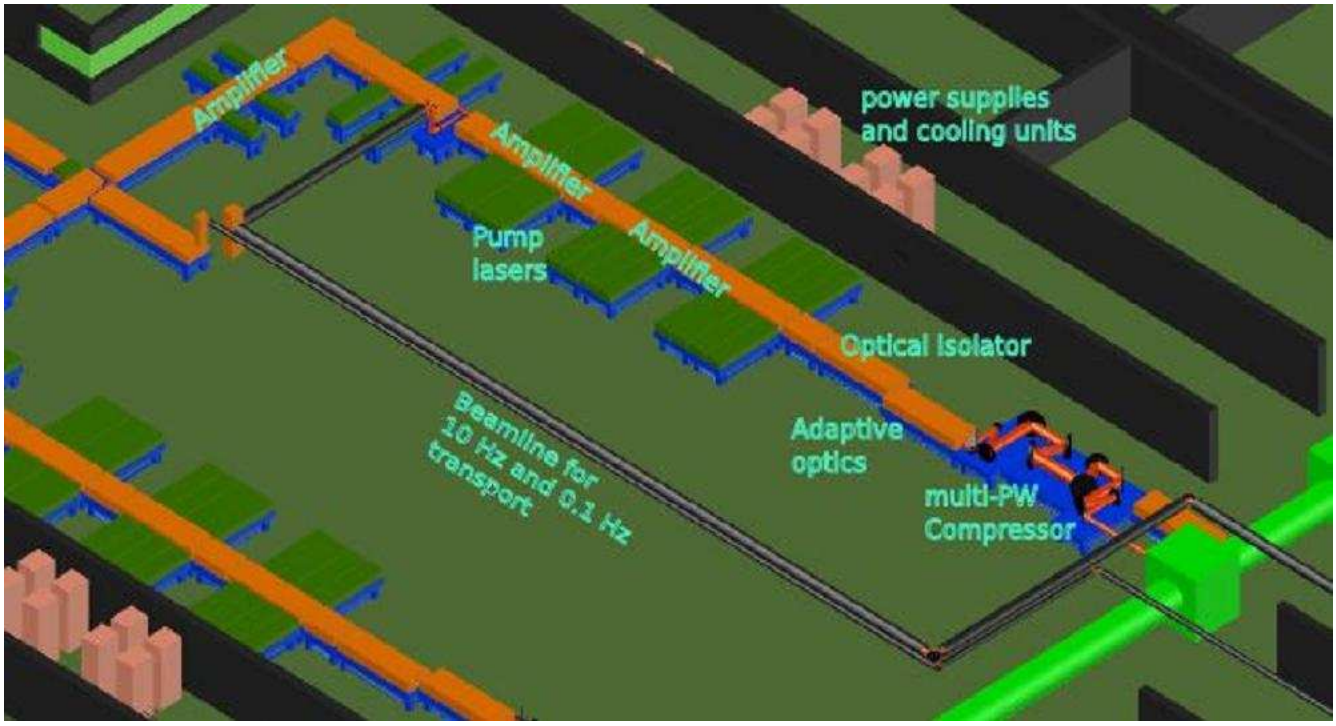

Figure 6: Detail of figure 5: Amplification arm layout with compresor position and beams to experimental areas

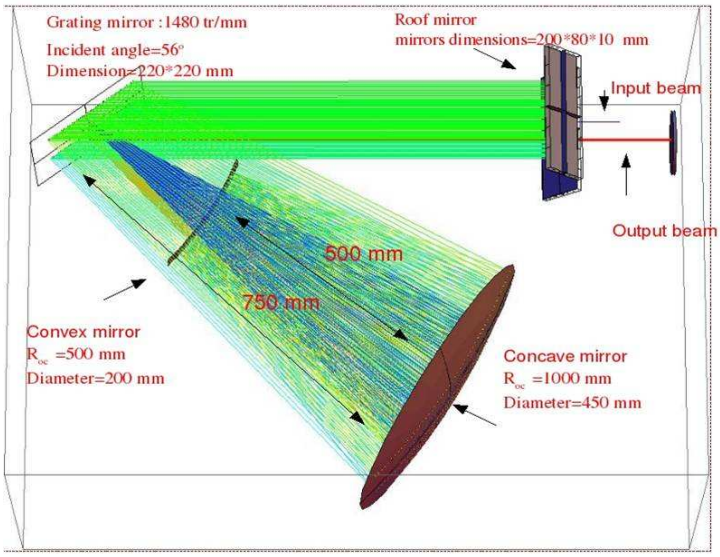

Figure 7: Possible Offner-type stretcher design for the Front End

- at the end of the amplification arm (multi-PW).

Up to the 1 PW class, there are solutions available on the market. To design a multi-PW class compressor is one of the challenges of ELI-NP project. A possible approach was presented in [23], implementing mosaic diffraction gratings. Ray-tracing of the system, presented in Fig. 8, shows that the dispersion of such compressor provides 14 ps/nm. We evaluated the temporal contrast induced by the hard clipping; this reaches 10^{-14} at 5 ps, in the range needed by the experiments.
For the multi-PW compressors, one needs 6 diffractive gratings, the vacuum chamber and the corresponding pumps (see section on beam transport), the mechanical mounts and diagnostics (see diagnostics). The price of the vacuum chamber for the compressor depends on the specific spectral composition of the pulse, as explained in the introduction of this subsection, and can be up to a factor

of two larger than the one estimated in the Apollon project.

3.4 Alignment and Diagnostics

For the laser diagnotics and alignment, we have envisaged a list of necessary equipments for the different laser parts:
1) after the fs oscillator: beam splitter, energy meter, CCD camera, quadrant photodiode detector and motorized iris diaphragm;
2) after the booster and strecher: beam splitter, energy meter, CCD camera, quadrant photodiode detector, fast photodiode, oscilloscope;
3) before the regenerative amplifier: beam splitter, energy meter, CCD camera, fast photodiode, oscilloscope;
4) before the multi-pass amplifier: beam splitter, energy meter, CCD camera, fast photodiode, quadrant photodiode detector;
5) at the Front End output: beam splitter, energy meter, CCD camera, fast photodiode, quadrant photodiode detector, compressor stage for test;
6) after the A1 and A2 amplifiers beam splitter, energy meter, CCD camera, fast photodiode, quadrant photodiode detector, motorized iris diaphragm, beam cleaning equipment;
7) after A3, A4 and A5 power amplifiers: beam splitter, energy meter, CCD camera, fast photodiode, quadrant photodiode detector, motorized iris diaphragm, beam cleaning equipment;
8) after the compressor: beam splitter, energy meter, CCD camera, SPIDER, autocorrelator 3^{rd} order.

3.5 Pulse shaping

There are several methods to shape the pulse: namely spatial, temporal, spectral and phase shaping. For the spatial shaping, adaptive mirror is planned after the A2 amplifier and possibly after the final amplifier.
Temporal and spectral shaping are complementary approaches in the sense that the pulse duration and spectral composition of the pulse are in a Fourier transform relation. Most of the shaping techniques refer to the spectral and phase shaping. The most appropriate technology will be used considering acusto-optic modulators for phase and amplitude, liquid crystals for 4f shaper or, in the case of OPCPA technique, spectral modulation by pump laser intensity modulation.

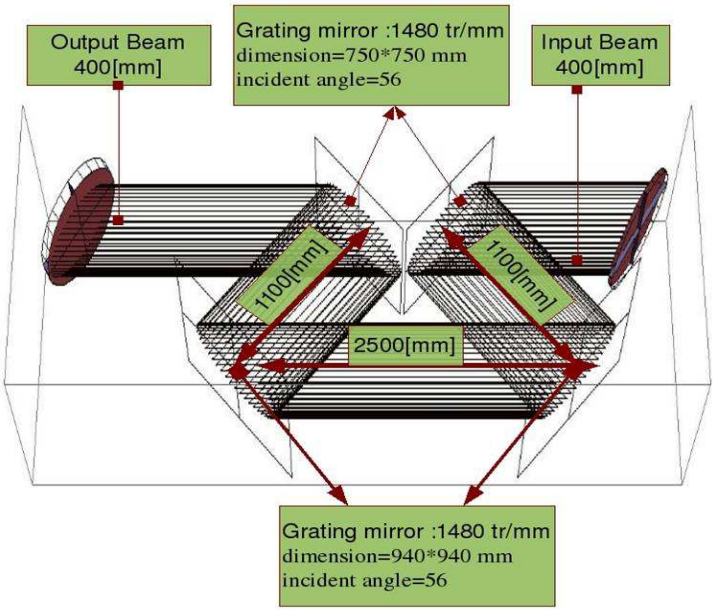

Figure 8: Possible configuration for the compressor

3.6 Control, supervision system (C2S)

The monitoring and control systems study comprehends the necessities and the particularities involved by the complexity and dimensions of ELI-NP project, and the actual technological capabilities (including commercial equipment software and service).
Regarding the ELI-NP project requirements, we identify three major types of control and monitoring systems, as presented in fig. 9:

1. Basis control system;
2. Automation;
3. System and ambient monitoring and data logging;

1. Basis control system
- include all control systems which assure laser synchronization devices, interlocks, optical path control, beam combination and shaping, control and command of auxiliary devices (pumping laser, vacuum pumps, valves, etc). Without one of the systems mentioned before, the system is not able to work. Generally the systems which control directly the laser systems, they are so called "Real-time" and "high-speed" systems. Later we will give a generic definition for the upper mentioned systems.

2. Automation
- include systems which assure automatic beam control, stage isolation, active mirrors etc. These systems looks like auxiliary devices, but these devices make the entire laser system to be more reliable robust and improve the long term stability. Another characteristic for this kind of systems is that they have to work in manual or automatic mode, or can be (remotely) started and stopped. Because here we are speaking about systems which means closed loops, in fact we are speaking, again about "Real-time" and "high-speed" systems.

3. System and ambient monitoring and data logging
- the purpose of these systems monitor and record a large types of system and environmental data, in order to have historical behavior and trends of the system. The monitoring and data logging system should be based on Supervisory Control And Data Acquisition (SCADA) concept, with hierarchical structure due the complexity and physical dimensions of the entire facility (many rooms filled with high complexity machines, usually involving local supervision, supervision by types of tasks and general supervision).

All control systems described before should be developed keeping in mind the human and device safety. The systems shall be implemented at different functional levels, well defined, with certain crossing connections between them as is shown in next diagram:
Real-time systems means systems when the result of a stimulus or an input data is offered at output of the system in an very well determined amount of time. When we deal with problems which involve event response within a specific deadline, or with closed loops controls, the only way to solve the problem is to use a "real-time" system.
High-speed systems means exactly the name suggest. There is no clear border between high-speed and low-speed. Any way, in laser systems we currently find requirements of delays up to few nanoseconds.
Example of real-time and high-speed systems, commercially available: real-time hardware and software from National Instruments, FPGA devices with embedded firmware, from ALTERA, LATTICE, XILINX, etc. This complex project will contain commercially available laser systems combined with systems in situ developed. Control system team should develop in situ laser control systems, among to integrate the commercially systems (acquired during the entire project development) into a general shell.

The next table describes the first version of Control-Command (C2) & Supervision system (C2S) for ELI laser system.

3.7 Coherent beam combining

Coherent beam combining (CBC) of multiple ultra-short laser beams represents an effective solution to obtain a high power laser for both continuous wave and pulsed systems. CBC method has been

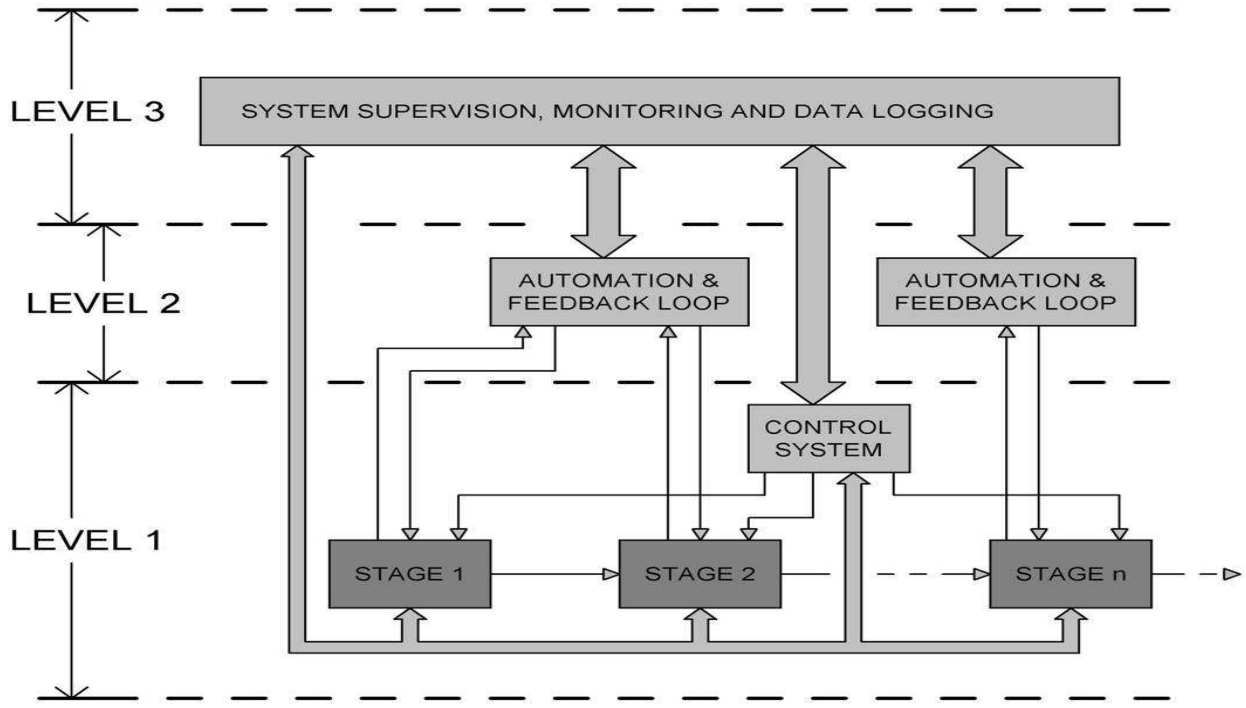

Figure 9: ELI control system organized on functional level

Table 7: Control-command (C2) & supervision system (C2S)

Functions	**Equipments to control and command**	**Environmental specs**	**Safety & Remarks**
C2S: -provides laser safety and security for the PSS (Personnel Safety System) -governs the operating and sequential modes of the machine -integrates a general view of the machine (supervision, system states, troubles, alarms) -manages the configuration of the machine equipments -manages the generated results and data	-security elements: door contacts, interlocks, shutters, obstructers, valves -HV supplies -lasers -oscilloscopes -multi-ways digital measuring apparatus -delay generators -energy-meters -spectrometers - CCD cameras -motors (mirror mounts, spatial filter sets, diffraction gratings, translation and rotation stages, filter gratings, plate holders, target holders, holders for frequency conversion crystals) -valves, pumps, gauges -ambient sensors (temperature, humidity, dust)	• indoor use • T = (0-55) ^{0}C, • h = (10-90)%, non-condensing • EMC: -emissions = EN 55011 Class A at 10 m -immunity = EN 61326:1997 + A2:2001 • V_{in} = 230 V • f_{in} = 50 Hz • I_{in} = 8 A	• laser • HV • X-rays -C2S requirements are generated by the experimenters or experimental results and are destined for the other big installations
C2: -operates the distribution of the laser beams from the pilot to the target -configures and operates the pumping lasers -adjusts the synchronization systems -operates the alignment and laser diagnosis systems -operates the vacuum systems			-C2 requirements are generated by the laser module developers / users

demonstrated with diode, solid-state, fiber, and gas lasers, but current efforts focus on fiber lasers and diode in continuous regime. Up to now, little work is related to pulsed lasers in the ns range and below. However, in order to scale the intensities of ultra-short pulse lasers in the femtosecond domain such CBC technique is needed.

Coherent beam combining technique requires that the sources are coherent and relative phases of combined beams are precisely controlled to a small fraction of the wavelength. The main difficulty is to obtain phase coherence at high power levels in a sufficiently stable manner, working not only in a quiet laboratory environment but also in a mechanically more noisy industrial setting. Another challenge is the need to match precisely and stably wavefronts and polarization directions.
One way to coherently combine the ultrashort pulses is to take several identical ultrashort pulses and overlap them directly on the target. Up to now no experimental report exists concerning this approach. However, if this works, there might be an alternative better solution that would allow to obtain significantly increased power on the target, by using laser pulses with complementing spectral composition.
One important issue in CBC relates to the mechanical stability of the entire laser amplification chain and to the possibility to measure and control the specific displacements. This might increase the cost of the mechanical components along the amplification path a factor of 2 or 3. Related interferometric methods for optical path stabilization are currently developed in INFLPR, within LASERLAB2 European project.

3.8 Laser Beam Transport System

In order to produce petawatt laser beams, a large section of the the ELI facility will be under vacuum. A system which will comprise a large chamber (compressor) hosting optical components and a long pipe for beam transport will be pumped down by a number of forevacuum and turbomolecular pumps. Alternatively, diffusion or cryopumps could be used for rapid air evacuation inside the largest volumes, down to 10^{-6} torr.
Realization of energy amplification will be possible by using an array of gratings for beam compression which will be achieved in the compressor chamber. The chamber will have a volume of 15 m^3 (5 m $\times$ 1.5 m $\times$ 2 m) if the pulse contains enough bandwidth. The thickness of the chamber walls depend on the materials used, whether it will be aluminum or stainless steel. In principle, aluminum will be the preferred material for weight and radioprotection considerations. Different solutions are currently analyzed for the design of the chamber. The chamber will be provided with several large windows and ports which will allow the access to the optical components hosted inside. Two large gratings with dimensions up to 90 cm, installed on precision mounts, will be the main parts of the compressor.
There will be 2 main vacuum systems which will deliver the 2 beams to the main target chambers and with the possibility to divert 2 beams to two separate smaller target chambers. Each system will have a multi-PW compressor and a long pipe. While the exact aperture of the beam has not been calculated, from the experience of other petawatt facilities it is expected that the diameter of the pipes used to transport the high-power beam (up to 10 Petawatt) will be 1 m. The thickness of the pipe wall, if Al is considered, will be about 15 mm. Sections with a length of 1.5 m will be bolted together creating the long pipe.

3.9 Further infrastructure

Supporting labs and mechanical workshops have to be organized at the ELI facility. These will be fully equipped for satisfying the demands for operation and maintenance of the equipments, preparation and running of the experiments.
1. **Optical workshops** are required for inspection, cleaning or treatment of various optical components such as gratings, mirrors, laser crystals, etc. The workshop has to be divided in three separate working areas providing specific working conditions for inspection of the optical components, respectively for their treatment or cleaning.
2. **Target microfabrication workshop**. Here the targets for experiments are produced. The designed targets could have different sizes and forms on different materials. Micromachining tools and sample preparation tools are used.
3. **Chemical workshop** is used for sample preparation. It has to be a different room to the Target microfabrication room, providing the necessary conditions for safely working in a chemical area. The

chemical workshop has to be placed close to the Target microfabrication room.
4. **Electrical workshop** is need for maintenance or testing of various electronic equipments, small equipments or electronic subsystems of the laser power supply, detectors, and control and acquisition systems. Here will also be assembled the electronic parts of the automations systems for the running experiments.
5. **Mechanical workshop**, equipped with necessary machining tools for processing mechanical parts used in experiments.

References

[1] D. Strickland and G. Mourou, Opt. Commun. 56, 219 (1985).

[2] M. D. Perry and G. Mourou, Science 264, 917 (1994).

[3] D. M. Pennington, M. D. Perry, B. C. Stuart, et al., in *Proceedings of the Solid State Lasers for Application to Inertial Confinement Fusion: Second Annual International Conference, London, 1997*, Proc. SPIE **3047**, 490–500 (1997).

[4] M. D. Perry et al., Opt. Lett. **24**, 160 (1999).

[5] Y. Kitagawa, H. Fujita, R. Kodama, et al., IEEE J. Quantum Electron. **40**, 281 (2004).

[6] C. N. Danson, P. A. Brummitt, R. J. Clarke, et al., Nucl. Fusion **44**, S239 (2004).

[7] M. Aoyama, K. Yamakawa, Y. Akahane, et al., Opt. Lett. **28**, 1594 (2003).

[8] V. V. Lozhkarev, G. I. Freidman, V. N. Ginzburg, et al., Laser Phys. Lett. **4**, 421 (2007).

[9] E. W. Gaul et al., Appl. Opt. 49, 1676-1681 (2010).

[10] I. N. Ross, P. Matousek, G. H. C. New, and K. Osvay, J. Opt. Soc. Am. B **19**, 2945 (2002).

[11] R. Li, Y. Leng, and Z. Xu, in *Proceedings of the Conference on Lasers and Electro-Optics, 2005*, p. CMB1.

[12] J. Hein, S. Podleska, M. Siebold, et al., Appl. Phys. B **79**, 419 (2004).

[13] C. P. J. Barty, M. Key, J. A. Britten, et al., in *Proceedings of the Conference on Lasers and Electro-Optics, OSA Trends in Optics and Photonics, San Francisco, CA, 2004* (Optical Society of America, Washington, 2004), p. JTuG4.

[14] L. J. Waxer, D. N. Maywar, J. H. Kelly, et al., Opt. Photonics News **16**, 30 (2005).

[15] E. W. Gaul, T. Ditmire, M. D. Martinez, et al., in *Proceedings of the Conference on Lasers and Electro- Optics, Baltimore,* 2005, p. JFB2.

[16] N. Blanchot, E. Bignon, H. Coic, et al., in *Proceedings of the Topical Problems of Nonlinear Wave Physics, 2005*, Proc. SPIE **5975**, 0C1-0C16 (2005).

[17] J. L. Collier, O. Chekhlov, R. J. Clarke, et al., in *Proceedings of the Conference on Lasers and Electro Optics, Baltimore, 2005*, p. JFB1.

[18] V. V. Lozhkarev, S. G. Garanin, R. R. Gerke, et al., JETP Lett. **82**, 178 (2005).

[19] V. Yanovsky et al., Opt. Express, 16, 2109-2114 (2008).

[20] S. K. Lee et al., *0.1-Hz 1-PW Ti:Sapphire Laser facility***,** LEI Conference, Brasov, Romania, October 16-21, 2009.

[21] Z. Wang et al., *Enhance XL III facility to Petawatt power with improved front-stage amplifier and optimized output energy*, LEI Conference, Brasov, Romania, October 16-21, 2009

[22] J. P. Chambaret, *The Extreme Light Infrastructure Project ELI and its prototype APOLLON/ ILE. "The associated laser bottlenecks"*, LEI Conference, Brasov, Romania, October 16-21, 2009.

[23] Projet CPER 2007-2013 APOLLON ILE 10-PW, 2009.

[24] A. Jullien et al., Opt. Express, vol. 14, pp. 2760–2769 (2006); A. Jullien et al., Appl. Phys. B, vol. 84, pp. 409–414 (2006); L. Canova et al., Appl. Phys. Lett., vol. 92, pp. 231102_1-3 (2008).

[25] I. N. Ross, J. L. Collier, P. Matousek, C. N. Danson, D. Neely, R. M.Allott, D. A. Pepler, C. Hernandez-Gomez, and K. Osvay, Appl. Opt.**39**, 2422-3427 (2000).

[26] Y. X. Leng, X. D. Yang, H. H. Lu, L. H. Lin, Z. Q. Zhang, R. X. Li, ,D. J. Yin, and Z. Z. Xu, Opt. Eng. **43**, 2994–2997(2004).

[27] Y. Leng, L. Lin, X. Yang, H. Lu, Z. Zhang, and Z. Xu, Opt. Eng. **42**, 862-866 (2003).

[28] K. Ertel, C. Hooker, S. J. Hawkes, B. T. Parry and J.L. Collier, Opt. Express **16**, 8039 (2008).

[29] J.H. Sung, S. K. Lee, T. J. Yu, T. M. Jeong and J. Lee, Opt. Lett. **18**, 3021 (2010).

Glossary

CBC – Coherent Beam Combination;
CCD – charge-coupled device;
CPA – Chirped Pulse Amplification;
ELI – NP - Extreme Light Infrastructures – Nuclear Physics;
FE – Front End;
FPGA – Field Programable Gate Array;
GDD – Group Delay Dispersion;
MP – multi-pass amplifiers;
NOPCPA – Non-collinear Optical Parametric Chirped Pulse Amplification;
OPCPA – Optical Parametric Chirped Pulse Amplification;
SHG – Second Harmonic Generation;
SPIDER – Spetral Interferometer for Direct Electric Field Reconstruction;
Ti:Sa – Sapphire doped with Titanium;
XPW – Cross Polarized Waves;

Infrastructure Producing High Intensity Gamma Rays for ELI Nuclear Physics Bucharest-Magurele, Romania

The ELI-Gamma Source working group

Editors:
Dietrich Habs, Ludwig-Maximilians-Universität München
Marian Toma, National Institute for Laser, Plasma and Radiation Physics
Dan Cutoiu, National Institute for Physics and Nuclear Engineering "Horia Hulubei"

Authors
G. Wormser[1], R. Hajima[2], C. Barty[3]

Affiliations
[1] Linear Accelerator Laboratory, Orsay, France
[2] ERL Development Group, Japan Atomic Energy Agency
[3] Lawrence-Livermore National Laboratory, USA

4 Infrastructure Producing High Intensity Gamma Rays for ELI Nuclear Physics Pillar

4.1 Introduction

This report contains a description of the proposed infrastructure producing high intensity gamma rays, an important component of the Extreme Light Infrastructure - Nuclear Physics facility (ELI-NP). For simplicity reasons, we will call the infrastructure producing high intensity gamma rays ¨the γ source¨. There are four main criteria for the comparison of high intensity γ ray sources, namely: the **energy of the γ beam**, the **total photon flux**, the **peak brilliance** and the **bandwidth**.
The **energy of the γ rays** range from a few keV to 100 MeV, although most radiation is in the range $50\,\mathrm{keV} - 6\,\mathrm{MeV}$.
The **total photon flux** is measured in *photons/sec at 100%BW*.

The driving force behind the development of light sources is the optimization of their brilliance (or spectral brightness), which is the figure of merit of many experiments. Brilliance is defined as a function of frequency given by the number of photons emitted by the source in unit time in a unit solid angle, per unit surface of the source, and in a unit bandwidth of frequencies around the given one. The units in which it is usually expressed are *photons/s/mm^2/mrad^2/0.1%BW*, where 0.l%BW denotes a bandwidth $10^{-3}\omega$ centered around the frequency ω. As one can appreciate from the definition, brilliance puts a premium not only on the photon flux (photons per second in a given bandwidth), but also on the high phase space density of the photons, i.e. on being radiated out of a small area and with high directional collimation. Liouville's theorem ensures that brilliance is a property of the source and not of the optics of the beamline which delivers the photons to the experimental station. An ideal set of optical elements can only preserve the brilliance, a real one will always degrade brilliance (as some photons get lost on the way down the beamline). The **peak brilliance** is defined as the instantaneous peak value obtained at peaks of light pulses.
The γ beam bandwidth is the width of the range (or band) of frequencies in which the beam energy spectrum is concentrated.
The γ source will produce a very intense and brilliant γ beam ($\mathrm{E}_\gamma = 1 - 13\,\mathrm{MeV}$ for the beginning and $\mathrm{E}_\gamma \leq 19.5\,\mathrm{MeV}$ latter), which is obtained by incoherent Compton back scattering of direct laser light with a very brilliant and intense electron beam ($\mathrm{E}_e \leq 0.6\,\mathrm{GeV}$). The experiments envisaged with the γ source suggests the parameters of the γ beam: bandwidth equal or lower than 10^{-3}, energy up to 19 MeV to access all GDR, total flux higher than 10^{13} photons/sec at 100%BW, peak brilliance higher than 10^{21} photons/mm^2/mrad^2/s/(0.1% BW). The high flux, narrow gamma-ray bandwidth and superb brilliance requires an excellent normalized emittance for the electron beam, in the range of 0.5 mm mrad. In addition, it is envisioned that the gamma source will be used in conjunction with the low repetition rate ELI-NP 10 PW laser beams for many experiments.
As for the implementation of ELI-NP γ source the following two principles were accepted as guideline:

1) a staged realization of the γ source

2) a flexible design of the γ source.

The first principle permits a sequential buildup of the facility according to the available resources. The first stage may target only the most basic physics topics and the basic facility components that need to be started immediately and may cover the period from 2011 - 2015. The second stage might start from 2016 for five years, including more ambitious programs. Subsequently the third stage might start from 2021 for maybe ten years. This stage might include the most ambitious and far reaching project.
The second principle requires that the first stage facility has to be flexible designed in such a way as to accommodate its future growth.
During the ELI-NP Executive Committee Meeting (April 12-13, 2010) three possible options for the γ source were presented: a storage ring, an energy recovery linac and a warm linac.
The storage ring is based on the ThomX project [1]. The ThomX machine is conceived to provide the maximum average flux in a fixed bandwidth. Consequently, the basic scheme takes into account a very

important collision repetition frequency and therefore the possibility to have Compton interaction in a storage ring. Electron bunches are injected and stored in the ring and discarded in a beam dump after 20 ms. To increase the pulse power of the light pulse the high average power laser is injected into a passive optical resonator (Fabry Perot cavity). Here the laser pulse is stacked on the pulse circulating in the cavity up to its limit given by the cavity finesse. The two systems are synchronized in a way that every turn the electron beam interacts with a laser pulse.
The main difficulty of the ThomX machine comes from the fact that 50 MeV storage rings are not very stable since the electrons are not sufficiently relativistic and that in addition the electron is strongly affected by the dispersion introduced in the bunches by the laser and the Compton scattering. For applications in Nuclear Physics of interest to the ELI project, the photon energy range lies in the 1-16 MeV range. This will require electron energies between 250 MeV up to 1 GeV, since in Compton scattering, the photon energy rises quadratically with the electron energy. Preliminary simulations show a much stable ring dynamics therefore, besides the small inconvenient to have to build a somewhat larger ring (ThomX 50 MeV ring diameter is only 3 m, ELI machine's one should be around 35 m), the expected photon yield should be larger for the MeV photon source. Unfortunately the majority of the nuclear physics experiments proposed for ELI requires a better than 10^{-3} FWHM which can not be obtained by this storage ring proposal. More, a ring configuration cannot be upgraded after 2015 (due to the fix diameter of the ring).
The energy recovery linac [2] has excellent performance, in some respect better than the warm linac (e.g. the negligible parasite electron dump), but is in an earlier R&D stage which posses serious concerns regarding the 2015 ELI deadline. The estimated price is also the highest due to cryogenics technology. But upgrade to ERL after 2015 is possible using the warm linac configuration.
The warm linac is based on the MEGa-ray project [3]. It fulfils the requirements for the γ beam and has a well established technology.
In order to guarantee a reliable and timely available technological solution for the startup phase of ELI-NP, a ¨warm¨ linac was selected. This choice ensures that ELI-NP will be the world-leading gamma beam facility at the time of its start of operation. In the second stage, this facility could be upgraded with a 100 mA ERL.

4.2 First stage warm linac in X-band RF plus 532nm laser

4.2.1 Description

The warm linac gamma source is based on technology developed for the MEGa-ray project [3]. This technology fulfils the requirements for the γ beam and is a well-established technology. This approach is based on the interaction of short pulse lasers with relativistic electrons, i.e. Compton scattering, to create ultra-bright Mono-Energetic Gamma-ray (MEGa-ray) beams. The scattered radiation is Doppler upshifted by more than 1,000,000 times and is forwardly-directed in a narrow, polarized, tunable, laser-like beam. The peak brilliance of an optimized MEGa-ray source is both revolutionary and transformative as in Fig. 10.

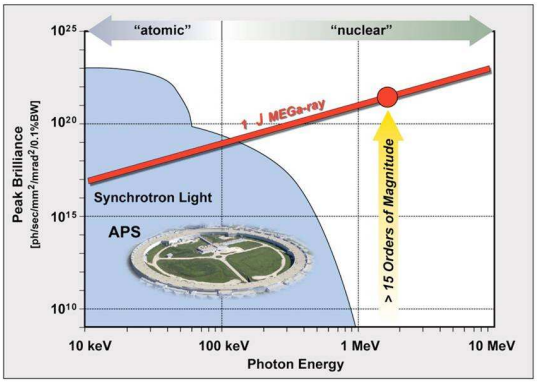

Figure 10: Peak brilliance for MEGa-ray

MEGa-ray is a third generation Compton machine following PEIADES [4] and T-REX [5] and has been optimized for peak brilliance and narrow bandwidth. The Thomson-Radiated Extreme X-ray Source (T-REX) project was the precursor project to MEGa-ray and produced monochromatic, highly collimated, tunable X-rays and gamma rays as a feasibility demonstration (see Fig. 11). With T-REX output researchers demonstrated an ability to use nuclear resonance flourescence to detect low density material (^{7}Li) shielded behind higher density materials (Al and Pb).

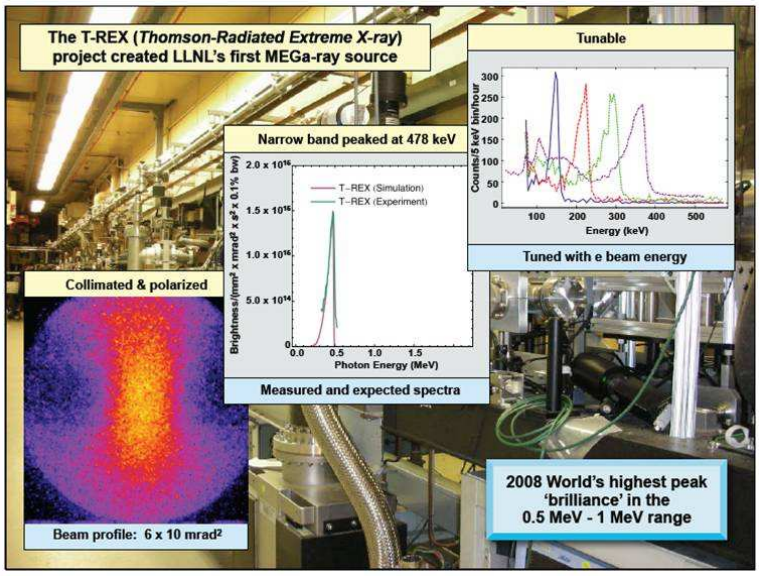

Figure 11: Feasibility of LLNL Thomson-Radiated Extreme X-ray

The T-REX project used the S-band accelerator technology (∼4 GHz and 10 MeV/m) for the accelerating structure. This technology could be easily scaled to higher energy (GeV scale) and work at higher flux and narrower bandwidth but is not compact and is relatively costly. One compact alternative is laser wakefield ¨acceleration¨ which can produce acceleration gradients of 10,000 MeV/m and can thus be extremely small. This technology however has relatively large energy spread and would produce gamma beams with >50% BW. Furthermore the lasers required for high flux wakefield acceleration would be very large, complicated and beyond the state of the art.
The best alternative is the high gradient X-band (∼12 GHz) technology developed at the SLAC National Accelerator Lab which provides a path to future compact MEGa-ray machines with up to 180 MeV/m acceleration gradients. The accelerating section presented in Fig. 12 is capable of 120 MeV on aprox. 1 m length! The X-band accelerator technology was developped for the International Linear Colider competition and recently has been adopted for use by CLIC, the planned next generation high energy physics machine after LHC.
LLNL's planned Center for Gamma-ray Applied Science (CGrAS) will house the world's first '3rd Generation' MEGa-ray capability based on X-band accelerator and diode pumped laser technologies. CGrAS aims to develop compact and rapid, isotope-specific material detection, assay and imaging technologies and will house a gamma source with a brightness higher than 1.5×10^{21} for 2 MeV photons energy at 0.1% BW.
The goals of MEGa-ray (Mono-Energetic Gamma ray) source at CGrAS are four fold:

a) to increase gamma-ray source precision (2 orders of magnitude better banwidth than T-REX)

b) to increase peak brilliance (6 orders of magnitude relative to T-REX)

c) to increase gamma beam flux (5 orders of magnitude relative to T-REX)

d) to reduce gamma-ray source size.

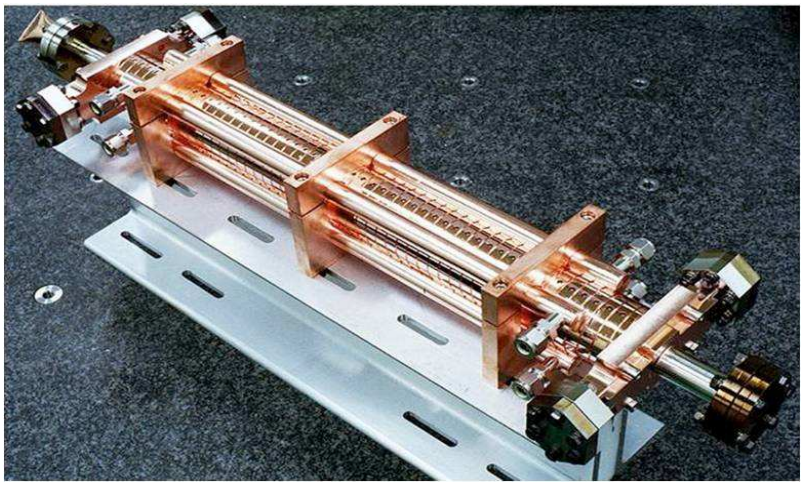

Figure 12: T53 accelerating structure

The project is under development and implementation phase for the construction of a precision 250 MeV X-band Linac for a MeV-class Compton scattering light source and is scheduled to be fully operational and ready for users at the end of 2013.
The linac is powered by a 400 MW, 11.424 GHz RF source and the requirements on rf phase and amplitude stability are very stringent as: 1^o rf phase (243 fs), and 0.1% stability. The design includes ScandiNova solid-state modulators and SLAC XL-4 klystrons with SLED-II delay lines. The RF distribution is presented in Fig. 13.

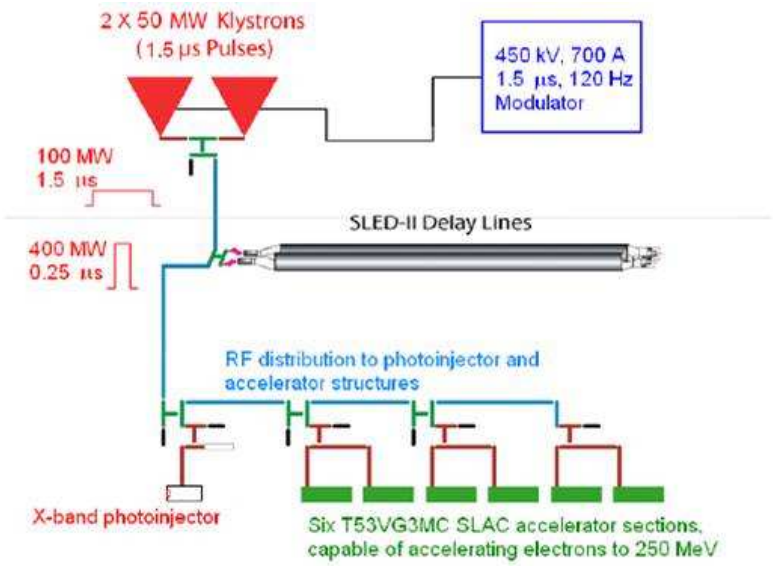

Figure 13: X-Band RF Power Distribution

A very important subsystem is the 5.59 cell X-band RF gun (Fig. 14) which is a modified version of SLAC's (Arnold Vliek) original 5.49 cell X-band gun with the following optimized parameters:

- Cathode electric field: 200 MV/m
- Bunch duration: 10^o, 2.5 ps
- Injection phase: optimized for each geometry; 20^o for 5.59-cells
- Nominal charge: 250 pC

- Emittance: as low as 0.18 mm×mrad obtained for the DC photocathode using high acceleration voltage of 500 kV and 250 pC electron bunches
- Emittance compensation magnet: anti-Helmholtz pair, 7 kG (Fig. 15)

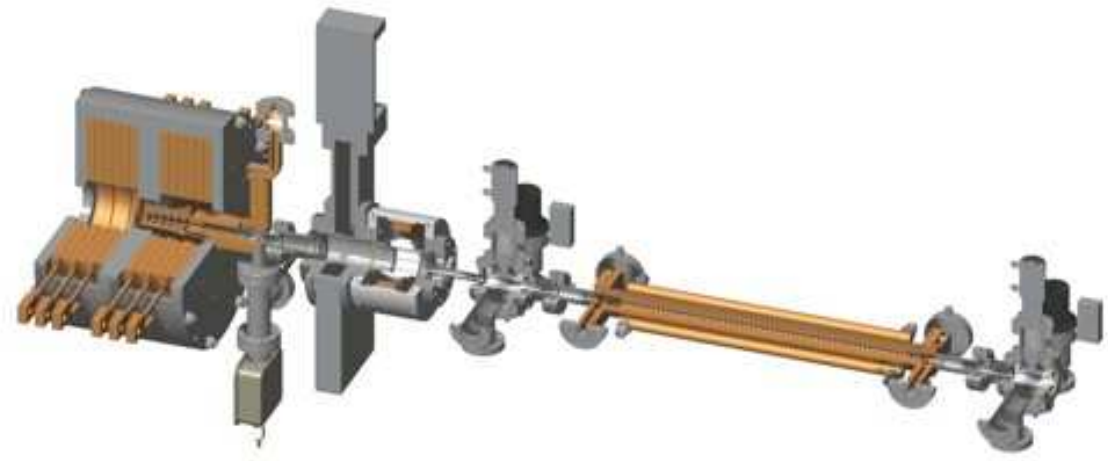

Figure 14: The RF gun and the first accelerator stage

Figure 15: Solenoid Magnet (Anti-Helmholtz)

The linac main architecture is presented in Fig 16 and the timing of the laser and electron beam subsystems are given in Fig. 17.

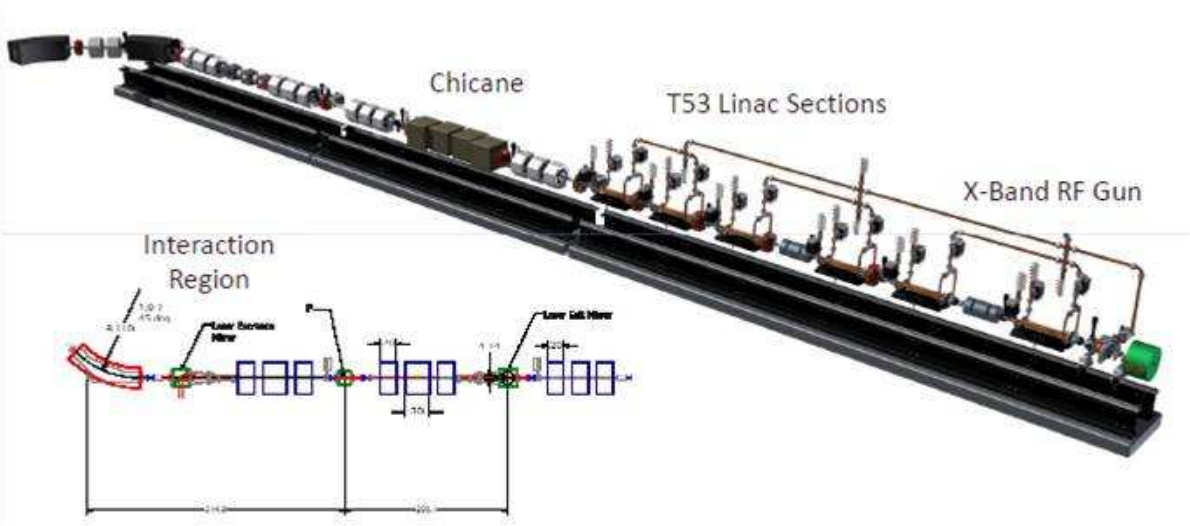

Figure 16: Architecture of 250 MeV X-Band Linac

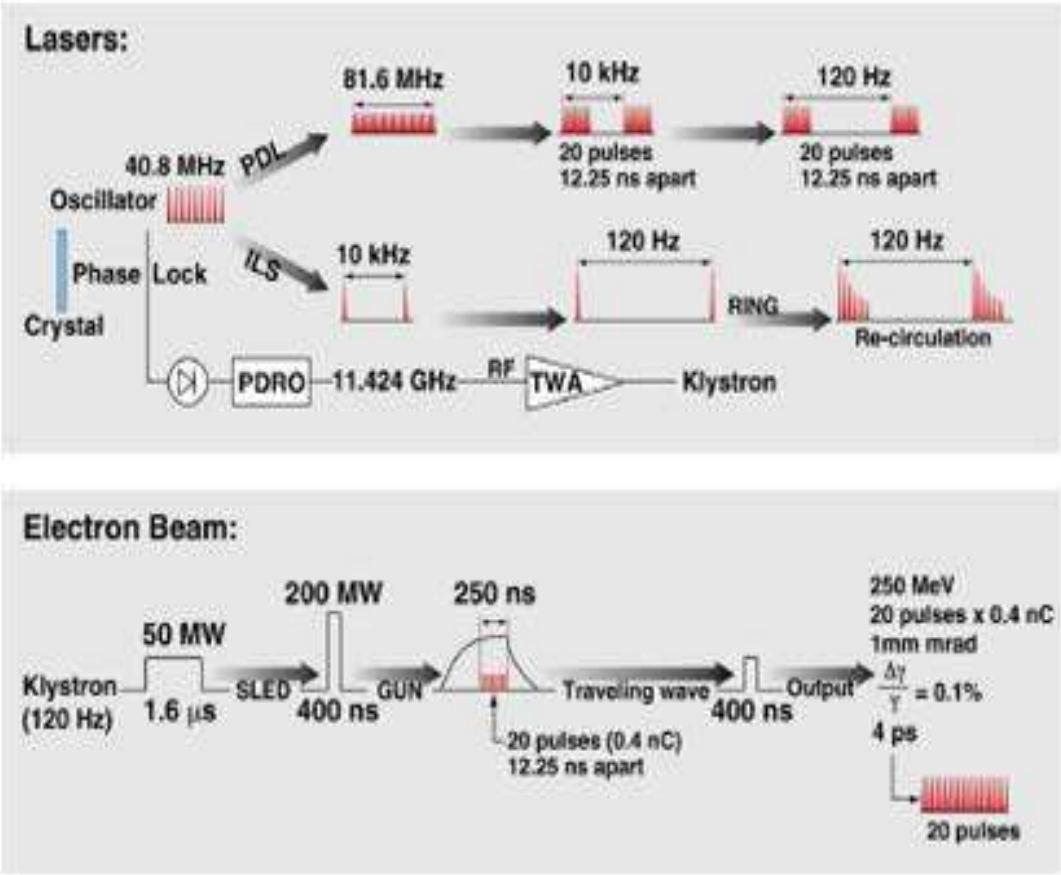

Figure 17: Sub-Picosecond Timing

Table 8: Technical parameters for the MEGa-ray facility currently being constructed at LLNL.

Quantity	**Value**	**Units**
Peak gamma brilliance	1.5×10^{20}	Photons/sec/mm^2/mrad^2/(0.1% BW)
Effective Beam repetition	12,000	Hz (100 micro-bunches at 120 Hz rep rate)
Gammas per pulse	8×10^{7}	Photons at 100% BW
Spectral beam flux	10^{6}	Photons/sec/eV
Gamma pulse duration	2	Picoseconds
Gamma collimation	0.1	mrad at 0.1% BW
Gamma bandwidth	10^{-3}	ΔE/E
Gamma source size	10	microns
Electron beam energy	250	MeV
Laser pulse energy	0.15	Joules
Gamma-ray energy	0.5−2.3	MeV

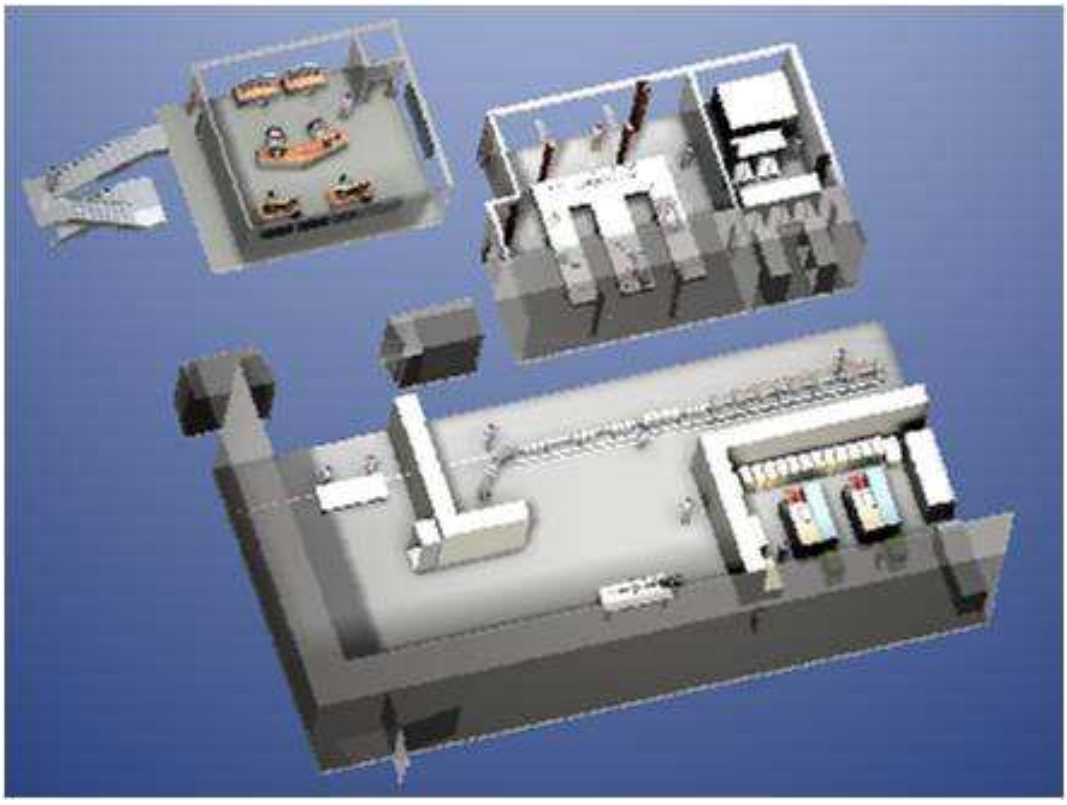

Figure 18: MEGa-ray Facility

A brief system overview is presented in Table 8 and the facility layout is described in Fig. 18. The interaction laser can run reliable at the high repetition rate of 120 Hz using diode pumping. By using a ring-down cavity for the laser pulse, within the macropulse of 120 Hz repetition rate, 100 micropulses can be realized, increasing the overall repetition rate to 12 kHz.
The predicted spectrum for the LLNL next MEGa-ray machine is shown in Fig. 19.

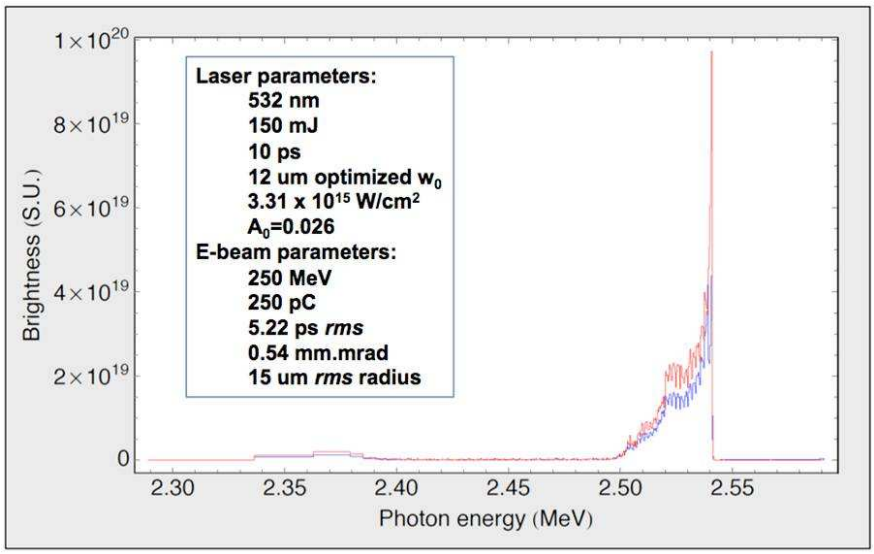

Figure 19: Predicted spectrum of an optimized MEGa-ray source at ∼2.54 MeV.

4.2.2 Specifications of the ELI-NP machine

The ELI-NP machine use identical X-band linac technology but extended from 250 MeV to 600 MeV, use identical state of the art 120 Hz diode pumped laser technology but extended from 1 J to 10 J and duplicate as much as possible the controls systems and hardware being developed for the LLNL machine. The accelerator structure will be capable of 75 MeV/m in order to avoid higher breakdown rates and higher dark current signals. Specifications for the ELI-NP machine are listed in Table 9.

Table 9: The main specifications of the ELI-NP machine

Quantity	**Value**	**Units**
Peak gamma brilliance	$>1.5\times10^{21}$	Photons/sec/mm^2/mrad^2/(0.1% BW)
Effective Beam repetition	12,000	Hz (100 micro-bunches at 120 Hz rep rate)
Gammas per pulse	8×10^8	Photons at 100% BW
Spectral beam flux	10^6	Photons/sec/eV
Gamma pulse duration	2	Picoseconds
Gamma collimation	0.1	mrad at 0.1% BW
Gamma bandwidth	10^{-3}	ΔE/E
Gamma source size	10	Microns
Electron beam energy	600	MeV
Laser pulse energy	1.5	Joules
Gamma-ray energy	1−13 (with 532 nm laser interaction)	MeV

This system will incorporate the latest in dark current noise mitigation and a fully documented and validated computer control system. It has to be stressed that 12,000 Hz is not the upper limit on repetition rate for this system and that 10^{-3} is not the lower limit on bandwidth.
Going beyond these points however will require significant R&D that is not included in the estimates for the ELI-NP project.
Schematic of 600 MeV X-band linac and power distribution system for ELI-NP project is presented in Fig. 20 and an overall view of the proposed γ-source is presented in Fig. 21.

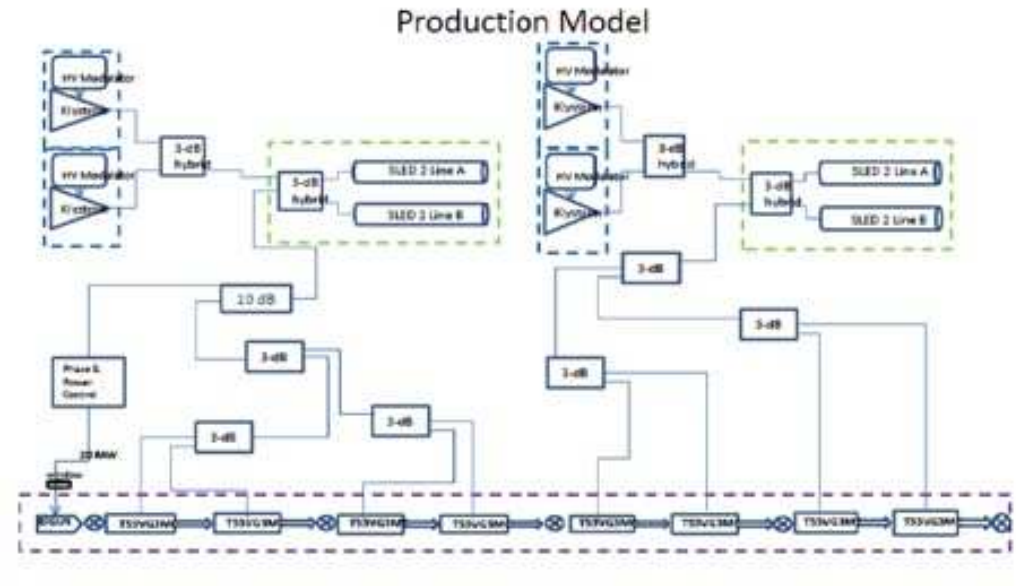

Figure 20: Schematic of 600 MeV X-band linac and power distribution system for ELI-NP project. SLAC XL-4 klystrons and T-53 linac sections are used.

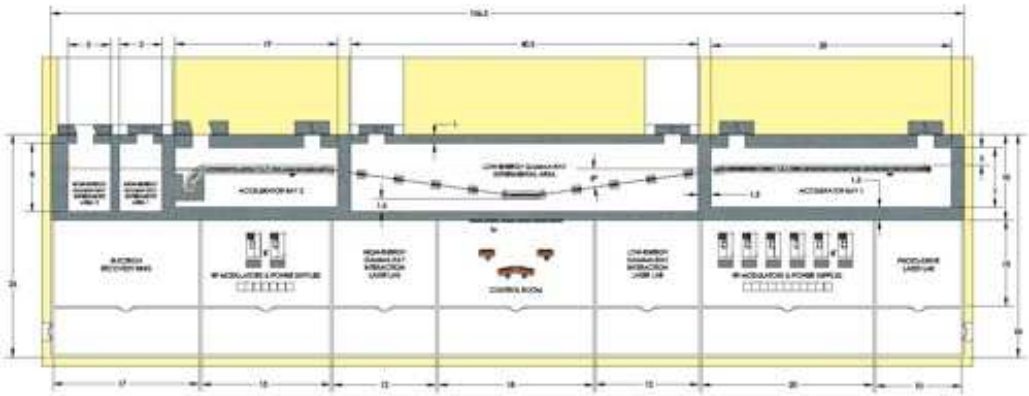

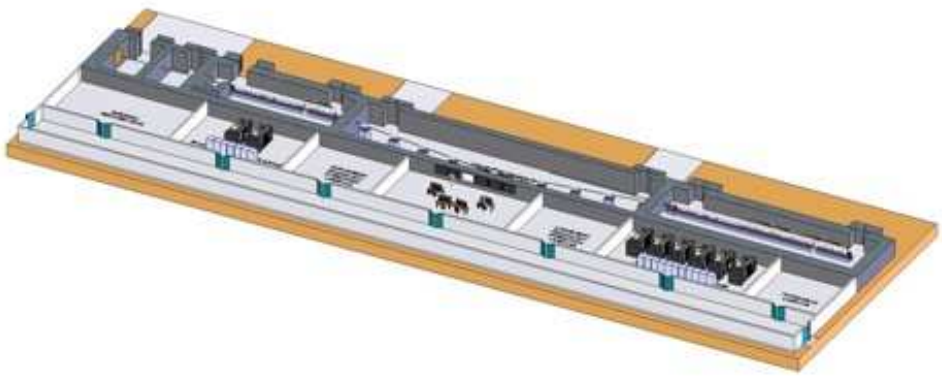

Figure 21: Overall view of the proposed ELI-NP γ source.

The proposed solution can be upgraded after 2015 as desired, e.g. by a 100 mA ERL. There is enough space to accommodate such an upgrade. Also, with a 355 nm laser instead of the 532 nm one, the γ output could be brought to 19.5 MeV. The upgrade is not trivial.
A number of significant activities are covered under this proposal. These include:
1) Development and test of a high energy laser and beam recirculation system which enables a gamma-ray flux that is 100× beyond LLNL's present machine.

a) Construction of a robust, femtosecond, fiber laser seed source that is synchronized to the linac X-band RF frequency.

b) Construction of a dispersion management system for narrowband chirped pulse amplification.

c) Construction of a 10 J-class interaction drive laser system with a base repetition rate of 120 Hz.

d) Construction and test of non-linear pulse recirculation hardware.

e) Construction and commissioning of a full suite of laser diagnostics.

2) Development of multi-bunch X-band linac technology and hardware for creation of high brightness 600 MeV electrons with an effective repetition rate of 12 kHz (see Fig.14).

a) Construction of an all fiber-laser-based photogun drive system synchronized to the linac X-band RF frequency.

b) Construction of a high brightness, multi-bunch compatible, high gradient X-band photogun.

c) Construction of 17 high gradient, X-band linac structures.

d) Construction of X-band power and power distribution system consisting of 8 klystrons and modulators.

e) Construction of X-band power pulse compressor for high gradient linac operation.

f) Construction of linac beam transport and dark current chicane.

g) Construction of laser-electron interaction region.

h) Construction and commissioning of a full suite of electron beam diagnostics.

3) Design, test and optimization of laser-electron interactions to maximize flux and/or minimize gamma-ray bandwidth.
4) Generation of an integrated computer control system for all components.
5) Generation of full construction, operation and maintenance documentation.
Four ELI-NP scientists should participate in the R&D, construction and test of the ELI-NP hardware at LLNL before it is shipped to Romania for installation there.

4.2.3 Possible upgrade in future

The proposed solution can be upgraded after 2015 as desired, e.g. by a 100 mA ERL. There is enough space to accommodate such an upgrade.

4.3 Second stage 100 mA Energy Recovery Linac

Energy-recovery linac (ERL) is a new class of accelerator which produces an electron beam of small-emittance and high-average current [6]. In an energy-recovery linac, an electron beam is accelerated by superconducting rf linac and the beam after use is decelerated in the same linac. Thus the electron energy is converted back into rf energy and recycled to accelerate succeeding electrons; this is ¨energy recovery¨.
This energy-recovery enables to accelerate an electron beam of high-average current with rf generators of small capacity. Moreover, the ERL is free from degradation of electron beam emittance caused by multiple recirculations of electrons, because an electron bunch in the ERL goes to a beam dump after deceleration and another fresh electron bunch is accelerated every turn.
The beam emittance of an ERL can be improved by adopting a small-emittance injector such as a photocathode electron gun. These features, generation of an electron beam with high-average current and small emittance, distinguish the ERL from other type of accelerators.
ERL has been developed for high-power free-electron lasers [7, 8] and now is considered as a platform for future X-ray light sources [9]. The ERL can also work for a high-flux and high-brilliance gamma-ray source in combination with laser Compton scattering as shown in Fig. 22 [10, 11]. A small-emittance electron beam from the ERL plays an essential role in the generation of high-flux and high-brilliance

gamma-ray generation. In the high-brilliance mode, the electron beam, $\varepsilon_n = 0.1$ mm-mrad, is almost diffraction limited, and the on-axis gamma-ray bandwidth is dominated by monocromaticity of the electron beam and has a symmetric spectrum, while the bandwidth in the high-flux mode is dominated by electron beam emittance and has an anti-symmetric spectrum.

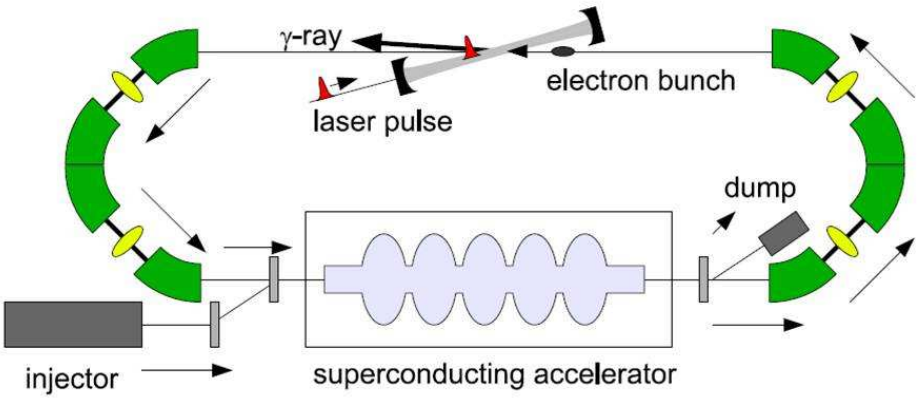

Figure 22: A schematic view of Compton gamma-ray source utilizing an energy-recovery linac (ERL)

Upgrade to 100-mA ERL can be made by adding superconducting ERL cavities under development in Japan [12]. After upgrade to 100-mA ERL, we can operate the gamma-ray source with parameters 80 pC, 130 MHz for the high-flux mode and 8 pC, 1.3 GHz for the high-brilliance mode. The flux and brilliance will be enhanced by 2 orders of magnitude.

4.4 Conclusions

Warm linac present and next future technology upgrades could provide for an affordable cost all requirements imposed by ELI. This facility is expected to be the best γ source worldwide, significantly better than the present best facility HIγS. By leveraging the LLNL activities it is believed that the working components for the ELI-NP machine could be constructed, tested and prepared for shipping to Romania in 3 years from the start of the project, i.e. receipt of funding.
Upgrade after 2015 is possible using the existing configuration. For example with 100mA ERL current one can get a γ flux of 5×10^{15} ph/sec and an incredible bandwidth of 4×10^{-5}.
The development with time of the most important parameters of the gamma ray sources (Fig. 23) shows an exponential improvement with time. The planned ELI-NP facility will have the world-wide best gamma source parameters at the start of operation. In the long run with 100 mA ERL's one can reach a significantly better bandwidth and peak brilliance for the gamma-beams compared to the 2015 approach.

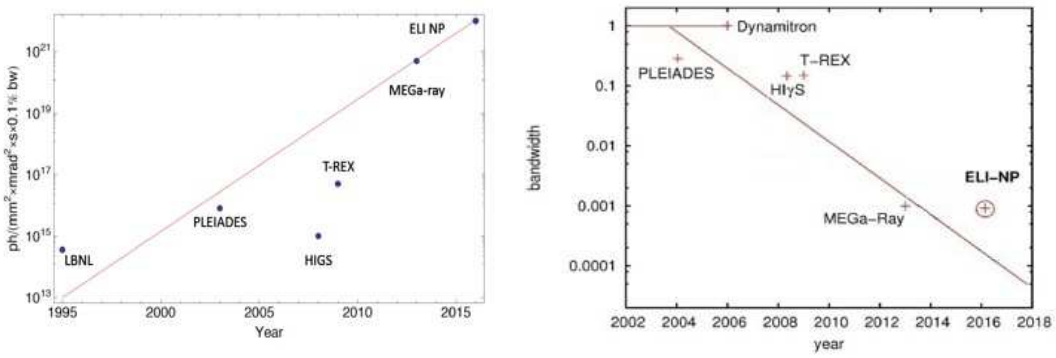

Figure 23: Development with time of the peak brilliance and bandwidth of the gamma ray sources, showing an exponential improvement with time.

References

[1] G.Wormser, Gamma Ray Source Working Group, http://www.eli-np.ro/documents/eli-excom-meeting/Wormser-Gamma-ray-source-working-group.pdf

[2] R.Hajima, High-Flux and High-Brightness g-ray Source Based on an Energy-Recovery Linac, http://www.eli-np.ro/executive-comittee-meeting-april-12-13.php ; R. Hajima and N. Nishimori, private communication (2010).

[3] Ch. Barty, Development of MEGaRay technology at LLNL, http://www.eli-np.ro/executive-comittee-meeting-april-12-13.php and private communication (2010)

[4] W.J.Brown et al:"Experimental characterization of an ultrafast Thomson scattering X-ray source with three-dimensional time and frequency-domain analysis" Phys.Rev. ST-AB 7 0607021-1 – 060702-12 (2004)

[5] F.Albert et al"Isotope specific detection of low-density materials with laser-based monoenergetic gamma-rays" Opt.Lett.35, 354-356 (2010)

[6] R. Hajima"Current status and future perspectives of energy-recovery linacs", in Proc. 2009 Particle Accelerator Conference (2009).

[7] G. R. Neil et al."Sustained Kilowatt Lasing in a Free-Electron Laser with Same-Cell Energy Recovery", Phys. Rev. Lett. 84, 662–665 (2000).

[8] R. Hajima et al."First demonstration of energy-recovery operation in the JAERI superconducting linac for a high-power free-electron laser", Nucl. Instr. Meth. A507, 115–119 (2003).

[9] S.M. Gruner et al."Energy recovery linacs as synchrotron radiation source", Rev. Sci. Instr. 73, 1402–1406 (2002).

[10] R. Hajima et al."Detection of radioactive isotopes by using laser Compton scattered γ-ray beams" , Nucl. Instr. Meth. A608, S57–S61 (2009).

[11] V.N. Litvinenko et al., "Potential uses of ERL-based gamma-ray sources", IEEE Trans. Plasma Sci. 36, 1799–1807 (2008).

[12] R. Nagai et al., submitted.

Glossary

BW - Band Width;
CGrAS - Center for Gamma-ray Applied Science;
CLIC - Compact LInear Collider;
ELI-NP - Extreme Light Infrastructures - Nuclear Physics;
ERL - Energy-Recovery Linac;
FWHM - Full Width at Half Maximum;
HIγS - High Intensity γ (Gamma) Source;
LAL - Laboratoire de l'Accélérateur Linéaire;
LLNL - Lawrence Livermore National Laboratory;
LHC - Large Hadron Collider;
LINAC - LINear ACcelerator;
MEGa-ray - Mono-Energetic Gamma-ray;
PLEIADES - Picosecond Laser Electron Inter-Action for the Dynamic Evaluation of Structures;
RF - Radio Frequency;
R&D - Research and Development;
SLAC - Stanford Linear Accelerator Center;
SLED - SLAC Energy Doubler;
ThomX - Thomson X-ray Source;
T-REX - Thomson -Radiated Extreme X-ray Source.

The Scientific Case of ELI Nuclear Physic Pillar

The ELI-Nuclear Physics Experiment working group

Editors:
Dietrich Habs, Martin Groß, Nicolae Mărginean,
Florin Negoiţă, Peter G. Thirolf, Matthias Zepf

Authors

M. Apostol[11], P. Böni[12], D. Bucurescu[11], A. Buţă[11], Gh. Căta-Danil[20], R. Chapman[26,27], C. Ciortea[11], F. Constantin[11], B. Constantinescu[11], V. Corcalciuc[11], L. Csige[21] L.C. Cune[11], B. Dietz[5], M.O. Dima[11], G. Dollinger[23], D. Dudu[11], D. Dumitriu[11], N. Elkina[3], A. Fedotov[10], D. Fluieraşu[11], M. Fujiwara[25], H. Gies[4], M. Ganciu[17], C. Ghica[19], T. Glodariu[11], M. Groß[3], M. Gugiu[11], I. Gurgu[20], D. Habs[3,8], R. Hajima[2], M.N. Harakeh[18], C. Harvey[16], M. Hassan[26,27], C. Haţegan[11], T. Hayakawa[1], T. Heinzl[16], A. Henig[3,8], R. Hörlein[3,8], Ch. Hugenschmidt[12], A. Ilderton[16], R.A. Ionescu[11], C. Ivan[11], E. Ivanov[11], D.A. Jaroszynski[26], D. Kiefer[3,8], U. Köster[22], A. Krasznahorkay[21], K.W.D. Ledingham[26,28,29], A. Lupaşcu[20], W. Ma[6,8], D. Macovei[19], M. Marklund[24], N. Mărginean[11], J. Melone[26,28], M. Naumova[6], F. Negoiţă[11], A. Negreţ[11], D. Niculae[11], S. Pain[26,27], D. Pantelică[11], G. Paulus[4], N. Pietralla[5], A.M. Popovici[20], N. Puşcaş[20], P.M. Racolţa[11], A.A. Răduţă[11,30], G. Rosner[26], H. Ruhl[3], D. Savran[5], K. Schreckenbach[12], J. Schreiber[8], R. Schützhold[15], T. Shizuma[2], J.F. Smith[26,27], K. Sonnabend[5], K.-M. Spohr[26,27], M. Stafe[20], C.M. Teodorescu[19], P. G. Thirolf[3], C.A. Ur[11,31], G. Vaman[11], I. Vâţă[11], A.M. Vlaicu[19], H.A. Weidenmüller[9], X.Q. Yan[8,14], N.V. Zamfir[11], M. Zepf[13].

Affiliations

[1] Advanced Photon Research Center, JAEA, Kizugawa, Kyoto, Japan
[2] Advanced Photon Research Center, JAEA, Tokai, Ibaraki, Japan
[3] Fakultät für Physik, Ludwig-Maximilians-Universität München, Munich, Germany
[4] Friedrich Schiller Universität, Jena, Germany
[5] Institut für Kernphysik, TU Darmstadt, Darmstadt, Germany
[6] Institute of Physics, CAS, Beijing, P.R. China
[7] Laboratoire d'Optique Appliquée, UMR 7639 ENSTA, Palaiseau, France
[8] Max-Planck Institute of Quantum Optics, Garching, Germany
[9] Max-Planck Institut für Kernphysik, D-69029 Heidelberg, Germany
[10] Moscow Engeniering Physics Institute, Moscow, Russia
[11] National Institute for Physics and Nuclear Engineering, Bucureşti-Măgurele, România
[12] Physik-Department E21, Technische Universität München, Garching, Germany
[13] Queen's University, Belfast, Northern Ireland, UK
[14] State Key Lab of Nuclear Physics and Technology, Peking University, Beijing, P.R. China
[15] Universität Duisburg-Essen, Duisburg, Germany
[16] University of Plymouth, Plymouth, PL4 8AA, UK
[17] National Institute for Laser Plasma and Radiation Physics, Bucureşti-Măgurele, România
[18] Kernfysisch Versneller Instituut, Zernikelaan 25, NL-9747 AA Groningen, The Netherlands
[19] National Institute for Materials Physics, Bucureşti-Măgurele, România
[20] Polytechnic University, Bucureşti, România
[21] MTA, ATOMKI Debrecen, Hungary
[22] ILL, Grenoble, France
[23] University of the Bundeswehr, Munich, Germany
[24] Umea University, Umea, Sweden
[25] Osaka University, Osaka, Japan
[26] Scottish Universities Physics Alliance, SUPA,

[27] Faculty of Engineering and Science, University of the West of Scotland, Paisley, PA1 2BE, United Kingdom
[28] Department of Physics, University of Strathclyde, Glasgow, G4 0NG, United Kingdom
[29] AWE, Aldermaston, Reading, Berkshire, RG7 4PR, United Kingdom
[30] Academy of Romanian Scientists, 54 Splaiul Independentei, Bucharest 050094, Romania
[31] Istituto Nazionale di Fisica Nucleare, Sezione di Padova(Italy)

5 The Scientific Case of ELI Nuclear Physic Pillar

5.1 Introduction to Envisioned Experiments at ELI Nuclear Physics Facility

ELI Nuclear Physics is meant as an unique research facility to investigate the impact of very intense electromagnetic radiation (**Extreme Light**) on matter with specific focus on nuclear phaenomena and their practical applications. The extreme light is realized at ELI-NP in two ways: by very high optical laser intensities and by the very short wavelength beams on γ-ray domain with very high brilliance. This combination allows for stand-alone experiments with a state-of-art high-intensity laser, stand-alone high resolution γ-beam experiments or combined experiments of both photon sources. In this way it will be possible to approach a broad range of frontier research topics of modern physics, as the production and study of radioactive species important to understand the genesis of elements in Universe which cannot be produced at existing radioactive-beam facilities or under construction, the investigation of rare processes taking advantage of the acceleration of compact bunches of matter with high-intensity lasers or the study of photonuclear processes using an unique tunable energy, high-resolution γ-ray beams.

The ELI-NP high-intensity laser will be based on APOLLON-type solution and will use OPCPA technology at the front-end and Ti:Sapphire high-energy amplification stages. The APOLLON-type high-intensity laser at ELI-NP facility will have two front-ends, which will temporally stretch and amplify initial ultrashort pulses with 800 nm central wavelength to the 100 mJ level, preserving the needed large bandwidth of the 15 fs laser pulses and the temporal contrast of the pulses in the range of 10^{-12}.

The pulses after the front end will be splitted and distributed to further laser amplifiers, reaching few Jules of energy at 10 Hz repetition rate and few tens of Joules at a repetition period of the order of few seconds. At these energy levels, the pulses can be extracted from the laser amplification chain and recompressed to shortest duration in vacuum compressors. Subsequently, they are distributed to the high repetition rate experimental areas.

Alternatively, the laser pulses will be further amplified in the amplification chains to energies of the order of 300 J. The repetition rate of the pump lasers will restrict the repetition period of the high energy pulses to the minutes range. Adaptive optics and optical isolation of the pulses will be implemented before the optical mosaic compressors. The ultrashort pulses will be distributed to the high energy experimental areas, where stand-alone experiments or combined nuclear physics experiments using the highly brilliant γ beam will be performed.

Coherent combination of the high power ultrashort pulses with the ultraintense and ultrashort pulses from the parallel amplification chains is envisaged, in order to reach intensities of the order of 10^{23} W cm^{-2} and above. The operation of the experiments will take place in parallel, the laser pulses being delivered to different experimental areas on request. Depending on technological developments, an upgrade of the high-intesity laser system in a second stage might be possible, allowing to obtain intensities above 10^{24} W cm^{-2}.

The γ source of ELI-NP will produce a very intense and brilliant γ beam (E_γ = 14 -16 MeV for the beginning and $E_\gamma \leq 19$ MeV in a second stage), which is obtained by incoherent Compton back scattering of direct laser light with a very brilliant and intense electron beam ($E_e \leq 0.6$ GeV).

The experiments envisaged with the γ source definded severe constraints for the parameters of the γ beam: bandwidth equal or higher than 10^{-3}, energy up to 19 MeV to access all GDR, repetition rate in the range of kHz to get about 1 event/pulse in the detector, total flux higher than 10^{13} photons/sec, peak brilliance higher than 10^{22} photons mm^{-2} mrad^{-2} s^{-1} (0.1% BW)$^{-1}$ in order to improve the ratio effect-background; the high flux and superb brilliance requires an excellent normalized emittance for the electron beam (in the range of 0.25 mm mrad). The solution adopted for producing the 600 MeV electron beam is to use a 120 Hz warm LINAC accelerator, similar with the accelerator foreseen for the MEGa-ray project of LLNL. The reflective laser for the production of γ-rays will run reliable at the high repetition rate of 120 Hz using diode pumping. By using a ring-down cavity for the laser pulse, within the macropulse of 120 Hz repetition rate, 100 micropulses can be realized, increasing the overall repetition rate to 12 kHz

Upgrade to 100-mA ERL will be possible in a second stage, by adding superconducting ERL cavities

currently under development in Japan. After upgrade to 100-mA ERL, it will be possible operate the gamma-ray source with parameters 80 pC, 130 MHz for the high-flux mode and 8 pC, 1.3 GHz for the high-brilliance mode. Consequently, the flux and brilliance will be further enhanced by 2 orders of magnitude, paving the way toward new experimental challenges at the frontier of physics.

5.2 Experiments with the APOLLON-type Laser used stand-alone

The APOLLON-type laser beam will not produce effects on nuclear dynamics directly, but the laser will be used for ion acceleration or to produce relativistic electron mirrors by laser acceleration followed by a coherent reflection of a second laser beam in order to generate very brilliant X-ray or γ beams. We plan to use these beams later to produce exotic nuclei or to perform new γ spectroscopy experiments in the energy or time domain. Most of the experiments proposed in this subsection may be done, with some limitations, at laser intensities of $10^{23}\,\mathrm{W/cm^2}$, and several other experiments require laser intensity of $10^{24}\,\mathrm{W/cm^2}$. The production of the electron sheet as relativistic mirror needs laser intensity of $10^{24}\,\mathrm{W/cm^2}$, and the fission-fusion mechanism to produce neutron-rich nuclei can be investigated as proof-of-principle at $10^{23}\,\mathrm{W/cm^2}$, but the real production experiments require intensities of $10^{24}\,\mathrm{W/cm^2}$ and greater.

5.2.1 Production of Neutron-Rich Nuclei around the $N = 126$ Waiting Point of the r-Process via the Fission-Fusion Reaction Mechanism using a Laser-Accerated Th Beam

D. Habs[1] and P.G. Thirolf[1]
[1] *Ludwig Maximilians University, Munich (Germany)*

According to a recent report by the National Research Council of the National Academy of Science (USA), the origin of the heaviest elements remains one of the 11 greatest unanswered questions of modern physics [1]. While the lower path of the r-process for the production of heavy elements is well explored, the nuclei around the $N = 126$ waiting point critically determine this element production mechanism, and at present basically nothing is known about these nuclei. We propose to produce neutron-rich nuclei in the range of the astrophysical r-process (the rapid neutron-capture process) around the waiting point $N = 126$ [2–4] by fissioning a dense thorium ion bunch with about 7 MeV/u in a ca. 3 mm thick thorium target (covered by a thin carbon layer), where the light fission fragments of the beam fuse with the light fission fragments of the target. Via laser Radiation Pressure Acceleration (RPA) [10, 11] we are able to produce very efficiently bunches of solid state density of ^{232}Th with about 7 MeV/u, which pass through a thin carbon layer and desintegrate into light and heavy fission fragments. In addition light ions (H,C) from the CH_2 backing of the first Th target will be accelerated as well, inducing the fission process of ^{232}Th in the second, thick Th foil. The expected strongly reduced stopping power for these very dense ion bunches helps to obtain intense fission fragment beams. The high density of the bunch and the target furthermore leads to a reasonable fusion yield. In contrast to classical radioactive beam facilities, where intense, low density radioactive beams of one isotope are merged with stable targets, we here study the fusion between neutron-rich short-lived target-like nuclei and neutron-rich, short-lived projectile-like nuclei. Since each of these mass distributions consists of a multitude of isotopes, we exploit the fluctuations in neutron number of both target and beam fragment to reach more neutron-rich nuclei. Also the neutron transfer before the first fission reaction will increase the fluctuations in neutron number of the light fission fragments. The new acceleration scheme allows to reach this so far unexplored region of neutron-rich nuclei with importance to nuclear physics and astrophysics. One expects for the 20 PW APOLLON-type laser with 300 J about 10^{12} accelerated thorium ions with a 9 μm beam diameter, 30 nm bunch length and 0.1 Hz repetition rate. This should result in about $10^5 - 10^6$ ions/shot of fused neutron-rich nuclei with masses close to $A = 180 - 190$. In a velocity filter the other species with $A \approx 232$, $A \approx 140$ and $A \approx 100$ can be separated from the beam-like nuclei of interest with $A = 180 - 190$. Since the yield of very neutron-rich fusion products grows strongly nonlinearly with laser energy, a final use of several coincident APOLLON-like lasers could be very advantageous, especially since the detection of the new ms-isotopes should be rather straightforward.

Radiation Pressure Acceleration (RPA) with solid state density ion bunches, which are about 10^{15} times more dense than classically accelerated ion bunches, allows for a high probability that generated fission products fuse again, when the thorium beam strikes a second close Th target. The fission fragments have a $1/\sin(\Theta)$ angular distribution and thus are predominantly emitted in beam direction and stay within the cylinder volume defined by the small spot diameter of the first Th target. In this two-step reaction neutron-rich light fission fragments of the beam fuse with neutron-rich light fission fragments of the target and we can reach more neutron-rich nuclei than with classical radioactive beams only. The produced beam of new radioactive nuclei will be analyzed with a (gas-filled) recoil separator, where the technical optimization is well known and one gets a very good suppression of background for nearly symmetric fusion reactions. The small repetition rate of the 20 PW APOLLON-type lasers of about 0.02 Hz with very short production pulses is stretched by the β-decay half-lives of the produced nuclei to counting rates acceptable to nuclear detectors. Very neutron-rich nuclei still have small production cross sections, because weakly bound neutrons ($B_N \geq 3$ MeV) are evaporated easily. It is important that the hindrance of fusion for nearly symmetric systems (break-down of fusion) only sets in for projectile and target masses heavier than 100 u [8, 9]. Thus for the fusion of light fission fragments we expect an unhindered fusion evaporation process. The velocity filter has to suppress the many fused nuclei close to the valley of stability. Here we want to look specifically for nuclei close to the waiting point at $N = 126$ of the r-process, which is decisive for the astrophysical production of heavy elements and was not accessible until now. We estimate sufficient rates for these interesting nuclei. We envision having behind the velocity filter a gas stopping cell for the preparation of the ions [10] prior to their injection into a Penning trap [11], where nuclear masses can be measured with high accuracy, thus giving access to nuclear binding energies.

References

[1] E. Haseltine, http://discovermagazine.com/2002/feb/cover

[2] K.L. Kratz et al., Prog. in Part. and Nucl. Phys. **59**, 147 (2007).

[3] M. Arnould, S. Griely, K. Takahashi, Phys. Rep. **450**, 97 (2007).

[4] I.V Panov and H.-Th. Janka, Astr. Astroph. **494**, 829 (2009).

[5] A. Henig et al., Phys. Rev. Lett. **103**, 245003 (2009).

[6] T. Tajima, D. Habs, X. Yan, *Laser Acceleration of Ions for Radiation Therapy*, RAST **2**, 221 (2009).

[7] G. Münzenberg et al., Nucl. Instr. Meth. **161**, 65 (1979).

[8] A.B. Quint et al., Z. Phys. **A 346**, 119 (1993).

[9] W. Morawek et al., Z. Phys. **A 341**, 75 (1991).

[10] J.B. Neumayr et al., Nucl. Instr. Meth. **B244**, 489 (2006).

[11] M. Block et al., Nature **463**, 785 (2010).

5.2.2 From Radiation Pressure Acceleration (RPA) and Laser-Driven Ion Pistons to Direct Laser Acceleration of Protons at Intensities up to 10^{24}W/cm^2

D. Habs[1], A. Henig[1], J. Schreiber[1], R. Hörlein[1], X.Q. Yan[2] and M. Zepf[3]
[1] *Ludwig Maximilians University, Munich (Germany)*
[2] *State Key Lab of Nuclear Physics and Technology, Peking University, Beijing, (P.R. China)*
[2] *Queen's University Belfast, Northern Ireland (UK)*

Since the pioneering work that was carried out 10 years ago [1–4], the generation of highly energetic ion beams from laser-plasma interactions has been investigated in much detail in the regime of target normal sheath acceleration (TNSA) [5]. Creation of ion beams with small longitudinal and transverse emittance and energies extending up to tens of MeV fueled visions of compact, laser-driven ion sources for applications such as ion beam therapy of tumors, fast ignition inertial confinement fusion or the generation of neutron-rich nuclei. However, new pathways are of crucial importance to push the current limits of laser-generated ion beams further towards parameters necessary for those applications.
To overcome the limitations of TNSA, a novel mechanism which is referred to as Radiation Pressure Acceleration (RPA) was proposed [6–9]. Here, much thinner foil targets of only nanometers are used so that the laser transfers energy to all electrons located within the focal volume. While for TNSA the accelerating electric field that is generated by hot electrons is stationary and ion acceleration is spatially separated from laser absorption into electrons, in RPA a localized longitudinal field enhancement is present that co-propagates with the ions as the accompanying laser pulse pushes the electrons forward. By changing the laser polarization to circular, electron heating and expansion are efficiently suppressed, resulting in a phase-stable acceleration that is dominated by the laser radiation pressure and is maintained for an extended time. Thus, the whole target is accelerated ballistically as a quasi-neutral, dense plasma bunch like a light sail. Just recently, this novel acceleration process has been observed for the first time in an experiment at intensities of 5×10^{19} W/cm^2 [10,11] and pulse energies below 1 J, generating a peaked spectrum of C^{6+} ions. Compared to quasi-monoenergetic ion beam generation within the TNSA regime [12], a more than 40 times increase in conversion efficiency was achieved.
A large number of theoretical studies lately predicted further improvement of the ion beam characteristics in terms of conversion efficiency as well as peak energy and monochromaticity when significantly higher laser pulse energies and intensities are used [13–17]. In particular, it is expected that the RPA process progresses much more stably when ions reach relativistic velocities already in the initial hole-boring phase before the whole target is set in motion (i.e., before the light sail stage). At intensities around 10^{23} W/cm^2 simulations show that protons become relativistic within one half-cycle of the laser pulse and acceleration by the laser radiation pressure is dominant even for linear polarization in what is referred to as the laser-piston regime [18,19]. Here, the target can be viewed as a relativistic plasma mirror with Lorentz factor γ being propelled by the reflected laser and the laser-to-ion conversion efficiency $\eta = 1 - 1/(4\gamma^2)$ approaches unity in the ultrarelativistic limit.
In all ion acceleration mechanisms discussed so far, the laser energy was not directly transfered to ions but mediated by electrons instead. For even higher laser intensities of $\sim 5 \times 10^{24}$ W/cm^2 at a wavelength of 1 μm, protons can be driven to relativistic velocities directly by the laser field. This regime of direct ion acceleration has not been studied in simulations so far since the new phenomenon of radiation damping strongly changes the laser-plasma interaction and is also expected to occur at 10^{24} W/cm^2, hence preventing the straightforward application of existing PIC codes [20,21]. Basically all theories of radiation damping suffer from more or less severe intrinsic inconsistencies [22] and only by comparison with experiment the proper theory can be established.
Employing the APOLLON-type laser unprecedented intensities on the order of 10^{24} W/cm^2 become available for experiments, allowing for improved RPA and for the first time study of the laser-piston regime as well as direct proton acceleration. According to theory, mono-energetic solid density ion bunches are expected at laser-to-ion conversion efficiencies approaching unity. Such a novel compact ion source could serve a wealth of experiments and applications, with an example being given by the production of neutron-rich nuclei around the N=126 waiting point as described in project 4.1.

References

[1] E. L. Clark et al., Phys. Rev. Lett. **85**(8), 1654–1657 (2000).

[2] A. Maksimchuk et al., Phys. Rev. Lett. **84**(18), 4108–4111 (2000).

[3] R. A. Snavely et al., Phys. Rev. Lett. **85**(14), 2945–2948 (2000).

[4] S. P. Hatchett et al., Phys. Plas. **7**(5), 2076–2082 (2000).

[5] S.C. Wilks et al., Phys. Plasma **8**, 542 (2001).

[6] A. Macchi et al., Phys. Rev. Lett. **94**(16), 165003 (2005).

[7] O. Klimo et al., Phys. Rev. ST Accel. Beams **11**, 031301 (2008)

[8] A.P.L. Robinson et al., New J. of Phys. **10**, 013021 (2008).

[9] X. Q. Yan et al., Phys. Rev. Lett. **100**(13), 135003–4 (2008).

[10] A. Henig et al., Phys. Rev. Lett. **103**, 245003 (2009).

[11] T. Tajima, D. Habs, X. Yan, *Laser Acceleration of Ions for Radiation Therapy*, RAST **2**, 221 (2009).

[12] B. M. Hegelich et al., Nature, **439**, 441–444 (2006).

[13] X. Q. Yan et al., Phys. Rev. Lett., **103**(13), 135001 (2009).

[14] B. Qiao et al., Phys. Rev. Lett. **102**, 145002 (2009).

[15] A.P.L. Robinson et al., Plasma Phys. Control Fusion **51**, 024004 (2009).

[16] A. Macchi et al., Phys. Rev. Lett. **103**, 085003 (2009).

[17] A. Macchi et al., *Radiation pressure acceleration of ultrathin foils*, New J. Phys. (2010), in press.

[18] T. Esirkepov et al., Phys. Rev. Lett. **92**, 175003 (2004).

[19] F. Pegoraro and S.V. Bulanov, Phys. Pev. Lett. **99**, 065002 (2007).

[20] T. Schlegel et al., Phys. Plas., **16**, 083103 (2009).

[21] M. Chen et al., *Radiation reaction effects on ion acceleration on laser foil acceleration*, arXiv:0909.5144v1(2009).

[22] I.V. Sokolov, JETP **109**, 207 (2009).

5.2.3 Deceleration of Very Dense Electron and Ion Beams

D. Habs[1], A. Henig[1], J. Schreiber[1], R. Hörlein[1], W. Ma[2] and M. Zepf[3], D. Dumitriu[4], C. Ciortea[4], M. Gugiu[4], D. Fluerașu[4]
[1] *Ludwig Maximilians University, Munich (Germany)*
[2] *Institute of Physics, CAS, Beijing, (P.R. China)*
[3] *Queen's University Belfast, Northern Ireland (UK)*
[4] *IFIN-HH, Bucharest, Romania*

In nuclear physics the Bethe-Bloch formula [2] is used to calculate the atomic stopping of energetic individual electrons [1] by ionization and atomic excitation:

$$-[\frac{dE}{dx}]_I = K \cdot z^2 \frac{Z}{A}\frac{1}{\beta^2}\left[\frac{1}{2}\ln\frac{2m_e c^2\beta^2\gamma^2 T_{\max}}{I^2} - \beta^2 - \frac{\delta}{2}\right] \tag{1.1}$$

and ions:

$$-\frac{dE}{dx} = 4\pi n_e \frac{Z_{\text{eff}}^2\, e^4}{m_e v^2 (4\pi\epsilon_0)^2}\left[\ln\left(\frac{2m_e v^2}{I(1-\beta^2)}\right) - \beta^2\right] \tag{1.2}$$

where I is the ionization potential, n_e the density of the electrons, m_e the mass of the electron, v is the ion velocity, $\beta = v/c$, $T_{\max}$ is the maximum kinetic energy which can be imparted to a single electron in a single collision, and Z_{eff} is the effective charge of the ions.
For relativistic electrons the other important energy loss is bremsstrahlung with:

$$-[\frac{dE}{dx}]_R = (4\pi n_e/(m_e c^2))\frac{Z}{137\pi}(\gamma - 1)ln(183Z^{-1/3}) \tag{1.3}$$

The approximate ratio of the two loss processes [2] is:

$$[\frac{dE}{dx}]_I/[\frac{dE}{dx}]_R = EZ/1600mc^2 \tag{1.4}$$

Thus radiation loss is dominant for high energy electrons e.g. E≥ 100 MeV and Z=10. If, however (see below), the atomic stopping becomes orders of magnitude larger by collective effects, the radiation loss can be neglected.
For laser acceleration the electron and ion bunch densities reach solid state densities, which are about 15 orders of magnitude larger compared to beams from classical accelerators. Here collective effects become important. One can decompose the Bethe-Bloch equation according to Ref. [3] into a first contribution describing binary collisions and a second term describing long range collective contributions:

$$-\frac{dE}{dx} = 4\pi n_e \frac{Z_{\text{eff}}^2\, e^4}{m_e v^2 (4\pi\epsilon_0)^2}\left[\ln(m_e v^2/e^2 k_D) + \ln(k_D v/\omega_p)\right] \tag{1.5}$$

Here k_D is the Debye wave number and ω_p is the plasma frequency of the electrons. Similar to bubble acceleration [4] but now with opposite phase for deceleration a strong collective field is built up by the blown-out electrons that decelerates them much faster than the processes that take effect for individual charged particles. Typical electric fields E are:

$$E = m_e\omega_p \cdot v \cdot \frac{n_b}{n_e\, e} \tag{1.6}$$

where n_b is the charge density of the bunch. In Ref. [6] we discuss this mechanism of collective deceleration of a dense particle bunch in a thin plasma, where the particle bunch fits into part of the plasma oscillation and is decelerated $10^5 - 10^6$ stronger than predicted by the classical Bethe-Bloch equation [2] due to the strong collective wakefield. For ion deceleration we want to use targets with

suitable low density. These new laws of deceleration and stopping of charged particles have to be established to use them later in experiments in an optimum way.
We may also discuss the opposite effect with a strongly reduced atomic stopping power that occurs when sending an energetic, solid state density ion bunch into a solid target. For this target the plasma wavelength ($\lambda_p \approx$1 nm) is much smaller than the ion bunch length ($\approx$ 100 nm) and collective acceleration and deceleration effects cancel each other. Only the binary collisions are important. Hence, we may consider the dense ion bunch as consisting of 300 layers with Å distances. Here the first layers of the bunch will attract the electrons from the target and – like a snow plough – will take up the decelerating electron momenta. The predominant part of the ion bunch is screened from electrons and we expect a $\approx 10^2$ fold reduction in stopping power. The electron density n_e is strongly reduced in the channel because many electrons are driven out by the ion bunch and the laser. Again all these effects have to be studied in detail.
It is expected that the resulted very dense electron and ion bunches should have a time evolution (decay in time) and the decay products are emitted at different times and angles. Therefore, for characterization of the dense bunches and their time evolution, the detection system need to capture the decay products, emitted at different times (analogous to time of flight measurements), and measure their angular distributions. Of course, the temporal evolution which can be followed vary greatly depending on the temporal resolution of the diagnosis system. In a preliminary phase, it is expected that electrons and ions are emitted due to the Coulomb explosion of a part of the initially formed bunch (pre-bunch emission) . Then, the remained bunch will have a slower temporal evolution, which can be followed in dependence of its time of flight in free space. The experimental study of deceleration of dense, high speed bunches of electrons and ions will require:

- Bunch's characterization in free space: its components, their energies and the ion charge states, their angular distribution and temporal evolution; due to the large number of particles, the detection solid angles must be small (of the order of 10^{-7} sr or less).
- Tracking the changes introduced by bunch's passing through different materials (solid or gas) and their deceleration study. Studies will be carried out depending on laser power and target type and thickness and for deceleration - depending on material type and its thickness.

The same detection system could be used for both diagnosis in free space and diagnosis after passing through a material. A rapid characterization may be done with a Thomson parabola ion spectrometer, and an electron magnetic spectrometer, implying measurements of the emissions at different times and possibly their angular distribution, in the case they are relevant. A more complete analysis will require a diagnosis system working in real-time, using magnetic spectrometers and detection systems with high granularity or with position sensitive reading in the focal plane (e.g., stacks ofΔE-E detectors, with ionization chambers and Si or scintillation detectors). Even if the laser pulse frequency is small, the nuclear electronics can be triggered in the usual way.

References

[1] Particle Data Group, Phys. Rev. **D 66**, 010001 (2002).

[2] S. Segre, *Nuclei and Particles*, 2nd edition, W.A. Benjamin, RA, London (1977)

[3] S. Ichimaru, *Basic Principles of Plasma Physics: A Statistical Approach*, Benjamin, Reading, MA (1973).

[4] A. Pukhov and J. Meyer-ter-Vehn; Appl. Phys. **B74**, 355 (2002).

[5] H.-C. Wu et al., *Collective Deceleration*, arXiv:0909.1530v1 [physics.plasm-ph] (2010).

5.2.4 The development and application of ultra-short duration high brilliance gamma rays probes for nuclear physics

D.A. Jaroszynski[1], G. Rosner[1], M. Ganciu[2], N.V. Zamfir[3],
Gh. Căta-Danil[3], N Mărginean[3]
[1] *Scottish Universities Physics Alliance, SUPA,*
[2] *Institute of Lasers, Plasma and Radiation, Bucharest-Magurele (Romania)*
[3] *National Institute for Physics and Nuclear Engineering, Bucharest-Magurele (Romania)*

The radiation sources that will be set up in the ELI-NP Bucharest laboratory will provide unique probes for investigating the structure of matter on unprecedented temporal and spatial scales. In addition, they could provide users with the means to create "extreme" states of matter. An important long term objective of the ELI project will be to produce very intense electric fields, approaching 10^{17} V/m, where QED effects become evident. Furthermore, the proposed narrow bandwidth gamma sources based on Compton back-scattering will give unique opportunities to investigate nuclear structure and nuclear processes.

To provide the groundwork for the teams enable them to take advantage of the proposed ELI facilities we will set up a collaborative Scottish-Romanian programme, which includes a strong training element drawing on the expertise in nuclear, plasma, accelerator physics of the two teams, to develop the new techniques that are necessary to probe matter using gamma rays and ultra-short duration bright electron bunches. This programme will include the development of high brilliance femtosecond duration gamma ray sources based on the laser-plasma wakefield accelerator. The source development, which is currently part of the Strathclyde team's ALPHA-X project, will include scaling up of a betatron laser-wakefield radiator from the current 200 keV (600 keV critical photon energy) to the range of 1–10 MeV, and beyond. This will be achieved by increasing the energy of the beams from the laser-driven plasma wakefield accelerator to several GeV by lowering the plasma density and increasing the laser intensity. The measured peak brilliance is currently in excess of 10^{22} phot/sec/mm2/mrad2/0.1% BW. This will be increased by several orders of magnitude when the photon energy is scaled up to the 1-10 MeV range. The expected photon flux should be in the range of 10^{10}–10^{12} photons/s depending on the laser repetition rate. The proposed experimental work will be carried out initially using the current 30 TW ALPHA-X laser, and then on the new SCAPA 200–300 TW laser, which will become operational in 2011-2012. The femtosecond duration polarised gamma ray source should provide a unique opportunity for developing new radiation delivery methods (focussing), time dependent pump-probe techniques and detectors necessary for the future ELI nuclear physics programme. It will also provide a very useful complementary source to the proposed Compton backscatter source because of its unique time structure. Furthermore, the electron bunches, with energies up to several GeV, could also be used directly in nuclear experiments.

One aspect of the programme will be collaboration in the development of the plasma media necessary for supporting the high electrostatic fields, and the transport of the ultra-short electron bunches. In addition to building on the existing collaboration between the Scottish and Romanian teams we will enlarge the collaboration to include all interested parties. It is the intention to provide training opportunities not only for new students and postdoctoral researchers entering this new and exciting field but also for the more senior scientists who will require retraining to develop new expertise in this rapidly evolving field. It is clear that to take full advantage of the new facilities new expertise will be needed in Romania. The hope is that this collaboration will help to provide this training while also growing competence within the wider ELI consortium.

An important adjunct to the source and technique development part of the collaboration is the development of a solid scientific applications programme. There are many opportunities that could be explored. With a view to furthering the overall goals of the ELI-NP project the Scottish-Romanian teams will use the radiation and particle beams at Strathclyde to carry out several initial studies of photo-nuclear isotope generation, which could have an impact on the development of new methods for the treatment of nuclear waste, or for the manufacture of medical isotopes. The gamma ray energy range of 1–15+ MeV covers several interesting spectral regions from giant to pigmy dipole resonances. Even though the relatively broad spectral width of betatron sources may not be immediately useful for directly studying these photonuclear processes spectroscopically, there are opportunities that take

advantage of the short temporal duration of the gamma ray pulses, which is of the order of 1 femtosecond, and could be decreased to several attoseconds. Another important part of the collaboration will include the study of radiation reaction in highly radiating systems such as betatron radiation in ion channels and also the collective scattering processes in plasma using the ultra-short duration high peak brightness and dense electron bunches from wakefield accelerators.

5.2.5 A Relativistic Ultra-thin Electron Sheet used as a Relativistic Mirror for the Production of Brilliant, Intense Coherent γ-Rays

D. Habs[1,2], D. Kiefer[1,2], R. Hörlein[1,2] and X.Q. Yan[2,3]
[1] *Ludwig Maximilians University, Munich (Germany)*
[2] *Max-Planck Institute of Quantum Optics, Garching (Germany)*
[2] *State Key Lab of Nuclear Physics and Technology, Peking University, Beijing, (P.R. China)*

In Ref. [1] we have proposed the use of an intense laser to drive a very dense electron sheet out of an ultra-thin Diamond-Like-Carbon (DLC) foil. The sheet then surfs on the half-wave of the laser pulse and gains a relativistic energy characterized by $\gamma = 1/\sqrt{1-\beta^2}$ with the total velocity $\beta = v/c$. We also introduce $\gamma_x = 1/\sqrt{1-\beta_x^2}$ with the velocity $\beta_x = v_x/c$ normal to the electron sheet. This relativistic electron mirror is expected to allow the reflection of a second laser beam for very brilliant, very intense, coherent X ray and γ beams with many unique applications.
Kulagin et al. [2,3] showed that the produced flat electron sheet stays together for some μm, having energies of $\gamma \approx a$, where a is the dimensionless laser intensity parameter. This γ is different from the $\gamma = 1 + a^2/2$ calculated for a single electron, which probably is to high for a dense electron sheet. We have experimentally observed this production of electron sheets for the first time at the Trident laser in Los Alamos for 500 fs laser pulses [4] and also at the laser of the Max Born Institute in Berlin with their 35 fs laser pulses [5].
If one would reflect optical photons of energy $E_0 = 1$ eV normally from this electron sheet with an energy characterized by γ_x, one naively would expect to obtain reflected γ photons of energy $E_\gamma = 4 \cdot \gamma_x^2 \cdot E_0$. However, Wu et al. [6,7] showed that the electron sheet also acquires a transverse velocity component v_x from the transverse laser E-field. Only later the $\vec{v} \times \vec{B}$ force leads to the dominant forward acceleration. The transverse velocity causes a much smaller Doppler boost of the reflected γ photons of $E_\gamma = 4 \cdot \gamma_x^2 \cdot E_0 = 2 \cdot \gamma \cdot E_0$, where γ is the total γ. However, recently Wu et al. [8] showed that one should place a second foil of about 2 times the skin depth (15 nm) in a 1-2 μm distance behind the first target foil, where the accelerating laser pulse is reflected. The reflected laser pulse completely cancels the transverse velocity component v_x, but basically leaves the longitudinal velocity component unchanged. In this way the originally expected full Doppler boost of the γ photons with $E_\gamma = 4 \cdot \gamma^2 E_0$ is recovered. While the preliminary simulations of Wu et al., [8] are very impressive more realistic ultrathin foils with much larger n_e/n_c for 1nm foils are required. The present simulations correspond to independent individual electrons, while then collective effects like expansion of the foil become important.
We invented a special target design with ultra-thin DLC foils and a very low-density carbon nanotube target as a spacer inbetween, in order to realize such a target for a perfectly reflecting electron sheet. The dense electron sheet then traverses the reflector target and shortly behind the reflector is bombarded with the second laser pulse (split off from the APOLLON-type laser with wavelength λ_0) to produce the γ photons with $\lambda_\gamma = \lambda_0/4\gamma^2$. The thickness d of the electron sheet determines up to which γ energy a coherent reflection occurs. In the inner rest frame of the electron sheet the photons have the wavelength $\lambda_i = \lambda_0/2\gamma$ before reflection. The requirement is $\lambda_i/2 \leq d$. Possibly the electron sheet is compressed during acceleration and also by the interaction with the reflected laser, reducing the thickness d. If we use $d = 1$ nm and $\lambda_0 = 1$ μm and $\gamma = 250$, we obtain reflected γ-photons of ≈ 250 keV. These γ pulses would be coherent and would have a pulse length of a few zeptoseconds. Since we will have about $N \approx 10^9 - 10^{10}$ coherently reflecting electrons, the reflected amplitude is increased by N. If we assume a spot diameter of the reflected laser pulse of 3 μm, we obtain a large reflectivity (1%) and expect due to the energy conservation of the laser accelerated electron sheet $\approx 10^{14}\,\gamma$/shot with $(6\ \mu\text{m})^2$, $(\approx 5$ mrad$)^2$, 10^{-20} s and 0.1 % BW. Thus a rough estimate of the

peak brilliance is 10^{37}/[s (mm mrad)^2 0.1 % BW]. With the APOLLON-type laser we easily can realize $a = 250$, but require in addition a very high contrast of 10^{16} for the survival of ultrathin foils during the prepulse. In this context careful experimental studies have to be performed aiming to characterize potential effects of reflectivity modifications by distortions of the reflecting mirror foil during the laser interaction.
In Ref. [9] we showed that a much larger reflecting force should occur, since the transition from the Lorentz force to the radiation damping force is strongly enhanced. While the Lorentz force scales with charge e, the radiation damping force or Landau-Lifshitz term scales with $(\frac{2}{3}\frac{e^3}{mc^3})$ [10] und thus if N electrons act coherently, the Lorentz force is proportional to N, while the Landau-Lifshitz force scales with N^2 and thus one obtains an acceleration due to radiation damping which is N fold enhanced. Thus 10^2 larger γ-energies may be reflected, reaching energies in the 25 MeV range. Here the ensemble of all electrons reflects like one macro-particle, which then takes up the recoil momentum as a whole. The electron sheet is trapped between the potential of the strongly reflecting laser and the Coulomb potential of the more backward layers of the electron sheet. This binding together of the electrons to a macroparticle is essential to result in a Mössbauer-like reflection scenario. If the Landau-Lifshitz force becomes dominant and higher order terms of the Landau-Lifshitz expansion series become important, even higher orders of N become relevant.
If these coherent intense γ pulses become available, many proposed experiments of ELI-NP with the incoherent γ beam like pair creation from the vacuum or excited multiple nuclear excitons will give orders of magnitude better results. Furthermore pump-probe experiments with two consecutive excitations of nuclei will become possible, which open a new field of studying highly excited states described by random matrix theory [6].

References

[1] D. Habs et al., Appl. Phys. **B 93**, 349 (2008).

[2] V.V. Kulagin et al., Phys. Rev. Lett. **99**, 124801 (2007).

[3] V.V Kulagin et al., Phys. Rev. **E 80** , 016404 (2009).

[4] D. Kiefer et al., Eur. Phys. J. **D 55**, 427 (2009).

[5] D. Kiefer et al., to be published.

[6] H.-C. Wu and J. Meyer-ter-Vehn., Eur. Phys. J. **D 55**, 443 (2009).

[7] J. Meyer-ter-Vehn and H.-C. Wu, Eur. Phys. J. **D 55**, 433 (2009).

[8] H.-C. Wu et al., *Laser-like X-Ray Sources Based on Optical Reflection from Relativistic Electron Mirror*, arXiv:1003.1739v2 (2010).

[9] D. Habs et al., *Proposed studies of radiation damping in laser interaction with an ultra-thin coherently refelcting electron sheet, regarded as a macro-particle*, ,Brasov Romania Conference, AIP1228, 287 (2009).

[10] L.D. Landau and E.M. Lifschitz; *Klassische Feldtheorie*, Volume 2, chapter 76, Verlag Harri Deutsch, 1992.

[11] J.Z. Gu and H.A. Weidenmüller, Nucl. Phys. **A 690**, 382 (2001).

5.2.6 Nuclear Techniques for Characterization of Laser-Induced Radiations

D. Bucurescu[1], Gh. Cata-Danil[1], C. Ivan[1], N. Mărginean[1], F. Negoiţă[1], C.A. Ur[1,2] and N.V. Zamfir[1]
[1] *National Institute for Physics and Nuclear Engineering, Bucharest-Magurele (Romania)*
[2] *Istituto Nazionale di Fisica Nucleare, Sezione di Padova(Italy)*

During the last decade it was experimentally proved that when a high-intensity laser beam hits a target it induces ionization and acceleration processes. Consequently, several kinds of radiations were observed following the irradiation: accelerated electrons, protons and ions arising from the primary ionization and acceleration process, but also neutrons and a very intense gamma flux generated in secondary processes as bremsstrahlung and nuclear reactions. The investigation of laser-based acceleration process and of the radiations generated in this way evolves very fast and there is a stringent need to collect experimental data in a systematic way in order to understand and properly evaluate the potential use of high-intensity lasers for nuclear physics experiments and applications. To be performed efficiently such systematic investigations require dedicated infrastructure and implies significant developments of detection techniques. Inside ELI-NP we propose therefore to adapt and develop modern techniques currently used in nuclear spectroscopy in order to build the detection infrastructure needed for systematic investigation of laser-induced radiations.

General overview

We briefly outline several characteristics of the laser-induced radiations as known in the present:

- Large particle and photon fluxes are produced in a very short (below 1 picosecond) time interval.
- Several kinds of radiations are generated in primary and secondary processes: electrons, protons, heavy ions, X and gamma rays. Each of these is distributed in a specific energy range, strongly depending on the irradiated target and on the power of the laser source.
- The emittance is different for different radiation types, i. e. electrons are better focused and protons or heavier ions have a relatively broad angular distribution.

According to the processes that lead to the generation of these radiations, one can classify them as follows:

Radiations arising from primary processes: These are accelerated electrons, protons and heavier ions, with energies and angular distributions strongly depending on the acceleration scheme, irradiation geometry and target characteristics. The well established acceleration scheme at laser intensities up to 10^{20} W/cm^2 is the so-called *Target Normal Sheath Acceleration* e. g. [1], when the electrons are pushed out from the target, form a negative charge cloud and the ions from the target are accelerated by the electrostatic potential created in this way. TNSA is low-efficiency accelerating mechanism, where the maximum ion energy scales with the square root of the laser intensity. Recently another acceleration mechanism was experimentally evidenced, the *Radiation Pressure Acceleration* [2]. When a nanometer-thick foil is irradiated with circular polarized high intensity laser pulse appears a cold compression of electron sheet followed by the acceleration of ions in the rectified dipole field created between electrons and ions. In this way are created macroscopically neutral bunches of ions and electrons traveling at the same speed. This RPA mechanism is more efficient than TNSA and scales linearly with the laser intensity. At laser intensities of 10^{24} W/cm^2 and higher, the H and He nuclei are expected to enter the relativistic regime, when they will be accelerated directly by the laser as the electrons for laser intensities greater than 10^{18} W/cm^2. The electron energies obtained in the present are up to several hundreds of MeV, while for heavy ions are about several MeV/nucleon and are expected to increase with one-two orders of magnitude at ~ 10 PW, 10^{24} W/cm^2 lasers.

Radiations from secondary processes: Following the interaction of accelerated electrons with matter an intense flux of bremsstrahlung photons is produced. This brilliant gamma flux might further produce photonuclear reactions. In addition, depending on their energy, the nuclei accelerated from the primary target might produce nuclear reactions. All these lead to the emission of a large variety of secondary radiations: neutrons, charged particles and gamma rays.

Taking into account the high instantaneous flux and the relatively low repetition rate specific to the present high-intensity lasers, the well-established event-counting and coincidence techniques from nuclear spectroscopy are very difficult to be applied directly. Instead, simple nuclear spectroscopy techniques as analysis of activated samples or Thomson spectrometers coupled with CR-39 plastic track detectors were used until now. These techniques are not real-time and provide information about the investigated radiation field in minutes or even hours after the irradiation. Recently several experiments e.g. [3] were performed using a microchannel plate (MCP) with phosphorous screen, which provides almost real-time response as track detector. A systematic and efficient investigation of laser-induced radiations requires further optimization of currently used diagnosis techniques and further development of new methods. In nuclear spectroscopy the high-resolution experiments are performed in an event-by-event mode, which means recording into so-called "events" the radiations detected in a time window typically ranging from nanoseconds to microseconds. Obviously the "prompt flash" of radiation produced by a high-power laser beam hitting a target would be recorded as one event, if the detectors were not already overloaded by the intense radiation flux. The event-by-event way to measure is based on accumulating statistics; therefore using it in combination with the low repetition rate of the high power lasers constitutes a challenge for the nuclear spectroscopy technology of present days. The solution is to use state-of-art high granularity detectors, in which case every single detector element will see a reduced flux of radiation and will be active even during the "prompt flash". The granularity might compensate partially also the low repetition rate since there are many elements detecting coincident radiations, and sensible statistics can be obtained in a reasonable amount of time. Several high-granularity detection systems and associated digital electronics are presently used and some others are under development. The scope is to use them to the high intensity and radioactive beam facilities under construction. One example is the European AGATA project, which develops a state-of-art highly segmented HPGe gamma detectors array to be used in sites like FAIR/GSI (Germany) or SPIRAL2/GANIL (France). There is a striking similarity between the experimental conditions expected at FAIR and the ones encountered in working with laser-induced radiations, since in both cases there is a "prompt flash" the detection system must stand, then recover and continue to measure. Thus many ongoing developments in nuclear radiation detector technology will find immediate use in spectroscopic studies with laser-induced radiations.

Spectroscopy of accelerated heavy ions

The main characteristics needed for the understanding of the laser-induced ion acceleration are energy, charge-state and angular distributions as well as their absolute number per pulse. As stated before direct event-counting methods typical for nuclear spectroscopy are very difficult to apply for the detection of the prompt radiation produced by the laser pulse. Thus several alternative techniques must be used, in parallel with an intense R&D activity for the development of faster response, high-resolution spectroscopic methods suitable for the spectroscopy of laser-induced radiations. Presently, for the spectroscopy of laser-accelerated ions several experimental techniques are suitable for use and further development.

Activation techniques: basically consist in placing a stack of thin foils in front of the beam, to be activated by the beam particles. The radioactivity of each foil is measured individually after irradiation, in this way the incident beam intensity can be estimated. The beam energy distribution might be estimated using threshold reactions or from the de-convolution of the number of final reaction products in each foil when the beam energy dependence of the cross section of reaction in which they were produced is reliably known. The activation method is mostly suited for proton beams, where the reactions cross-sections are better known and have well-defined threshold behavior. This method might be further refined using low-background, high-efficiency HPGe spectrometer stations. Besides the optimized shielding for low-background counting, the HPGe detectors can have BGO anti-Compton shields which will reject the Compton scattering background and will improve the peak-to-total ratio, thus the spectrometer sensitivity. The "response time" of the method can be increased using in parallel several counting stations, as it was demonstrated in Ref. [4] where several scintillator were used in parallel. Low-granularity angular distributions can also be obtained if an array of foil stacks is used; in this case the radioactivity per foil will be lower and very efficient counting spectrometers must be used.

Thomson spectrometers: are compact devices using a configuration with parallel static electric and magnetic fields to deviate ions on a parabolic trajectory according to the mass-over-charge ratio and energy. With Thomson spectrometers one can measure the charge-state and energy distributions of the accelerated ions, on the limits defined by the acceptance of the spectrometer and the sensitivity of the detection system. The Thomson spectrometer is normally used coupled with CR-39 plastic track detectors, thus the "response time" of this detection system is long. Being compact devices, arrays of Thomson spectrometers can be used to increase the granularity and to cover a larger solid angle. With proper collimation a Thomson spectrometer might be used for preselecting ions with defined A/q ratio or energy range, which can be further analyzed by large-acceptance magnetic spectrometers with a faster response time for the focal plane detectors.
Scintillation-based techniques with digital image recording: few experimental solutions were already investigated, i.e. the coupling of a Multi-Channel Plate with a phosphorus screen at the exit from an Thomson spectrometer and digital acquisition of the image obtained during the irradiation with heavy ions. An interesting development came very recently from RAL(UK), when the image obtained on very fast plastic scintillator foils at irradiation with laser-accelerated protons was recorded with gated CCD cameras, avoiding in this way the signals by electrons or X-rays [5]. With this detection device were obtained relatively precise angular distributions of protons integrated over several energy ranges defined by the thickness of the scintillation foil. The scintillator-gated CCD camera detection has almost instant response time and can be used continuously for many successive laser shots, being thus a very promising technique.
De-convolution of the pulse shape (proposed development): with a very fast plastic scintillator coupled with a fast phototube one can obtain a well-defined detector signal for one charged particle, signal with few nanoseconds width. When the detector is irradiated with a bunch of ions the output signal can be recorded with a (triggered) high-frequency digitizer. If the temporal dispersion of the ion bunch is larger than the standard one-particle signal width the output signal will have a pulse shape function of the distribution of the ion bunch in time. This temporal dispersion can be obtained with time-of-flight techniques. In this way it will be possible to obtain an estimate of the velocity distribution of the ions inside the bunch from the de-convolution of the digitally recorded pulse shape. The energy distribution of the ions can be thus obtained. This kind of detector is appropriate for the construction of medium granularity arrays with small individual elements, and can provide also information about the angular distribution of the ions. The saturation effects, which might appear when the scintillator is irradiated with high dose, must be taken into account when the detector is designed. Moreover, special geometries with light guides should be investigated in order to prevent the accelerated electrons travelling faster than the ion beam to enter directly in the phototube.
Dispersion magnetic spectrometers with large momentum acceptance and relatively small coverage of the solid angle might become a powerful tool to investigate the energy, charge-state and angular distributions of the ions. The magnetic spectrometer design can be similar to that of existing large-acceptance heavy-ion spectrometers like VAMOS or PRISMA: one quadrupole element to enhance collection followed by a large magnetic dipole for dispersion and a large (1 m) focal plane detection area. The particular conditions for the laser-accelerated ions prevent the use of any start detectors and ion-by-ion counting, thus a small entrance opening of the spectrometer is required and the "start" signal for the time-of-flight must be given by the laser pulse. In the focal plane special detectors should be designed, since more than one ion per pulse will be detected. Digital recording of a scintillation image might be a possibility, with the limitation that the time-of-flight information will be lost. A more suitable solution, which needs technical developments, is based on fast scintillators and de-convolution of digital signals idea described above. A high granularity focal-plane array of fast scintillators can be constructed at reasonable price. With this focal plane detector the "stop" signal for the time-of-flight can be obtained with good resolution, therefore the velocity distribution of the ions will be measured with higher precision. In order to simplify the image obtained in the focal plane, devices like the Thomson spectrometer or a Wien velocity filter might be used.

Spectroscopy of accelerated electrons

Similar with protons and heavier ions, the parameters that must be measured for accelerated electrons are energy and angular distributions as well as the beam intensity. However, not having to

deal with charge-state distribution simplifies the design of electron spectrometers, and the small mass respect to protons allows more compact solutions. Although the techniques used for detection of laser-accelerated electrons are relatively well established, further developments might significantly improve them as well.
Characteristic X-ray tracers, based on the observation of K? lines (typically of Cu) focused in crystals are a powerful tool to measure the angular distribution of electrons with high resolution [6]. This method is however limited, and cannot provide the energy distribution for the electron beam.
it Thomson spectrometers can be used for electrons as well, with the advantages and disadvantages mentioned in the previous section. With these devices one can obtain the energy distribution with moderate resolution and also the beam intensity.
Scintillation foils with triggered CCD camera might be used to detect the angular distribution. As for the X-ray tracers, the information obtained about energy distribution is rather limited.
Magnetic spectrometers based on dispersion are very efficient for measuring the energy distribution of the electrons with high resolution. Typically, in the focal plane are placed track detectors or a phosphor screen imaged on a CCD camera. A possible use of fast scintillators in the focal plane would give also the time-of-flight of the electrons and might further improve the quality of energy measurements.

References

[1] S.C. Wilks et al., Phys. Plasmas **8**, 542 (2001).

[2] A. Henig et al., Phys. Rev. Lett. **103**, 245009, (2009).

[3] H. Schwoerer et al., Nature **439**, 445 (2006).

[4] M.M Aleonard et al., *NATALIE, a multidetector system for activation techniques to characterize laser produced energetic particles,* **ELI Nuclear Physics Workshop**, Bucharest, Feb. 2010, http://eli-np.ro.

[5] J.S. Green et al., CFL Ann. Rep. 2008/2009, p. 311.

[6] B. Ramakrishna et al., CLF Ann. Rep. 2008/2009, p. 34.

5.2.7 Modelling of High-Intensity Laser Interaction with Matter

M. Apostol[1] M. Ganciu[2] L.C. Cune[1] and G. Vaman[1]
[1] *Institute of Physics and Nuclear Engineering, Magurele-Bucharest*
[2] *Institute of Lasers, Plasma and Radiation, Magurele-Bucharest*

One of the most interesting prospects of both fundamental and applied research opened up in 1979, with an important paper by Tajima and Dawson,[1] who suggested that pulses of electrons could be accelerated up to relativistic energies by high-intensity laser beams. In the 1990s this suggestion became reality by a revolutionary technique discovered by Mourou and collaborators,[2] who succeeded in producing such high-intensity lasers. Today, bunches of electrons up to energies in the GeVs range are currently produced by this method, as well as accelerated ions (including heavy ions) and associated intense gamma radiation. Such new tools offer a unique and challenging occasion of both fundamental and applied studies of a large variety of new phenomena, pertaining to both condensed matter physics and nuclear physics, involving mainly the interaction of high-intensity electromagnetic radiation with matter and its constituents. It is the purpose of the present research project to pursue theoretical and experimental studies in this subject, with the general aim of further enhancing our understanding of such complex phenomena. Recently, the present authors developed a new concept regarding the electron acceleration by high-intensity polaritonic laser pulses.[3, 4] The novelty consists in identifying the plasmon and polariton elementary excitations of the electromagnetic field interacting with an ideal plasma, realizing that plasma oscillations, in contrast with polaritons, cannot be propagated with a group velocity, constructing a polaritonic wave packet and highlighting the key control parameters of such an object. According to our preliminary studies, the electrons can be accelerated appreciably in a rarefied plasma, e.g. up to cca 17 MeV for a plasma density $10^{18}\mathrm{cm}^{-3}$. The acceleration energy does not depend on the laser intensity. On the contrary, the number of electrons in the pulse goes like the square root of the laser intensity, and, at the same time, as the 3/2-power of the pulse size. For instance, for a laser intensity $10^{18}\mathrm{W/cm}^2$ and a pulse size 1 mm we may get a number of accelerated electrons as high as 10^{11} per pulse. It is for the first time that the number of electrons in the pulse is computed by a theory which looks consistent. It is also shown that the efficiency process goes like the inverse square root of laser intensity. The 10-pettawatt laser at ELI-NP, Magurele-Bucharest, offers the possibility of testing experimentally such theoretical predictions. We emphasize that the current research in this subject is exclusively based on numerical simulations and modelling, requiring sometimes huge computational resources, like 500 state-of-the-art processors running continuously for 2 years,[5] in contrast with our theory which is practically entirely analytic.

Specifically, our first goal is to test the dependence of the electron flux on the laser intensity and pulse size in the range $10^{18}\mathrm{W/cm}^2$, size 1 mm to $10^{22}\mathrm{W/cm}^2$, size ∼10microns. The second goal is to test the acceleration energy over a wide range of plasma densities, from $10^{17}\mathrm{cm}^{-3}$ to $10^{21}\mathrm{cm}^{-3}$. These two goals will be achieved by a typical experiment of electron acceleration by laser pulses, involving, in particular, the focusing on various regions of an inhomogeneous plasma (created by usual ultrasonic nozzles), increasing the plasma density by applying high pressure (up to 100 torr), and measuring the electron energy by usual techniques of stopping power in thin metallic foils[6]. The general experimental approach will follow closely the one employed in Ref. [7]. Detailed specifications of the experiment will be shortly presented. The third goal pertains to further theoretical studies, regarding both the refinement of the present theoretical model and its extension to higher plasma densities, acceleration of injected electrons, destabilization of the pulse by a second laser pulse, characterization of the wake field by reflection and refraction of a laser beam, as well as the role of the polaritonic pulses in the mechanism of "collective" acceleration of ions in thin foils (the usual mechanism of light pressure).

The research in the polaritonic pulse as described above is the first main theme of the present project. Its second theme regards the highly-interesting question of whether a gamma-ray laser could be possible. As it is well-known, this idea was pursued both theoretically and experimentally by many groups of researchers all around the world, without success yet, or with controversial, ambiguous results. It seems that the current consensus is that such a process would in fact be impossible, though, however, the convincing reason and motivation are still missing.

Recently, a new idea emerged, of coupling a two-level nuclear system (for instance a giant resonance) with the bremsstrahlung gamma (or X-ray) radiation produced by fast electrons accelerated by high-

intensity laser pulses[8]. This may raise hope for an efficient pumping, and may give a new impetus to the research in the field. Consequently, it is the second theme of the present project to pursue studies, both experimental and theoretical, in this matter. Such studies are essentially based on the previous experience of the authors in, on one hand, creating directional sources of high-intensity X-rays by the cruise effect of accelerated electrons conducted over the surface of dielectric fibres,[8] and, on the other hand, theoretical studies of coherent interaction of matter with electromagnetic field.[9] A superradiance transition was shown to occur in polarizable matter coupled with electromagnetic radiation, provided a certain critical condition imposed upon the strength of the coupling is fulfilled. While in some special cases of atomic matter such a transition may indeed occur, in a nuclear two-level system it is beyond any hope. However, in the presence of a sufficiently high external field, the coherent interaction may, in principle, lead to a lasing effect.

The fourth goal of the present research project is to analyze the mechanism of the coherent lasing effect and to provide numerical estimates for a possible gamma-ray (or X-ray) laser. Such estimations will be corroborated with the results of the fifth goal of the project, which consists in experimental characterizaton of the cruise effect with highly-energetic electrons provided by the high-intensity laser and their production of X- and, possibly, gamma rays. Apart from a basic advance in fundamental knowledge, we hope that such a combined research may help in settling the question of the possibility of a gamma-ray laser.

References

[1] T. Tajima and J. M. Dawson, Phys. Rev. Lett. 43 267 (1979).

[2] G. Mourou et al, Revs. Mod. Phys. 78 309 (2006).

[3] M. Apostol and M. Ganciu, J. Theor. Phys. 186 1 (2010).

[4] M. Apostol, Seminar, Institute of Atomic Physics, April 8, 2010, http://www.ifa-mg.ro/

[5] See, for instance, S. F. Martins et al, Nature Physics 6 311 (2010).

[6] M. Ganciu, Seminar, Institute of Atomic Physics, May 6, 2010, http://www.ifa-mg.ro/

[7] A. Giulietti et al, Phys. Rev. Lett. 101 105002 (2008).

[8] See, for instance, M. Ganciu, Final Report, Contract F61775-00-WE061, September 2001 (http://handle.dtic.mil/100.2/ADA398179), and M. Ganciu, Seminar, Institute of Atomic Physics, May 20, 2010, http://www.ifa-mg.ro/

[9] M. Apostol, Phys. Lett. A373 379 (2009).

[10] M. Apostol, Seminar, Institute of Atomic Physics, May 13, 2010, http://www.ifa-mg.ro/

5.2.8 Studies of enhanced decay of ^{26}Al in hot plasma environments

K.-M. Spohr[1,2], S.D. Pain[1,2], K.W.D. Ledingham[1,3,4], S. Brien[1,2],
R. Chapman[1,2], M. Hassan[1,2] J. Melone[1,3], J.F. Smith[1,2]
[1] *Scottish Universities Physics Alliance, SUPA,*
[2] *Faculty of Engineering and Science, University of the West of Scotland, Paisley, PA1 2BE, United Kingdom*
[3] *Department of Physics, University of Strathclyde, Glasgow, G4 0NG, United Kingdom*
[4] *AWE, Aldermaston, Reading, Berkshire, RG7 4PR, United Kingdom*

Properties of unstable nuclei which play a key role in explosive stellar environments have been the paramount interest of astrophysical nuclear research since its emergence more than 50 years ago [1]. With the projected ELI intensities, a new world of possibilities opens up to study their behavior for the first time under the extreme temperature and pressure conditions present in the inner cores of planets and stars. The quest to study nuclear astrophysics with ELI should focus on the most prominent puzzling systems. Hence the SUPA collaboration proposes to study the possible enhancement of the decay of the long-lived ^{26}Al radioisotope in astrophysical environments with ELI. This endeavor would be a complementary effort to already established successful experimental research projects of current SUPA physicists (S.D. Pain) at the Holifield Radioactive Ion Beam Facility at Oak Ridge.
The γ-ray mapping of the ^{26}Al decay across the galaxy provides one of the most interesting constraints on nuclear physics parameters in astrophysical environments. The ^{26}Al nucleus was the first radioisotope detected in the interstellar medium, by the observation of the characteristic 1809 keV γ-emission associated with the decay of its ground state [2]. As the half life ^{26gs}Al (5^+) state is 7.2×10^5 years, the presence of this nucleus provides evidence of ongoing galactic nucleosynthesis. Wolf-Rayet stars and Asymptotic Giant Branch (AGB) stars and novae [3] have been suggested as possible sources of the origin of ^{26}Al. At a temperature of T=0.03 GK, the ^{26gs}Al(p,γ)^{27}Si reaction is expected to be the main destruction mechanism for the ^{26}Al isotope. However, at these hot stellar temperatures, the dominant contribution to the ^{26gs}Al(p,γ)^{27}Si reaction rate is capture through low-lying resonances, for which the strengths have not been measured and an experimental benchmarking of theoretical studies, such as Hauser-Feshbach based calculations [4], remains elusive. The disintegration process of ^{26}Al is further intricated by the presence of a 0^+ isomer at 228 keV above the ground state. This isomer which originates like the ground state from the coupling of the two unpaired nucleons in the odd-odd ^{26}Al system, is prohibited to decay into ^{26gs}Al due to the large spin difference.^{26m}Al decays via β^+ emission with $T_{1/2} = 6.35$ s directly to ^{26gs}Mg (0^+). This is a very specific and complicated scenario. Equilibration between ^{26gs}Al and ^{26m}Al can only proceed via the coupling through a sequence of intermediate states (IS), for which no branching ratios are experimental established.
Theoretical work [5] based on shell-model calculations predicts the a dramatic reduction of the effective life time τ_{eff}(^{26gs}Al) by a factor of 10^9 within the temperature range from 0.15 to 0.4 GK, superseding previous estimates by Ward and Fowler [6] by orders of magnitude. This significant decrement of τ_{eff} is due to a variety of physical processes triggered and influenced by hot plasma environments which will gradually become accessible with the emerging ELI project. At high densities the increasing Fermi energy of the electron opens up electron capture channels otherwise energetically forbidden. Moreover, hot bremsstrahlung radiation will lead to an enhancement of the coupling of ground and isomeric state via the manifold of known as well as hitherto unresolved IS at several MeV where the nuclear level density is high. The population of these states and thus their contribution to the true astrophysical disintegration rate, will reflect an overlap of Boltzmann distributions from ground *and* excited state in the hot and dense environmental conditions provided [7]. The ELI laser system will deliver energetic particle and radiation bursts of sufficient intensity to create planet and stellar-like environmental conditions. Most importantly these radiation pulses are ultrashort in time and synchronous, thus providing ideal conditions for an 'astrophysical laboratory' capable of resolving *ps* time scales. In a first instance, we want to expose a miniature ^{26}Al target specimen to an isochorically heated environment with ELI. Work by Patel *et al.* shows that isochorical heating by laser induced thermally distributed proton beams with end-energies of only a few MeV can be used to create very localised ($\oslash$=50μm) high energy-density plasma states [8]. In this study a 'modest'

10 J, 100 fs high intensity laser system was able to produce several tens of eV within the ps time domain. The ELI system, even in the first phase, will be able to surpass this values by several orders of magnitude, especially once the onset of the pressure dominant acceleration regime is established as predicted by Esirkepov [9]. For increasing laser intensity the electromagnetic field will eventually start to directly interact with the nucleus, thus presumably contributing further to an enhancement of the decay probability. In all instances the spatial confiment of particles and radiation emerging from laser acceleration will help this particular investigation tremendously. The isotope ^{26}Al is only available in minute quantities, which will just allow the production of miniature pellet targets or thin layers on backing or radiator materials. The onset of an enhanced transition rate and the coupling of ground and isomeric state via IS can be deciphered via the 511 keV annihilation radiation following the β^+ decay of ^{26m}Al. The coincident 511 keV photons are measurable with semiconductor or scintillation detector systems and would exhibit a characteristic temporal behaviour with $T_{1/2} = 6.35$ s. Ideally, a fast target transportation would need to be developed to retrieve the target probe from the interaction zone after irradiation.

We are aware of the many conceptual and technical aspects that need to be addressed prior to such an experimental engagement with ELI. Most importantly, once ELI parameters are firmly established, precise yield estimates have to be undertaken. Furthermore we have to consider the reaction yield for the ^{26}Al(γ,n)^{25}Al channel with $S_n(^{26}\mathrm{Al})$=11.4 MeV which also causes the emergence of 511 keV annihilation radiation with $T_{1/2}$=7.18 s, as ^{25}Al is a β^+ emitter. This suggests e.g. the use of neutron detectors for discrimination. Moreover, as the decay of ^{25}Al also produces a coincident 1612 keV γ-ray with low branching, intensity measurements with a high resolution germanium detector will allow to estimate the background contribution from this intruding reaction channel. To achieve isochorical heating, a series of conceptual studies have to be performed to derive an ideal setup for the miniature aluminum targets, which will include fabrication, alignment and the encapsulation of the tiny probes. Additionally, as particle reaction channel yields have to be estimated, Hauser-Feshbach calculations have to be performed for increasing temperatures [10]. Besides theoretical codes, GEANT4, SRIM [11] and LASNEX [12] simulations need to be undertaken. Furthermore there may be a need to development of a special target chamber due to the radioactivity of the target probe. We also propose to implement prima facie experiments on bulk targets of stable isotopes that have a low-lying isomeric states with similar life-times as proof of concept studies (e.g. ^{107,109}Ag). Results will be first and foremost interpreted in light of the theoretical evaluations shown in [5]. The study of ^{26}Al could become a benchmark experiment as it would manifest ELI as a novel accelerator system, providing environments of astrophysical interest. It will align and allow a further development of existing projects with radioactive beam facilities that will deliver a lot of interesting results for nuclei of pronounced astrophysical interest in the next years.

References

[1] Burbidge E.M, Burbidge G.R., Fowler W.A. and Hoyle F., Rev Mod Phy **29**, 547, 1957

[2] Mahoney, W.A., *et al.*, Astrophys. J. **286**, 578, 1984.

[3] Prantzos, N. and Diehls R., *et al.*, Phys. Rep. **267**, 1, 1996.

[4] Hauser, W. and Feshbach H., Phys. Rev. **87**, 366, 1952.

[5] Coc A. *et al.*, Phys. Rev. C **61**, 015801, 1999.

[6] Ward, R.A. and Fowler W.A., Astrophys. J. **238**, 266, 1980.

[7] Utsunomiya, H *et al.* Nucl. Phys. A **777**, 459, 2006.

[8] Patel P.K. *et al.*, Phys. Rev. Lett. **91**, 125004, 2003.

[9] Esirkepov T. *et al.*, Phys. Rev. Lett. **92**, 175003, 2004.

[10] Rauscher T. *et al.*, arXiv:astro-ph/9609012v1, 1996.

[11] Biersack J.P. and Haggmark L., Nucl. Instr. and Meth. **174**, 257, 1980.

[12] Zimmermann, G.B. and Kruer W.L., Phys. Controlled Fusion **2**, 51, 1975.

5.2.9 Nuclear phases and symmetries

A. A. Răduţă[1,2]
[1)] *Institute of Physics and Nuclear Engineering, Bucharest, POB MG6, Romania*
[2)] *Academy of Romanian Scientists, 54 Splaiul Independentei, Bucharest 050094, Romania*

Nuclear clusters

The laser beam of ELI carries a huge amount of energy and therefore it is expected that nuclei loose their identity being melt into a nucleonic plasma. Such a scenario reminds us the way metallic clusters are prepared, the melting process being followed by an adiabatic cooling which result in obtaining a cluster of atoms characterized by an inter-atomic distance larger than that of molecules and smaller than that of a compound system. This field, although very old (in Middle Eve the coloured glass was prepared by inserting clusters of metals in the melted glass) [1-3], was developed very rapidly since 1985 when Knight [4] discovered a shell structure for spherical clusters. Using the mean field approach theoretical methods were formulated also for deformed clusters [5-8]. Actually the studies on atomic clusters may be considered precursors of nanoscience which put much emphasis on the possible technological consequences. Similarly, one could expect that cooling the nuclear system a cluster could show up. The idea of nuclear clusters was advanced long time ago by Broomley and Greiner's group in connection with nuclear molecules. Nuclear molecules, in their model, are formed out for a very short time in a heavy ion collision [9].

Superheavy nuclei

Since Mendeleev invented the Periodic Table people searched for new elements. Nowadays the elements to be discovered are supposed to be short lived nuclei and most probable to be with Z close to the stability islands. Where is that stability island is established by theoretical models describing the binding energy as function of Z. The first calculations predicted Z=114 and several years later a more realistic calculation suggested Z=118 to be the magic number for protons. The difficulties in achieving a superheavy element consists in choosing the most suitable pair of projectile and target nuclei. That happens because a composite system with Z=Z1+Z2 is characterized by a high Coulombian barrier and therefore requires a large bombarding energy. On the other hand at such a high energy the channel of neutron evaporation is open. If the Coulombian barrier is diminished by heating the two components of the superheavy nucleus, one may have a chance to get superheavy elements by overcoming the difficulties raised by the barrier.

Superdense nuclear matter

Another way of diversifying the microscopic world is to study a given nucleus in extreme conditions such as a superdense metastable state. Long time ago, in a collaboration with Giu Do Dang (Orsay) [10], we calculated the energy of 12C as a function of nucleon density using Skyrme interactions and an alternative layer structure for nucleons in a spherical shell model states. To our surprise we found out that this function exhibits two minima, the superdense one being situated at about 30 MeV above the ground state. The secondary minimum is determined by the tensorial forces between two consecutive layers. Identifying with ELI a superdense state of a heavy nucleus would be a major contribution to the field of nuclear structure and nucleon-nucleon interaction.

Nuclear properties measured in the domain of low energy are associated to the so called cold nuclei. However nuclei might be heated in the process of a relativistic heavy ion collisions [11,12]. With the Eli device the nuclei are heated by the laser beam. Many properties of the heated system are modified by increasing the temperature. Here is a short list of them: nuclear density, the compressibility, the nucleon binding energy, the position and the width of the giant resonances, the decaying properties of the nuclear levels. All these features could be studied experimentally with Eli.

It is interesting to remark that in the traditional experiments the nuclear levels are excited, for example, by Coulomb interaction of the projectile and the target. This suggests that a coincidence experiment of a laser beam and a hevy ion collision allow us to study the temperature dependence of the nuclear collective levels. In this way one could see whether the symmetries of the could system are preserved or violated.

Parity Violation

Aiming at solving the $\tau - \theta$ puzzle T. D Lee and C. N. Yang [11] advanced the hypothesis that parity is not conserved by weak interactions. This idea was confirmed by the famous experiment of Wu et al [12]. In this experiment the electrons resulting from the decay

$$^{60}Co \rightarrow ^{60} Ni + e^{-} + \tilde{\nu} \tag{1.7}$$

were recorded.In this experiment the nuclei of Co were kept at a very low temperature (0.1K) and placed in an intense magnetic field. The ground state of Co is 5^{+} while that of Ni is 4^{+}.Since the transition is changing the spin with a unity it is of Gamow- Teller type. Moreover the transition is an allowed transition. At a space reflection transformation the nuclear angular momentum (an axial vector) and magnetic field do not change while the spin and the direction of electron and neutrinos motion are changed. If the process is invariant to the space reflection, the number of electrons emitted to the direction of the nuclear angular momentum would be equal to the number of electrons emitted in the opposite direction. The result was that electrons were emitted predilectly to the direction opposite to the nuclear angular momentum. The conclusion was that the electron helicity is negative. The linear momentum conservation requires that the anti-neutrino has the right hand helicity. The final conclusion was that parity is not conserved during the beta decay.

Parity is a symmetry which is met everywhere. For example an axially deformed nucleus has a parity symmetry while an octupole deformed nucleus does not exhibit a parity symmetry. Indeed, there exists no point O in space, with the property that the image of an arbitrary point of the nuclear surface, with respect to O, is a point belonging also to the nuclear surface. We say that such a surface emerges from a quadrupole deformed nucleus by a spontaneous breaking of the space reflection symmetry. Since any symmetry breaking is associated to a new nuclear phase one expects that nuclei with octupole deformation exhibit new properties [15,16]. Coming back to beta decay, the electroweak interaction may change a right handed component into a left handed component for neutrino. At ELI one could prepare nuclei with large neutron excess and having an octupole deformed shape. Due to the neutron excess such nuclei are unstable due to their β^{-} decay [17-19]. Since the mean field of the single nucleon motion has not a good parity symmetry one expects that the asymmetry in the beta decay rate for octupole deformed nuclei is particularly large.

References

[1] W. A. Heer, Rev. Mod. Phys. 65 (1993) 611.

[2] M. Brack, Rev. Mod. Phys. 65 (1993) 677.

[3] Vitaly V. Kresin, Physics Reports 220 (1992) 1.

[4] K. Knight et al., Phys. Rev. Lett. 52 (1984) 2141.

[5] K. Clemenger, Phys. Rev. B32 (1985) 1359.

[6] A. A. Raduta, Ad. R. Raduta and Al. H. Raduta, Phys. Rev. B 59 (1999) 8209.

[7] A. A. Raduta, E. Garrido and E. Moya de Guerra, Eur. Phys. Jour. D 15 (2001) 65.

[8] A. A. Raduta, R. Budaca and. Al. H. Raduta, Phys. Rev. A 79 (2009) 023202.

[9] W. Greiner, J. Y. Park and W. Scheid, Nuclear Molecules, World Scientific, 1995.

[10] Giu Do Dang and A. A. Raduta, J. Physique, Letters, 41 (1980) 585.

[11] D. Spencer, Il Nuovo Cimento, Vol. 105 A, No 1 (1992) 47.

[12] W. Greiner, H. Stocker, Scientific American (ISSN0036-8733) vol. 252 (1985) 76-82,84,86,87.

[13] T. D. Lee, C. N. Yang, Phys. Rev. 104 (1956) 254.

[14] C. S. Wu, et al., Phys. Rev. 105 (1957) 1413.

[15] A. A. Raduta, Al. H. Raduta and C. M. Raduta, Phys. Rev. C 74 (2006) 044312.

[16] A. A. Raduta and C. M. Raduta and A. Faessler, Phys. Rev. C 80 (2009) 044327.

[17] A. A. Raduta et al., Phys. Rev. C69 (2004) 064321.

[18] A. A. Raduta et al., Phys. Rev. C 71 (2005) 034317.

[19] A. A. Raduta and C. M. Raduta, Phys. Lett. B 647 (2007) 171.

5.3 APOLLON-Type Laser + γ/e^- Beam

All experiments listed in this subsection require laser intensity of $10^{24}\,\mathrm{W/cm^2}$, except the streaking technique to measure nuclear lifetimes, where the time-definition of the laser pulse is a critical parameter. Combining the high-intensity laser system with the gamma beam represent a big technical challenge for the project, considering both the spatial overlap of the beams and their temporal synchronization.

5.3.1 Probing the Pair Creation from the Vacuum in the Focus of Strong Electrical Fields with a High Energy γ Beam

R. Schützhold[1]. H. Gies[2], G. Paulus[2], C. Harvey[4], A. Ilderton[4], T. Heinzl[4], D. Habs[3], M. Gross[3] and P. G. Thirolf[3]
[1] *University Duisburg-Essen,, Duisburg (Germany),*
[2] *Friedrich Schiller Universität, Jena (Germany),*
[3] *Ludwig Maximilians University, Munich (Germany),*
[4] *University of Plymouth, Plymouth, PL4 8AA (UK)*

The experiments will allow for a new experimental window into the largely unexplored domain of nonperturbative quantum electrodynamics (QED). This has implications not just for QED, but also for fundamental issues in quantum field theory, as well as nuclear, atomic, plasma, gravitational and astro-physics. Whereas there are impressive confirmations of the precision of perturbative QED, we know very little about the nonperturbative regime of QED, arising in ultra-strong external fields.
The long-standing spectacular prediction of spontaneous decay of the vacuum in terms of Schwinger pair production, i.e., production of electron-positron pairs, in strong electric fields exists already since the early days of quantum field theory [1–3]. Based on constant-field calculations, this break-down of the vacuum is expected to occur near a critical field strength $E \sim E_{cr} = m^2c^3/(e\hbar) \simeq 1.3 \times 10^{16} V/cm$. The rate of pair creation is given by:

$$R_{e^+e^-} = \frac{e^2E^2}{4\pi^3} \sum_{n=1}^{\infty} \frac{1}{n^2} exp(-n\pi \frac{E_{cr}}{E}) \tag{1.8}$$

The critical intensity $I_{cr} = 4.3 \cdot 10^{29}\mathrm{W/cm^2}$ is still orders of magnitude beyond upcoming future laser capacities.
Recent new theoretical ideas suggest that lasers such as those planned for ELI may be able to reach this elusive and exponentially suppressed nonperturbative regime. The Schwinger mechanism can be *dynamically assisted* [4] by superimposing a strong electric field with a weak but rapidly varying field. Thereby, it is possible to enhance significantly the pair creation rate, as the effective spectral gap between the electron states and the Dirac sea, i.e., the relativistic tunneling barrier, is decreased. A realistic experimental scenario is given by a new catalysis mechanism for Schwinger pair production [5], where a strongly focused optical laser pulse in a purely electric standing wave mode is superimposed by a plane-wave γ-ray probe beam. This superposition leads to a dramatic enhancement of the expected yield of e^+e^- pairs, and brings the vacuum pair production effect significantly closer to the observable regime.
While in Ref. [4,5] only probe γ beams up to 1 MeV have been discussed, Baier and Katkov recently gave a comprehensive overview in pair creation in constant electric field reaching up to 10 GeV for the γ beams [8]. The basic results for such high energy γ beams where even obtained in 1968 by N.B. Naroshny [9]. The dominant exponential dependance of the rate of pair creation in a field with field strength E and incoherent γ beam photons of high energy $\hbar\omega$ is given by:

$$R_{e^+e^-} \propto exp(-\frac{8}{3} \frac{E_{cr}}{E} \frac{mc^2}{\hbar\omega}) \tag{1.9}$$

The equations shows that for a 100 MeV γ quantum the pair creation is similar to Schwingers formular with a 200 fold increased E-field. The formular again corresponds to exponentially suppressed nonperturbative regime. The expoments in the equations depend on the two Lorentz invariant quantities

f=$e^2F^2_{\mu,\nu}/2m^4$ and $\kappa = [e^2(k_\mu F_{\mu,\nu})^2]^{1/2}/m^3$, where $F_{\mu,\nu}$ is the electromagnetic field tensor of the laser and k_μ is the 4-momentum of the high energy photons.
Figure 24 shows the number of pairs produced by an incident high-energy photon, traversing a strong electric field of 1μ length, as a function of incoming photon frequency ω during one day of operation. The strong field is assumed to be produced in a standing-wave mode of a focussed laser beam at an intensity of $I = 10^{24}W/cm^2$. The two curves correspond to two sets of parameters: 10^{13} high-energy photons per pulse with 1 shot per minute repetition rate (blue curve), and 10^{15} high-energy photons per pulse with 100 kHz repetition rate (purple curve). We observe that the threshold of 1 pair per day is crossed right near $\omega \simeq 10 \ldots 20$MeV. Beyond this threshold, i.e. for higher photon frequency or higher field strength, pair production increases exponentially as is characteristic for a nonperturbative phenomenon.

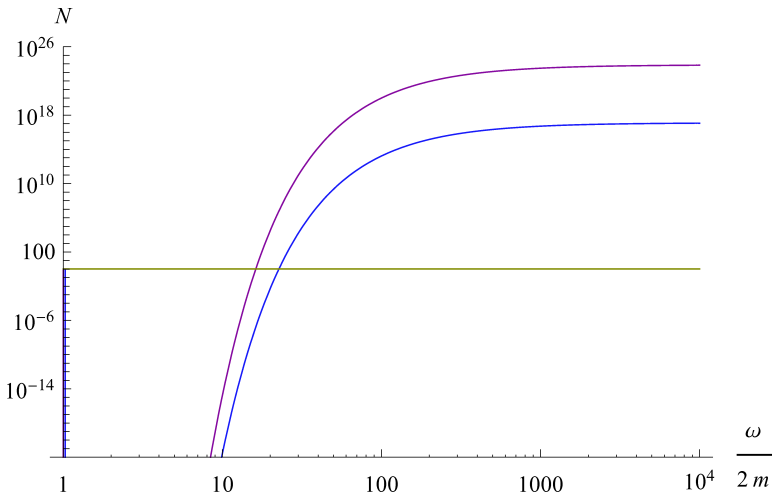

Figure 24: Number of pairs produced by an incident high-energy photon of frequency ω, traversing a strong electric field of 1μ length, during one day of operation. The strong field corresponds to a laser intensity of $I = 10^{24}W/cm^2$. Parameter sets: 10^{13} high-energy photons per pulse with 1 shot per minute repetition rate (blue curve), and 10^{15} high-energy photons per pulse with 100 kHz repetition rate (purple curve).

This prediction has been confirmed with very different theoretical methods [6, 7], pointing towards a close conceptual connection between Schwinger pair production, Hawking radiation of black holes and the decay of metastable strings.
The proposal of a catalyzed Schwinger mechanism on the one hand introduces a strong amplification mechanism for pair production by a tunnel barrier suppression, but on the other hand fully preserves the nonperturbative character of the Schwinger mechanism. Its experimental discovery has the potential to open up an entirely new domain in the parameter space of quantum field theories, with the prospect of further fundamental discoveries as well as practical applications.

The tremendous increase in catalytic pair creation by about 35 orders of magnitude when going from 10 MeV to 100 MeV γ quanta shows that we should produce a γ beam up to 100 MeV by using surface harmonic for the linear Compton backscattering γ facility. The 10. harmonic compared to the first harmonic has a $\approx 10^3$ times reduced yield, but is overwelmed by the factor of $\approx 10^{35}$ for pair production. Thus high flux, very high energy γ with small emittance have to be optimized. The single shot laser for the γ ray generation first produces high harmonics, which then are Doppler boosted in energy via the relativistic electron bunch. Apparently for the very high energy γ-quanta $\approx$ 100MeV one quantum produces several e^+e^- pairs in the APOLLON-type laser focus and we can study this production in detail as a function of the energy of the γ quanta and the intensity in the laser focus and will not have counting rate problems. For the detection of the e^+e^- pairs we need magnetic spectrometers with good acceptance angle, where the electric laser field boosts the energies of the electrons and positrons to about 1 GeV.

Once such an electron-positron pair is produced, it may be possible that these electrons and positrons get accelerated in the laser focus that much, that cascades of pairs develop, which drastically change the signal for detection of pair creation by cascading. If on the other hand a single electron can induce such cascades of pairs, one has to be more concerned about background reactions e.g. from imperfect vacuum conditions, and optimizing the vacuum in the laser focus will become a serious experimental issue. Thus finally it may even be advantageous to perform catalytic pair creation under conditions, where a single slow electron cannot induce these cascades of pairs – the sparking of the vacuum – to suppress contributions from insufficient vacuum conditions. While A.R. Bell and J.G. Kirk [15] predict cascades of pairs already for 10^{24}W/cm^2, Ruhl et al. in dedicated numerical simulations expect this only for higher intensities (see chapt.6.3). It may be a large advantage if the focused laser or the high energy γ beam do not produce cascades of positron electron pairs from a single slow electron or positrons but the pair creation only shows up in their joint action.

References

[1] F. Sauter, "Über das Verhalten eines Elektrons im homogenen elektrischen Feld nach der relativistischen Theorie Diracs," Z. Phys. **69**, 742 (1931).

[2] W. Heisenberg and H. Euler, "Consequences of Dirac's Theory of Positrons", Z. Phys. **98**, 714 (1936); English translation at arXiv:physics/0605038.

[3] J. Schwinger, "On gauge invariance and vacuum polarization", Phys. Rev. **82** (1951) 664.

[4] R. Schützhold, H. Gies and G. Dunne, Phys. Rev. Lett. **101**, 130404 (2008) [arXiv:0807.0754 [hep-th]].

[5] G. V. Dunne, H. Gies and R. Schützhold, Phys. Rev. D **80**, 111301 (2009) [arXiv:0908.0948 [hep-ph]].

[6] A. Monin and M. B. Voloshin, Phys. Rev. D **81**, 025001 (2010) [arXiv:0910.4762 [hep-th]].

[7] A. Monin and M. B. Voloshin, arXiv:1001.3354 [hep-th].

[8] V. N. Baier and V. M. Katkov, arXiv:0912.5250 [hep-ph].

[9] N.B. Narozhny, Zh. Eksp. Teo. Fiz. **54**, 676 (1968).

[10] A. R. Bell and J. G. Kirk, Phys. Rev. Lett. **101**, 200403 (2008); J. G. Kirk, A. R. Bell and I. Arka, arXiv:0905.0987 [hep-ph].

5.3.2 The Real Part of the Index of Refraction of the Vacuum in High Fields: Vacuum Birefringence

C. Harvey[1], A. Ilderton[1], T. Heinzl[1], M. Marklund[2], D. Habs[3] and P. G. Thirolf[3]
[1] *University of Plymouth, Plymouth, PL4 8AA (UK)*
[2] *University of Umea, SE-901 87 Umea (Sweden)*
[3] *Ludwig Maximilians University, Munich (Germany),*

In ultra-high laser fields the vacuum shows a changed index of refraction, where the imaginary part corresponds to the electron positron pair creation (discussed in the preceeding proposal) and the real part results in a birefingence for light traversing the laser focus. Both quantities are related by a Kramers-Kronig relation [1] to the same integal of the polarisation tensor. Thus again we learn something about nonperturbative QED, however the measurement of the birefringence appears more difficult and the production of positron electron pairs for the imaginary part is a very unique signature. The polarized vacuum acts as a medium with preferred directions dictated by the external fields which we assume to be generated by a high-power laser of frequency ω. Accordingly, there are two different refractive indices for electromagnetic probe beams of different polarization states. These are

$$n_\pm = 1 + \frac{\alpha\epsilon^2}{45\pi}\left\{11 \pm 3 + O(\epsilon^2\nu'^2)\right\}\left\{1 + O(\alpha\epsilon^2)\right\} \ , \tag{1.10}$$

to the lowest order in (dimensionless) laser intensity $\epsilon^2 \equiv E^2/E_{cr}^2 = (a_0\nu)^2$ and probe frequency $\nu' = \omega'/m$. Note the frequency dependence in terms of the product $\epsilon\nu'$ which is essentially the Lorentz invariant $\kappa \equiv e\sqrt{(F^{\mu\nu}k'_\nu)^2}/m^3 = 2\epsilon\nu'$. Adopting an optimal value of $a_0 \simeq 5\times 10^2$ corresponding to an intensity of 10^{24} W/cm^2 and an X-ray probe of $\omega' = 500$ keV, one may achieve values as high as $\epsilon \simeq 10^{-3}$ and $\nu' \simeq 10^0$.
The experimental proposal [5] is to send a linearly polarized probe beam of sufficiently large frequency ω' into a high-intensity region of extension d generated by one laser beam (or two counter-propagating laser beams) and measure the ellipticity signal, $\delta^2 \sim \nu'^2(n_+ - n_-)^2$ caused by a phase retardation of one of the polarization directions, see Fig. 25.

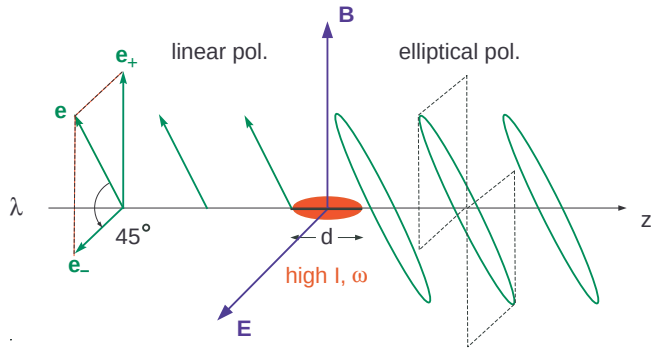

Figure 25: Schematic experimental setup to measure vacuum birefringence via an ellipticity signal.

To the leading order in probe frequency ν' and intensity parameter a_0^2, assuming a laser photon energy $\omega = 1$ eV, one finds a signal of size

$$\delta^2 = 1.1\times 10^{-17}\left(\frac{d}{\mu\mathrm{m}}\,a_0^2\,\nu'\right)^2 \tag{1.11}$$

which grows quadratically with the dimensionless parameters ν' and a_0^2 as well as the spot size d (taken to be the Rayleigh length). For ELI one expects a maximal value of $\delta^2 \simeq 10^{-4}$, assuming $\nu' = 10^0$, $a_0 = 5\times 10^2$ and $d = 10$ μm. γ ray polarimetry via NRF should be sensitive to ellipticities of about 10^{-4}. So one indeed requires intensities in the upper range of ELI specifications (10^{24} W/cm^2). However, the situation changes if one could produce polarized photon beams of MeV energies. Then

the signal should increase significantly (with an expansion in $\epsilon\nu' = O(1)$ no longer possible). In this case one becomes sensitive to the frequency dependence of the refractive indices in a regime where a Kramers-Kronig relation is expected between real and imaginary parts, the presence of the latter being tied to anomalous dispersion, $\partial n/\partial\nu' < 0$ [**?**]. This would be an alternative signal for vacuum pair production,see Fig. 26.

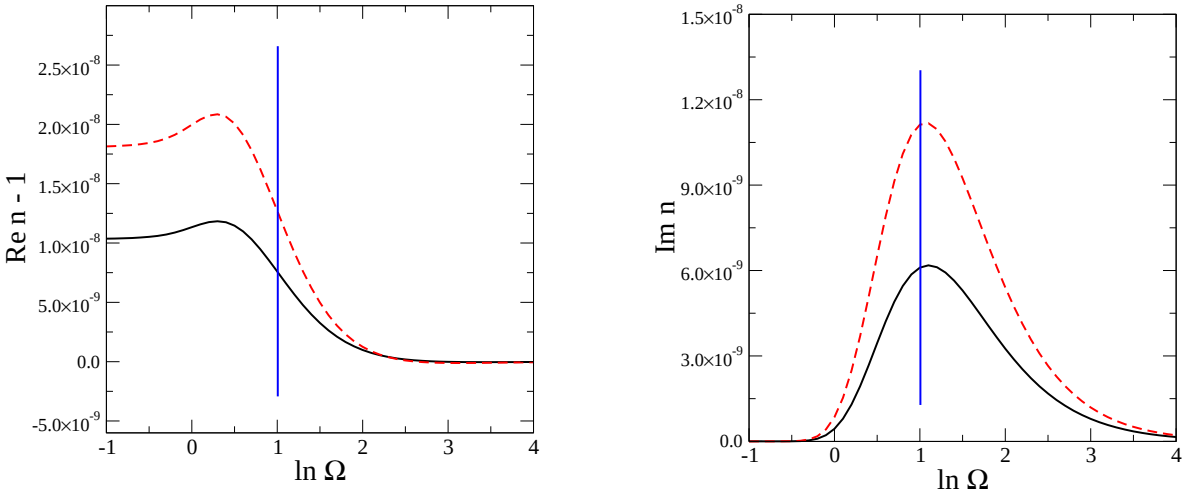

Figure 26: Real and imaginary parts of the QED refractive indices as a function of $\ln\Omega \equiv \ln\epsilon\nu'$. Dashed line: n_+, full line: n_-, vertical line: $\ln\Omega = 1$, achieved for 2 eV photons backscattered off 1.5 GeV electrons.

The requirements on the incoherent γ beam in these two experiments on the refractive index of the vacuum are very different, but also indicate the requirements for other experiments which intend to use the very high fields in the focus of APOLLON-type laser. For an optimized positron production we just require the most intense γ beam and do not critically care about the energy spread. In the second study of the quantum vacuum we want to measure the birefringence of the vacuum by the small turn of the linear polarisation of the γ beam, which we can measure very sensitively using NRF. Thus here we need a γ beam with a rather good energy resolution and we have to observe the modification of the pronounced minimum in the angular distribution of the $0^+ \to 1^- \to 0^+$ cascade. Perhabs in the future another phase sensitive or phase velocity sensitive method can be found, which is less stringent on the γ beam energy.

References

[1] J.D. Jackson; *Classical Electrodynamics*, Third edit., John Wiley, chapt 7.10 (2001).

[2] T. Heinzl, A. Ilderton and M. Marklund, arXiv:1002.4018.

[3] J. Toll, (1952), PhD thesis, Princeton, 1952.

[4] T. Heinzl and A. Ilderton, Opt. Commun. **282**, 1879 (2009), arXiv:0807.1841.

[5] T. Heinzl *et al.*, Opt. Commun. **267**, 318 (2006), hep-ph/0601076.

[6] T. Heinzl and O. Schröder, J. Phys. **A39**, 11623 (2006), hep-th/0605130.

[7] T. Heinzl and A. Ilderton, Eur. Phys. J. D **55**, 359 (2009) [arXiv:0811.1960 [hep-ph]].

5.3.3 Cascades of e^+e^- Pairs and γ-Rays triggered by a Single Slow Electron in Strong Fields

H. Ruhl[1], N. Elkina[1] and A. Fedotov[1]
[1] *Department of Physics, LMU Munich, 80333 Munich (Germany)*

Vacuum breakdown Field assisted vacuum breakdown is likely to be important at intensities envisioned at ELI. Recently Bell and Kirk [1, 2] prediced a prolific pair production at laser intensities approaching $10^{24}\mathrm{W/cm}^2$ by analytic methods. Here we consider a scenario where a single slow electron is initially present in a very intense electromagnetic field. In the context of those strong external fields the latter electron is capable of emitting photons at enhanced rates, which in turn seed e^+e^--pairs. The process leads to a multiplication effect and sets in about two orders of magnitude in the external field earlier than the production of a pair from photons only. The simuations show that pair creation is overestimated by analytic models.

The quantum efficiency parameter In order to observe the emission of a photon in the context of a strong electromagnetic field it is necessary to maximize the external electric field at the location of an electron or positron. Calculations done by Nikishov and Ritus identify the quantum efficiency parameter for the emission of radiation from charges

$$\chi_e \;=\; \frac{e\hbar}{m^3c^4}\sqrt{-\left(F^{\mu\nu}p_\nu\right)^2} = \frac{\gamma}{E_s}\sqrt{\left(\vec{E}+\vec{v}\times\vec{B}\right)^2-\left(\frac{\vec{v}\cdot\vec{E}}{c}\right)^2}\,, \tag{1.12}$$

where

$$\gamma \;=\; \sqrt{1+\frac{\vec{p}^2}{m^2c^2}}\,, \qquad \vec{v}=\frac{c\vec{p}}{\sqrt{m^2c^2+\vec{p}^2}}\,, \qquad E_s=\frac{m^2\,c^3}{e\,\hbar}=1.32\cdot10^{18}\,\frac{V}{m} \tag{1.13}$$

that has to be as large as possible. The parameter χ_e can be calculated for simple situations neglecting hard photon emission. If a circularly polarized standing wave is assumed to be present at the position of an electron, where $\vec{B}=0$ holds, the equations of motion of an electron initially at rest in the field of the latter are

$$\frac{d\vec{p}}{dt} \;=\; -e\,\vec{E}\,, \qquad \vec{p}(0)=0\,, \tag{1.14}$$

where

$$\vec{E}(t) \;=\; E_0\begin{pmatrix}\cos\omega t\\ \sin\omega t\end{pmatrix}. \tag{1.15}$$

The solutions for $\vec{p}(t)$ is

$$\vec{p}(t) \;=\; -\frac{e\,E_0}{\omega}\begin{pmatrix}\sin\omega t\\ 1-\cos\omega t\end{pmatrix} \tag{1.16}$$

and for $\vec{v}(t)$

$$\vec{v}(t)=-\frac{e\,E_0^2}{m\,\omega\,\gamma(t)}\begin{pmatrix}\sin\omega t\\ 1-\cos\omega t\end{pmatrix}, \tag{1.17}$$

where $\gamma(t)$ is

$$\gamma(t) \;=\; \sqrt{1+4\,a^2\,\sin^2\frac{\omega t}{2}}\,, \qquad a=\frac{e\,E_0}{m\,\omega\,c}\,. \tag{1.18}$$

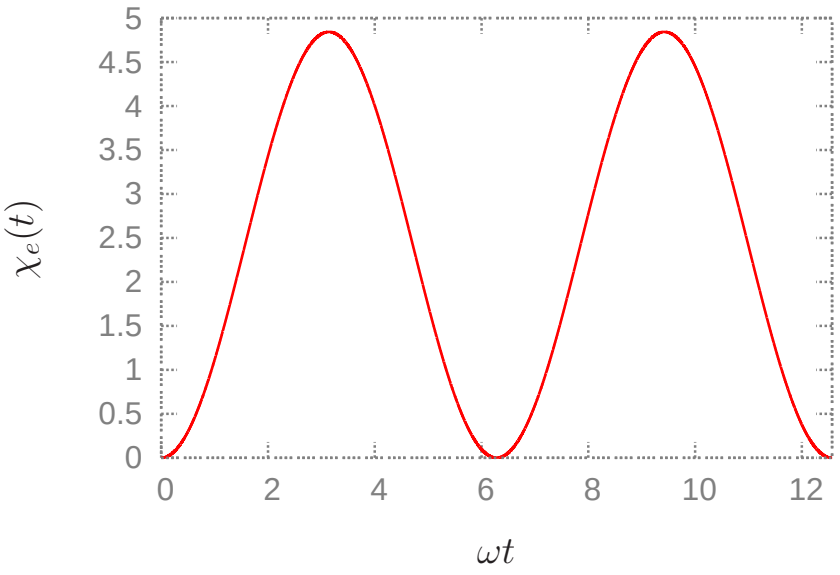

Figure 27: The parameter $\chi_e(t)$ for a circular polarized electric field at $a = 1000$ and $\omega = 1.88 \cdot 10^{15}\ \mathrm{s}^{-1}$.

Now $\chi_e(t)$ can be calculated to be

$$\chi_e(t) \;=\; \frac{E_0}{E_s}\sqrt{1+4\,a^2\,\sin^2\frac{\omega t}{2}-a^2\,\sin^2\frac{\omega t}{2}} = \frac{a\,\hbar\,\omega}{m\,c^2}\sqrt{1+4\,a^2\,\sin^4\frac{\omega t}{2}}\,, \tag{1.19}$$

where

$$\frac{\hbar}{m\,c^2} \;=\; 1.288\cdot 10^{-21}\,sec\,. \tag{1.20}$$

Figure 27 shows $\chi_e(t)$ neglecting the emission of hard photons.

Hard photon emission and pair production If hard photon emission is included $\chi_e(t)$ has to be computed numerically since the momentum of the emitting electron changes in the course of hard photon emission. We make the following assumptions

$$\vec{k} \;=\; \frac{\vec{p}}{p}\frac{\omega}{c}\,, \qquad \vec{p}^{\,\prime} = \frac{\vec{p}}{p}\sqrt{\left(\sqrt{m^2c^2+p^2}-\frac{\hbar\,\omega}{c}\right)^2 - m^2c^2}\,, \qquad p>0\,, \qquad \theta \approx \frac{1}{2\gamma}\,, \tag{1.21}$$

where $\vec{k}$ is the photon wave vector, $\vec{p}^{\,\prime}$ is the post-emission electron vector, and θ is the angle between emitting electron and emitted photon. Figure 28 shows $\chi_e(t)$ with hard photon emission included. Due to hard photon emission the parameter $\chi_e(t)$ is essentially prevented from becoming large. The red line in the figure shows the case without photon emission. The blue lines give $\chi_e(t)$ with photon emission included. Since pairs are generated at arbitrary phase of the external field (blue lines at later times) their quantum efficiency parameters $\chi_e(t)$ can become very large (be above the red line). A similar parameter holds for the production of a e^+e^--pair from a photon

$$\chi_\gamma \;=\; \frac{e\hbar^2}{m^3c^4}\sqrt{-\left(F^{\mu\nu}k_\nu\right)^2} = \frac{\hbar\omega}{mc^2}\,\frac{1}{E_s}\sqrt{\left(\vec{E}+\frac{c\vec{k}}{k_0}\times\vec{B}\right)^2-\left(\frac{\vec{k}\cdot\vec{E}}{k_0}\right)^2}\,, \tag{1.22}$$

where $k_0 = \omega/c$ and $\vec{k}$ is obtained from Eqn. (1.21).

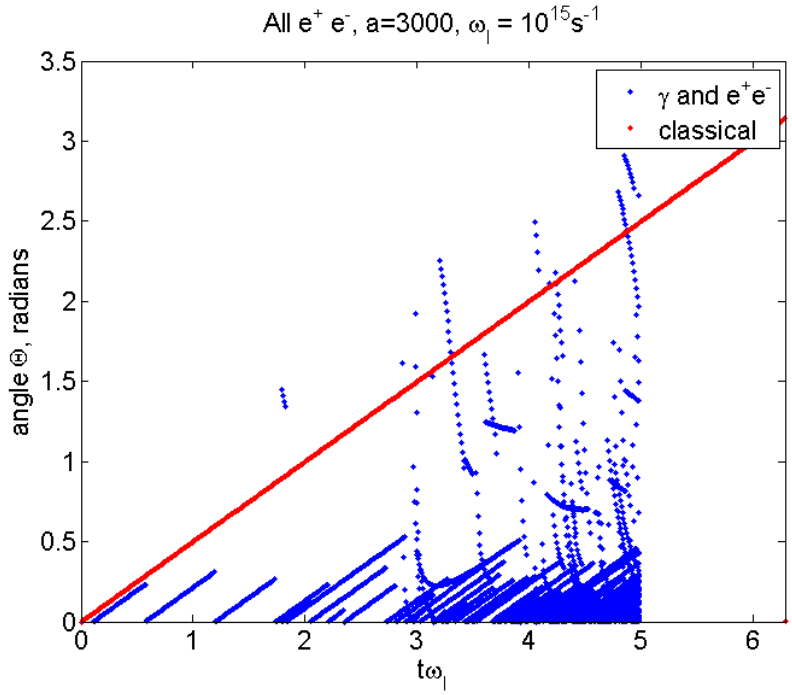

Figure 28: The parameter $\chi_e(t)$ from numerical computation including hard photon emission at $a = 3000$ and $\omega = 10^{15}\,\mathrm{s}^{-1}$.

Transition rates in strong external fields The total transition rate for photon emission in the limit of $\chi_e(t) \gg 1$ is given by

$$W_\gamma(t) \approx \frac{\alpha\, m^2\, c^4}{\hbar\, \epsilon(t)}\, \chi_e^{\frac{2}{3}}(t) = \frac{\alpha\, m\, c^2}{\hbar \sqrt{1 + 4\, a^2\, \sin^2 \frac{\omega t}{2}}} \left(\frac{a\, \hbar\, \omega}{m\, c^2} \sqrt{1 + 4\, a^2\, \sin^4 \frac{\omega t}{2}} \right)^{\frac{2}{3}} . \tag{1.23}$$

The transition rate for photon emission neglecting hard photon emission at $a = 1000$ and $\omega = 1.88 \cdot 10^{15}\,\mathrm{s}^{-1}$ is plotted in Figs. 29 and 30. The total transition rate for pair creation in the limit of $\chi_\gamma(t) \gg 1$ is given by

$$W_{e^+e^-}(t) \approx \frac{\alpha\, m^2\, c^4}{\hbar\, \epsilon(t)}\, \chi_\gamma^{\frac{2}{3}}(t) . \tag{1.24}$$

The pair creation rates have to be computed numerically. However, at large electron energies they are of a magnitude comparable to hard photon emission.

Time and length scales There are a few important time and length scales connected with QED-cascading. The formation length and time scales at $a = 1000$ and $\omega = 1.88 \cdot 10^{15}\,\mathrm{s}^{-1}$ are

$$l_{cr} \approx \frac{m\, c^2}{e\, E_0} = \frac{c}{a\, \omega} \approx 1.59 \cdot 10^{-10}\,\mathrm{m} , \qquad t_{cr} \approx \frac{l_{cr}}{c} = \frac{1}{a\, \omega} \approx 5.32 \cdot 10^{-19}\,\mathrm{s} . \tag{1.25}$$

Those scales represent thresholds that have to be overcome before the vacuum can be unstable. They typically cannot be resolved on a computer and are dealt with within analytical theory. Other useful time and length scales are those on which $\chi_e(t) \approx 1$ is reached. They represent the time and length scales on which the electron accelerates and hence can enlarge $\chi_e(t)$. Yet other length and time scales are given by

$$l_{free} = \frac{c}{t_{free}} , \qquad \int_0^{t_{free}} d\tau\, W^{tot}_{\gamma, e^+e^-}(\tau) \approx 1 . \tag{1.26}$$

Those are the time and length scales between two events.

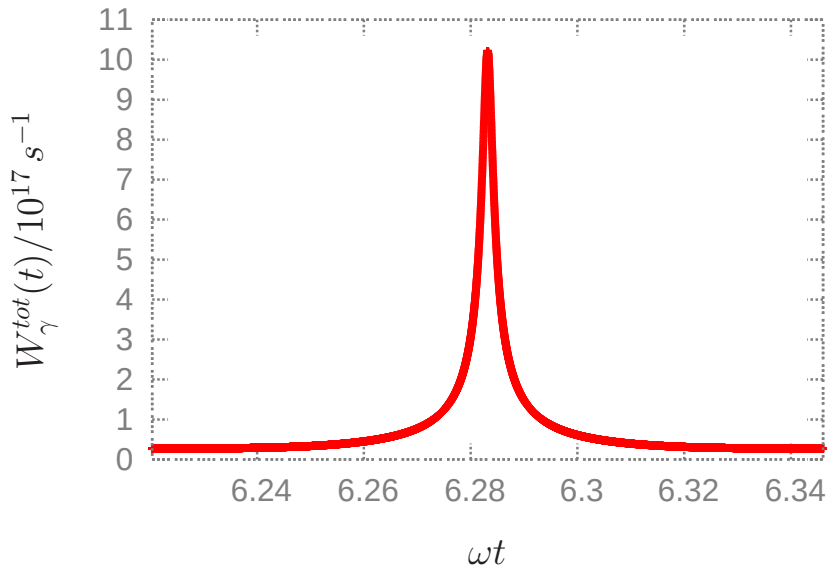

Figure 29: The total transition rate $W_\gamma^{tot}(t)$ for a circular polarized electric field at $a = 1000$ and $\omega = 1.88 \cdot 10^{15}\,\mathrm{s}^{-1}$.

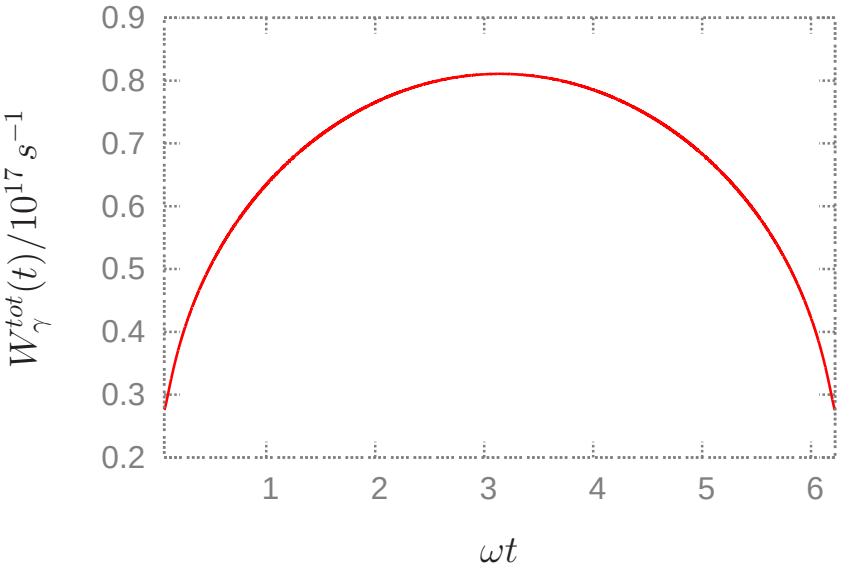

Figure 30: The total transition rate $W_\gamma^{tot}(t)$ for a circular polarized electric field at $a = 1000$ and $\omega = 1.88 \cdot 10^{15}\,\mathrm{s}^{-1}$.

Transport equations Neglecting higher order effects as annihilation of pairs and classical radiation reaction effects the system consisting of electrons, positrons, and radiation can be described by transport equations of the following kind

$$\begin{aligned}\left(\partial_t + \vec{v}\cdot\partial_{\vec{x}} - e\left(\vec{E}+\vec{v}\times\vec{B}\right)\cdot\partial_{\vec{p}}\right) f_\pm(\vec{x},\vec{p},t) \\ = \int_{\omega>\omega_0} d^3k\, W_\gamma^{\vec{E},\vec{B}}(\vec{k},\vec{p}+\vec{k})\, f_\pm(\vec{x},\vec{p}+\vec{k},t) - f_\pm(\vec{x},\vec{p},t)\int d^3k_{\omega>\omega_0}\, W_\gamma^{\vec{E},\vec{B}}(\vec{k},\vec{p}) \\ + \int_{\omega>\omega_0} d^3k\, W_{e^+e^-}^{\vec{E},\vec{B}}(\vec{k},\vec{p})\, f_\gamma(\vec{x},\vec{k},t)\end{aligned} \tag{1.27}$$

$$\begin{aligned}\left(\partial_t + \frac{\partial\omega}{\partial\vec{k}}\cdot\partial_{\vec{x}}\right) f_\gamma(\vec{x},\vec{k},t) \\ = \int d^3p\, W_\gamma^{\vec{E},\vec{B}}(\vec{k},\vec{p})\, [f_+(\vec{x},\vec{p},t) + f_-(\vec{x},\vec{p},t)] \\ - f_\gamma(\vec{x},\vec{k},t)\int d^3p\, W_{e^+e^-}^{\vec{E},\vec{B}}(\vec{k},\vec{p})\ ,\end{aligned} \tag{1.28}$$

which for $\omega < \omega_0$ have to be coupled to Maxwell's equations with the current

$$\vec{j}(\vec{x},t) \;=\; e\int d^3p\,\vec{v}\,[f_+(\vec{x},\vec{p},t) - f_-(\vec{x},\vec{p},t)]\ . \tag{1.29}$$

It has to be made sure that radiation contained in $\vec{E}$, $\vec{B}$, and f_γ will not lead to double counting of radiation, hence the $\omega < \omega_0$ threshold.

Pair production Simple analytical estimates yield

μ	$I\left[\frac{W}{cm^2}\right]$	$N_\pm$
0.1	$3\cdot 10^{23}$	non
1.0	$3\cdot 10^{25}$	$\approx 10^4$
2.0	$1.2\cdot 10^{26}$	$\approx 10^{10}$

where the production rates depends on a parameter $\mu = E_0/\alpha E_s$. The simulations, however, show that pair creation is over-estimated by the analytical model but still strong. We obtain a linear growth with time for various amplitudes a. Figure 31 shows the distribution of hard photons (black arrows), electrons (red lines), and positrons (blue lines) after one full cycle of the external fields. The yellow dots indicate pair creation events. Figure 32 shows a logarithmic plot of the number of electrons and positrons as a function of time. The growth rate that can be infered is $\Gamma \approx 10^{16}\,\mathrm{s}^{-1}$ for $a = 3000$ and $\omega = 10^{15}\,\mathrm{s}^{-1}$. In conclusion, a novel numerical code has been presented that is capable of calculating the effects of vacuum instability. Starting from a single initial electron a cascade consisting of radiation, electrons and positrons is obtained with a growth rate of about $\Gamma \approx 10^{16}\ \mathrm{s}^{-1}$ at $a = 3000$ and $\omega = 10^{15}\,\mathrm{s}^{-1}$. With growing a the laser energy distributed over electrons, positrons and hard photons shifts. At large a radiation is suppressed in favor of matter.
Injecting low energy electrons into the laser focus the cascades of higher energy electrons can be measured with the planned magnetic spectrometers and the theoretical predictions can be tested in detail.

References

[1] A. R. Bell and J. G. Kirk, Phys. Rev. Lett. **101**, 200403 (2008);

[2] J. G. Kirk, A. R. Bell and I. Arka, Plasma Phys. Ontrol. Fusion **51**, 085008 (2009).

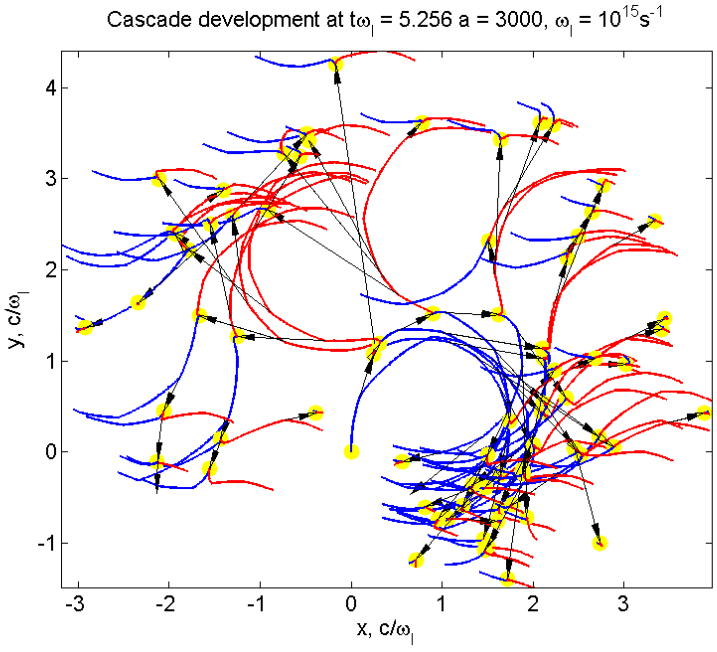

Figure 31: The γe^+e^--cascade for a circular polarized electric field at $a = 3000$ and $\omega = 10^{15}\,\mathrm{s}^{-1}$.

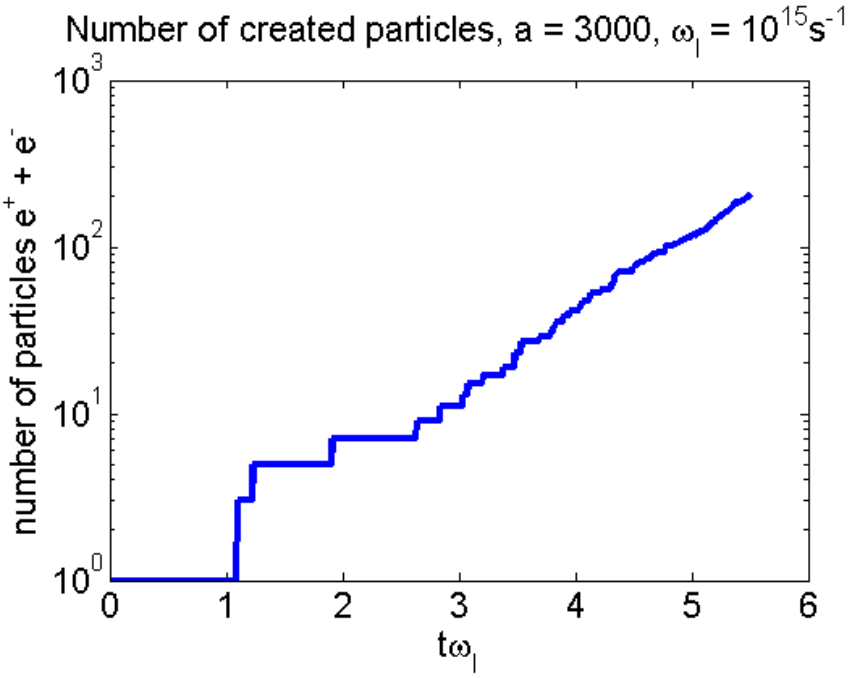

Figure 32: The total number of electrons and positrons as a function of time for a circular polarized electric field at $a = 3000$ and $\omega = 10^{15}\,\mathrm{s}^{-1}$.

5.3.4 Compton Scattering and Radiation Reaction of a Single Electron at High Intensities

T. Heinzl[1], N.M. Naumova[2] D. Habs[3], and P. G. Thirolf[3]
[1] *University of Plymouth, Plymouth PL4 8AA, (UK),*
[2] *Laboratoire d'Optique Appliquée, UMR 7639 ENSTA, Palaiseau (France)*
[3] *Ludwig Maximilians University, Munich (Germany)*

The process in question is the collision of an electron and a high intensity laser beam, such that a photon γ' is scattered out of the beam. The relevant physical parameters are the laser frequency, ω, the electron energy measured in terms of their gamma factor, $\gamma = E_{\rm el}/m$, and the dimensionless laser amplitude,

$$a_0 = \frac{eE}{m\omega} \,. \tag{1.30}$$

This represents the energy gain of an electron (charge $-e$, mass m) traversing a laser wavelength, $\lambda\!\!\!^{-} = \lambda/2\pi = 1/\omega$, in an r.m.s. field E, in units of the electron rest energy, m (employing natural units, $\hbar = 1 = c$). Thus, when a_0 is of order unity, the electron quiver motion becomes relativistic. It is useful to rewrite (1.30) in terms of laser intensity I and wavelength λ,

$$a_0 = 6 \times 10^2 \sqrt{I/I_{24}}\ \ \lambda/\mu{\rm m} \,, \tag{1.31}$$

where $I_{24} \equiv 10^{24}$ W/cm^2 is the intensity envisioned for the Romanian ELI subproject.
Using the theory of quantum electrodynamics (QED) nonlinear Compton scattering has been analysed already in the early sixties (soon after the invention of the laser) treating the laser field as an infinite plane wave [2–5]. In this case, one can utilise an exact solution of the Dirac equation going back to Volkov which provides a quantum description of the quivering electron. In QED jargon, such an

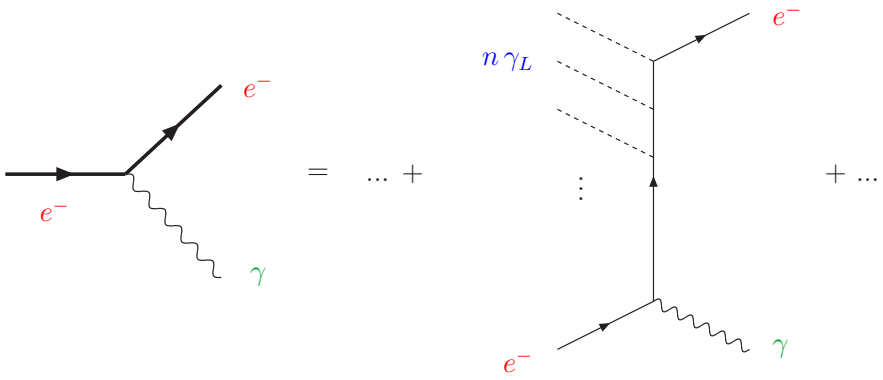

Figure 33: Feynman diagrams for nonlinear Compton scattering.

electron is said to be 'dressed' by the background field and may be depicted as shown on the left-hand side of Fig. 33 which, when expanded in the number of laser photons involved, becomes a sum of diagrams of the type shown on the right-hand side representing the processes

$$e + n\gamma_L \to e' + \gamma' \,. \tag{1.32}$$

Here, the electron absorbs an arbitrary number n of laser photons γ_L of energy $\omega \simeq 1$ eV before emitting a single photon γ' of energy ω'.
Note that the tree-level diagrams involved have a classical limit which is a good description of the process when the electron mass m is the dominant energy scale [6]. This classical limit is referred to as Thomson scattering. It is valid as long as the following frame independent inequality holds,

$$\nu_0 \equiv \frac{k \cdot p}{m^2} \ll 1 \,, \tag{1.33}$$

where k and p are the asymptotic four-momenta of laser photons and electrons, respectively. In the electron rest frame one has $\nu_0 = \hbar\omega_0/mc^2$ (temporarily reinstating $\hbar$ and c). In terms of lab

quantities, this implies $\gamma \ll m/2\omega \simeq 10^5 \ldots 10^6$, in agreement with the folklore that the Thomson scattering is the a low-energy limit. With an electron linac producing electrons in the 600 MeV range γ will be of order 10^3 so that one is starting to move away from the Thomson (towards the Compton) regime. In any case, it is important to stress that, unlike say pair creation, the processes (1.32) are not suppressed by any threshold effects. Thus, one can study intensity effects at arbitrarily low centre-of-mass energies both for photons and electrons. This is quite a unique feature of nonlinear Thomson/Compton scattering and singles out this process from a particle physics point of view.

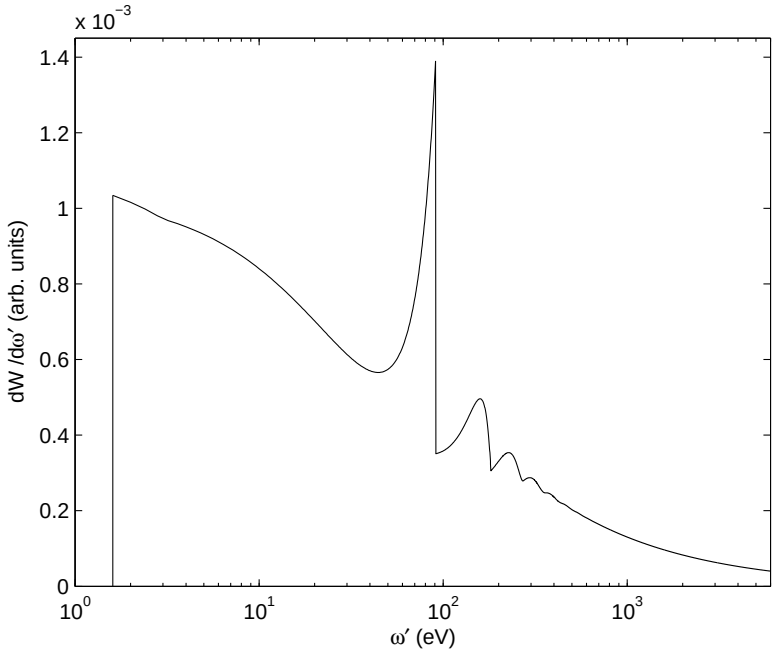

Figure 34: Nonlinear Compton spectrum for ELI parameters (intensity parameter $a_0 = 500$, laser energy $\omega = 1.5$ eV and electron energy $E_{\rm el} = 1$ GeV).

In Fig. 34 we show the photon emission rates as a function of the emitted photon frequency, ω'. The central peak corresponds to the first harmonic ($n = 1$) located at scattered frequency $\omega_1' \simeq 4\gamma^2\omega/a_0^2 \simeq 10^2$ eV. Note that this is substantially *red-shifted* from the linear Compton edge, $4\gamma^2\omega \simeq 25$ MeV. The side maxima to the right of the global maximum correspond to higher harmonics, $\omega_n' \simeq n\omega_1'$. In the lab frame, for the parameter values chosen, there is still some energy transfer from electrons to the scattered photons, hence the blue-shift $\omega \to \omega_n' > \omega$. In an astrophysical context such a process is referred to as 'inverse Compton scattering'. This is to be contrasted with 'normal' Compton scattering (Compton's original experiment) where the electrons are at rest in the lab and one observes a red-shift of the photon frequency, $\omega' < \omega$. The inverse Thomson/Compton up-shift is now being routinely used to create γ beams, for instance at Lawrence Livermore National Laboratory, where the T-Rex facility is the world's highest peak brightness MeV γ source.
The details of nonlinear Compton scattering have recently been reviewed in [7] with an emphasis on lab frame signatures, treating the laser as an infinite plane wave. In this case the red-shift of the linear Compton edge may be understood in terms of the electron mass shift,

$$m_* = m\sqrt{1 + a_0^2}\,, \tag{1.34}$$

which may be interpreted as being due to an averaging over the electron quiver motion. This adds an intensity dependent, longitudinal contribution to the electron four-momentum p resulting in the *quasi-momentum*

$$q = p + \frac{a_0^2 m^2}{2k\cdot p}\,k\,. \tag{1.35}$$

Using the fact the photons are massless ($k^2 = 0$), it is easy to see that $q^2 = m_*^2$. Thus, as the

electron 'gains weight' ($m \to m_*$) it will recoil less, reducing the energy transfer to the final state photon, hence the red-shift in the maximum photon energy[1], see Fig. 34. The associated spectra are characterised by momentum conservation using electron *quasi*-momenta, i.e. $q + nk = q' + k'$, with the momenta in one-to-one correspondence with the particles of (1.32). Among other things, this conservation law determines the spectral ranges, in particular its minimum and maximum values, or 'Compton edges' [7].

In the lab frame there is an interesting interplay between laser intensity and electron energy. We have seen that backscattering off high-energy electrons ($\gamma \gg 1$) produces a blue-shift ('inverse' Compton). On the other hand, high intensity ($a_0 \gg 1$) produces a red-shift, hence works in the opposite direction. It turns out that there is exact balance in the centre-of-mass frame of the Volkov electrons and the n laser photons, that is when $4\gamma^2/a_0^2 \simeq 1$ [7]. This can obviously be achieved by fine-tuning γ and a_0: for 1 GeV electrons the associated a_0 is about $2\gamma \simeq 4 \times 10^3$. Hence, for a_0 of this order or larger one expects an overall red-shift, $\omega' < \omega$, as the Volkov electron has become so heavy that it appears almost 'static' from the photons' point of view. On the other hand, assuming the ELI value $a_0 \simeq 500$, one would just need 100 MeV electrons to test this interesting spectral regime. Fig. 35 gives an idea of how sensitively the spectra depend on the magnitude of a_0 choosing $\gamma = 100$ so that the critical $a_0 \simeq 200$.

As stated above, the critical value of $a_0 \simeq 2\gamma$ defines an intensity dependent centre-of-mass frame where the total momentum vanishes,

$$\vec{P} \equiv \vec{q} + n\vec{k} = \vec{p} + \left(\frac{a_0^2 m^2}{2k \cdot p} + n \right) \vec{k} = 0 \, . \tag{1.36}$$

As $k \cdot p > 0$ this obviously requires that $\vec{p}$ and $\vec{k}$ are anti-parallel (head-on collision). Again, note the explicit dependence on the laser strength parameter a_0.

It is important to stress that the electron mass shift, though predicted long ago [5, 8], has never been directly confirmed in an experiment as intensities have been too small until recently. Nonlinear Compton scattering (1.32) has been observed and analysed in the SLAC E-144 experiment [9] using 47 GeV electrons from the SLAC beam and a Terawatt laser with $a_0 \simeq 0.4$. This was a high energy ($\gamma \simeq 10^5$) and low intensity ($a_0 < 1$) experiment (hence deep in the 'inverse' Compton regime). Photon spectra were not recorded and hence no red-shift was observed [9]. ELI should rectify this omission by recording detailed photon spectra in the complementary regime of intermediate energies and high intensities ($\gamma \simeq a_0 \simeq 10^3$), thus exploring this uncharted region of the standard model for the first time.

The considerations above are valid for an infinite plane wave. This should be a good approximation as long as the pulse duration T is large compared to the laser period, $T \gg 2\pi/\omega$. In this case the electron 'sees' sufficiently many cycles to be dragged along with the pulse which effectively increases its mass, $m \to m_*$. For ultra-short pulses of a few cycles this picture has to be modified [6,10]. The spectra will then be dominated by finite size effects in both space and time. Qualitatively, the following features can be seen to arise. In an infinite plane wave, the Compton edge becomes red-shifted such that the photon emission signal above $\omega_1' = 4\gamma^2\omega/a_0^2$ is entirely due to higher harmonics ($n > 1$) and strongly suppressed (see Fig. 34). For a short pulse, the gap between this nonlinear and the linear Compton edge ($\omega' = 4\gamma^2\omega$) gets 'populated' with an oscillatory signal (substructure) which, however, remains suppressed compared to the principal maximum at the nonlinear edge [6]. Thus, for large a_0, one should not expect a substantial yield of frequency up-shifted photons.

This extreme sensitivity to beam characteristics may, nevertheless, be turned into a bonus by using nonlinear Compton/Thomson scattering as a diagnostic tool both for the electron beam [11] and the laser [6]. In particular, it has been suggested to gain information on the carrier phase of the pulse in this way [12].

As pointed out by McDonald [13] the QED (hence *quantum*) analysis of Compton scattering should contain corrections to Thomson scattering due to radiative reaction. The basic reason is energy momentum conservation which in a scattering process equates the total four-momenta of incoming

[1]Therefore, if one is interested in a large energy up-shift, e.g. to produce γ rays, one should rather use low intensity beams ($a_0 < 1$) to scatter off from the electrons.

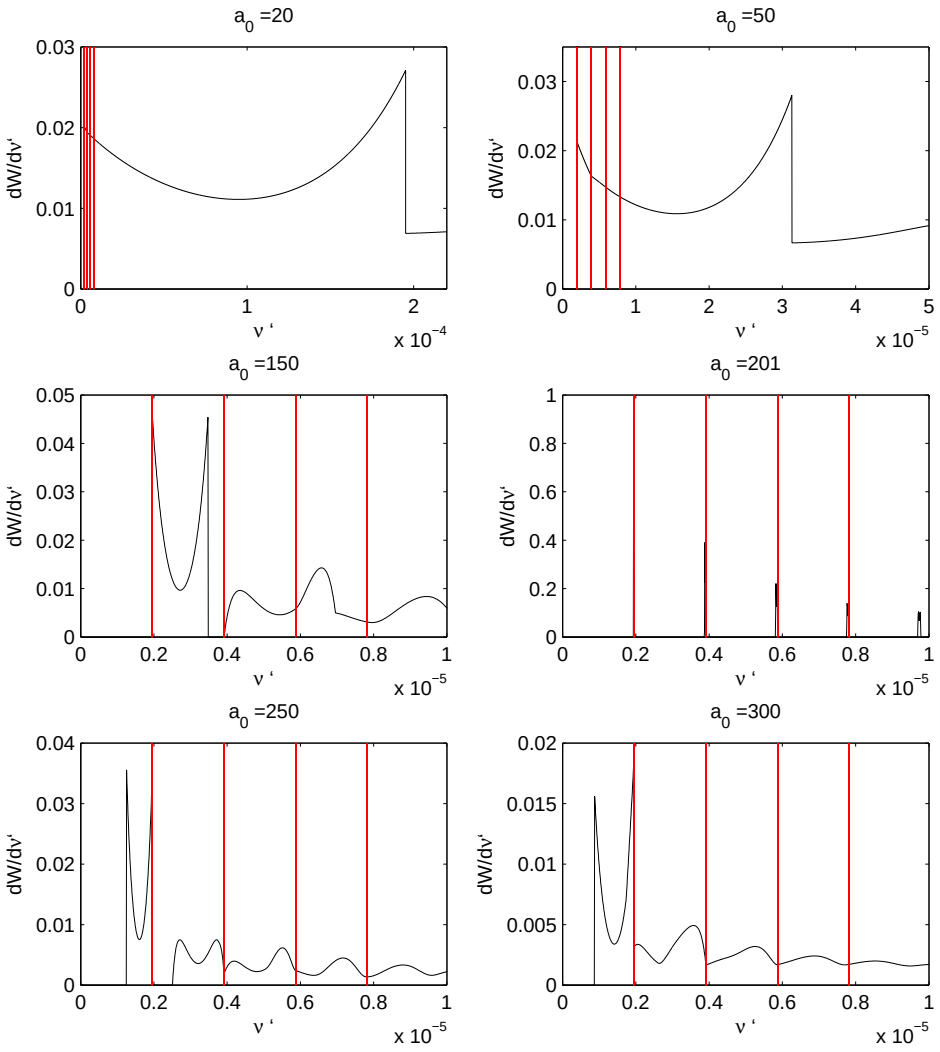

Figure 35: Photon emission spectra as a function of $\nu' = \omega'/m$ for different values of a_0, $\gamma = 100$ and incoming frequency $\nu = \omega/m = 2 \times 10^{-6}$ assuming a head on collision of the incoming particles. The vertical (red) lines correspond to frequencies $n\nu$ [7].

and outgoing asymptotic particles. Recall that in the QED analysis with an infinite plane wave it is the *quasi*-momenta (1.35) that enter the conservation law. A nice interpretation of radiation reaction and its relation to QED may be given as follows [13]. One writes the force $F_{\rm RR}$ of radiation resistance in an ambient electric field E_0 as

$$F_{\rm RR} = \frac{2}{3} e^2 F_L \sqrt{\nu_0^2 + \epsilon_0^2}\,, \tag{1.37}$$

where F_L is the Lorentz force, while the parameters ν_0 from (1.33) and $\epsilon_0 \equiv E_0/E_S$ measure photon energy and electric field strength in the electron rest frame[2] assuming a head-on collision of laser and electron beam. As usual, $E_S \equiv m^2c^3/e\hbar = 1.3 \times 10^{18}$ V/m denotes Sauter's critical field strength, beyond which the QED vacuum 'breaks down' via pair creation. We have temporarily reinstated $\hbar$ to show that radiation resistance can be interpreted as a quantum phenomenon that 'knows' about radiative energy-momentum losses or gains which in the classical picture correspond to (proper) time integrals of the force terms[3]. This point has recently been corroborated through a QED derivation of

[2]The Lorentz invariant definition of ϵ_0, often denoted χ, is $\epsilon_0 = e\sqrt{(F^{\mu\nu}p_\nu)^2}/m^3$ where $F^{\mu\nu}$ is the laser field strength tensor.

[3]In principle, there may be additional contributions to what classically is radiative reaction stemming from higher-

a modified Lorentz-Abraham-Dirac equation [1, 14] based on the original QED analysis [2].
Continuing with our analysis of (1.37) we note that backreaction becomes important when either ν_0 or ϵ_0 become of order unity. Let us discuss both parameters one after the other. We have already seen (in Footnote 1) that $\nu_0 \ll 1$ implies that we are in the Thomson rather than Compton regime. For ELI parameters one finds $\nu_0 = \gamma(1+\beta)\nu \simeq 10^{-2}$ so quantum corrections associated with electron recoil should be at the percent level. On the other hand, one calculates $\epsilon_0 = \gamma(1+\beta)E/E_S = O(1)$ upon assuming an r.m.s. lab field of magnitude $E \simeq 10^{-3}E_S$. Thus, when radiative reaction is large due to large ϵ_0, then, in its own rest frame, the electron sees an electric field of the order of Sauter's critical field! Accordingly, with the present ELI parameter values we are right at the pair production threshold E_S or, for optimal values, even slightly above. One may thus expect to see positrons generated by the particular combination of high intensity for the laser photons and sufficiently high energy for the electrons ($\gamma \simeq a_0 \gg 1$). This may even lead to prolific pair creation via cascading processes 'maintained' by subsequent repeated laser acceleration of the produced pairs [15–17].
There is, however, a caveat here: the SLAC experiment has shown that the energy threshold for pair creation becomes intensity dependent, $s > 4m_*^2$, where s is the usual invariant defining the total energy in the centre-of-mass frame, $\sqrt{s}$. This increase is due to the fact that pairs with *effective* mass m_* need to be produced which, in turn, suggests that the critical field increases as well, $E_S \to E_S^* \equiv m_*^2/e$. Again, this may depend on pulse duration and possible other finite size effects which makes it all the more important to actually *probe* the details of the mass shift experimentally.
After all, it is this very mass shift which determines the size of the radiative reaction. Upon rewriting (1.37) as

$$F_{\rm RR}/F_L = \frac{2}{3}e^2\nu_0\sqrt{1+a_0^2}\,, \tag{1.38}$$

it becomes manifestly proportional to the mass scaling factor, cf. (1.34), and, reassuringly, yields the same numerical value as (1.37). We thus can conclude that it is indeed the appearance of a_0 in (1.38), as well as in the quasi-momenta q and q' and the associated conservation law, which signals backreaction. That's why the analysis of Thomson scattering in [18] using the purely classical language of radiation reaction is nothing but a reinterpretation of the intensity dependent centre-of-mass dynamics characterised by (1.36) and depicted in Fig. 35. The connection is provided by (1.38), the right-hand side of which is just the radiation reaction parameter R defined in [18], multiplied by a_0.
The scattering between laser photons and relativistic electrons is governed by three dimensionless, Lorentz invariant parameters, which can be conveniently written as

$$\nu_0 = \omega_0/m = 10^{-5}\,E_{\rm el}/{\rm MeV}\,, \tag{1.39}$$

$$a_0 = \frac{eE_0}{\omega_0 m} = 6\times 10^2\,\sqrt{I/I_{24}}\;\;\lambda/\mu{\rm m}\,, \tag{1.40}$$

$$\epsilon_0 = \frac{E_0}{E_S} = 6\times 10^{-3}\,\sqrt{I/I_{24}}\;\;E_{\rm el}/{\rm MeV}\,. \tag{1.41}$$

The last identity, adapted from [1], is plotted in Fig. 36. The subscripts "0" refer to the electron rest frame with the lab frame electric field being given by $E = \gamma(1-\beta)E_0$ and likewise for the laser frequency ω.
It is important to note that the parameters (1.39–1.41) are not independent as $\epsilon_0 = a_0\nu_0$. However, all three are useful as they characterise different physics. When $\nu_0 = O(1)$ we are in the genuine quantum (Compton rather than Thomson) regime. As also stated there, $a_0 = O(1)$ implies that the electron quiver motion in the laser becomes relativistic. Finally, when $\epsilon_0 = O(1)$ the electron 'sees' an electric field of the order of the critical one in its rest frame which implies the onset of pair creation. The authors of [1] have fittingly dubbed the electric fields in the last two cases as "relativistically strong" and "QED strong", respectively.
According to a recent paper by Sokolov et al., [1], for $I = 10^{24}{\rm W/cm^2}$ and a 1 GeV electron beam, photons of ≈15% of electron beam energy can be generated efficiently for values of ϵ_0 in the range

order radiative corrections (final state interactions and loop diagrams). These are obviously not included in the lowest order diagrams of Fig. 33. Not much is known about such corrections and we do not include them in this discussion.

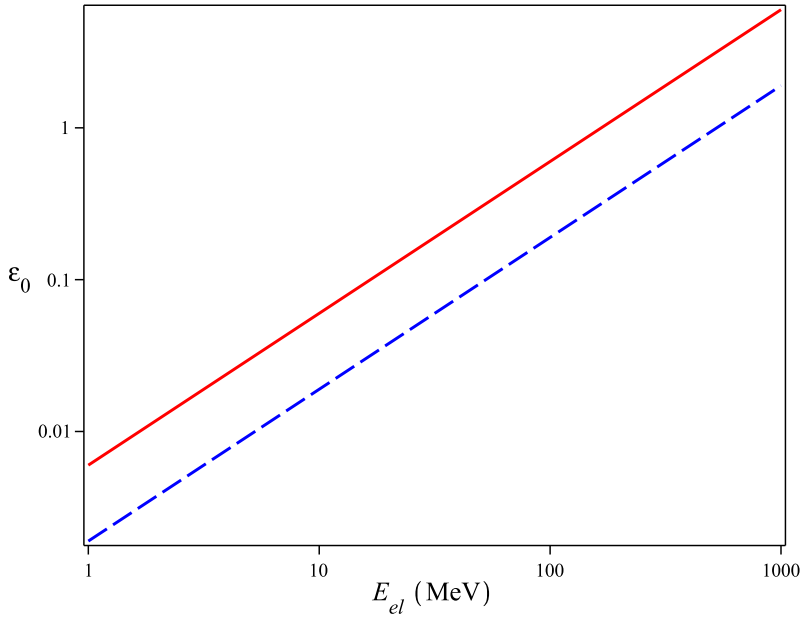

Figure 36: Dependence of the parameter ϵ_0 from (1.41) on the electron energy $E_{\rm el}$ and the intensity I of the counter-propagating laser beam. Full line: $I = I_{24} = 10^{24}$ W/cm^2. Dashed line: $I = 10^{23}$ W/cm^2.

between 1 and 10. It means that ≈ 150 MeV photons are expected for a 1 GeV electron beam. It is necessary to note that ≈ 100 MeV electrons are easily generated during the interaction of such intense laser pulses with plasmas, what leads to the production of ≈ 15 MeV photons.

References

[1] I.V. Sokolov, J.A. Nees, V.P. Yanovsky, N.M. Naumova, and G.A. Mourou, *Emission and its back-reaction accompanying electron motion in relativistically strong and QED-strong pulsed laser fields*, Phys. Rev. **E 81** (2010);arXiv:1003.0806v1.

[2] A. I. Nikishov and V. I. Ritus, *Zh. Eksp. Teor. Fiz.* **46** (1963) 776–796. [Sov. Phys. JETP **19**, 529 (1964)]; A. I. Nikishov and V. I. Ritus, *Zh. Eksp. Teor. Fiz.* **46** (1964) 1768–1781. [Sov. Phys. JETP **19**, 1191 (1964)].

[3] N. B. Narozhnyi, A. Nikishov, and V. Ritus, *Zh. Eksp. Teor. Fiz.* **47** (1964) 930. [Sov. Phys. JETP **20**, 622 (1965)];

[4] I. I. Goldman, Phys. Lett. **8**, 103 (1964).

[5] L. S. Brown and T. W. B. Kibble, Phys. Rev. **133**, A705 (1964).

[6] T. Heinzl, D. Seipt and B. Kämpfer, Phys. Rev. A **81**, 022125 (2010).

[7] C. Harvey, T. Heinzl and A. Ilderton, Phys. Rev. A **79**, 063407 (2009) [arXiv:0903.4151 [hep-ph]].

[8] N. Sengupta, Bull. Math. Soc. (Calcutta) **44** (1952) 175–180.

[9] C. Bamber *et al.*, Phys. Rev. D **60**, 092004 (1999).

[10] G. Krafft, Phys. Rev. Lett. **92**, 204802 (2004).

[11] W. Leemans *et al.*, Phys. Rev. Lett. **77**, 4182 (1996).

[12] F. Mackenroth, A. Di Piazza and C. H. Keitel, arXiv:1001.3614 [Unknown].

[13] K.T. McDonald, *Limits on the Applicability of Classical Electromagnetic Fields as Inferred from the Radiation Reaction*, unpublished preprint, available from http://www.hep.princeton.edu / mcdonald/examples/radreact.pdf.

[14] I.V. Sokolov *et al.*, arxiv:0910.4268 [physics.plasm-ph].

[15] A. R. Bell and J. G. Kirk, Phys. Rev. Lett. **101**, 200403 (2008).

[16] J. G. Kirk, A. R. Bell and I. Arka, PPCF **51**, 085008 (2009), arXiv:0905.0987 [hep-ph].

[17] A. Fedotov, N. Narozhny and G. Mourou, Report on the ELI Grand Challenges Meeting, ed.s G. Korn and P. Antici, Paris 2009.

[18] A. Di Piazza, K. Z. Hatsagortsyan and C. H. Keitel, Phys. Rev. Lett. **102**, 254802 (2009) [arXiv:0810.1703 DOC-TYPE = PREPRINT [Unknown]].

[19] T. Heinzl., Journ. of Phys.: Conference Series **198** 012005 (2009).

[20] T. Heinzl et al., arXiv:0911.1622v2[hep-ph] 14 Dec 2009

5.3.5 Nuclear Lifetime Measurements by Streaking Conversion Electrons with a Laser Field.

D. Habs[1], M. Gross[1] and P. G. Thirolf[1]
[3] *Ludwig Maximilians University, Munich (Germany)*

Nuclear levels have lifetimes down to the zeptosecond range once one reaches excitation energies beyond the particle emission threshold, while nuclear levels have lifetimes longer than typically 10 fs below the particle threshold [1]. We plan to study this drastic change in lifetime and predicted changes in decay laws for the first time. We modulate the energy of emitted conversion electrons in a phase-locked laser field and carry over the technique used to measure *as* lifetimes of atomic levels [2] to nuclear systems. Only for heavier nuclei we will get sufficiently large conversion coefficients. We will follow the modulated energies of the accompanying conversion electrons of the particle decay. We induce the particle decay by the γ beam, which is locked to the APOLLON-type laser or the γ's from the relativistiv mirror (project 4.4). Since we do not require the maximum laser fields, we may use laser light from an earlier amplifier state, which is delivered with higher repetition rate like 10 Hz. We want to induce the particle decay with very short γ-pulses, where we hopefully reach times below 1 as for the relativistic mirror. The emitted conversion electrons have energies, where the K binding energy is subtracted from the γ beam energy (typically 6-8 MeV). They can be observed in an electron spectrometer under angles where laser accelerated electrons from the target do not contribute.
Fig. 37 shows some nuclear lifetimes as a function of the excitation energy above the ground state for E1 and M1 transitions. In comparison also typical atomic lifetimes as a function of level energy are shown. Until now only time integrated particle spectra have been measured and it was not possible to measure the particle spectra as a function of the emission time. Typical particle emission times in the range of 10^{-20} s are obtained from statistical model calculations for higher excitation energies. If it were possible to follow the emission spectra as a function of time, e.g. a much better understanding of dissipation and damping processes in the energy region of overlapping resonances above ~15 MeV excitation energy could be obtained.

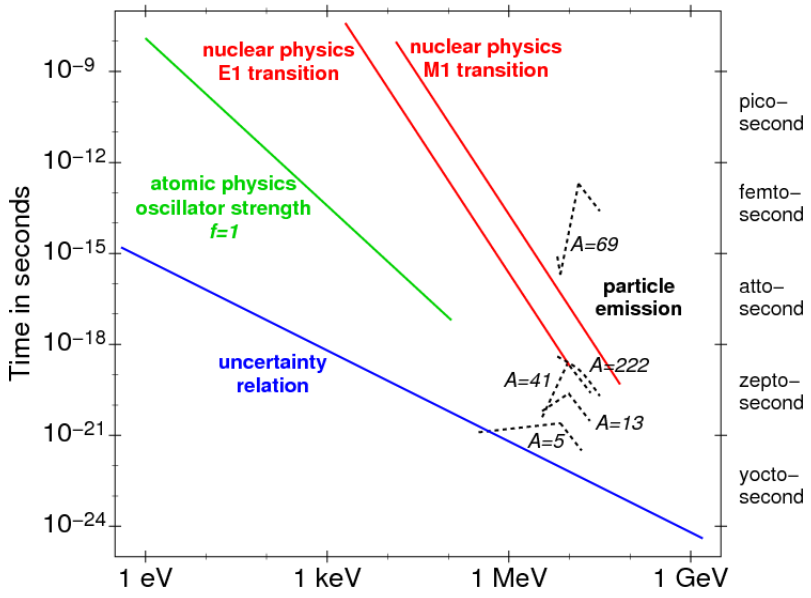

Figure 37: Correlation between nuclear lifetime and energy. The curve in green corresponds to atomic levels with oscillator strength f=1, the red curves represent single particle estimates for nuclear E1 and M1 γ transitions, while the blue line denotes the limit given by the uncertainty relation for a single-cycle laser pulse. The dashed black lines indicate lifetimes of nuclear levels after particle emission for different mass numbers A.

Experimental access to these ultrashort sub-attosecond lifetimes can be gained by exploiting the production technique for brilliant photon beams, where laser pulses are Compton-backscattered from a relativistic electron mirror, thus resulting in an energy boost by a factor of $4\,\gamma^2$, while the corresponding

pulse duration is reduced by a factor $1/(4\gamma^2)$. For a single cycle pulse the energy versus time relation would be described by the uncertainty principle. This demonstrates that excitations with gγ pulses much shorter than the expected lifetimes are possible. Though many experimental methods have been developed in different time ranges for different decay modes, transfering the well-established streaking technique of atomic physics to the regime of even shorter lifetimes in nuclear physics will enable to disentangle different channels of nuclear decay processes, where complex energy spectra could be followed as a function of time.

Properties of the decay in time of the compound nucleus Ultrashort light pulses offer the possibility to study photonuclear reactions up to 10 or 15 MeV from a different and completely new perspective. The band width $\Delta E = \hbar/\Delta t$ defined by the length (in time) Δt of the pulse may be large compared to the mean spacing d between adjacent levels of the same spin and parity. For medium-weight and heavy nuclei, d is typically 100 keV near the ground state and decreases exponentially with excitation energy, so that typically $d \sim 10eV$ at the neutron threshold, i.e. there are about 10^6 levels above the ground state. Below the neutron threshold, the average decay width Γ of nuclear levels is due to γ emission and has typical values of 10 meV. Right above the neutron threshold, particle decay increases Γ to typical values of about 1 eV. From here on Γ increases monotonically with excitation energy, until it reaches typical values of 50 or 100 keV (corresponding to a lifetime of 10^{-21} s) at the upper end of the energy interval here considered. Until now, photonuclear reactions were investigated with continuous beams of fairly poor energy resolution (measured in terms of the values of Γ and d discussed above) and have yielded only gross features of nuclear excitation functions, with the exception of the study of individual levels in the ground state domain. In particular spectroscopic properties of levels in the energy range between several 100 keV of excitation energy and the neutron threshold are unknown. Neutron time-of-flight spectroscopy has offered a window to study spacing distributions and other statistical properties of levels (i.e. neutron resonances) right above the neutron threshold. The outstanding feature of that gross structure is the emergence of giant resonances, especially the giant dipole resonance, that were investigated in considerable detail.
With a band width $\Delta E > d$, several or even many nuclear states will be simultaneously excited. In that case, meaningful theoretical statements can be made only if $\Delta E >> d$ or, if $\Gamma >> d$, for $\Delta E >> \Gamma$. Then the decay in time of the excited nucleus is determined by the Fourier transform of the photonuclear autocorrelation function. With S_{ab}(E) being the scattering amplitude leading from the incident photon channel to the final channel b, that function is defined as

$$S_{ab} = \int |g(E)|^2 S_{ab}(E + 1/2\epsilon) \cdot S^*_{ab}(E - 1/2\epsilon). \tag{1.42}$$

Here $|g(E)|^2$ describes the distribution in energy of the photon intensity and is centered at energy E_0 with width ΔE. The autocorrelation function is a running average over energy of the two scattering amplitudes with arguments separated by the energy ϵ. For the energy average to be representative, we must have $\Delta E >> d, \Gamma$. At the same time, ΔE should be small in comparison with the characteristic energy scale of gross features of photonuclear excitations. For the giant dipole resonance that is the resonance width with typical values around several MeV. The numbers given above for d and Γ then define the desirable band width for short light pulses. It is given by $\Delta E = Nmax(d, \Gamma)$, where N determines the relative statistical accuracy $1/\sqrt{N}$ of the energy average. The spectroscopic data taken with neutron time-of-flight spectroscopy are consistent with a random matrix description and suggest that the compound nucleus is chaotic. It is probable that this feature prevails at lower excitation energies. The hallmark of that description is a non-exponential decay in time of the compound nucleus when few channels are open. Only for many open channels is the expected exponential decay attained (mean lifetimes are always defined in terms of the values of Γ that pertains to the energy interval of interest). Measurements on the decay in time of nuclei excited by short light pulses could confirm this theoretical expectation. In particular such data could cast light on hitherto unexplored properties of excited nuclear states below the neutron threshold.
H.A. Weidenmüller et al., [5] are studying the decay of such compound nuclear resonances within random-matrix theory [3] and find an exponential decay below the particle threshold, while they predict an exponential decay folded by a power law above the particle threshold. Weidenmüller et al.

state that such measurements "comprise information on amplitude correlations in compound nucleus resonances, which cannot be obtained from other observables and that they would establish a new unambigous test of random-matrix theory for nuclear physics".

Streaking of electrons Experimental access to sub-attosecond nuclear lifetimes can be expected from an adaptation of the well-established streaking technique of atomic physics [1,2] to decay processes in excited nuclei. Nuclear levels below the particle emission threshold ($\sim$ 6-8 MeV) not only decay by γ emission but also are accompanied by prompt conversion electrons with a fraction given by the conversion coefficient. The dominant peaks in the conversion electron spectrum are the K-conversion lines. Now we excite a level of a stable nucleus with a γ beam of suitable energy. In parallel we superimpose a laser field to the nucleus with a tunable delay between the photonuclear excitation and the streaking field for the conversion electron. The energy modulation of the conversion electron should be in the range of 5 keV, requiring only moderate laser intensities of about $10^{14} W/cm^2$. With a magnetic transport and filter system ('Mini-Orange' spectrometer [3]) for conversion electrons we can choose the transmission curve to select a narrow range of the conversion electron spectrum with high efficiency, while fully suppressing all electrons being directly accelerated from atomic shells. By varying the delay of the streaking field, lifetimes in the range of 1-100 fs can be measured. For the release of the conversion electrons we need γ beams of 10 keV - 5 MeV. Metallized tapes with stable target nuclei would be ideal targets. The measurements would allow to determine the spins and parities of the excited levels. From the transition matrix elements many properties of their wave functions could be deduced.

References

[1] D. Habs et al., Eur. Phys. J. **D 55**, 279 (2009).

[2] E. Goulielmakis et al., Science **317**, 769 (2007).

[3] H.A. Weidenmüller and R. Dietz; *Photonuclear Reactions induced by Intense Short Laser Pulses*, to be published (2010).

[4] H.A. Weidenmüller and G.E. Mitchell, Rev. Mod. Phys. **81**, 539 (2009).

[5] J. Itatani et al., Phys. Rev. Lett. 88 (2002) 173903.

[6] R. Kienberger et al., Nature 427 (2004) 817.

[7] J. v. Klinken and K. Wisshak, Nucl. Instr. Meth. 98 (1972) 1.

5.4 Stand-alone γ/e^- Facility for Nuclear Spectroscopy

5.4.1 Measuring Narrow Doorway States, embedded in Regions of High Level Density in the First Nuclear Minimum, which are identified by specific $(\gamma, f), (\gamma, \alpha), (\gamma, p), (\gamma, n)$ Reactions and allow to map out the Nuclear Potential Landscape

D. Habs[1], M. Gross[1], P. G. Thirolf[1], A. Krasznahorkay[2] and L. Csige[2]
[1] *Ludwig Maximilians University, Munich (Germany)*
[3] *MTA, ATOMKI, Debrecen (Hungary)*

We want to make use of the unique high resolution of the γ beam to selectively identify doorway states with a small damping width via the (γ, x) reaction. A prototype example are states in the second or third potential minimum of actinide nuclei, which due to their tunneling through the inner barrier show a small damping width. These transmission resonances can be uniquely identified by their fission decay. Due to the high level density in the first minimum, there are always states in the first minimum which completely mix with the states in the 2. and 3. minimum and can be nicely excited via the γ beam. This concept of weakly coupled doorway states in fission can be carried over to p,n or α decays, where strongly deformed halo states again are particle unstable and we can identify them as rather sharp resonances in photonuclear reactions. We prefer to use odd target nuclei, because then we can populate several members of a rotational band with E1,M1 or E2 transitions.
The present photon energy resolution of the HIγS facility at 6-8 MeV with 300 keV does not allow to identify these resonances, while a few keV are equivalent to the the resolution of particle-induced reactions, where we identified such resonances [16]. In this way vibrational and rotational bands in the second and third minimum can be identified [2]. From the rotational bands the moments of inertia can be determined for the states in the different minima.
We plan to employ multi-layer actinide targets, which allow to measure the fission fragment angular distributions for rather thick overall targets. From the rotational and vibrational states the potential landscape of the nuclei can de deduced. At higher excitation energies a reasonable transmission through the barrier exists and good yields can be expected. The spin and parity selectivity of the γ excitation is important. Also the damping width is an important parameter.

References

[1] P.G. Thirolf and D. Habs; Prog. in Part. and Nucl. Phys. **49**, 325 (2002).

[2] M. Hunyadi et al., Phys. Lett. **B 505** (2001) 27.

5.4.2 Precision Tests of Fluctuating Quantities in Nuclear Physics of Highly Excited Nuclear Levels in Comparison to Random-Matrix-Theory and Quantum Chaos

D. Habs[1], P. G. Thirolf[1] , H.A. Weidenmüller[2], B. Dietz[3] and N. Pietralla[2]
[1] *Ludwig Maximilians University, Munich (Germany),*
[2] *Max-Planck Institut für Kernphysik, Heidelberg (Germany),*
[3] *Institut für Kernphysik, TU Darmstadt, Darmstadt (Germany)*

A very detailed theory of highly excited compound nuclear states has been developed over the last 70 years. It started with the compound nucleus picture of Bohr [1], where a nucleon collides with a nucleus and shares its energy with many nucleons and after many collisions the energy is concentrated again in a nucleon, which then is reemitted. This started the random-matrix theory by Wigner and Dyson [2] and finally led to the recent reviews on random matrices and chaos in nuclear physics [3, 4]. The theory represents a prototype for quantum chaos and leads to many generic predictions for fluctuating quantities, like Porter-Thomas distributions for decay widths or nearest-neighbor-spacing (NNS) level distributions of the Gaussian Orthogonal Ensemble (GOE).
Until now only smaller ensembles of quantities have been studied experimentally and seem to confirm this theory. Here we want to perform precision measurements for levels above the particle threshold with the new intense, brilliant γ facility. One example are precise measurements of the energy levels and their strength of (γ, n) resonances via a longer neutron flight path setup ($\approx$100m). Here the high intensity of the γ beam, the very precise start signal (3 ps), the larger Breit-Wigner cross section and the good band width of the γ beam allow precision measurements with several orders of magnitude larger ensembles than obtained in earlier measurements.
Thus we can test the generic predictions and perhaps additional refinements become necessary. E.g. deviations from the GOE description are expected when the spreading time or equilibration time becomes comparable to the compound nucleus decay time [4]. At the same time many new predictions are being developped in much more detail within random-matrix theory and they can be tested in high resolution experiments in the energy or time domain.
The former studies of the double excitation of the giant dipole resonance [6, 7] can be regarded as a first prototype of new pump-probe experiments with γ beams, exploring the interference of different amplitudes of states, populated by damping into other compound states and then excited a second time. If the expected higher flux for γ beams can be realized with the relativistic mirror approach, such pump-probe experiments become possible for the given Breit-Wigner resonance cross sections and more detailed time dependent studies of developments in quantum chaos.
Also the decay of these compound nucleur states in time frequently are not simple exponentials, but show power law components [5,8]. Here new precision measurements in the as and zs time range (see Project 5.4) will allow to test a rich new world of predictable decay patterns.
A fourth class of experiments may explore the violation of symmetries and invariances [4]. An example are parity violating amplitudes in E1/M1 mixing (see also project 6.4), where close lying parity doublets will increase these amplitudes with increasing excitation energy, because more levels of opposite parity move closer and closer together.
Thus these precision experiments will lead to a deeper understanding of higher-lying nuclear levels and quantum chaos. We will be able to predict the strong component of the many very weak, unobservable transitions of the pygmy dipole resonance more accurately via the random matrix theory of this fluctation strength and obtain better predictions for the element production in astrophysics.
The measurement of the (γ,n) resonances also can have a large impact on the improved operation of a future phase of the γ beam facility with an ERL. Here we can measure the γ beam energy above $\approx$7 MeV with an accuracy of better than 10^{-7} by measuring the Time Of Flight (TOF) of the neutrons. By subtracting the large fixed neutron binding energy, by obtaining rather slow neutrons and having a very good start signal for the TOF, we get a very high resolution. The development of keV neutron TOF systems with good efficiency and resolution here are a major task. Thus we can measure the average γ energy and the width of the γ beam within $\approx 100\mu$s without perturbing the γ facility. This signal can be used in a feedback loop to stabilize the electron beam energy very accurately. In several measurements one wants to perform a controlled variation of the γ beam energy, which again becomes very easy.

For an improved future γ beam band width in a second phase other quantities have to be adjusted: One probably has to reduce the bunch charge to 1 pC and increase the repetition rate. It should not be a problem to improve the band width of the super cavity, as we know from LIGO cavities. Thus the photons have more periods N and smaller angular divergence. It is clear that the emittance of the γ beam is a convolution of the emittance of the electron beam and the photon beam. Thus we need the best normalized emittance from the photo cathode of the electrons. One will use a larger spot size within the diffration limit to get the best γ beam band width. Presently the high voltage ripple of the clystrons limits the achievable stability to $2 \cdot 10^{-5}$ of the cavities in ERL's and this is the area where further improvements have to focus on [9].
An improved resulution will open up a complete spectroscopy of 1^- and 1^+ levels up to 8 MeV excitation energy. In this way the vision in nuclear physics becomes possible, to study the transition from regular collective nuclear motion to chaotic motion for many nuclear species in detail. The changes in neighbour spacing of levels or changes in the γ strength distribution and its fluctuations can be studied with high accuracy.

References

[1] N. Bohr, Nature **137**, 344 (1936).

[2] C.E. Porter, *Statistical Theories of Spectra: Fluctuations*, Academic Press, New York (1965).

[3] H.A. Weidenmüller and G.T. Mitchell, *Random marices and chaos in nuclear Physics:Nuclear structure*, Rev. Mod. Phys. **81**, 539 (2009).

[4] G.E. Michell, A. Richter and H.A. Weidenmüller, *Random Matrices and Chaos in Nuclear Physics: Nuclear Reactions*, arXiv:1001.2411v1[nucl-th]14 jan 2010.

[5] H.A. Weidenmüller and B. Dietz, *Photonuclear Reactions induced by Intense Short Laser pulses*, to be published (2010).

[6] J.Z. Gu and H.A. Weidenmüller, Nucl. Phys. **A 690**, 382 (2001).

[7] H.A. Weidenmüller and G.T. Mitchell, *Random marices and chaos in nuclear Physics:Nuclear structure*, Rev. Mod. Phys. **81**, 539 (2009); chapter IV.C2 .

[8] G.E. Michell, A. Richter and H.A. Weidenmüller, *Random Matrices and Chaos in Nuclear Physics: Nuclear Reactions*, arXiv:1001.2411v1[nucl-th]14 jan 2010; Chapter V.C, *Decay in Time of the Compound Nucleus.*

[9] M. Liepe et al., ERL-09 workshop, p. 49-52 (2009).

5.4.3 Precision measurement of the dipole polarizability α_D of ^{208}Pb with high intensity, monoenergetic MeV γ-radiation for the evaluation of neutron skin and the enhancement of UNEDF theory

K.-M. Spohr[1,2], K.W.D. Ledingham[1,3,4], R. Chapman[1,2], M. Hassan[1,2]
J. Melone[1,3], S. Pain[1,2], J.F. Smith[1,2]
[1] *Scottish Universities Physics Alliance, SUPA,*
[2] *Faculty of Engineering and Science, University of the West of Scotland, Paisley, PA1 2BE, United Kingdom*
[3] *Department of Physics, University of Strathclyde, Glasgow, G4 0NG, United Kingdom*
[4] *AWE, Aldermaston, Reading, Berkshire, RG7 4PR, United Kingdom*

The creation of an Unified Nuclear Energy Density Functional (UNEDF) is the biggest collaborative effort in nuclear theory worldwide in the moment. Combining coherent efforts of 15 leading US-institutions the main aim is to find an optimum 'nuclear' functional informed by the nucleonic Hamiltonian and existing experimental data [1]. By establishing a microscopic description of all measured nuclear properties in the future, the UNEDF working group envisages to exactly reproduce known and predict new observables in hitherto undiscovered finite nucleonic systems as well as for extended asymmetric systems of astrophysical dimensions such as neutron stars. It is hoped that this quest to establish the UNEDF will unify and revolutionize theoretical nuclear physics in the same manner as it was achieved by Kohn's original work [2] on electron energy functionals for the fields of chemistry and condensed matter physics. As for heavier nucleonic systems, UNEDF is complementing and extending *ab-initio* calculations which are currently limited to nuclei with $A \leq 60$, by simplifying the computational approach using adequate functionals. The quality of these functionals is benchmarked by their ability to represent useful, quantifiable observables and, as importantly, by the uncertainty of this representation which strongly limits UNEDF's predictive powers. Work by Perlinska *et al.* [3] shows that including a particle-hole (*p-h*) mixing term, the energy density functional of a heavy system can be described as $\bar{H}(r) = \int \left(\frac{\hbar^2}{2m}\tau_0(r) + \sum_{t=0,1} (\chi_t(r) + \breve{\chi}_t(r)\right) dr^3$, where $\chi_t(r)$ is the *p-h* and $\breve{\chi}_t(r)$ is the particle-particle *p-p* interaction energy density. Both depend for $t = 0$ quadratically on the isocalar density $\rho_0 = \rho_n + \rho_p$ and for $t = 1$ on the isovector density $\rho_1 = \rho_n - \rho_p$ of which the neutron skin of a heavy system $r_{skin} = r_n^{rms} - r_p^{rms}$ is strongly dependent. In a very recent paper, Reinhard and Nazarewicz [4] quantified a strong relationship between the dipole polarizability $\alpha_D = 2 \sum_{n \in RPA} (| < \Phi_n|\hat{\mathrm{D}}|\Phi_0 > |)^2 \,/\, E_n$ and the neutron skin of ^{208}Pb based on an extensive covariance analysis. They found that α_D, which is measurable for finite nuclei, and the neutron skin r_{skin} are almost perfectly correlated with $c_{(r_{skin},\alpha_D)} = 0.98$. Moreover, they were able to show that a precise determination of the neutron radius r_n^{rms} with an experimental relative error of $\leq 0.4\%$ will dramatically reduce theoretical uncertainties in their calculations deriving the neutron matter equation of state (EoS). A sophisticated and model independent measurement of α_D will thus allow to test their newly proposed Skyrme-force based functional and its validity for describing the neutron EoS. Their calculation predicts r_{skin} to be 0.191(24) fm. Unfortunately, due to the poor quality and inconsistencies in the currently available experimental data sets, this recent advance in theory remains experimentally untested the moment. Measurements as long as four decades ago determined $\alpha_D = 13.3(14)\,\mathrm{fm^2MeV^{-1}}$ [5] and Lipparini *et al.* derived a value of $\alpha_D = 13.6(14)\,\mathrm{fm^2MeV^{-1}}$ in 1989 [6]. The situation with regard to the experimental determination of r_{skin} is not much better either. Measurements of the π^+/π^- ratio resulted in $r_{skin} = 0.0(1)$ fm [7], elastic proton scattering for different energies gave 0.14(4) fm [8] and 0.20(4) fm [9]. Inelastic α scattering results suggest 0.19(9) fm [10]. Based on these heavy discrepancies Karataglidis *et al.* [11] extracts in an overview article a value for r_{skin} of 0.17 fm, but emphasize strongly that a potential presence of systematic uncertainties in the analysis of high-energy proton scattering data would result in an overall experimental error which at worst is in the same order as the suggested value for r_{skin}. Other estimates depicted e.g. in [12] state that currently, at best, $r_{skin}(^{208}\mathrm{Pb})$ has still to be evaluated with an uncertainy of more than 5%. The nuclear community has long planned to react on the need to determine r_n^{rms} of ^{208}Pb. The proposed PREX (^{208}Pb Radius Experiment) investigation to be performed at the Jeffer-

son Laboratory (JLAB) can be seen to be the flagship initiative in this respect [13]. In the original proposal from 1999 PREX promises to establish the neutron skin thickness of ^{208}Pb with an accuracy of less than 1%.
Besides its important role in the quest to establish functionals, ^{208}Pb has long been advocated as an ideal case to unambiguously establish the existence of neutron skins and to test fundamental physics such as parity violation. With the foreseen implementation of a highly intense monoenergetic MeV source at the ELI-NP in mind, the new calculations of Reinhard and Nazarewicz [4] now suggest a measurement of the potentially readily accessible dipole polarizability of ^{208}Pb with a laser driven system in the future. As α_D is an excellent indicator to derive a precise conclusion on r_n^{rms}, an alternative and exciting experimental route has opened up. We therefore propose these studies to be performed with the intense, high energy, quasi-monochromatic γ-ray beam to be expected from ELI-NP. Our findings will allow to complement any forthcoming PREX results promising a similar level of accuracy. Our laser driven experiment will be photon based and thus is of different nature to PREX. This will allow to estimate model dependent influences in any potential JLAB measurements. The PREX investigation is e.g. heavily dependent on specific assumptions regarding the interpretation of the electron scattering data. Amongst others, the equality of normalized proton and neutron densities is assumed, as well as specific electron form factors. For our proposed the ELI experiments a thick ^{208}Pb target would be placed facing the impinging tunable MeV photon beam. The measurement of photo-transmission of the highly directional and monochromatic MeV-gamma radiation with radiation hardened semiconductor detectors will be the preferred method of detection. For these devices the experimental energy resolution matches the expected value of dE/E of $\sim 0.1\%$ of the γ-beam in the MeV regime, which can be seen as the lowest estimate for the expected uncertainties. With this projected beam quality, we will be able to deduce the total intensity of the resonant dipole absorption as function of energy with hithertho unknow precision. Hence α_D could be derived with high accuracy and a very precise study of the GDR resonance in ^{208}Pb will be obtained. Obviously, α_D derives from the sum of the amplitudes of the dipole operators expectation values in random phase approximation, weighted with $1/E$. Thus energies from $\sim 5\,$MeV up to the region of the GDR resonance in ^{208}Pb $\sim 13.6\,$MeV are of highest relevance to achieve a robust measurement. Moreover, as depicted in [4], an identification of r_n^{rms} within the proposed values in our experiment will allow discrimination between different energy functional models in the region of heavy elements. The method should also be easily transferable to a series of selected stable isotopes of theoretical interest, for which calculations could be obtained in the forthcoming years. Based on such an experimental campaign the ELI-NP system could become an established facility to inform theory in the ongoing global quest to establish an Universal Energy Density Functional.

References

[1] Bertsch, G.F.; Dean, D.J. and Nazarewicz W., *Universal Nuclear Energy Functional, Computing Atomic Nuclei*, SCIDAC Review, Winter 2007, www.scidacreview.org, 2007.

[2] Kohn, W., Reviews of Modern Physics **71** (5), 1253, 1999.

[3] Perlinska, E., *et al.* Phys. Rev. C **69**, 014316, 2004.

[4] Reinhard, P.-G. and Nazarewicz W., arXiv:1002.4140v2 [nucl-th], 2010.

[5] Veyssiere, A. *et al.*, Nucl. Phys. A. **159**, 561, 1970.

[6] Lipparini, L and Stringari S. *et al.*, Phys. Rep. **175**, 103, 1989.

[7] Allardyce, B.W. *et al*, Nucl. Phys. A. **209**, 1, 1973.

[8] Hoffmann, G.W. *et al.*, Phys. Rev. C **21**, 1488, 1980.

[9] Starodubsky, V.E. and Hintz N.M. *et al.*, Phys. Rev. C **49**, 2118, 1994.

[10] Krasnahorkay, A. *et al.*, Nucl. Phys. A **567**, 521, 1994.

[11] KARATAGLIDIS, S. *et al.*, Phys. Rev. C **65**, 044306, 2002.

[12] MICHAELS, R. *et al.*, *Proposal fo Jefferson Lab PAC 29*, http://hallaweb.jlab.org/parity/prex, 2005.

[13] HOROWITZ, C.J. *et al.*, Phys Rev C **63**, 025501, 2001.

5.4.4 Use of high-resolution inelastic electron scattering to investigate deformed nuclear shapes and the scissors mode

D. Habs[1], M. Gross[1], P. G. Thirolf[1], N. Pietralla[2] and A.A. Răduţă[3,4]
[1] *Ludwig Maximilians University, Munich (Germany),*
[2] *Institut für Kernphysik, TU Darmstadt, Darmstadt (Germany)*
[3)] *Institute of Physics and Nuclear Engineering, Bucharest, POB MG6, Romania*
[4)] *Academy of Romanian Scientists, 54 Splaiul Independentei, Bucharest 050094, Romania*

There are more than thirty years since the collective scissors mode has been predicted by Lo Iudice and Palumbo [1]. These authors considered a simple model of two axially symmetric rotors associated to the proton and neutron systems, respectively. These objects perform a scissors like angular oscillation and a rotation as a whole around the bisector line of the angle determined by the proton and neutron symmetry axis. Although the predicted M1 strength was too large, the name 'scissors mode' was kept by both phenomenological and microscopical calculations. This mode was discovered, few years later, by A. Richter in an $(e, e^{'})$ experiment at backward angles, in ^{156}Gd. The mode is lying around 3 MeV and is characterized by a M1 strength of 1-3 μ_N^2 . During more than one decade many efforts, from both theoretical and experimental sides, have been focused on discussing various features of this mode [2]. One major result shows that the M1 strength is proportional with the nuclear deformation squared which in fact proves the collective character of the mode. Therefore the large $M1$ strength is expected for the well deformed nuclei. The results have been confirmed by other experiments such as $(n, n^{'})$ at forward angles and $(\gamma, \gamma^{'})$ measurements using bremsstrahlung radiation. It is interesting to mention that the three experiments mentioned above were performed in different laboratories. For example the $(e, e^{'})$ measurements were made in the Institut für Kernphysik, Technische Universität Darmstadt, $(n, n^{'})$ in Lexington, Kentucky, while the $(\gamma, \gamma^{'})$ experiments (or fluorescence experiments) at the Dynamitron accelerator from Stuttgart.
At this point one should stress the fact that ELI is able to substitute the standard sources of electrons, neutrons and γ and therefore will be possible to perform all these three different types of experiment devoted to measuring the characteristics of the collective magnetic states in a single place, ELI-NP Bucharest.
There are many interesting properties of magnetic states which are to be studied. Here we mention only two of such features. a) Microscopic formalisms indicates that the pure orbital mode (scissors mode) is actually mixed with a spin-like mode. A simultaneous study of scissors and spin excitations may lead to a better understanding of these phenomena. b) Non-scissors-mode behavior of isovector magnetic dipole orbital transitions involving isospin transfer was not enough studied. We studied the response of isovector orbital magnetic dipole (IOMD) transitions to the quadrupole-quadrupole (QQ) interaction, to the isospin-conserving pairing interaction (ICP) and the combination of both. We found qualitatively different behaviors for transitions in which the final isospin differs from the initial isospin versus cases where the two isospins are the same. For N=Z even-even nuclei with $J = 0^+, T = 0$ ground state such as ^{8}Be and ^{20}Ne, the summed $T = 1 \rightarrow T = 2$ IOMD from the ground state to all the $J = 1, T = 1$ states in the $0\hbar\omega$ does not vanish when the QQ interaction is turned off. The pairing interaction (ICP) alone leads to a finite transition rate. For $J = 0^+, T = 1$ ground state such as ^{10}Be and ^{22}Ne, the summed $T = 1 \rightarrow T = 1$ IOMD does vanish when the QQ interaction is turned off, as is expected in a good scissors behavior. However this is not the case for the corresponding sum of the $T = 1 \rightarrow T = 2$ IOMD transitions. In ^{22}Ne (but not ^{10}Be) the sum of the $T = 1 \rightarrow T = 2$ IOMD transitions is remarkably insensitive to the strengths of both the QQ and ICP interactions. In ^{22}Ne an energy-weighted sum is similarly insensitive. Calculations were carried out in the $0\hbar\omega$.

On the other hand, we want to use the high quality, high energy electron beam for inelastic scattering experiments when the transfer of larger spins compared to the γ beam is required. An interesting case is the study of transmission resonances in the (e,e'f) reaction for ^{238}U. Here we want to determine the depth of the third minimum in ^{238}U. For ^{236}U,^{234}U and ^{232}U we observed a third minimum with a depth comparable to the second potential minimum and theoretically a similarly deep second minimum is expected for ^{238}U [16]. Due to the lack of targets this isotope could not be studied by e.g. (d,p) reactions in the same way as the lighter uranium isotopes. Starting from the 0^+ ground state we want to identify by inelastic scattering rotational bands in the second and third minimum of ^{238}U. We aim at identifying several members of the band to determine the moment of inertia. Also systematic studies of E0, E2, E3, and E4 modes of heavy nuclei will be possible at ELI Nuclear Physics Pillar in Bucharest.

References

[1] Lo Iudice and F. Palumbo, Phys. Rev. Lett. 74 (1978) 1046.

[2] G. De Francheschi, F. Palumbo and N. Lo Iudice.

[3] D. Bohle, A. Richter et al. Phys. Rev. Lett. 137 B (1982) 27.

[4] D. Zawischa, J. Phys. G 24 (1998) 683.

[5] S. Richter, Prog. Part. Nucl. Phys. 34 (1995) 261.

[6] N. Lo Iudice, . Part. Nucl. Phys. 34 (1995) 309.

[7] A. A. Raduta, A. Faessler and V. Ceausescu, Phys. Rev. C 36 (1987) 2111.

[8] A. A. Raduta, A. Faessler and I. I. Ursu, Nucl. Phys. A 489 (1988) 20.

[9] A. A. Raduta, Phys. Rev. C 51 (1995) 2973.

[10] A. A. Raduta, I. I. Ursu and D. S. Delion, Nucl. Phys. A 475 (1987) 439.

[11] A. A. Raduta and D. S. Delion, Nucl. Phys. A 491 (1989) 24.

[12] N. Lo Iudice, A. A. Raduta and D. S. Delion, Phys. Lett. B 300 (1993) 195; Phys. Rev. C 50 (1994) 127.

[13] A. A. Raduta, D. S. Delion and N. Lo Iudice, Nucl. Phys. A564 (1993) 185.

[14] A. A. Raduta et al., Phys. Rev. C 65 (2002) 024312.

[15] A. A. Raduta and N. Lo Iudice, Z.fuer Physik A 334 (1989) 403.

[16] P.G. Thirolf and D. Habs; Prog. Part. Nucl. Phys. **49**, 325 (2002).

5.4.5 Parity violation in a $(e, e^{'})$ process

A. A. Răduţă[1,2]
[1)] *Institute of Physics and Nuclear Engineering, Bucharest, POB MG6, Romania*
[2)] *Academy of Romanian Scientists, 54 Splaiul Independentei, Bucharest 050094, Romania*

The electron scattering from a nucleus is represented schematically in Fig. 38, showing cross-section variables and the Feynman diagram of the process, and Fig. 39 showing the lepton waves. The three-momentum transfer is denoted by $\mathbf{q}$ and defined as difference between the initial,$\mathbf{p}$, and the final,$\mathbf{p}^{'}$, lepton momenta, respectively. The moduli of these vectors are denoted by q, p and respectively. The angle between the initial and final momenta, $\mathbf{q}$ and $\mathbf{q}^{'}$, θ, is called dispersion angle. The transferred energy ω is the difference between the initial, ϵ and final, $\epsilon^{'}$, kinetic energies of the lepton. Since the process considered is elastic, the total kinetic energy is constant; therefore the nuclear target is not excited and the energy transfer is just the kinetic energy of the recoiling target. The kinetic energy of the projectile and the transferred energy, using natural units, are defined by:

$$\epsilon = \sqrt{m_e^2 + p^2} - m_e, \;\; \omega = \sqrt{M^2 + q^2} - M. \tag{1.43}$$

The relation between the momentum transfer, the energy of the incoming electron and the scattering angle is obtained by an elementary manipulation:

$$\begin{aligned} q^2 &= (\vec{p} - \vec{p}^{'})^2 p^2 + p^{'2} - 2pp^{'}\cos\theta \approx \epsilon^2 + \epsilon^{'2} - 2\epsilon\epsilon^{'}\cos\theta \\ &= \epsilon^2 + (\epsilon - \omega)^2 - 2\epsilon(\epsilon - \omega)\cos\theta \approx 2\epsilon^2(1 - \cos\theta = 4\epsilon^2 \sin^2(\theta/2). \end{aligned} \tag{1.44}$$

The notations m_e and M stand for the electron and target masses, respectively.

$$Q^{\mu} = (\omega, \vec{q}); \;\; Q^2 = q^2 - \omega^2. \tag{1.45}$$

In calculating the form factor of the $(e, e^{'})$ process the following kinematic factors are used:

$$\kappa = \frac{q}{2m_N}, \;\; \tau = \frac{q^2 - \omega^2}{4m_N^2}. \tag{1.46}$$

The Feynman diagram from Fig. 38 shows that whenever a photon is exchanged between two charged particles, a Z^0 is also exchanged. At the energies of interest in electron scattering the strength of the weak process mediated by the Z^0 boson is negligible compared to the electromagnetic strength. Hence the Z^0 exchange does not play any role in the electron scattering process unless an experiment is set up to measure the parity violation observable. While the electromagnetic interaction conserves parity, the weak interaction does not and it is through parity violation that we are sensitive to Z^0 -exchange in electron scattering.
A direct way to measure the degree of parity violation in the process is by means of the parity-violating asymmetry,

$$A = \frac{d\sigma^{+} - d\sigma^{-}}{d\sigma^{+} + d\sigma^{-}}, \tag{1.47}$$

which is proportional to the difference between the cross section of incoming electrons longitudinally polarized parallel and anti-parallel to their momentum.
Since the weak interaction operator contains vector and axial-vector components which behave differently under the parity transformation, a process involving a weak interaction is clearly distinguishable from its mirror image.
Indeed, as shown in Fig. 40 an electron polarized parallel to its momentum becomes in its mirror image polarized anti-parallel to its momentum. This happens due to the axial-vector character of spin (does not change the sign when the parity transformation is performed).

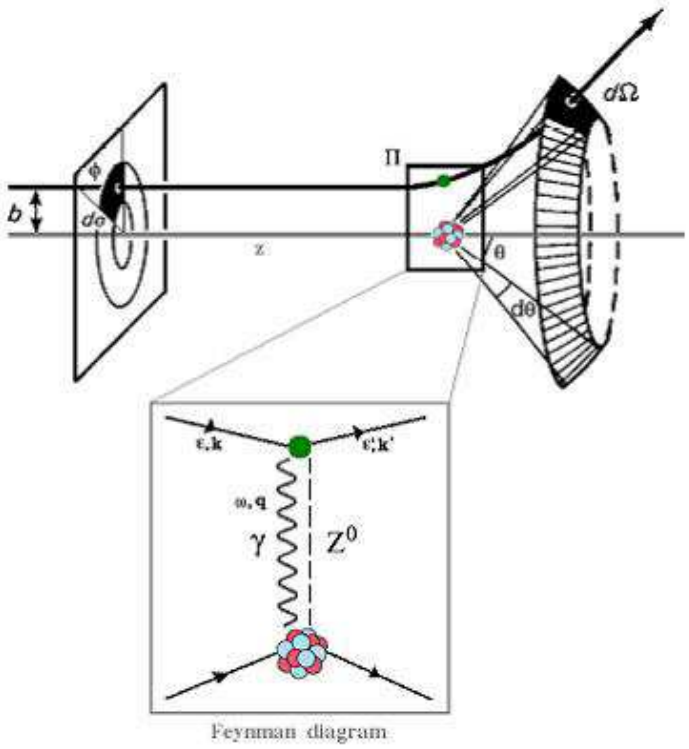

Figure 38: Top: Schematic representation of an electron scattering off a nucleus, showing the impact parameter b, the scattering angle θ, the differential cross-section $d\sigma$, the corresponding differential solid angle $d\Omega$, and the scattering plane Π. Bottom: First-order Feynman diagram of the process of interest, in which a photon and Z^0 are exchanged between the electron and the nucleus.

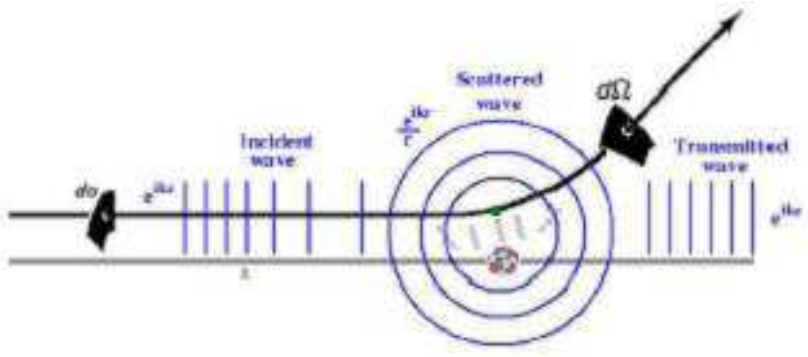

Figure 39: Schematic representation of the scattering process, showing the incident (plane), the scattered (plane) and the transmitted (plane) waves of the electron

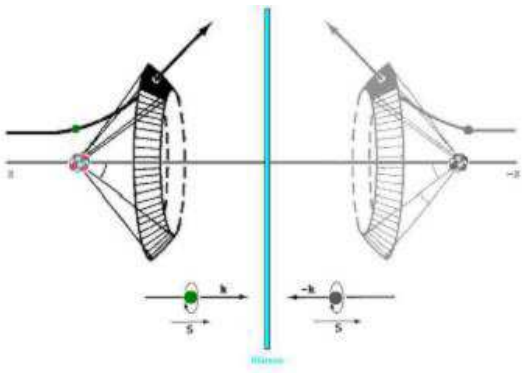

Figure 40: Schematic representation of the scattering process and its mirror (parity transformed) image. Spin and momentum of the scattered electron in both sides of the mirror are also shown.

One can consider the exchange of a single gauge boson for each interaction with charged lepton wave function unaffected by the nuclear target field, i.e. within plane wave Born approximation (PWBA); in this way the parity-violation asymmetry can be written as:

$$A = \frac{G_F}{2\pi\alpha\sqrt{2}} Q^2 \frac{W^{PV}}{W^{PC}}, \tag{1.48}$$

where G_F and α are the Fermi and fine-structure constants, respectively,W^{PV} and W^{PC} are the parity-violating and parity conserving responses, and Q is the four- momentum transfer in the scattering process. The parity violating (PV) and parity conserving (PC) responses can be separated into longitudinal W_L and transversal W_T responses and written in terms of the Coulomb, electric, and magnetic form factors of different multipolarities J (F_{CJ}, F_{EJ}, F_{MJ} respectively), as well as in terms of vector and axial-vector current form factors for the electromagnetic $F(EM)$ and the weak neutral $\tilde{F}, \tilde{F}^A$ (WNC) currents. If we restrict ourself to elastic scattering of $J = 0^+$ nuclear targets the ratio of the PV and PC responses becomes:

$$\frac{W^{PV}}{P^{PC}} = \frac{2C_A^e F_{C0}(q)\tilde{F}_{C0}(q)}{F_{C0}^2(q)} = \frac{2C_A^e \tilde{F}_{C0}(q)}{F_{C0}(q)} \tag{1.49}$$

because only Coulomb-type monopole operators (C0) can induce the elastic transition. Further on, every form factor can be decomposed into isospin-projected terms, namely the isoscalar ($T = 0$) and isovector ($T = 1$) ones. When considering an $N = Z$ nuclear target with pure isospin $T = 0$ in its ground state, only the isoscalar part of the form factors is nonzero and the EM and WNC form factors become proportional, yielding

$$\frac{W^{PV}}{W^{PC}} = 2c_A^e \beta_V^0, \tag{1.50}$$

where $c_A^e = -0.5$ and $\beta_V^0 = -2\sin^2\theta_W$ (Standard Model constant expressed in terms of the mixing angle). The corresponding asymmetry is:

$$A = A^0 \equiv \left[\frac{G_F Q^2}{2\pi\alpha\sqrt{2}}\right] 2c_A^e \beta_V^0 \approx 3.22 \cdot 10^{-6} Q^2, \tag{1.51}$$

with the momentum transfer measure in fm^{-1}. Starting from this reference value one can establish deviations proportional to the reference value itself,

$$A = A^0(1 + \Gamma). \tag{1.52}$$

The deviation is influenced by isospin mixing in the nuclear states, isospin impurities in the nucleon (strangeness content) or distorted-wave treatment of incoming and outgoing electron wave functions

[2-10]. These effects were analyzed for four even-even, N=Z isotopes, namely ^{12}C, ^{24}Mg, ^{28}Si and ^{32}S , which are the most abundant isotopes of the corresponding element in Ref.[1]. Here I will present only the PV asymmetry with ^{28}Si as target with the effects of nuclear isospin mixing and Coulomb distortion of incident electron analyzed separately. When nuclear isospin mixing is not considered (superscript 0) which is computed by fixing the same proton and neutron densities, the PWBA asymmetry A^0_{PW}, should show a linear Q^2 behavior. As a matter of fact this behavior is shown in Fig. 41. If to these circumstances we add the Coulomb distortion for the electron wave function, the corresponding asymmetry, A^0_{DW} shows a dip. The inclusion of isospin mixing (superscript I) in the plane wave (PW) case gives rise to extreme, divergent modifications of the asymmetry A^I_{PW} due to the diffraction minima of the WNC and EM form factors occurring now at different momenta. The effect of considering distortion in this last case is to fill in or to smooth out the diffraction minima and therefore to avoid the divergence in the asymmetry A^I_{DW}.

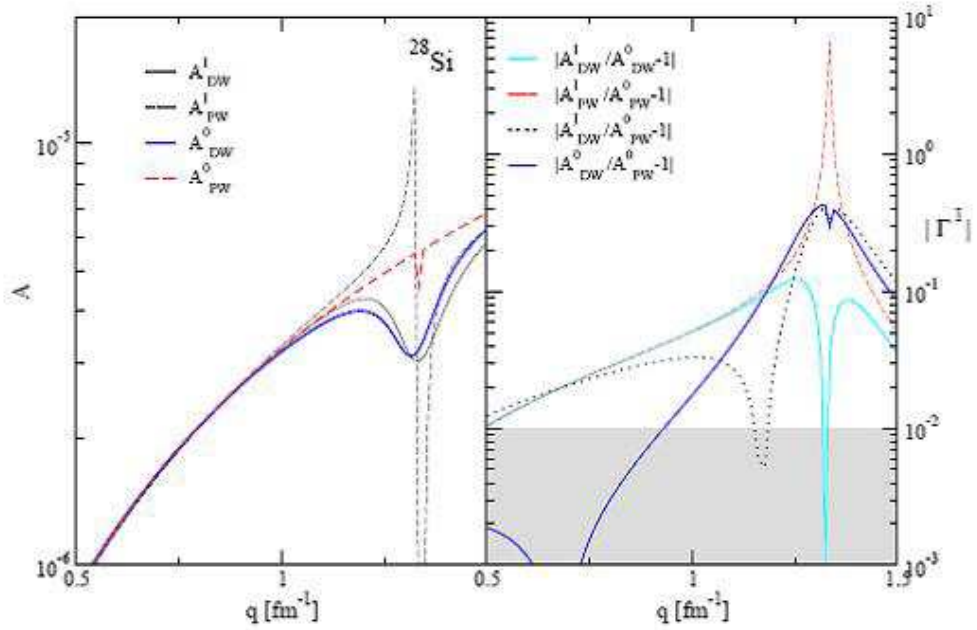

Figure 41: Left-hand panel: PV asymmetry for ^{28}Si with isospin mixing (A^I) and without it (A^0), for a PWBA calculation (A_{PW}) and allowing distortion (A_{DW}). Right-hand panel: Asymmetry deviations for ^{28}Si due to pure isospin mixing effects in DW (solid line) and in PWBA (dashed line), due to isospin mixing and distortion effects together (dotted line) and due to distortion effects only (thick solid line).

In Ref [1] the PV asymmetry was analyzed also for N different of Z nuclei where the fact that proton and neutron densities are different may play an important role. The PV asymmetry in elastic electron scattering from the HF ground state of ^{208}Pb is shown in Fig. 42 in PWBA and DWBA.
The quantity R_{np} is expressed in terms of proton and neutron Coulomb form factors as:

$$R_{np} = |F_n/F_p - 1| \approx \Gamma. \tag{1.53}$$

Summary
A new device is usually used to explore new phenomena to be discovered in the field considered. On the other hand old subjects could be viewed from a completely new angle. One of the major task of an experiment is to unveil a new symmetry of the nuclear matter or fix the conditions when such symmetries are broken. I believe the subject I have described before belongs to the class of objectives of the nature mentioned above. Indeed, in a process governed by the weak interaction the parity is not conserved. This was proved long time ago in the experiment of Wu [11] for the

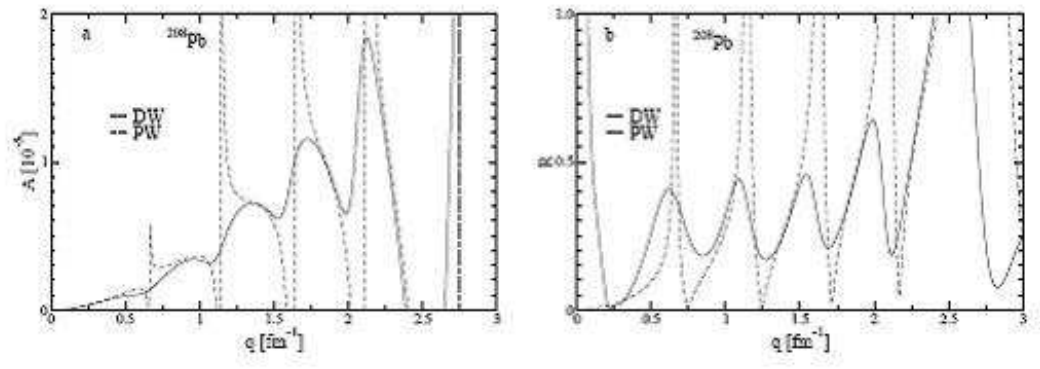

Figure 42: Left panel: Plane wave (PW) and distorted wave (DW) PV asymmetries of ^{208}Pb in its ground state. Right panel: for the same nucleus, the quantity R_{np} in plane wave (PW) and distorted wave (DW).

single beta decay. Weak interaction is mediated by the boson Z0. If the parity violation is a general signature of weak interactions than that phenomenon should take place in an () experiment where the weak interaction between the projectile and one nucleon from the target shows up. There are some attempts to interpret the asymmetry of the process cross section as a prove for the parity violation. The arguments presented here were taken from the PhD thesis of Oskar Moreno from Madrid [1]. There are several open questions related to the involved phenomena. One of them, which deserves attention, is whether this interpretation is unique. Investigations on this line are possible at ELI given the fact that the electrons delivered there, could be accelerated in a synchrotron and then used in an () process.

References

[1] Oskar Moreno Diaz, Electroweak processes in nuclei, PhD thesis, Universidad Complutense de Madrid, 2010.

[2] J. E. Amaro et al., Nucl. Phys. A 602 (1996), 263.

[3] J. E. Amaro et al., Nucl. Phys. A 611 (1996) 163.

[4] S. Jeschonnek and T.W. Donnelly, Phys. Rev. C 48 (1993), 960R.

[5] C. J. Horowitz et al., Phys. Rev. C 63 (2001) 025501.

[6] P. Raghavan, At. Data and Nucl. Data Tables 42 (1989) 189.

[7] I. Sick and J. S. McCarhty, Nucl. Phys. A 150 (1970) 631.

[8] W. Reuter, Thesis, KPH Mainz, 1981.

[9] G. C. Li, et al., Phys. Rev. C 9 (1974) 1861.

[10] E. W. Lees, et al., J. Phys. G 2 (1976) 105.

[11] C. S. Wu et al., Phys. Rev. 105 (1957) 1413.

5.4.6 Nuclear Transitions and Parity-violating Meson-Nucleon Coupling

D. Habs[1], M. Gross[1], P. G. Thirolf[1], K. Sonnabend[2], N. Pietralla[2], D. Savran[2],
A. Krasznahorkay[3],L. Csige[3] and M. Fujiwara[4]
[1] *Ludwig Maximilians University, Munich (Germany),*
[2] *Institut für Kernphysik, TU Darmstadt, Darmstadt (Germany),*
[3] *MTA, ATOMKI, Debrecen (Hungary)*
[4] *Osaka University, Osaka (Japan)*

In Ref. [1] light nuclei with known highly excited parity doublets in ^{14}C,^{14}N,^{15}O,^{16}O,^{18}F and ^{20}Ne are investigated theoretically for the enhancement of parity mixing amplitudes of E1/M1 or E2/M2 transitions. According to first order perturbation theory calculations, the mixing is strongly enhanced, because the parity violating matrix element is divided by the small energy difference of the two levels of opposite parity. The doublet levels are at excitation energies between 5 MeV and 12 MeV and can be nicely reached with the high resolution γ beam facility, where $\Delta E_\gamma/E_\gamma \leq 10^{-3}$ is expected to be realized, but even extensions to 10^{-5} appear possible. Until now many nuclei with a possible E1/M1 mixing have been investigated like ^{19}F (1080keV); ^{19}F (109.9 keV); ^{21}Ne (2789 keV); ^{175}Lu (396 keV); however, experimental accuracies were insufficient. With the brilliant, tunable, polarized and monochromatic γ beams the effect of parity non-conservation (PNC) will be studied at higher excitation energies. For circularly polarized γ beams a forward-backward asymmetry, which is linear in the parity mixing amplitude, can be used to measure mixed parity transitions, where a high sensivity is reached by switching the sign of the circular polarisation. The experiments will allow to understand the fundamental role of the exchange processes of weakly interacting bosons in the nucleon-nucleon interaction [3–5]. Fig.43 illustrates this exchange process.

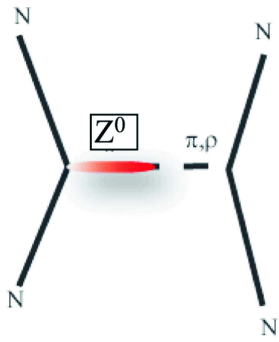

Figure 43: Parity-violating nucleon-nucleon interaction. The Z_0 graph is not plotted to scale, since its Compton wavelength of 0.02 fm is very small.

The results can also be compared with chiral perturbation theory, furthering the development of effective couplings between Z_0 and π, ρ and ω mesons.
^{20}Ne seems to be most interesting case with largest enhancement. The two highly excited parity doublet levels where observed in particle-induced reactions and not in a (γ, γ') reaction. Their energies are quoted in the Nuclear Data Sheets as 11262.3(19) keV for the 1^+ state and 11270(5) keV for the 1^- state. Both states are assigned to be T=1 states and thus the isospin quantum number does not prevent their mixing. Their excitation energy difference is thus $\Delta E = 7.7(5.7)$ keV. If their total widths are comparable to their energy difference, then mixing due to the effects of the maximum parity-violating weak interaction must be expected. Observation of such a mixing effect would represent a rare precision test of the weak interaction on nuclear structure. Unfortunately, the current accuracy of the enrgy difference is insufficient for an estimate of the amount of parity mixing. The width of the 1^- is known to be smaller than 0.3 keV. The total width of the 1^+ state is unknown. Its ground state $M1$ decay width is $\Gamma_0 = 11 \pm 2$ eV. Thus, besides the forward-backward assymetry due to parity mixing, also the other properties of the doublet, like the energy splitting of the two levels and their decay widths, have to be measured accurately. Also the purity of the circular polarisation of the γ beam has to be determined. Direct investigations in high-resolution ($\gamma\gamma'$) reactions with large-volume

Table 10: Candidate for PNC asymmetry in light nuclei

Nucleus	Transition	E_{f1}	E_{f2}	Amplif. fac.
^{14}C	$(0^+,1) \rightarrow (2^-,1)$	7340 keV	7010 keV	31±6
^{14}N	$(1^+,0) \rightarrow (1^+,0)$	6203 keV	5691 keV	7.0± 2.0
	$(1^+,0) \rightarrow (0^+,1)$	8624 keV	8776 keV	40 ± 5
	$(1^+,0) \rightarrow (2^-,1)$	9509 keV	9172 keV	45 ± 5
^{15}O	$(1/2^-,1/2) \rightarrow (1/2^-,1/2)$	11025 keV	10938 keV	37±7
^{16}O	$(0^+,0) \rightarrow (2^-,0)$	8879 keV	6917 keV	18±2
^{18}F	$(1^+,0) \rightarrow (1^-,0+1)$	5605 keV	5603 keV	590±110
^{20}Ne	$(0^+,0) \rightarrow ((1^-,0)$	11270 keV	11262 keV	670±7000

Germanium detectors are highly desirable.

References

[1] A.I. Titov et al., J. Phys. G: Nucl. Part. Phys. **32**, 1097 (2006).

[2] U.E.G. Berg et al., Phys. Rev. **C 27**, 2981 (1983).

[3] E. Adelberger et al., Nucl. Phys. **A 396**, 221c (1983).

[4] E. Adelberger et al., Ann. Rev. Nucl. Sci. **35** , 501 (85).

[5] B. Desplanques., Phys. Rep. **297**, 1 (1998).

[6] R. Hajima et al., Nucl. Instr. and Meth. **A 608**, 557 (2009).

5.4.7 Study of pygmy and giant dipole resonances in lead isotopes by direct γ excitation

C. Borcea[1], M.N. Harakeh[2], A. Negret[1] and N.V. Zamfir[1]
[1]*Horia Hulubei National Institute for Physics and Nuclear Engineering, Bucharest - Magurele, 070125, Romania*
[2]*Kernfysisch Versneller Instituut, Zernikelaan 25, NL-9747 AA Groningen, The Netherlands*

Pygmy dipole resonances (PDRs) in nuclei are frequently interpreted as a collective phenomenon representing an oscillation of the neutrons in excess (to protons) with respect to the N=Z core while giant dipole resonances (GDRs) are seen as oscillations of the proton and neutron fluids with respect to each other. PDRs are placed much lower in energy than GDRs and they represent only a small fraction of the total E1 strength (few percents), while GDRs, highly placed in energy, exhaust almost fully the E1 strength (TRK sum rule). The PDR occurs close to the neutron emission threshold and its decay is governed by the coupling to the large number of states around the threshold. Most frequently microscopic models (RPA, RRPA, QPM, TDHF theory) are invoked to interpret and understand the experimental results. From the experimental point of view, many measurements were carried out throughout the chart of nuclides, much more for GDR than for PDR. The resonances were excited by various means like light-particle or heavy-ion bombardment or directly by γ rays. Subsequent particle and/or γ decay were recorded. When excited by γ rays, these were produced by positron-annihilation in flight, by bremsstrahlung, by Coulomb excitation (virtual γ rays) and more recently by dedicated γ sources based on Compton backscattering. The last technique has substantial advantages like: the narrow width in energy, the easy energy variation and the fact that γ beams are polarized. The present proposal intends to measure the excitation function of the γ scattering cross section on separated lead isotopes in a range of energies covering both PDR and GDR, i.e. until about 18 MeV. The measurements will be carried out at the high-resolution and high peak brilliance γ source of ELI-NP, using polarized beams. The expected output of the experiment consists of measured excitation functions for elastic and inelastic γ scattering revealing possible fine structures/splitting of PDR and GDR, excitation function with high resolution for (γ,n) and (γ,charged particle) channels, allowing to determine the branching ratios for various decay channels. The polarized beam will also allow determining the E1 or M1 type of excitation for the observed structures. The experimental setup will include large efficiency Ge detectors arranged in the vertical and horizontal planes as well as silicon telescopes for charged particles set up in a thin-wall evacuated reaction chamber around the target. The beam monitoring will be done by measuring with a Ge detector the incident γ flux scattered on a high-Z material at a small angle, few meters downstream from the target. The very well-defined γ beam would allow an effective shielding of the detectors used in the experiment from the monitoring system. Though the present proposal is rather exploratory for the potential of the γ source for such type of measurements, significant improvement and enrichment of present experimental data is expected. The experiment will be a first step in a sequence of systematic investigations of PDR and GDR in neutron-rich nuclei.

5.4.8 Gamma scattering on nuclei
The Pygmy Dipole Resonance (PDR) of deformed nuclei

D. Savran[1], N. Pietralla[1], K. Sonnabend[1],
R.A. Ionescu[2], D. Pantelica[2], C. Haţegan[2]
[1] *Institut für Kernphysik, TU Darmstadt, Darmstadt (Germany)*
[2] *IFIN-HH, Bucharest (Romania)*

Radiative (gamma ray) strength functions, especially dipole strength functions, are an important ingredient for the analysis of photodisintegration reactions (e.g. (γ, n)) and their inverses, radiative capture reactions (e.g. neutron radiative capture, (n, γ), and proton radiative capture, (p, γ)).
The radiative neutron capture is responsible for the production of heavy elements (elements beyond iron) in stars [1]. Neutron capture processes divide into two classes:

1. the slow neutron capture process (s-process) where the produced nucleus decays to a stable nucleus before further neutron capture occurs

2. the rapid neutron capture process (r-process) where the neutron flux is so high that the nucleus capture many neutrons before it can decay

When the capture cross section is small we expect a build-up leading to larger abundances. This happens when the number of neutrons is magic (N=50, 82, 126) and this corresponds in beta stable nuclei to mass number A=90 (^{90}Zr), $\sim$ 140 (^{138}Ba and ^{140}Ce - the most abundant of the rare earth elements), and 208 (^{208}Pb which is double magic).
Moreover, the proton radiative capture at small (at nuclear scale) energy and radiative disintegration (p-process responsible for production of some neutron deficient stable isotopes: N=50 ^{92}Mo, Z=50 ^{112}Sn, N=82 ^{144}Sm) play an important role in stellar evolution.
The standard theoretical tool to derive neutron capture cross sections for unstable isotopes relevant for the s- and r-processes is the Hauser-Feshbach statistical model. The ingredients for the model are the radiative strength functions and the neutron strength functions.
Dipole strength functions can be obtained from photoabsorption cross sections σ_γ using (γ, n) reactions. These experiments are restricted to the energy region above the neutron separation energy where the giant dipole resonance is located. Starting with [2, 3] it has been found that in the energy region from 10 to 30 MeV the cross sections for all nuclei exhibit a resonance like structure due to dipole electrical (E1) multipolarity of incoming gamma. With the availability of monoenergetic photons from in flight annihilation of fast positrons obtained by pair production from bremsstrahlung (typical 1% energy resolution) and tagged bremsstrahlung the emphasis changes from the exploration of the absorption process to the understanding of the giant resonance states especially in light nuclei where the density of states is smaller than in heavier nuclei (see [4] for a review).
The giant dipole resonance corresponds to the fundamental frequency of absorption of electric dipole radiation by the nucleus and is most simply understood as the oscillations of the neutrons against the protons in the nucleus (semiclassical hydrodynamic models of Goldhaber and Teller [5] and Steinwedel and Jensen [6]). Microscopically one construct the giant resonance from a superposition of (quasi)particle-(quasi)hole states based on the shell model or its extensions (HFB) [7]. In the schematic model of Brown and Bolsterli for doubled closed shell nuclei it was proven that one 1^- state from many possible particle-hole states is pushed up in energy due to the residual interaction and it collects all the dipole electric transition strength.
Therefore, the presence of the giant dipole resonance is a well established fact in all nuclei. Nevertheless, the precise knowledge of the dipole strength on the low energy tail of the giant dipole resonance, especially the properties of the dipole strength at varying number of proton and neutrons, is an open problems in nuclear physics. Moreover the dipole strength at low energy (below and around the neutron emission threshold) can have electric (pygmy dipole resonance) or magnetic character. Both parts, the electric dipole strength in vibrational nuclei (1^- quadrupole-octupole two-phonon states, pygmy resonances close to the particle emission threshold [8]) as well as the magnetic dipole excitations (low lying orbital scissors mode in deformed nuclei, high lying spin-flip mode [8, 9]) are interesting topics in nuclear physics of stable and radioactive nuclei.

One clean way to probe the structure of the states of an atomic nucleus is to use electromagnetic probes: (forward) proton scattering, electron scattering and photon scattering (virtual photon scattering, i.e. Coulomb excitation/breakup or real photon scattering). The photon scattering is an ideal tool to investigate low-lying dipole strength in stable nuclei because of its selectivity to low spin states: the states excited by electric and magnetic dipole transition from the ground state dominate the resonant gamma scattering.
The new photon scattering experiments use two sources of photons: (partially linearly polarized) bremsstrahlung (high flux, $10^6 photons/(keV \cdot s)$, but continous spectrum) at Stuttgart Dynamitron (shut down in 2005), at S-DALINAC in Darmstadt, at 15MeV Linac in Gent [10] and at high current electron accelerator ELBE in Rossendorf and the high-flux, quasi-monochromatic photon sources, tuneable in energy, and of nearly 100% linear polarization by laser Compton back-scattering (lower total flux, $10^6 photons/s$, but small energy spread of the order of 100 keV at 10 MeV) at HIγS at Duke [11] and in Japan. The monochromaticity of this novel photon beam together with high resolution and high efficiency γ-spectrometres will allow a detailed study of the fragmentation of the dipole strength and its dependence on the parameters characterizing different nuclei: shell efects, deformation etc.
The critical parameters of the photon beam are: **small energy spread** to reduce both the background Compton scattering and to allow a selective excitation of states if the density of dipole excited states in the energy region of interest is low (spherical nuclei) or at least to explore with high energy resolution the dipole strength when the density of excited states is large (deformed nuclei) and **high intensity** to obtain statistically relevant experimental data in resonable time and with smaller target (especially important for long-lived beta unstable nuclei or isotopically pure targets).
Even for very good energy resolution, the energy width of the beam (keV) is large compared to the level radiative widths ($\mu eV - eV$), and the experimental signal is the cross section integrated over resonance which is proportional with the radiative width.
Up to now the experimental studies of the low lying electric dipole strength was done for few light nuclei, ^{26}Mg [12], ^{27}Al [13] and for nuclei with magic number of protons and/or neutrons: N=50 (^{87}Rb [14], ^{88}Sr [15], ^{89}Y [16], ^{90}Zr [17]) or close to N=50 (^{92}Zr and ^{96}Mo [18], even Mo isotopes [19], Zr isotopes [20]), Z=50 (Sn isotopes [21]), N=82 (^{138}Ba [22]), or close to N=82 (^{142}Ce [23]), N=126, Z=82 (^{208}Pb [24]) and Pb isotopes [24].
As possible higly interesting experimental topics we propose:

- Studies of the pygmy dipole resonance via resonant photon scattering for neutron closed shell nuclei

  This nuclei are important for the slow neutron capture process in stars and the systematic study of the pygmy dipole resonance below the particle emission threshold will allow to understand the source of this strength decoupled from the giant resonance. We mention that Lane, who introduced the concept of "pygmy resonance" in 1971 [25], discussed the possibility that the dipole electric strength decoupled from the giant resonance in the region of neutron emission threshold is due to the small overlap with other states of some low angular momentum neutron single particle threshold states (they spread out of the nucleus at the expense of being depressed inside). This avoided mixing of some states into the giant dipole resonance due to boundary conditions is worth studying with the modern experimental facilities as it will constraints also the behaviour of this pygmy strength in nuclei far from stability. We are not aware of any test of this idea in recent photon scattering experiments, but the behaviour of the pygmy dipole strength in N=50 stable even isotones (^{136}Xe - ^{144}Sm) [26] indicates a larger pygmy dipole strength around 6MeV for ^{136}Xe (neutron separation energy $\sim$ 8 MeV) than for ^{144}Sm (neutron separation energy $\sim$ 11 MeV). The same behaviour is apparent for Z=50 Sn isotopes [27].

- Studies of the pygmy dipole resonance via resonant photon scattering for deformed nuclei

  The behaviour of the low lying electric dipole strength for deformed nuclei is an other interesting topic. The main question is how the incresed deformation for nuclei far from closed shell affect the total strength in the pygmy resonance region. One expects that the deformation will increase

the 1^- level density (for even-even nuclei) in the pygmy resonance energy region and the strength will be spreaded over many more individual resonances.

- Studies of the dipole strength in light nuclei

  The light stable nuclei are involved in radiative proton capture processes in stars and the behaviour of their dipole electric strength both below and above proton separation threshold is relevant for nuclear astrophysics. In this light nuclei the electric dipole strength is fragmented due to the low density of states. Therefore the investigation of individual resonances is experimentally easier. Moreover it seems that the measurement of radiative width above the proton separation threshold is feasible (the neutron threshold is higher and the proton width remains small, comparable with the radiative width, due to the Coulomb barrier). Such measurements will better constrain the radiative width for resonances relevant for proton capture reactions at stellar energies.

Phenomena in nuclear physics which have recently attracted great interest of experimentalists as well as theoreticians are collective electric dipole modes below the Giant Dipole Resonance, frequently denoted as Pygmy Dipole Resonances (PDR) [8, 28]. Evidence for such excitation modes has been found in many stable spherical nuclei below the particle separation energies [4,5,26,29,30]. In addition above threshold energies a similar observation has been made recently in exotic nuclei with a large neutron excess [33, 34]. The experiments are accompanied by intense theoretical investigations to explain the nature of this nuclear phenomenon, see e.g. [35] and references therein. Understanding the nature of the low-lying E1 strength will, e.g., help to constrain the symmetry energy in atomic nuclei [36] and has an impact on reaction rates of astrophysical interest [37, 38] as well as on the photodisintegration of ultra-high-energy cosmic rays [39]. However, the experimental database is still scarce, especially for non-magic nuclei. Consequently the influence of deformation on the PDR strength has yet not been investigated experimentally, while recently first relativistic Random Phase Approximation (RPA) calculations of low-lying E1 strength in deformed nuclei became available [40, 41]. It is thus of mandatory importance to extend the experimental investigations towards deformed nuclei in order to provide the necessary test grounds for these modern calculations.
The method of choice for the investigation of low-lying E1 strength below the particle threshold in stable nuclei is the method of real photon scattering [8, 42]. It assures a clean excitation mechanism and allows a model independent extraction of quantum numbers such as multipolarities, absolute strengths, decay branching ratios, and parities. Up to now, nearly exclusively bremsstrahlung has been used as high energy photon source. However, the investigation of the E1 strength close to the particle thresholds in deformed nuclei has been hindered by the extremely high level densities. In addition, the determination of parities is mandatory for the clean identification of E1 strength in deformed nuclei, which is difficult to achieve with unpolarized bremsstrahlung. These drawbacks can be overcome by using Linear Compton Backscattered (LCB) photons, as has partly been shown in [5, 43]. The benefits of using a monoenergetic polarized LCB source is two-fold:

- The monoenergetic character of the beam will allow a energy dependent determination of the photon absorbtion cross sections even in the vicinity of very high level densities.
- The polarized character of the beam will allow for an unambiguous disentanglement of E1, M1 and E2 contributions to the photon absorption cross section.

Compared to the experiments using LCB photons performed in [5, 43], the superior properties of ELI will improve the sensitivity of the experiments by at least one order of magnitude and thus will allow the investigation of the PDR also in deformed nuclei.

References

[1] E.M. Burbidge, G.R. Burbidge, W.A. Fowler, F. Hoyle, Rev. Mod. Phys. **29** (1957) 547

G. Wallerstein et al., Rev. Mod. Phys. **69** (1997) 995

C. Iliadis, *Nuclear Physics of Stars*, Wiley-VCH Verlag, Weinheim, 2007

[2] W. Bothe, W. Gentner, Z. Physik **106** (1937) 236

[3] G.C. Baldwin, G.S. Klaiber, Phys. Rev. **71** (1947) 3

[4] B.L. Berman, S.C. Fultz, Rev. Mod. Phys. **47** (1975) 713

[5] M. Goldhaber, E. Teller, Phys. Rev. **74** (1948) 1046

[6] H. Steinwedel, H. Jensen, Z. Naturforsch. **5A** (1950) 413

[7] G.E. Brown, M. Bolsterli, Phys. Rev. Lett **3** (1959) 472

[8] U. Kneissl, N. Pietralla, A. Zilges, J. Phys. G **32** (2006) R217.

[9] K. Heyde, P. von Neumann-Cosel, A. Richter, nucl-ex/1004.3429, to appear in Rev. Mod. Phys.

[10] K. Govaert et al., Nucl. Inst. Meth. **A337** (1994)265

[11] H.R. Weller et al., Prog. Part. Nucl. Phys. **62** (2009) 257

[12] R. Longland et al., Phys. Rev. **C80** (2009) 055803

[13] N. Pietralla et al., Phys. Rev. **C51** (1995) 1021

[14] L. Kaubler et al., Phys. Rev. **C65** (2002) 054315

[15] N. Pietralla et al., Phys. Rev. **C65** (2002) 047305
L. Kaubler et al., Phys. Rev. **C70** (2004) 064307
R. Schwengner et al., Phys. Rev. **C76** (2007) 034321

[16] N. Benouaret et al., Phys. Rev. **C79** (2009) 014303

[17] R. Schwengner et al., Phys. Rev. **C78** (2008) 064314

[18] C. Fransen et al., Phys. Rev. **C70** (2004) 044317

[19] G. Rusev et al., Phys. Rev. **C79** (2009) 061302(R)
M. Erhard et al., Phys. Rev. **C81** (2010) 034319

[20] H. Utsunomiya et al., Phys. Rev. Lett. **100** (2008) 162502

[21] H. Utsunomiya et al., Phys. Rev. **C80** (2009) 055806

[22] R.-D. Herzberg et al., Phys. Rev. **C60** (1999) 051307
N. Pietralla et al., Phys. Rev. Lett. **88** (2002) 012502
A.P. Tonchev et al., Phys. Rev. Lett. **104** (2010) 072501

[23] A. Gade et al., Phys. Rev. **C69** (2004) 054301

[24] N. Ryezayeva et al., Phys. Rev. Lett. **89** (2002) 272502
J. Enders et al., Nucl. Phys. **A724** (2003) 243

[25] A.M. Lane, Ann. Phys. **63** (1971) 171
B. Gyarmati, A.M. Lane, J. Zimanyi, Phys. Lett. **50B** (1974) 316
L.P. Csernai, J. Zimanyi, B. Gyarmati, R.G. Lovas, Nucl. Phys. **A294** (1978) 41

[26] S. Volz, N. Tsoneva, M. Babilon, M. Elvers, J. Hasper, R.-D. Herzberg, H. Lenske, K. Lindenberg, D. Savran, A. Zilges, Nucl. Phys. **A779** (2006) 1

[27] B. Ozel et al., Nucl. Phys. **A788** (2007) 385c

[28] G. A. Bartholomew, E. D. Earl, A. J. Ferguson, J. W. Knowles, M. A. Lone, Adv. Nucl. Phys. **7** (1973) 229.

[29] K. Govaert, F. Bauwens, J. Bryssinck, D. De Frenne, E. Jacobs, W. Mondelaers, L. Govor, V. Y. Ponomarev, Phys. Rev. C **57** (1998) 2229.

[30] R. Schwengner, G. Rusev, N. Benouaret, R. Beyer, M. Erhard, E. Grosse, A. R. Junghans, J. Klug, K. Kosev, L. Kostov, C. Nair, N. Nankov, K. D. Schilling, A. Wagner, Phys. Rev. C **76** (2007) 034321.

[31] D. Savran, M. Fritzsche, J. Hasper, K. Lindenberg, S. Müller, V. Y. Ponomarev, K. Sonnabend, A. Zilges, Phys. Rev. Lett. **100** (2008) 232501.

[32] A. P. Tonchev, S. L. Hammond, J. H. Kelley, E. Kwan, H. Lenske, G. Rusev, W. Tornow, N. Tsoneva, Phys. Rev. Lett. **104** (2010) 072501.

[33] P. Adrich, A. Klimkiewicz, M. Fallot, K. Boretzky, T. Aumann, D. Cortina-Gil, U. Datta Pramanik, Th. W. Elze, H. Emling, H. Geissel, M. Hellström, K. L. Jones, J. V. Kratz, R. Kulessa, Y. Leifels, C. Nociforo, R. Palit, H. Simon, G. Surowka, K. Sümmerer, W. Walus, Phys. Rev. Lett. **95** (2005) 132501.

[34] A. Klimkiewicz, P. Adrich, K. Boretzky, M. Fallot, T. Aumann, D. Cortina-Gil, U. D. Pramanik, T. W. Elze, H. Emling, H. Geissel, M. Hellstroem, K. L. Jones, J. V. Kratz, R. Kulessa, Y. Leifels, C. Nociforo, R. Palit, H. Simon, G. Surowka, K. Suemmerer, S. Typel, W. Walus, Nucl. Phys. **788** (2007) 145.

[35] N. Paar, T. Niksic, D. Vretenar, P. Ring, Phys. Lett. B **606** (2005) 288.

[36] J. Piekarewicz, Phys. Rev. C **73** (2006) 044325.

[37] S. Goriely, Phys. Lett. B **436** (1998) 10.

[38] S. Goriely, E. Khan, M. Samyn, Nucl. Phys. **A739** (2004) 331.

[39] E. Khan, S. Goriely, D. Allard, E. Parizot, T. Suomijärvi, A. J. Koning, S. Hilaire, M. C. Duijvestijn, Astro. Phys. **23** (2005) 191.

[40] D. Pena Arteaga, P. Ring, Phys. Rev. C **77** (2008) 034317.

[41] D. Pena Arteaga, E. K. P. Ring, Phys. Rev. C **79** (2009) 034311.

[42] U. Kneissl, H. H. Pitz, A. Zilges, Prog. Part. Nucl. Phys. **37** (1996) 349.

[43] N. Pietralla, Z. B. V. N. Litvinenko, S. Hartman, F. F. Mikhailov, I. V. Pinayev, G. S. M. W. Ahmed, J. H. Kelley, S. O. Nelson, R. Prior, K. Sabourov, A. P. Tonchev, H. R. Weller, Phys. Rev. Lett. **88** (2001) 012502.

5.4.9 Fine-structure of Photo-response above the Particle Threshold: the (γ ,α), (γ,p) and (γ ,n) Reactions

N. Pietralla[1], D. Savran[1], K. Sonnabend[1],
A. Negret[2] and V. Corcalciuc[2]
[1] *Institut für Kernphysik, TU Darmstadt, Darmstadt (Germany)*
[2] *IFIN-HH, Bucharest, Romania*

The excitation energy region around the particle separation threshold is of particular importance for nuclear physics. On one hand side this energy region is of interest for theoretical reasons because the coupling of bound quantum states to the continuum of unbound states requires an extended formalism, the mastering of which becomes extremely important for exotic nuclei near the drip-lines where all structures are weakly bound [1]. Examples are the famous halo-nuclei like e.g. ^{11}Li [2]. On the other hand this energy region covers the Gamow-window of thermally driven reactions of nucleons with heavy nuclei. Its understanding is a prerequisite for the modelling of nuclear reaction cascades in hot cosmic objects and thus for nucleosynthesis.
Below the threshold all excited resonances must decay by γ emission. They can be studied with the typical high energy resolution of semiconductor-detector technology (e.g., 5 keV at 8 MeV). The photo-response below the particle separation energy is currently investigated in nuclear resonance fluorescence experiments [1] at existing γ-beam facilities such as the bremsstrahlung facilities at the S-DALINAC electron accelerator in Darmstadt, Germany, [4] or at the High Intensity γ-ray Source (HIγS) at Duke Univ., Durham, NC, U.S.A [5].
Above the threshold the particle-decay channel opens up. Either no γ rays can be observed at all or their intensity cannot be used as a measure for the total electromagnetic excitation strength to the resonance due to the unknown particle-decay branching ratio. Neutrons cannot be measured with a competitive energy resolution at acceptable solid-angle coverage.
An intense and high-energy resolving γ-ray beam from ELI-NP will open up new horizons for the investigation of the nuclear photo-response at and above the separation threshold. Alternatively to nuclear fluorescence, a photo-transmission experiment could be performed. A reduction in the photo transmission is directly proportional to the photo-excitation cross section. A measurement of the transmitted intensity is sensitive to the fine-structure in the energy window of the photon beam. A high-resolution γ-ray beam with energy width dE/E $\leq 10^{-3}$ will allow for the performance of transmission experiments with semiconductor-detector resolution even in the regime of unbound resonances. We expect a tremendous increase of insight into nuclear structure in the continuum and a deepened understanding of the structure of the nuclear Gamow-window.
The gamma induced nuclear reactions mentioned in the title were extensively studied during the years using mostly the gamma rays from bremsstrahlung and to a smaller extent, Compton back scattering. Generally, there is a clear difference among the three reactions because the Coulomb barrier makes the study of the (γ,α) reaction more difficult than the study of the (γ,p) reaction which is more difficult than (γ,n). Consequently, in the cross section data base EXFOR [6] there are 21 entries for (γ,α) cross sections, 278 entries for (γ,p) cross sections and 832 entries for (γ,n) cross sections. Further, the NSR database [7] displays 104 references for the (γ,α) reaction, 1052 references for the (γ,p) reaction and 1394 references corresponding to the (γ,n) reaction.
A major scientific interest related to the study of these reactions comes from Astrophysics. The nuclei heavier that Z=26 (iron) are synthesized mainly by neutron-capture reactions (r- and s- processes). The neutron deficient stable isotopes with Z>34 (Se) and Z<80 (Hg) that are shielded from rapid neutron capture by stable nuclei are referred as p-nuclei and their formation occurs, most probably, during the supernova explosions. All p-nuclei can be synthesized from the destruction of pre-existing nuclei of the s- and r-type by a combination of (p,γ) captures and (γ,n), (γ,p) or (γ,α) photoreactions. It is to observe that in the nuclear mass region of interest for the p-process and not too far from stability, the (γ,α) reactions usually have much larger rates than the (γ,p) reactions because in that region the α particles have small or even negative binding energies, whereas typical proton separation energies are of the order of several MeV. Therefore, when the α particle is replaced by a proton, the smaller Coulomb barrier does not compensate the strong increase in binding energy $S_p - S_\alpha$ and the

(γ,α) reaction operates at significantly lower photon energies and thus higher photon densities than the (γ,p) reaction.
One question raised by the p-process studies is to know to what extend the calculated p-nuclei abundances do reproduce the solar system ones. A variety of explosive stellar sites in which matter is heated to temperatures in the range T_9 = 1.5-3.5 (T = 2-3$\times 10^9$ K) succeed in synthesizing p-nuclides with relative abundances in rough agreement with the solar system isotopic content. However a serious discrepancy concerns the large isotopic ratios of the Mo and Ru p-nuclei in the Solar system (of the order of 10 % of the corresponding elemental abundances), for which no satisfactory explanation has been found so far.
Other problems raised by the p-process nucleosynthesis concern the production of the rare odd-odd nuclei $^{180}Ta^m$ and ^{138}La. In both cases (γ,n) reaction rates on these nuclei and on their much more abundant neighbors ^{181}Ta and ^{139}La are the essential nuclear quantities which will determine their final abundances. The rarest stable nucleus in the Solar system and the only naturally occurring isomer, $^{180}Ta^m$, has been shown by to be a natural product of the p-process in the supernovas of second type (SNe-II).
The temperature reached during supernova explosions T_9 = 2-3 corresponds to gamma energies of E_γ = 8-10 MeV. Therefore the reactions occur well below the Coulomb barrier (typically around 15 MeV for the α particles) and consequently have very small cross sections. The very intense gamma flux during the explosion makes these processes important for the astrophysical models.
We will summarize a few cases were the study of (γ,α), (γ,n) and (γ,p) reactions are of Astrophysical interest.
In Ref. [8] the authors measure ^{92}Mo(α,α)^{92}Mo at the cyclotron of ATOMKI in order to determine the α - ^{92}Mo optical potential, to extrapolate it and to calculate the reaction rates of the ^{96}Ru(γ,α)^{92}Mo reaction at T_9 = 2-3 (corresponding to E_γ=8-10 MeV or E_α =6-8 MeV for the inverse reaction; the Coulomb barrier is about 15 MeV).

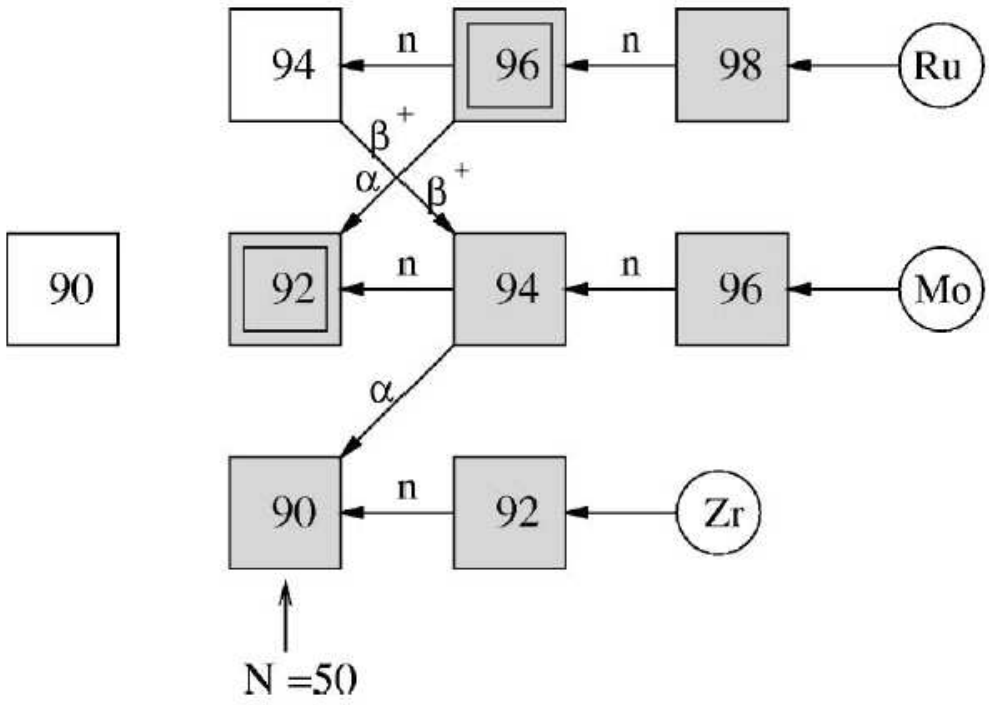

Figure 44: Nucleosynthesis of ^{92,94}Mo

Nucleosynthesis path for p nuclei ^{92,94}Mo:
^{96}Ru → 2 times (γ,n) → ^{94}Ru → 2 times β^+ → ^{94}Mo
^{96}Ru →(γ,α) → ^{92}Mo
To a large extent, the relative abundance of ^{92}Mo and ^{94}Mo depend on the (γ,n) and (γ,α) reaction

rates on ^{96}Ru (for details the rp contribution to ^{92}Mo and the s contribution to ^{94}Mo should also be known). When the astrophysical reaction rates for the (γ,α) reaction are calculated with various potentials, they come out within two orders of magnitude. The authors claim that their extrapolation leads to an error of 15% for this reaction rate; however their result is a factor 2 lower than the presently recommended value.
Theoretical studies addressing a very similar issue are presented in Refs. [9, 10]: the ^{146}Sm/^{144}Sm abundance that depends on the ^{148}Gd(γ,n)^{147}Gd / ^{148}Gd(γ,α)^{144}Sm reaction rates. The authors of these studies pledge for the experimental determination of the cross sections.
Ref. [11] presents a recent study where the photodisintegration reactions of nuclei of interest for Astrophysics were directly measured. The authors measured the photodisintegration of ^{92}Mo and ^{144}Sm using the activation method. The bremsstrahlung facility ELBE was used: electron beam with energy up to 20 MeV, average current 1 mA, and photon flux of 10^9 cm^{-2}s^{-1}MeV^{-1}. The targets are discs or powder of 2-4 g and diameter of 20 mm. A pneumatic delivery system transports the activated samples to the measurement site (HPGe detectors). The measurements are relative to the ^{197}Au(γ,n) standard cross section.
Finally, we mention the experiments performed at the National Institute of Advanced Industrial Science and Technology (AIST) using also a gamma source based on laser inverse Compton scattering (LCS). There, the γ beam with a rather limited intensity (10^{4-5} photon/s) has been used to measure cross sections of ^{9}Be(γ,n)$\alpha\alpha$ of interest for the nucleosynthesis in supernovae [16], of ^{181}Ta(γ,n)^{180}Ta for the p-process nucleosynthesis [17], and D(γ,n)p for big bang nucleosynthesis [18]. The γ energy is varied in the region of 1-40 MeV by tuning the electron beam energy from 200 to 800 MeV. An energy resolution of 1-10% in FWHM and nearly 100% polarization are achieved. Because of the monochromaticity, the LCS γ beam is best suited to excitation function measurements of photoneutron reactions near threshold with enriched-target material of the order of 1 g. In addition, photo-activation of natural foils can be done for nuclei whose isotopic abundance is sufficiently large.
In conclusion, the gamma-induced nuclear reactions of astrophysical interest were extensively studied during the years but still represent a challenge for the experimental and theoretical work. The difficulty arises from the very small cross sections due to the fact that the reactions occur deep below the Coulomb barrier especially for the case of (γ ,α) reactions. Therefore a very intense gamma source would be of interest for such reactions.
The particle detection techniques cover a variety of methods: from direct detection of neutrons (scintillators), activation of targets, direct detection of charged particles etc. For low energy charged particles (particularly alpha particles), a variety of active reaction chambers have been designed (TPC-time projection reaction chambers). They act in the same time as target and as detector, offering the advantage of a near 4π detection geometry, a nearly 100% detection efficiency etc. Often, in measurements using TPC, the background events are dominant (sometimes 90% or more of all events) and special care must be taken in order to eliminate them.

References

[1] B. Jonson, Phys. Rep. **389** (2004) 1

[2] J. Dobaczewski, I. Hamamoto, W. Nazarewicz, J.A. Sheikh, Phys. Rev. Lett. 72 (1994) 981.

[3] U. Kneissl, N. Pietralla, A. Zilges, J. Phys. G **32** (2006) R217.

[4] D. Savran, M. Fritzsche, J. Hasper, K. Lindenberg, S. Müller, V. Y. Ponomarev, K. Sonnabend, A. Zilges, Phys. Rev. Lett. **100** (2008) 232501.

[5] A. P. Tonchev, S. L. Hammond, J. H. Kelley, E. Kwan, H. Lenske, G. Rusev, W. Tornow, N. Tsoneva, Phys. Rev. Lett. **104** (2010) 072501.

[6] Experimental Nuclear Reaction Data (EXFOR), http://www.nndc.bnl.gov/exfor/exfor00.htm

[7] Nuclear Science References Database (NSR), http://www.nndc.bnl.gov/nsr/index.jsp

[8] Zs. Fulop et al, Physics Review C 64, 065805 (2009).

[9] T. Rauscher, F.K. Thielemann and H. Oberhummer, The Astrophysical Journal 451, L37 (1995).

[10] S.E. Woosley and W.M. Howard, The Astrophysical Journal 354, L21 (1990).

[11] C. Nair et al., Journal of Physics G35, 014036 (2008).

[12] M. Gai et al., TUNL XLVII Progress report, 118 (2008).

[13] M. Gai et al., TUNL XLVII Progress report, 154 (2008).

[14] H. Weller et al., Progress in Particle and Nuclear Physics 62, 257 (2009).

[15] H. Utsunomiya, P. Mohr, A. Zilges, Nucl. Phys. A777, 459 (2006).

[16] K. Sumiyoshi, et al, Nucl. Phys. A709, 467 (2002).

[17] H. Utsunomiya, et al, Phys. Rev. C67, 015807 (2003).

[18] K.Y. Hara, et al, Phys. Rev. D68, 072001 (2003).

5.4.10 Nuclear Resonance Fluorescence on Rare Isotopes and Isomers

N. Pietralla[1], D. Savran[1], K. Sonnabend[1]
[1] *Institut für Kernphysik, TU Darmstadt, Darmstadt (Germany)*

Nuclear studies with the powerful experimental method of Resonance Fluorescence have been possible up to now only if sufficient amounts of (preferably isotopically enriched) target material on the order of about 1 g has been available. The production of such an amount of target material is not always possible at a reasonable cost (e.g., the worlds rarest naturally occuring isotope ^{180}Ta costs about $ 10,000 per mg at an enrichment of 5%). The advances in γ-ray beam brilliance at ELI will increase the sensitivity of NRF experiments by the same factor and thus it offers the opportunity to perform NRF studies on small target samples whose amounts could be reduced with respect to todays NRF experiments by the same factor. This opens up an entire new area of applicability of the NRF method to materials that may be available only in quantities of a few mg.
The dipole response of the long-lived radioactive isotope ^{14}C, the basis of radio-carbon dating method, will be accessible. These experiments will shed light on the neutron-spectroscopic factors for the *p*- and *sd*-shell orbitals in that mass region that nowadays is accessible to ab initio no-core shell models calculations.
Nuclear high-spin K isomers are known to be examples of highly-deformed nuclear structures. Due to their simple Nilsson-model wave function they offer a unique laboratory for the study of very deformed nuclear systems. Nuclear spectroscopy experiments with hadronic probes have previously been performed on the the long-lived K-isomer of ^{178}Hf. An investigation of the $E1$ and $M1$ response of the highly-deformed isomer using NRF on an enriched isomeric sample of a few mg will enable us to study the phenomenon of quadrupole-octupole coupling (E1) or the nuclear scissors mode (M1) at a nuclear deformation that has not been accessible for these types of investigations before.

References

[1] U. Kneissl, N. Pietralla, A. Zilges, J. Phys. G **32** (2006) R217.

5.4.11 Multiple Nuclear Excitons

R. Schützhold[1], D. Habs[2], P. Thirolf[2] and M. Fujiwara[3]
[1] *University od Duisburg-Essen, Duisburg (Germany),*
[2] *Ludwig Maximilians University, Munich (Germany),*
[3] *Osaka University, Osaka (Japan)*

The development of the laser based on stimulated emission was a giant breakthrough in quantum optics. It enabled us to create light with unprecedented accuracy, intensity, and control – thereby facilitating many novel applications. However, so far these applications are mostly restricted to the optical regime. The free electron laser (FEL) is a very interesting approach to achieve similar goals at higher energies. However, the free electron laser (in its usual design) is not a laser in the same sense as the optical laser, because the former is not really based on stimulated emission whereas the latter is. Therefore, the free electron laser does not incorporate all the advantages known from the optical laser. Within this project, we study the possibility to build a laser based on stimulated emission working at higher (e.g., keV) energies. To this end, we intend to use nuclear excitonic states known from Mössbauer sprectroscopy instead of the electronic excitations of atoms/molecules used in optical lasers. These coherent excitations [1] spread over many nuclei (Dicke states) [3] possess many advantages and are thus perfect candidates for our purpose. As a result, we expect such a "nuclear exciton laser" to be able (in principle) to outperform a conventional FEL/XFEL facility in terms of energy and momentum accuracy and possibly even intensity.
For nuclear transitions up to 100 keV the recoilless Mößbauer γ resonance absorption [5, 6] has been observed and is widely used as spectroscopic technique, where for bound nuclei the photon recoil may be taken up by the crystal without lattice excitation. A prototype nucleus is ^{57}Fe with its 14.4 keV Mößbauer M1 transition, which has a mean lifetime of 141 ns, a line width of 4.7 neV, a relative line width of $\Delta E/E = 3 \cdot 10^{-13}$ and a K-conversion coefficient $\alpha_K = 10$. At synchrotron facilities the non-resonant radiation could be suppressed sufficiently by nuclear Bragg reflection. Here the delocalized excitation of a nuclear ensemble - called nuclear exciton [9] - was studied in detail. Its delayed propagation through a crystal, showing quantum beats due to the interference of different transitions between hyperfine components was observed. This coherent γ-ray optics shows many new phenomena [14]. Although the brilliance of synchrotron γ beams much increased over the years, the chance to excite several nuclear excitons in a single bunch was negligible.

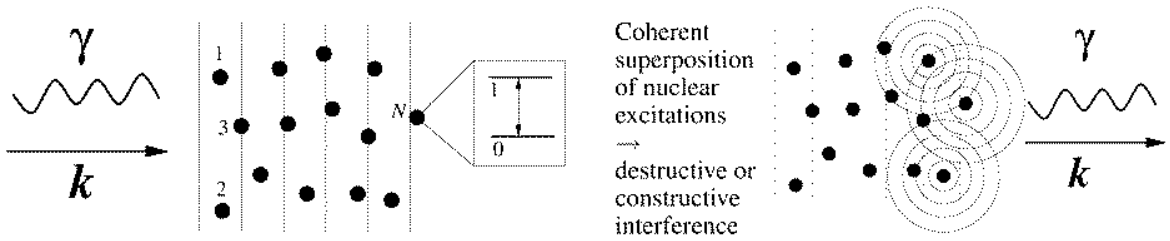

Figure 45: Excitation (left) and deexcitation (right) of a coherent nuclear ensemble, leading to directed X ray emission ('polariton laser') when the delocalized coherent nuclear ensemble is destroyed 'on demand'.

Fig. 45 schematically displays the excitation process of a nuclear polariton in an ensemble of nuclei (left) by X ray photons with wave number k. On the right-hand side it is depicted how a coherent superposition of nuclear excitations will result in a constructive or destructive interference during the deexcitation process, leading to a directed coherent emission exclusively in forward direction if the coherent multi-exciton state is destroyed. Thus a potential application of such multi-exciton states could lead to an 'exciton laser' with coherent X ray emission 'on demand'. Studying the collective properties of these bosonic condensates opens up a new and exciting perspective of coherent nuclear physics.
For an incoherent pulse of γ's the exciton number N_p grows linear with intensity. If one calculates within the Weisskopf-Wigner approach [7], the exciton decay rate (or γ width) increases with the

number of nuclei in the wave length volume and soon exceeds the width due to conversion. Then an avalanche-like growth of the linewidth occurs and more and more photons of the much broader driving X-ray beam may join the multiple exciton condensate. Due to the required recoilless Mössbauer-like absorption we here will use rather low energy γ rays in the 100 keV range. While we get multiple excitons with the γ beam, the exciton laser should be excited with coherent γ photons from the relativistic mirror. In this scenario a quadratic growth of the exciton number could be expected for coherent pumping with X rays produced by the ELI-NP laser and a relativistic mirror.] A coherently excited nuclear state in a rotating sample aquires a phase shift and the radiative decay of the excited state proceeds in the rotated direction. This effect is called light house effect [17–21] and can be used to separate the radiation from the nuclear decay from the primary exciting beam.

References

[1] D. Habs et al., Eur. Phys. J. **D 55**, 279 (2009).

[2] G.V. Smirnov et al., *Propagation of nuclear polaritons through a two-target system: Effect of inversion targets*, Ohys. Rev. **a 71**, 023804 (2005).

[3] R.H. Dicke; *Coherence in spontaneous radiation processes*, Phys. Rev. **93**, 99 (1954).

[4] T. Holstein and H. Primakoff, Phys. Rev. **58**, 1098 (1940).

[5] R.L. Mössbauer, Z. Physik **151**, 124 (1958), Naturw. **45**, 538 (1958).

[6] R.L. Mössbauer, Z. Naturforsch. **14a**, 211 (1959).

[7] M.O. Scully and M.S. Zubairy, *Quantum Optics*, Cambridge University Press, Cambridge, England (1997).

[8] H.J. Lipkin; *Coherent effects in the transitions between states containing several nuclear excitons* p. 128; in " Multiple Facets of Quatization and Supersymmetry, Michael Marinov Memorial Volume; edt.: M. Olshanetsky and A. Vainstein, World Scientific (2000).

[9] G.V. Smirnov et al., *Propagation of nuclear polaritons through a two-target system: Effect of inversion targets*, Ohys. Rev. **a 71**, 023804 (2005).

[10] U.v. Bürck; Hyp. Int. **123/124**, 483 (1999)

[11] M.O. Scully et al., Phys. Rev. Lett. **96**, 010501 (2006).

[12] D.C. Burnham and R.Y. Chao; Phys. Rev. **188**, 667 (1p69).

[13] D. Fröhlich et al., Phys. Rev. Lett. **67**, 2343 (1991).

[14] J.P. Hannon and G.T. Trammell; *Coherent γ-optics*, Hyp. Int. **123/124**, 127 (1999).

[15] N.E. Rehler and J.H. Eberly; *Superradiance*, Phys. Rev. **A 3**, 1735 (1971).

[16] Y.Y. Shuydku et al., Phys. Rev. Lett. **77**, 3232 (1996).

[17] R. Roehlsberger et al., Phys. Rev. Lett. **84**, 1007 (2000).

[18] R. Roehlsberger et al., Nucl. Inst. and Meth. **A 467**, 1473 (2001).

[19] T. Roth et al., Phys. Rev. **B 71**, 140401(R) (2005).

[20] I. Sergneev et al., Phys. Rev. Lett. **99**, 097601 (2007).

[21] I. Sergneev et al., Phys. Rev. **B 78**, 214436 (2008).

5.5 Stand-alone γ/e^- Facility for Astrophysics

The production of heavy elements in the Universe, a central question of astrophysics, will be studied within ELI-NP in several experiments. While we want to address the s-process and p-process with the γ beam, we also plan to study the r-process at the N=126 waiting point by producing these neutron-rich nuclei via fission-fusion reactions with the APOLLON-type laser. This close interaction between nuclear physics and astropyhisics will be very productive.

5.5.1 Neutron Capture Cross Section of s-Process Branching Nuclei with Inverse Reactions

K. Sonnabend[1], N. Pietralla[1], D. Savran[1]
[1] *Institut für Kernphysik, TU Darmstadt, Darmstadt (Germany)*

The heavy elements above the so-called iron peak are mainly produced in neutron capture processes: the r process (r: rapid neutron capture) deals with high neutron densities well above 10^{20} cm^{-3} and temperatures in the order of $2-3\cdot10^9$ K. It is thought to occur in explosive scenarios like *e.g.* supernovae [1, 2]. In contrast, the average neutron densities during s-process nucleosynthesis (s: slow neutron capture) are rather small ($n_n \approx 10^8$ cm^{-3}), *i.e.* the neutron capture rate λ_n is normally well below the β-decay rate λ_β and the reaction path is close to the valley of β stability [3–5]. However, during the peak neutron densities branchings occur at unstable isotopes with half-lives as low as several days. While the half-lives of these branching points are normally known with high accuracy at least under laboratory conditions and rely only on theory for the extrapolation to stellar temperatures [6], the neutron capture cross sections are only in special cases accessible to direct experiments. Besides the production of a sufficient amount of target material, the intrinsic activity of the target mainly hinders the experimental access especially in the case of the short-lived branching points.
However, the predictions in the Hauser-Feshbach model yield different results due to the underlying parameter sets. Additionally, the single studies on long-lived branching points (*e.g.* ^{147}Pm [7], ^{151}Sm [8, 9], ^{155}Eu [10]) showed that the recommended values of neutron capture cross sections in the Hauser-Feshbach statistical model [11] differ by up to 50% from the experimentally determined values. Thus, any experimental constraints on the theoretical predictions of these crucial values are welcome. Therefore, the inverse (γ,n) reaction could be used to decide for the most suitable parameter set and to predict a more reliable neutron capture cross section using these input values. This method has been applied to the branching nuclei ^{185}W and ^{95}Zr using a continuous-energy bremsstrahlung spectrum [12] and Laser-Compton backscattered photons [13].
In addition, data of the inverse (γ,n) reaction is also supposed to yield information for the calculation of Stellar Enhancement Factors (SEF) in some special cases like *e.g.* ^{151}Sm [14]. The inverse ^{152}Sm(γ,n) reaction only populates excited states in ^{151}Sm for energies close to the reaction threshold. Using the high resolution of ELI would allow measuring the matrix elements of the transitions to the particular states and, hence, measure the SEF which is the main source of uncertainty for the stellar cross section of ^{151}Sm(n,γ).

References

[1] K.-L. Kratz *et al.*, Astrophys. J. **403** (1993) 216.

[2] G. Wallerstein *et al.*, Rev. Mod. Phys. **69** (1997) 995.

[3] F. Käppeler, Prog. Part. Nucl. Phys. **43** (1999) 419.

[4] F. Käppeler, A. Mengoni, Nucl. Phys. **A777** (2006) 291.

[5] I. Dillmann, C. Domingo Pardo, F. Käppeler, A. Mengoni, K. Sonnabend, Publications of the Astronomical Society of Australia **25** (2008) 18.

[6] K. Takahashi, K. Yokoi, Nucl. Phys. **A404** (1983) 578.

[7] R. Reifarth *et al.*, Astrophys. J. **582** (2003) 1251.

[8] U. Abbondanno *et al.*, The N Tof Collaboration, Phys. Rev. Lett. **93** (2004) 161103.

[9] K. Wisshak *et al.*, Phys. Rev. C **73** (2006) 015802.

[10] S. Jaag, F. Käppeler, Phys. Rev. C **51** (1995) 3465.

[11] Z. Y. Bao *et al.*, At. Data Nucl. Data Tables **76** (2000) 70.

[12] K. Sonnabend *et al.*, Astrophys. J. **583** (2003) 506.

[13] K. Sonnabend *et al.*, AIP, 2009, Volume 1090, (p. 481–485).

[14] A. Mengoni, AIP, 2005, Volume 769, (p. 1209–1212).

5.5.2 Measurements of (γ, p) and (γ, α) Reaction Cross Sections for p-Process Nucleosynthesis

K. Sonnabend[1], N. Pietralla[1], D. Savran[1]
[1] *Institut für Kernphysik, TU Darmstadt, Darmstadt (Germany)*

Photodesintegration rates – like (γ,n), (γ,p), and (γ,α) – play an important role in the nucleosynthesis of the so-called p nuclei. These proton-rich, in general very low-abundant isotopes cannot be produced by neutron capture reactions. Complete network calculations on p-process nucleosynthesis include several hundred isotopes and the corresponding reaction rates. Therefore, theoretical predictions of the rates, normally in the framework of the Hauser-Feshbach theory, are necessary for the modelling. The reliability of these calculations should be tested experimentally for selected isotopes.
Different approaches are available and necessary to improve the experimental data base for the p process. While the (γ,n) cross sections in the energy regime of the Giant Dipole Resonance around 15 MeV have already been measured extensively several decades ago (see *e.g.* [1]), many efforts using continuous bremsstrahlung spectra have been made at the S–DALINAC at Darmstadt [2,3] and the ELBE setup at Forschungszentrum Dresden [4] to determine the reaction rates without any assumptions on the shape of the cross section's energy dependence in the astrophysically relevant energy region close above the reaction threshold. A determination of the reaction rates by an absolute cross section measurement is also possible using monoenergetic photon beams produced by Laser Compton Backscattering [5].
In contrast, the experimental knowledge about the (γ,p) and (γ,α) reactions in the corresponding Gamow window is worse. In fact, the experimental data is based on the observation of the time reversal (p,γ) and (α,γ) cross sections, respectively [6–10] for the proton-rich nuclei with mass numbers around 100. Due to the difficulties concerning the experimental accessibility of the (γ,α) reaction rates a method using elastic α scattering has been established [11,12].
Therefore, it would be a tremendous advance to measure these rates directly. However, the impact on the understanding of p-process nucleosynthesis would not be the measurement of one or two selected reactions but the development of a broad database. This is only possible if the time needed for one experiment is kept very short as it will be provided by the high intense γ beam of ELI.

References

[1] B. L. Berman, S. C. Fultz, Rev. Mod. Phys. **47** (1975) 713.

[2] K. Vogt, P. Mohr, M. Babilon, J. Enders, T. Hartmann, C. Hutter, T. Rauscher, S. Volz, A. Zilges, Phys. Rev. C **63** (2001) 055802.

[3] K. Sonnabend, K. Vogt, D. Galaviz, S. Müller, A. Zilges, Phys. Rev. C **70** (2004) 035802.

[4] M. Erhard, A.R. Junghans, R. Beyer, E. Grosse, J. Klug, K. Kosev, C. Nair, N. Nankov, G. Rusev, K.D. Schilling, R. Schwengner, A. Wagner, Eur. Phys. J. A **27** (2006) s01.135.

[5] H. Utsunomiya, H. Akimune, S. Goko, M. Ohta, H. Ueda, T. Yamagata, K. Yamasaki, H. Ohgaki, H. Toyokawa, Y.-W. Lui, T. Hayakawa, T. Shizuma, S. Goriely, Phys. Rev. C **67** (2003) 015807.

[6] T. Sauter, F. Käppeler, Phys. Rev. C **55** (1997) 3127.

[7] J. Bork, H. Schatz, F. Käppeler, T. Rauscher, Phys. Rev. C **58** (1998) 524.

[8] N. Özkan, A. S. J. Murphy, R. N. Boyd, A. L. Cole, M. Famiano, R. T. Güray, M. Howard, L. Şahin, J. J. Zach, R. deHaan, J. Görres, M. C. Wiescher, M. S. Islam, T. Rauscher, Nucl. Phys. **A710** (2002) 469.

[9] W. Rapp, M. Heil, D. Hentschel, F. Käppeler, R. Reifarth, H. J. Brede, H. Klein, T. Rauscher, Phys. Rev. C **66** (2002) 015803.

[10] G. Gyürky, Z. Fülöp, G. Kiss, Z. Máté, E. Somorjai, J. Görres, A. Palumbo, M. Wiescher, D. Galaviz, A. Kretschmer, K. Sonnabend, A. Zilges, T. Rauscher, Nucl. Phys. **A758** (2005) 517.

[11] Z. Fülöp, G. Gyürky, Z. Máté, E. Somorjai, L. Zolnai, D. Galaviz, M. Babilon, P. Mohr, A. Zilges, T. Rauscher, H. Oberhummer, G. Staudt, Phys. Rev. C **64** (2001) 065805.

[12] D. Galaviz, Z. Fülöp, G. Gyürky, Z. Máté, P. Mohr, T. Rauscher, E. Somorjai, A. Zilges, Phys. Rev. C (2005) in press.

5.6 Applications and Industry Relevant Developments at ELI-NP

Having at ELI-NP at the same place a brilliant γ beam, a brilliant X-ray beam, a brilliant micro neutron source and a brilliant micro positron source will be very advantageous in material science and life sciences because the same target can be studied with the different techniques which complement each other.

5.6.1 Industrial Applications for the Management of Nuclear Materials

T. Hayakawa[1], T. Shizuma[1], R. Hajima[2], and T, Glodariu[3]
[1] *Advanced Photon Research Center, JAEA, Kizugawa, Kyoto (Japan),*
[2] *Advanced Photon Research Center, JAEA, Tokai, Ibaraki (Japan),*
[3] *IFIN-HH, Bucharest (Romania)*

In the current geopolitical environment, proliferation of nuclear and radiological materials is a major concern. Many efforts are underway to develop a system that can rapidly identify and characterize illicit nuclear and radiological materials. Approaching such developments is an important mission for any major nuclear physics facility, and will constitute an important support for the IAEA policy. A comprehensive approach to the detection of weapons of mass destruction containing special nuclear materials (SNM) requires the ability to rapidly and efficiently determine a region of interest (ROI) in three dimensions where Z is high and subsequently identify and quantify the nuclear isotopes such as ^{235}U and ^{239}Pu in that region of space. The probability of finding SNM must be very high and the false alarms must be very low to ensure effective detection without impeding the flow of commerce. Similarly, detecting explosives or toxic substances requires the ability of finding ROI where Z is generally low and subsequently identifying in that region of space the amounts of carbon, nitrogen and oxygen along with identifiers (for toxic substances) such as sulfur, fluorine, phosphorus and arsenic or explosive enhancers such as magnesium and aluminum. NRF [15] provides a signal that is unique and present for almost all nuclei with $Z > 2$. Isotopes have different NRF signatures enabling, for example, the discrimination between ^{235}U from ^{238}U. The possibility of misidentify because of accidental overlap is demonstrated to be very small. Such confusion can be avoided by using second or third lines present in most NRF spectra [1]. The resonant energies in NRF are in the 1 to 10 MeV range. As a result, the attenuation path-lengths for NRF photons are much longer than x-ray photons and thermal neutrons used in other assay techniques, allowing the technique to work through many inches of lead or steel or several feet of hydrogenous material. NRF can provide the possibility for rapid scanning of seagoing containers, trucks and other vehicles in short times while providing high detection probabilities with low false alarm rates for SNM, explosives, toxic substances and other contraband. Systems can be designed to involve minimal operator intervention, to minimize dose to the sample, and to provide high throughput at commercial seaports, airports and other entry points [16].

Nuclear resonance fluorescence photon beams and detection system

The process of NRF corresponds to the excitation of a nuclear state by photons and having that state decay by the emission of a photon to the ground state or an excited state. If the state is unbound to neutron emission or another strongly interacting particle, generally the photon decay is not strong enough to observe in competition with particle decay. Thus, most of the useful states are below particle threshold and generally have ground state radiative widths of about 30 meV or larger.

$$\sigma(E) = \sum_i \frac{\pi}{2} \cdot \lambda^2 \cdot g \cdot \frac{\Gamma_0 \Gamma_i}{(E - E_0)^2 + \frac{\Gamma^2}{4}}$$

NRF cross sections typically have very large peak values at E = E0 that correspond to hundreds of barns for E0 in the range of a few MeV. The states are broadened by the zero-point motion of the atom and thermal motion. For light nuclei the broadening can be approximately 20 eV. For the detection of materials it is useful to think of NRF in two modes. One is in the mode wherein the scattered photons are detected back of 90. The second mode makes use of the dominance of the NRF process and examines the transmitted photon spectrum for absorption lines. The detectors for NRF are back

of 90 because there is no single electromagnetic process that produces a photon above 0.5 MeV at this angle and the background for NRF states in the MeV range is minimized. A clever method of measuring the outgoing photon beam was proposed by Bertozzi et al [1] is illustrated on the right hand side of Fig. 46. The basic idea is to let nature do most of the detecting for us. Since building detectors capable of directly observing a 1 eV wide resonance would be extremely difficult, we instead observe a physical process sensitive to resonant photons. This is accomplished by placing a small test sample of the suspected material in front of the beam exiting the container. An array of photon detectors measures the rate of resonant scattering within this sample and so determines the flux of resonant photons in the beam exiting the cargo. The flux of off-resonant photons is measured with a simple transmission detector placed directly in the path of the beam. If a specific material is present in the path of the photon beam, the spectrum is attenuated by standard non-resonant electromagnetic processes. In the regions where the NRF states of the material exist, the attenuation will be dominated by the nuclear absorption resulting a prominent depletion of resonant photons, or notch that are a few eV wide, and holes will be generated in the photon spectrum. If the same material (sample foil) is placed in the photon beam after the container, the NRF scattering from this material will display the greater attenuation caused by the resonant nuclear absorption of the NRF states of the same material in the container. The increased absorption directly yields the amount of the material that is in the container. This produces a two dimensional isotopic image of the contents of the container. The transmission detector searches only for the materials that are selected as reference scatterers. There can be several reference scatterers since the overlap of the NRF states is very unlikely.

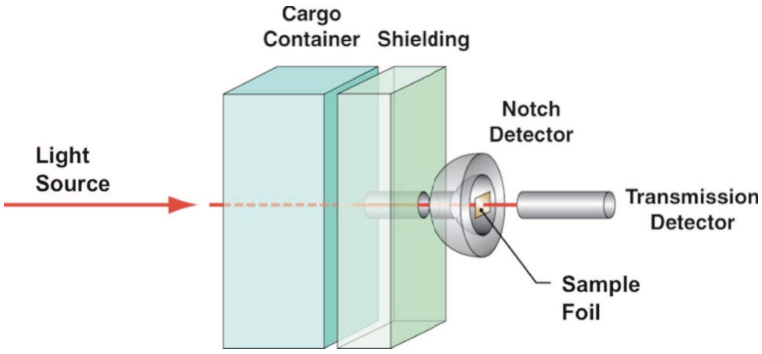

Figure 46: Schematic representation of the detection system. A photon beam is sent to interrogation cargo. After passing through the container the flux of resonant and off-resonant photons is measured. Resonant flux is measured by notch detectors that observe NRF within a small sample foil made of the isotope that is being looked for (reference scatterers). The flux of off-resonant photons is measured with a simple transmission or current detector.

Performance of the NRF-based detection systems depends sensitively on properties of the beam of interrogating photons. To give an idea of the range of possibilities Pruet et al. [3] considered two different, and in some sense limiting, photon beam types. The first is a broadband beam comprised of bremsstrahlung photons created as relativistic electrons are deflected or stopped in a dense metal target. These beams are common, well studied and characterized, and relatively inexpensive. They can have rather high end point photon energies tens of MeV and have an energy resolution of order unity. The angular distribution of such beams is of the order of the inverse Lorentz factor of the electrons, typically about 0.1 rad. The second type of source that they considered was a photon beam produced by a high intensity laser light which collide head on with a relativistic electron beam. Incident laser photons that are Compton back scattered by the relativistic electrons are Doppler up-shifted to large energies. Remarkably, the spectral brightness of these sources is calculated to scale as the square of the incident electron energy, meaning that the problem of generating high-quality beams becomes easier with increasing photon energy. The interrogation system studied by Pruet et al. [3] relies on detecting the absence of resonant photons, or notch,in the beam exiting scanned cargo. Any scattering that refills this notch could result in a false negative detection and defeat of the interrogation system. Processes that lead to photons observed by the notch detector can be divided

into four categories. The first one includes the resonant absorption and re-emission of photons. This is the desired signal used to determine whether or not a notch is present in the beam escaping cargo. The second one include the Compton scattering. Compton scattering events will overwhelmingly dominate production of photons emitted by the sample foil. Because photons suffering large-angle collisions are left with small energies (<0.5 MeV) they are readily filtered out or shielded against. This is the basic motivation for placing notch detectors to observe rays traveling perpendicular to or anti-parallel to the incident beam. The third category include the coherent elastic scattering. Coherent elastic scattering of multi-MeV photons is represented as a sum of DelbrÃ¼ck scattering, Rayleigh scattering, nuclear Thomson scattering, and scattering via virtual excitation of nuclear resonances. Delbrŭck scattering refers to scattering caused by the production and annihilation of an e+ /e- pair in the Coulomb field of a nucleus. Roughly, the contribution of Rayleigh scattering to the total elastic cross section is expected to scale as Z^2, with Z the atomic number of target nuclei. Delbrŭck and nuclear Thomson scatterings are expected to scale as Z^4/M^2 Z^2, with M the mass of target nuclei. Scattering via virtual excitation of resonances in heavy nuclei is not important for photons with energy smaller than about 6 MeV. The last category include the bremsstrahlung following photoelectric absorption or Compton scattering. From this four categories Compton scattering of photons with energies larger than the resonance energy has the potential to detrimentally redistribute photon energies in this way. Rayleigh and Delbrŭck scattering play a smaller role in notch refilling. Cross sections for these interactions are small relative to the Thomson cross section and many of these processes are essentially elastic. Mainly the flux of resonant photons recorded by the notch detector depends on the areal density of the suspected material, backgrounds, and notch refilling. Notch refilling is potentially more problematic because it depends on details of the cargo other than the integrated optical depth given by the transmission detector. For light sources with fine energy and angular resolution notch refiling is very small, while for bremsstrahlung sources the influence of notch refiling is larger but can be ameliorated with careful collimation [3]. For nearly monoenergetic light sources the background is expected to be dominated by elastic scattering events at energies within a few hundred keV of resonance energy. In principle, a simple threshold detector would work as well as germanium or other energy resolving detectors for these sources because the beam resolution is comparable to the detector resolution of the best high efficiency detectors. NRF experiments that use a bremsstrahlung source observe a background which falls to a small value within a few hundred keV of the beam end point energy and which rises approximately exponentially with decreasing photon energy. This makes characterization of NRF lines in heavy nuclei difficult when the line is more than 1 MeV away from the beam end point energy. For this broadband sources the background can be minimized by tuning the beam end point to be near the energy of the interesting NRF resonance.

Nuclear Data and Nuclear Structure Study

An advantage of the NRF system is to assay most radioactivities of long-lived fission products and fissionable isotopes, for example 237Np, 241Am, and 245,247Cm. A key nuclear data for the NRF assay is an excitation energy and a resonance width of an exited state in nucleus of interest. These nuclear data have not been, however, studied well for long-lived radioactivities. The excitation energies of excited states which may excited directly from the ground state by photon-induced reactions for minor actinide are known but their resonance widths have not been measured. Recently, Bertozzi et al. studied the excited states on 235U and 239Pu using NRF with Bremsstrahlung γ-rays and reported the strong dipole resonances above 2 MeV [11]. The nuclear data for 232Th [12], 235U [11], 236U [13], 238U [12], 239Pu [11] show that there exist strong magnetic dipole (M1) resonances around an excitation energy of 2 MeV, which can be understood by scissors mode of nuclear collective motion in viewpoint of the nuclear physics [13]. This suggests that there are probably M1 resonances around 2 MeV in most actinide isotopes. The nuclear structure study of these M1 resonances and the related nuclear data are important for the NRF assay of minor actinide.

Safety issues

Other characteristics that contribute to interrogation system performances are scan time and dose measures. For a given dose, a narrow band source can interrogate regions that are considerably thicker than can be interrogated by a broadband source. For the comparison between proposed laser-/linac-based sources and bremsstrahlung sources the difference in optical depth for a given dose is about $\ln(E_{end}/\Gamma_{beam})$ 6. For hydrogenous cargo with density of order of 1 g/cm3 six optical depths

corresponds to approximately 150 cm of material, about enough to satisfy the maximum weight allowed in sea-going cargo containers. Broad comparisons regarding scan time are harder to make. Bremsstrahlung sources can be very bright, potentially with the flux of order 10^{16} photons/ s needed to compete with proposed laser-/linac-based sources when interrogating modestly thick cargos. For very optically thick cargos the amount of angular collimation needed to overcome notch refilling when using a broadband source will prevent even the brightest bremsstrahlung sources from being able to interrogate quickly. High-brightness sources in which gamma rays are generated by scattering laser light from energetic electrons are more naturally suited to NRF-based detection. These sources are associated with a radiological dose and scan time per unit integrated brightness that is about 1000 times smaller than for bremsstrahlung sources.

Experimental plan

The principal ingredients in order to use an interrogation system based on NRF are the signatures lines of different isotopes corresponding to their resonant energies. In the case of detecting explosives or toxic substances almost all the candidates have very known signatures. The only one which need further experimental investigations is arsenic. In the case of special nuclear materials, recently Bertozzi et al. studied the excited states on 235U and 239Pu using NRF and reported the strong dipole resonances close to 2 MeV [11]. However, further effort will be required to determine the spin assignments of excited states and to establish the dynamics of the excitations involved. In addition, searching for new resonances at higher energies is critical because higher energy resonances may provide a significant performance enhancement in practical systems exploiting NRF to detect special nuclear materials. Therefore, for the arsenic, uranium isotopes and plutonium, additional experimental investigations of new resonances up to 10 MeV would be required. Following the experimental procedure described in [11]] the γ-rays will be measured with two HPGe detectors at about 50 cm from the target, and $+/-120^o$with respect to the beam direction. Both detectors should be encased in thick Pb shielding for the background minimization and collimated to view only the NRF target. Also, the detector openings should be covered with Pb absorbers of various thicknesses to reduce dead time. .

References

[1] W. Bertozzi and R.J. Ledoux, Nucl. Instrum. Methods B 241 (2005) 820.

[2] M. Haruyama, M. Takase, H. Tobita, T. Mori, High-sensitive detection by direct interrogation of 14 MeV AccNeutrons, (I) Uranium-contained metal matrix in a wast dram, Nihon-Genshiryoku-Gakkai Wabun-Ronbushi (J.At. Energy Soc. Jpn.), 3[2], 185–192 (2004) [in Japanese].

[3] J. Pruet, D.P. McNabb, C.A. Hagmann, F.V. Hartemann, and C.P.J. Barty, J. Appl. Phys. 99 (2006) 123102.

[4] R. Hajima, T. Hayakawa, N. Kikuzawa, E. Minehara, J. Nucl. Sci. Technol. 45 (2008) 441.

[5] N. Kikuzawa, R. Hajimam, N. Hishimori, E. Minehara, T. Hayakawa, T. Shizuma, H. Toyokawa, H. Ohgaki,Applied Physics Express 2 (2009) 036502.

[6] T. Hayakawa, H. Ohgaki, T. Shizuma, R. Hajima, N. Kikuzawa, E. Minehara, T. Kii, H. Toyokawa, Rev. Sci. Inst.80 (2009) 045110.

[7] R. Hajima, N. Kikuzawa, T. Hayakawa, E. Minehara, Proc. 8th International Topical Meeting on Nuclear Applications and Utilization of Accelerators (AccApp-07), 2007, p.182.

[8] K. Umemori, T. Furuya, S. Sakanaka, T. Suwada, T. Takahashi, H. Sakai, K. Shinoe, M. Sawamura, "Design of L-band superconducting cavity for the energy recovery linacs", Proc. Asian Particle Accelerator Conference 2007 (APAC 2007), 2007, p.570.

[9] T. Schreiber, C. Nielsen, B. Ortac, J. Limpert, and A. Tŭnnermann, "131 W 220 fs fiber laser system", Optics Letters 30 (2005) 2754.

[10] N. Pietralla, Z. Berant, V. N. Litvinenko, S. Hartman, F. F. Mikhailov, I. V. Pinayev, and G. Swift, M.W. Ahmed, J.H. Kelley, S. O. Nelson, R. Prior, K. Sabourov, A. P. Tonchev, and H. R.Weller, Phys. Rev. Lett. 88 (2002) 012502.

[11] W. Bertozzi, J.A. Caggiano, W. K. Hensley, M. S. Johnson, S. E. Korbly, R. J. Ledoux, D. P. McNabb, E. B.Norman, W. H. Park, and G. A. Warren, Phys. Rev. C 78 (2008) 041601(R).

[12] R.D. Heil, H.H. Pitz, U.E.P. Berg, U. Kneissl, K.D. Hummel, G. Kilgus, D. Bohle, A. Richter, C. Wesselborg, P.von Brentano, Nucl. Phys. A 476 (1988) 39.

[13] J. Margraf, A. Degener, H. Friedrichs, R. D. Heil, A. Jung, U. Kneissl, S. Lindenstruth, H. H. Pitz, H. Schacht, U.Seemann, R. Stock, and C. Wesselborg, Phys. Rev. C 42 (1990) 771.

[14] A. Zilges, P. von Brentano, R.-D. Herzberg, U. Kneissl, J. Margraf, H. Maser, N. Pietralla, and H.H. Pitz, Phys. Rev. C 52 (1995) 468(R).

[15] U. Kneissl, H.H. Pitz, A. Zilges, Prog. Part. Nucl. Phys. 37 (1996) 349 (and references therein). This reference provides a comprehensive review of theory and data.

[16] W. Bertozzi et al. / Nucl. Instr. and Meth. in Phys. Res. B 261 (2007) 331–336

5.6.2 Radioscopy and Tomography

M. Iovea[1]
[1] *Faculty of Physics, University of Bucharest, Romania*

An ultra-bright, energy-tunable and monochromatic gamma ray source in the range of 0.5-30 MeV produced by Laser - Compton Backscattering (LCB) technique is ideal for the Non-Destructive Testing (NDT) application [1, 2]. Practically, the new source could be a perfect solution for fulfilling all technical requirements for the large-size and complex products investigation in aeronautics, automotive, die-cast or sintered industries, new materials and technologies development, for archaeological artifacts and work of art objects analysis and many others.
The specific main advantages are:

- The source beam intensity is with many orders of magnitude higher than any other gamma ray source available, increasing substantially the penetration length and respectively the maximum size of investigated objects.
- The quasi-monochromatic and high-intensity source characteristics allow acquiring an energy-selected data from the entire scattered and attenuated beam. For example, only by considering the small-angle scattered rays, a significantly improvement in image sharpness is obtained even for large-size and strongly scattering objects;
- The small beam width, in the size of tens of microns, allows achieving good resolution images for in depth large objects technologies investigation, like: bonding in aeronautics, welding and machining accuracy in automotive industry, large concrete parts in construction [1], etc.
- The source tunable feature is very useful in adapting the energy range with the scanned object composition, for correctly revealing in the image the combination of different-attenuation materials, like plastic or ceramic with metals parts. Based on this feature, the dual/multi-energy technique could be also applied for scanning an object at different energies and obtaining information about its component materials like, for example, Density and Atomic effective number.

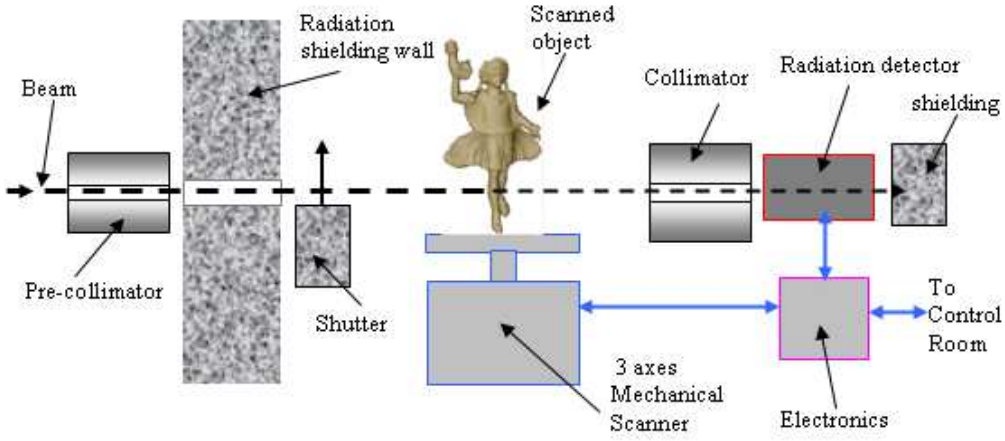

Figure 47: Schematic view of Digital Radioscopy and Tomography set-up

To fully exploit the above unique and very useful characteristics we propose to design and implement a complex **Digital Radioscopy and Tomography** Equipment (DRT) as a dedicated tool for developing NDT analysis at LCB facility. The DRT set-up we propose will be specialized in non-invasive experiments and analysis by performing 2D transmission images and 3D reconstructed tomograms of the scanned objects, revealing the internal fine structure and composition, very useful in the development of processes for new technologies and materials and also for industrial complex structures analysis. Figure 47 show a schematic view of our proposed DRT set-up, where the main components have the following meaning:

- **Scanned object**: maximum of 1.5 x 1.5 x 1.5 m3 and 200 Kg.
- **Mechanical scanner**: 3 axes with electronic control, 1 vertical translation of 1.5 m, 1 horizontal translation of 1.5 m and a continuous rotating table;
- **Radiation detector**: Spectroscopic detectors with MCA and SCA for high-count rate.

We should mention that this set-up could be used for the precise analysis of radionuclides in nuclear waste [3] and could be the starting point for very interesting techniques for interrogation of the fissile material in luggage and cargo for airport security-related applications.

References

[1] H. Toyokawa, Nucl. Instr. and Meth. Phys. Res. A 608 (2009) S41-S43.

[2] H. Toyokawa, H. Kanada, T. Kaihori, M. Koike, K. Yamada, IEEE Trans. Nucl. Sci. 55 (2008) 3571.

[3] R. Hajima , Journal of Nuclear Science and Technology, Vol. 45, No. 5, p. 441-451 (2008).

5.6.3 High Resolution, high Intensity X-Ray Beam

D. Habs[1], P. Thirolf[1], C.M. Teodorescu[2], A.M. Vlaicu[2],C. Ghica[2] and D. Macovei[2]
[1] *Ludwig Maximilians University, Munich (Germany)*
[1] *National Institute of Materials Physics, Bucharest-Magurele (Romania)*

High resolution X-ray beams are available at high energy synchrotron light sources using monochromators. There is a large interest in small compact devices for many applications like protein crystalline structure analysis [4] or Extended X-ray Absortion Fine Structure (EXAFS) for studying the structures of local neighbouring shells [1]. Here new developments with small storage rings and super-cavities are underway [2, 3]. However, for many applications the 10%-3% energy resolution of the 50 keV X-rays from compact storage rings is rather marginal and machines which would offer a direct bandwidth of 10^{-3} or better would be ideal. The diffration patterns at several wavelength around absorption edges can be measured. This technique of Multi-wavelength Anomalous Diffraction (MAD) is used to determine complex protein structures [1]. Thus technological developments for better bandwidth – as required for ELI-NP – would be very decisive to serve a much larger community. Thus the ELI-NP γ facility could serve as a demonstrator for such technologies and applications. Here the low energy beamline for Mössbauer transitions and multiple nuclear excitons could be used.
X-ray absorption spectroscopy
The XAS (*X-ray Absorption Spectroscopy*) techniques provide structural and chemical information regarding a certain atomic species selected of whatever complex materials or systems, by the analysis of the X-ray absorption spectra on the high-energy side of the absorption edge.

Most often, the data analysis is carried out by two distinct methods, EXAFS and XANES, distinguished by the approached energy range and the required information:

- EXAFS (*Extended X-ray Absorption-Edge Fine Structure*) describe the absorption oscillations up to 800-1000 eV above the edge. These oscillations are due to the elastic backscattering of the ejected photoelectrons on the neighbours of the absorbing atom, up to distances of 5-6 $\mathring{A}$. The contribution of more distant neighbours to EXAFS is severely dampened by inelastic scatterings. Therefore, EXAFS spectroscopy provides information about the local environment of the absorbing atom: interatomic separation, coordination numbers (number of neighbours), chemical nature of neighbours, structural disorder. The method has significant advantages with respect to the traditional X-ray diffraction: element selectivity, consisting of the separate description of the local structure around each atomic species in a material, regardless its complexity; high sensitivity, enabling to investigate highly diluted or dispersed species; same mathematical formalism in the data analysis for periodical (crystals) or disordered structures (amorphous, glasses). As a support of the EXAFS utility, it is one of the few techniques able to determine the location of the doping atoms in various host matrices [5–7], difficult to find out by traditional techniques of X-ray diffraction or electron microscopy.
- XANES (*X-ray Absorption Near-Edge Structure*) defines the spectrum details in the first 10-15 eV above the edge, corresponding to the photoelectron transitions from the initial atomic state ($1s$, $2p$) on unoccupied states with the symmetry allowed by the dipolar transition rules (Δl = $\pm$1; Δj = 0, $\pm$1). XANES reflects the density of unoccupied states, so being sensitive to the chemical state of the absorbing atoms: valence, oxidation degree, nature of the chemical ligands etc [8].

Other details of the spectra can also provide useful information. Faint pre-edge peaks, at energies before the edge, are present in the spectra of the transition metals and rare earths. They describe the electron transitions on free states, but of symmetry forbidden by the transition rules ($1s \rightarrow 3(4)d$, $2p \rightarrow 4f$) in the free atom. However, in solid matrices, configurations of low symmetry (e.g. tetrahedral) around the absorbing atom superpose states of different angular moments. This can increase the probability of the forbidden transitions, enhancing the pre-edge peaks. Their amplitude thus allows a fast estimate of the local symmetry around the absorbing species [9].

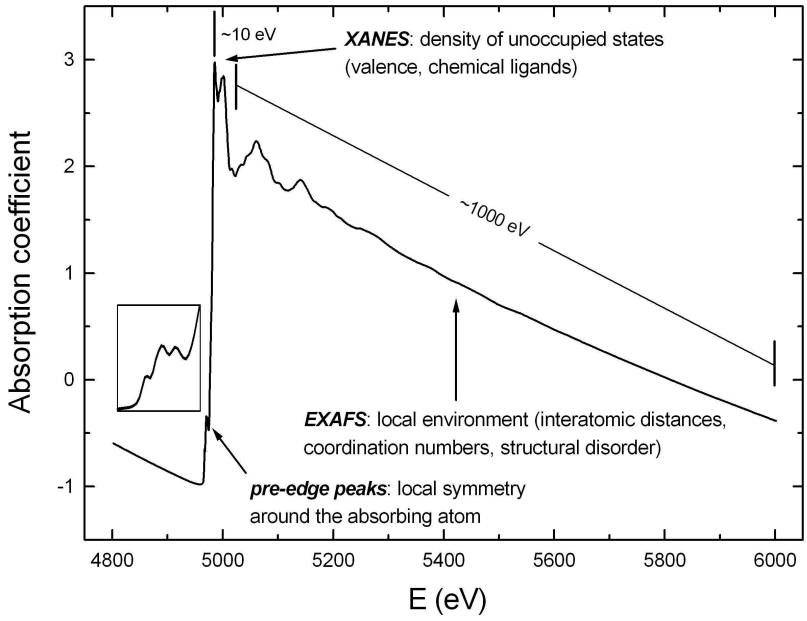

The EXAFS/XANES techniques have known a tremendous development in the last two decades, with applications in the study of a large variety of materials, like: metallic [10] and silicate glasses [11], metallofullerenes [12], catalysts [13], superconductors [14], liquid crystals [15] etc. EXAFS has also proved its capabilities in the research of biological systems, with valuable contributions to the description of metal environment in the complex structure of metalloproteins [16–18]. It is worth noting that the Chapter devoted to the ELI-NP applications (Chap. 8: "*Stand-alone γ Facility for Applications*"), in "*The Scientific Case of ELI Nuclear Physics*" (April 2010), specifically indicates the MAD (Multi-wavelength Anomalous Diffraction) and EXAFS techniques as appropriate applications of ELI-NP high-resolution and high-intensity X-ray beam in the study of complex protein structures [19]. The same proposal is reiterated in Chap. 9 ("*Industry Relevant Developments at ELI-NP*").

Multi-wavelength Anomalous Diffraction (MAD)

The **multi-wavelength anomalous diffraction** method, developed by W. Hendrickson (Hendrickson, W. A., 1991, "Determination of macromolecular structures from anomalous diffraction of synchrotron radiation." *Science*, *254*, 51-58.), is an approach to solving the phase problem in protein structure determination by comparing structure factors collected at different wavelengths, including the absorption edge of a heavy-atom scatterer. As a consequence of the wavelength dependence of anomalous dispersion, the structure factors $f = f^0 + f' + if''$ will be significantly perturbed, both in amplitude and in phase, by resonant scattering off an absorption edge. By comparing diffraction patterns measured at wavelength matching the absorption edge of a scattering atom, and again at a wavelength away from the absorption edge, it is possible to obtain information about the phase differences and solve the crystal structure.

Photoemission Electron Microscopy (PEEM) and High-Resolution Photoelectron Spectroscopy (HRPES) (Soft X-ray beamline: 100 - 2000 eV)

Such a beamline (e.g. composed by a plane grating monochromator PGM and spherical focusing mirrors) produces photons in the range 100 - 2000 eV with a resolving power E/ E of some 20 000. The resolving power depends critically on the source dimension. If the source is represented by an extremely compressed bunch of electrons, as is expected to be the case of the electron beam in a linac, the resolving power is expected to further increase. The above energy range is of prime importance, since it includes many interesting energy levels, such as:

- 1*s* levels for C, N, O, F, etc. - up to Si. These are of high importance for organic chemistry and also for Al metallurgy, semiconductors (Si), minerals (Na, Mg);
- levels for all 3d metals;

- levels for all 4d metals;
- levels for rare earths.

The corresponding near-edge X-ray absorption fine structure (NEXAFS) spectroscopy evidences $1s \rightarrow 2p$ transitions for elements from organic compounds, $1s \rightarrow 3p$ for Na, Mg, Al, Si, thus allowing the direct investigation of valence states. Concerning transition metals, one realises $2p \rightarrow 3d$ transitions; in the case of rare earths, transitions $3d \rightarrow 4f$ are induced. Hence, in the latter two cases one investigates directly the outer energy levels responsible for magnetic properties. Consequently, one of the applications of this facility will be NEXAFS spectroscopy of organic compounds [20] and another the determination of element-specific orbital and spin moments by X-ray magnetic circular dichroism (XMCD) [21].
Aside for NEXAFS and XMCD spectroscopies, the soft X-ray (SXR) beamline will be provided with several complex equipments: (i) the first one by combining X-ray photoelectron spectroscopy with electron microscopy (photoemission electron microscopy PEEM) [22]; (ii) a second for high resolution photoelectron spectroscopy (HRPES) [23]. A schematics of the setup is represented in Fig. 48. Regarding these two methods, one may mention the following: (i) A low-energy electron microscope and photoemission electron microscope (LEEM-PEEM) is expected to be commissioned in September 2010 in NIMP. This installation provides a spatial resolution of 4 nm and an electron energy resolution of 0.25 eV. The setup that is intended to be purchased at ELI-NP represents the more advanced version of the PEEM family, with an additional aberration corrector which yields to a spatial resolution of 2 nm (in NIMP this version could not be purchased due to the funds limitation). In order to ensure the optimum operation of the PEEM system, a very important condition is the extreme focusing of the soft X-ray beam (10 nm). The PEEM connected to the SXR yields informations such as XPS-like data (composition, chemical states, valence bands, dispersion laws) with a resolution exceeding that of actual scanning electron microscopes (SEM). Such a facility is not yet available anywhere in Europe. (ii) At the same time, the energy resolution of a PEEM system is rather moderate, as compared with the resolution possibilities of the SXR (250 meV as compared to some 10 meV). Thus, we consider necessary the coupling of a high resolution ($> 10\ 000$) electron spectrometer on the beamline, possibly using the same analysis chamber. One of the application of such high resolution photoelectron spectroscopy (HRPES) performed at a SXR is the possibility of detecting different vibrational states at surfaces and interfaces and also the separation without ambiguity the bulk, surface, interface (etc.) components.
Consequently, this facility will allow the access to NEXAFS, XMCD, PEEM and HRPES in a single installation, which will be unique in Europe. No other synchrotron radiation beamline offers actually so many techniques simultaneously. For instance, Ref. [24] was amongst the few papers that presented combined XMCD and HRPES for *in situ* prepared Fe/InAs(001) samples and was rather well received by the community (15 citations up to now).

References

[1] J. Als-Nielsen and D. McMorrow; *Elements of Modern X-ray Physics*, WILEY (2009).

[2] C. Bruni et al., *THOMX, Conceptual Design Report*, LAL/RT 09-28; SOLEIL/SOU-RA-2678 , (2009).

[3] M. Bech et al., Journ. of Synchr. Rad. **16**, 43 (2009)

[4] PSI-whitepaper; *Opportunities for Structural Genomics Beyond 2010, Creating Partnerships for the future*, (2008).

[5] W. Li, A.I. Frenkel, J.C. Woicik, C. Ni, S. Ismat Shah, *Phys. Rev. B* **72**, 155315 (2005).

[6] F. Vasiliu, L. Diamandescu, D. Macovei, C.M. Teodorescu, D. Tarabasanu, A.M. Vlaicu, V. Parvulescu, *Top. Catal.* **52**, 544 (2009).

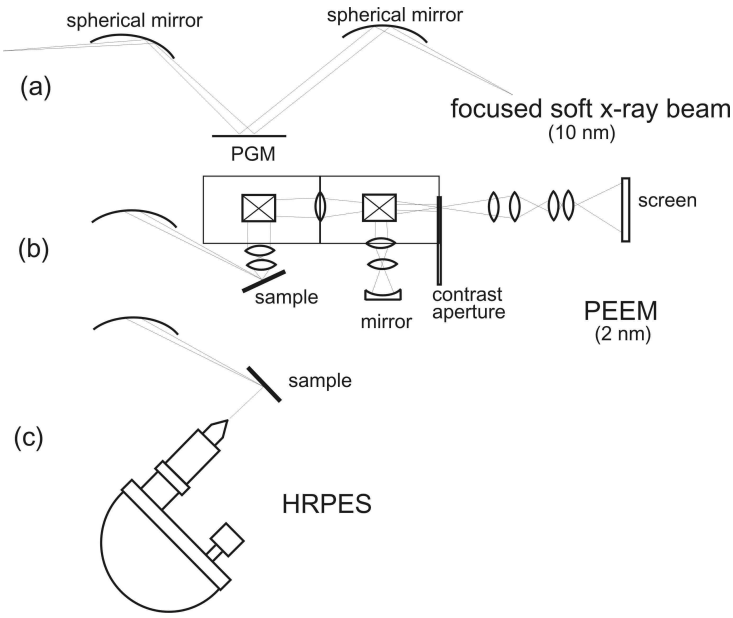

Figure 48: Setup of the soft X-ray beamline facility: (a) schematics of the SRX beamline with extreme focalization; (b) the analysis configuration in case of using PEEM; (c) the analysis configuration for using HRPES.

[7] N.D. Afify, G. Dalba, C. Armellini, M. Ferrari, F. Rocca, A. Kuzmin, *Phys. Rev. B* **76**, 024114 (2007).

[8] M. Schwidder, M.S. Kumar, K. Klementiev, M.M. Pohl, A. Bruckner, W. Grunert, *J. Catal.* **231**, 314 (2005).

[9] H. Yamashita, Y. Ichihashi, S.G. Zhang, Y. Matsumura, Y. Souma, T. Tatsumi, M. Anpo, *Appl. Surf. Sci.* **121-122**, 305 (1997).

[10] H.W. Sheng, W.K. Luo, F.M. Alamgir, J.M. Bai, E. Ma, *Nature* **439**, 419 (2006).

[11] G.N. Greaves, A. Fontaine, P. Lagarde, D. Raoux, S.J. Gurman, *Nature* **293**, 611 (1981).

[12] M. Takata, B. Umeda, E. Nishibori, M. Sakata, Y. Saito, M. Ohno, H. Shinohara, *Nature* **293**, 611 (1995).

[13] J. Corker, F. Lefebvre, C. Lecuyer, V. Dufaud, F. Quignard, A. Choplin, J. Evans, J.M. Basset, *Science* **271**, 966 (1996).

[14] J.M. Tranquada, S.M. Heald, A.R. Moodenbaugh, G. Liang, M. Croft, *Nature* **337**, 720 (1989).

[15] J. Stohr, M.G. Samant, J. Luning, A.C. Callegari, P. Chaudhari, J.P. Doyle, J.A. Lacey, S.A. Lien, S. Purushothaman, J.L. Speidell, *Science* **292**, 2299 (2001).

[16] C.E. MacBeth, A.P. Golombek, V.G. Young, C. Yang, K. Kuczera, M.P. Hendrich, A.S. Borovik, *Science* **289**, 938 (2000).

[17] L.X. Chen, W.J.H. Jager, G. Jennings, D.J. Gosztola, A. Munkholm, J.P. Hessler, *Science* **292**, 262 (2001).

[18] J.U. Rohde, J.H. In, M.H. Lim, W.W. Brennessel, M.R. Bukowski, A. Stubna, E. Munck, W. Nam, L. Que, *Science* **299**, 1037 (2003).

[19] D. Habs and P. Thirolf, in ***The Scientific Case of ELI Nuclear Physics*** Eds. D. Habs, M. Groß, P.G. Thirolf, M. Zepf), April 2010, p.74.

[20] J. Stohr, ***NEXAFS Spectroscopy***, Springer, Berlin, (1992).

[21] G. Schutz, W. Wagner, W. Wilhelm, R. Kienle, R. Zeller, R. Frahm, G. Materlik, *Phys. Rev. Lett.* **58**, 737 (1987) ; C.T. Chen, F. Sette, Y. Ma, S. Modesti, *Phys. Rev. B* **42**, 7262 (1990) ; B.T. Thole, P. Carra, F. Sette, G. van der Laan, *Phys. Rev. Lett* **68**, 1943 (1992) ; P. Carra, B.T. Thole, M. Altarelli, X. Wang, *Phys. Rev. Lett.* **70**, 694 (1993) ; C.T Chen, Y.U. Idzerda, H.-J. Lin, N.V. Smith, G. Meigs, E. Chaban, G.H. Ho, E. Pellegrin, F. Sette, *Phys. Rev. Lett.* **75**, 152 (1995).

[22] F.M. Ross, R.M. Tromp, M.C. Reuter, *Science* **286**, 737 (1999) ; B.T. Thole, F.-J. Meyer zu Heringdorf, M.C. Reuter, R.M. Tromp, *Nature* **412**, 517 (2001).

[23] W.L. Yang, J.D. Fabbri, T.M. Willey, J.R.I. Lee, R.M.K. Carlson, P.R. Schreiner, A.A. Fokin, B.A. Tkachenko, N.A. Fokina, W. Meevasana, N. Mannella, K. Tanaka, X.J. Zhou, T. van Buuren, M.A. Kelly, Z. Hussain, N.A. Melosh, Z.-X. Shen, *Science* **316**, 1460 (2007) ; P. Ruffieux, K. Ait-Mansour, A. Bendounan, R. Fasel, L. Patthey, P. Groning, O. Groning, *Phys. Rev. Lett.* **102**, 086807 (2009).

[24] C.M. Teodorescu, F. Chevrier, R. Brochier, V. Ilakovac, O. Heckmann, L. Lechevalier, K. Hricovini, *Eur. Phys. J. B* **28**, 305 (2002).

5.6.4 Producing of medical isotopes via the (γ, n) reaction

D Niculae[1]

[1] *IFIN-HH, Bucharest, Romania*

There is a growing concern about the ageing, safety and reliability of nuclear reactors that produce medical isotopes, including molybdenum-99, following a series of well publicized technical problems and unscheduled plant shutdowns. Alternatively, new approaches and methods for producing such radioisotopes are urgently needed to prevent future shortages. The feasibility of producing a viable and reliable source of photo fission / photo nuclear-induced molybdenum-99 (Mo-99) and other medical isotopes used globally for diagnostic medical imaging and radiotherapy is sought. Such a method should also provide a potential alternate solution through which to supplement the production capacity of Mo-99, and to lessen the reliance on existing nuclear research reactors.
We propose the use of the intense laser beam backscattered on high energy electron bunches to produce monoenergetic directed brilliant pulsed gamma-rays by the Compton backscattering process. In this technique a large amount of MeV gamma-rays may be generated and typical nuclear reaction and nuclear excitations may be induced. Electron bunches may be provided by an adjacently installed conventional linac. MeV gamma-photons may also be generated from solid targets and highly compressed by laser acceleration of ultrathin foil targets, based on Thomson backscattering process. Firing this highly intense photon beam at various targets may create molybdenum-99 based on photo-fission reaction. There are also photo nuclear reactions that can be employed, such as $^{100}\mathrm{Mo}(\gamma, n)^{99}\mathrm{Mo}$ (photon energy > 20 MeV). Specific separation methods for Mo-99 (or other medical isotopes) have to be investigated, selected and optimized. Moreover, efficient Tc-99m extraction technologies have to be developed.

5.6.5 Medical Radioisotopes produced by γ Beams

D. Habs[1], U. Köster[2]

[1] *Ludwig Maximilians University, Munich (Germany)*
[2] *ILL Grenoble*

In Ref. [1] about 50 radioisotopes are describes, which can be produced much better by γ beams and are of interest to medicine for diagnostic and/or therapeutic purposes. With the small band width γ beams for many of the isotopes we will find specific gateway states or groups of resonant states where the production cross sections can be increases by 2-3 orders of magnitude compared to Ref. [1],

making them even more interesting for largescale industrial applications. Here we shell focus on some of the most interesting isotopes to give a flavour of the possiblities:

^{195m}Pt Determining the efficiency of chemotherapy for tumors and the optimum dose by nuclear imaging

In chemotherapy of tumors most often platinum cytotoxic compounds like cisplatin or carbonplatin are used. We want to label these compounds with ^{195m}Pt for pharmacokinetic studies like tumor uptake and want to exclude "nonresponding" patients from unnecessary chemotherapy and optimizing the dose of all chemotherapy. For such a diagnostics a large scale market can be foreseen, but it would also save many people from painful treatments. We estimated in Ref. [1] that several hundred patient-specific uptake measurements could be produced with a γ beam facility, However this probably may be increased to 10^5, if optimum gateway states are identified by scanning the isomer production with high γ beam resolution. ^{195m}Pt has a high $13/2^+$ spin isomer at 259 keV, halflife ($T_{1/2}$= 4 d) with SPECT transitions of 130 keV and 99 keV to the $1/2^-$ groundstate.

^{117m}Sn An emitter of low energy Auger electrons for tumor therapy

Auger electron therapy requires targeting into individual tumor cells, even into the nucleus or to DNA, due to short range below 1μm of the Auger electrons; but there it is of high REB due to the shower of many 5-30 Auger electrons produced. On the other hand Auger radiation is of low toxicity, while being transported through the body. Thus Auger electron therapy needs special tumor specific transport molecules like antibodies or petides. Many of the low lying high spin isomers produced in (γ, γ') reactions have strongly converted transions, which trigger these large showers of Auger cascades.

A $^{44}Ti \rightarrow^{44}$Sc generator for the γ-PET isotope ^{44}Sc with much improved resolution in nuclear imaging

In recent years PET (Positron Emission Tomography) with typical spacial resolution of (3-10 mm) was supplemented by multi-slice X-ray CT (Computer Tomography) of much better resolution, leading to the novel technology of PET/CT. The coregistration and the reference frame of CT are very helpfuk for the interpretation of PET images. CT and PET require comparable dose. Looking at such images it is very apparent, that an order of magnitude improvement in the resolution of PET is highly desirable and might even make accompanying CT obsolete. ^{44}Sc is the best candidate to supply the two 511 keV annihilation quanta together with a strongly populated 1.157 keV transition. By measuring the position and direction of this γ quantum accurately with a Compton spectrometer together with the two 511 keV quanta the location of the emitting nucleus can be located in 3 dimensions. In conventional PET the two collinear 511 keV quanta only allow to determine a 2 dimensional localisation on a line. Thus a much better spacial resolution can be achived for the same dose with γ-PET compared to PET. With ^{44}Ti (half life $T_{1/2}$= 59 a) the production with a very promising generator for ^{44}Sc ($T_{1/2}$= 3.9 h) becomes available with γ beams. Again a much stronger population via the fine structure of the Giant Dipole Resonance (GDR) in the ^{46}Ti(γ,2n)^{44}Ti is expected for the ^{44}Ti core consisting of the doubly magiv ^{40}Ca and an α particle. The long halflife of ^{44}Ti requires a large transmutation with an intense γ beam, but on the other hand leads to a very valuable, longlived generator. The production of ^{44}Ti in the (γ,2n) reactions require rather large γ-energies of 23-24 MeV, and would require an increase of the maximum presently planned γ energy at ELI-NP of 19 MeV.

Many further new interesting medical radioisotpes can be produce (see Ref. [1]): " New matched pairs" of isotopes of the same element become available, one for diagnostics the other for therapy, allowing to contol and optimize the transport of the isotope by the bioconjugate to the tumor. Also new therapy isotopes become available like ^{225}Ac, where 4 consecutive α decays can cause much more double strand breaking. Devellopping these techniques and applications is a promising task of ELI-NP with a strong sociosocietal component.

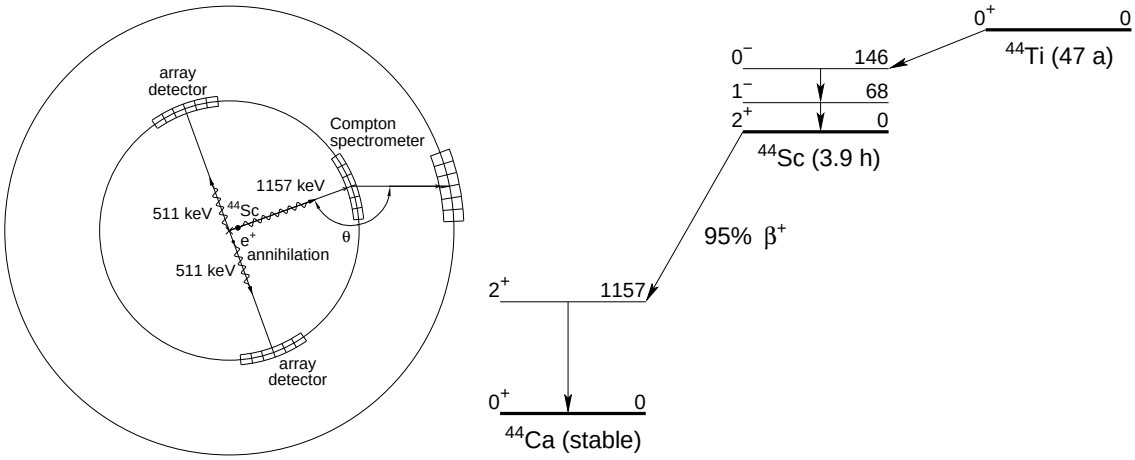

Figure 49: Schematic picture for the combined γ-PET and the ^{44}Ti/^{44}Sc generator

References

[1] D. Habs and U. Köster, *Produktion of Medical Radioisotopes with High Specific Activity in Photonuclear Reactions with γ Beams of High Intensity and Large Brilliance*, arXiv-1008.5336v1[physics.med-ph]2010, submitted to Appl. Phys. B.

5.6.6 Extremely BRIlliant Neutron-Source produced via the (γ, n) Reaction without Moderation (BRIN)

D. Habs[1], M. Gross[1], P. G. Thirolf[1] and P. Böni[2]
[1] *Ludwig Maximilians University, Munich (Germany),*
[2] *Physik-Department E21, Technische Universität München, D-85747 Garching,(Germany)*

Presently, thermal and cold neutron beams are produced at large-scale facilities like reactors or spallation neutron sources via moderation of MeV neutrons down to 1/40 eV. Moderators and shielding result in very large sources with ≈ 10 m diameter and accordingly reduced flux density. We propose to produce a brilliant pulsed neutron source directly without moderation by generating it with brilliant γ beams of 5–8 MeV via the (γ,n) reaction with energies up to 1000 meV above the neutron threshold [1]. This development became possible because very brilliant γ sources are being developed with spectral densities of $7 \cdot 10^8$/[s eV] at 100mA electron current, where the γ rays will be produced by incoherent Compton back-scattering of laser light from brilliant high-energy electron bunches. The γ energy spread is presently limited to 10^{-3} by the energy spread of $4 \cdot 10^{-4}$ of the electron beam due to the stability of the accelerator voltage. Presently, in the most advanced control system (for example at the Euro-XFEL) a stability of the amplitude of 0.01% and for the phase of 0.01^0 can be achieved. These numbers are corresponding to 10^{-4} energy stability. This is the limitation of the present technology, but hopefully the feedback system can be improved in the near future and so a few times 10^{-5} may be achievable. Such an improvement in γ-energy spread is very essential and will result in large gains of brilliance. Very small beam size γ beams with 20 μm diameter can be produced, which due to the strong collimation of the γ beam can be transfered to the place of neutron production. Thus we can obtain $7 \cdot 10^8$ neutrons with energies below 1 eV, which may be pulsed by macro-pulsing the electron beam. It emerges from a source with a diameter of 20 μm. We prefer to select states which neutron-decay by p waves, resulting in an angular distribution peaked normal to the orbital angular distribution. Since the spin of the polarized γ beam is transfered to the neutron-emitting nuclei and if the excitation starts from a 0^+ ground state, we can choose the projection of the orbital angular momentum of the neutrons with respect to the recoil direction of the emitting nucleus. Due to this $\sin^2$-like neutron distribution, the neutron brilliance in the detector region is increased by a factor of about 10 compared to an isotropic distribution. Selecting the right spin direction is very important. Futhermore the neutron energy spectrum becomes strongly angular dependent due to the recoil and within the 10% solid angle of the neutron guide system will have a narrow energy bandwidth. In this way a rather high brilliance neutron beam with 10^5n/[s (mm mrad)^2 0.1% BW] is obtained, which is roughly 2 orders of magnitude larger than the one at existing high-flux reactors and comparable to spallation sources. The highly divergent neutron beams can be extracted over a wide band of wavelengths (100-0.1Å) by means of elliptic guides using the latest supermirror technology and transported to the instruments for neutron scattering and imaging.

In neutron scattering there is a large development ongoing towards cold and thermal micro-neutron-beams for studying the structure and dynamics of small samples under ambient extreme conditions, for example in the area of solid state and soft matter physics. The large field of reflectometry and small-angle neutron scattering will also profit from highly brilliant and small beams. A large research field in fundamental physics as well as in applied physics can be opened up by such a new facility with a large user community with long-term experience in thermal neutron scattering. The investment costs and running costs of such a facility are 1 - 2 orders of magnitude smaller compared with present large-scale neutron facilities and may be installed even at universities. Moreover the large amounts of radioactive waste and the efforts for safety and security are minimized. The photon recoil of the γ rays causes a recoil momentum of the neutron emitting nucleus, which corresonds to a neutron energy of about 200 meV. Depending on the neutron emission this neutron momentum has to be added vectorially to the momentum of the emitted neutrons, resulting in strongly angle dependent neutron spectra with narrow band width, reaching down to rather low energies.

Here several neutron beamlines with elliptical or parabolic neutron guides [3, 4, 8] are foreseen for neutron scattering and imaging. Experiments with Small Angle Neutron Scattering (SANS), Time Of Flight (TOF) measurements with choppers or Tripple Axis Spectrometers (TAS) are foreseen.

References

[1] D. Habs et al., Eur. Phys. J. **D 55**, 279 (2009).

[2] Guide to Neutron Research facilities at the ILL, The Yellow Book, Grenoble, (1988).

[3] R. Valicu and P. Böni, *Focusing Neutron Beams to Sub-Millimiter Size*, subm. to NIM , (2010).

[4] M. Schneider, J. Stahn and P. Böni., Nucl. Instr. and Meth. **A 610**, 530 (2009).

[5] P. Böni, Nucl. Instr. and Meth. **A586**, 1 (2008).

[6] C. Grünzweig et al., Appl. Phys. Lett. **91**, 203504 (2007).

[7] Ch. Schanzer et al., Nucl. Instr. and Meth. **A 529**, 63 (2004).

[8] M. Janoschek et al., Nucl. Instr. Meth. A **613**, 119 (2010).

5.6.7 Neutron diffraction techniques for materials science

C.M. Teodorescu[1], A.M. Vlaicu[1],C. Ghica[1] and D. Macovei[1]
[1] *National Institute of Materials Physics, Bucharest-Magurele (Romania)*

The structure and sometimes dynamics investigations by X-ray and thermal neutrons scattering are among the obligatory requirements in production of the new materials. Although the X-ray radiation is used most frequently, especially for structure determination, the wonderful properties of the neutron make it an instrument preferred in some cases and not replaceable in other. Non-systematic variation with Z of the scattering length and its wave vector comparative with those of the collective movements in crystals make the neutron much appropriate to localize the light atoms, to distinguish between neighbouring atoms in the Mendeleyev table and for determination of phonon dispersion relations. Having no electric charge but having spin the neutron becomes the unique instrument for investigation in bulk materials and of the magnetic structure and dynamics.

Neutron production, condensed matter investigations, drawbacks
At this moment neutron beams to be used for condensed matter investigations are produced by nuclear reactors and by spallation. In the same time there are two major drawbacks: very high price per neutron and the impossibility to have neutron sources of brilliance comparative with those of X-ray, impeding the construction of high resolution spectrometers and diffractometers. The second drawback was partially removed once with the birth of the spallation sources. Because these are pulsed, the scattering methods naturally associated with the spallation sources are the time-of-flight methods (energy-dispersive for diffraction, by contrast with the angular dispersive method at the stationary reactors). An element contributing to resolution deterioration of the time-of-flight instruments is the impulse broadening caused by moderator.

Photonuclear reaction (γ, n): an efficient method to generate thermal neutrons at ELI facility.
Other methods to produce neutrons are known from a long time but because of their very low efficiency these were not used to profile beams for condensed matter studies. One of these methods is the photonuclear reaction (γ, n). If a heavy nucleus with the neutron binding energy B_n of magnitude of MeV, is irradiated with γ quanta of energy E_γ slightly higher than the resonance energy $E_\gamma = B_n + \Delta'$, the excited nucleus expels a neutron of energy Δ with a probability given by Breit-Wigner formula. If Δ is of magnitude of tenths up to hundreds meV the wavelength of the expelled neutron is in the range specific to diffraction on real structure of materials. The diffraction becomes measurable *without need to moderate the neutrons* if the target brilliance is enough large.

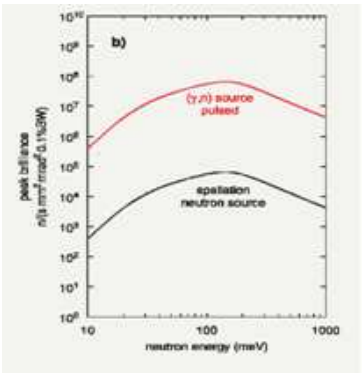

In the case of ELI facility the large target brilliance is due two factors: (i) - the huge intensity of incident beam and (ii) - focusing of this beam on very small surface of a very thin target, resulting in an active volume of magnitude 10^{-3} mm^3. The above mentioned authors estimate a brilliance of two order higher than those of the European spallation source in a wide wavelength range, of 0.3-3 $\AA$ (see left-side figure). This wide range can be obtained provided that the target is manufactured from a large number of heavy nuclei, actinides and sub-actinides, resulting in a convenient spreading of resonances on this range. At this moment numerous quantities essential for rigorous calculation of thermal neutron distribution like resonances of different heavy nuclei, breadths in Breit-Wigner formula, etc., are not yet known. Consequently the distribution shown before is rather a rough, qualitative estimation. Other necessary characteristics: pulsed source, frequency between 100 and 1000 Hz, width at half high of the neutron pulse is 0.1 μs.

Two possible diffractometers

At this stage when only rough estimations on the neutron source are available, we propose two possible geometries of diffractometers for powder samples, one using the time-of-flight method, the other one working in the angular dispersive method. Both are of Debye-Scherrer type and are conceived for recording the neutrons on the whole diffraction cone. Consequently small volume samples (mm^3) can be used. If the neutron spectra is enough large (as described before) it is preferred realization of the first geometry.

Geometry 1 is a classical one, being used for example at 'High resolution powder diffractometer", installed at the spallation source ISIS, Rutherford-Appleton Laboratory, UK. The difference is only the length of the flight basis, 7 m here, comparatively with 100 m at ISIS. This comes from the ratio between pulse widths, 0.1/20. The major contributions to resolution here are coming from the sample and detector thicknesses.

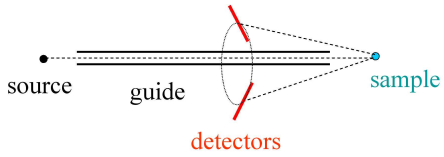

The scintillation detectors are mounted to realize time focusing in the angular range $2\theta \in (160°, 170°)$. It must be mentioned that if the facility runs with the frequency higher than 100 Hz, a chopper should be used in the incident beam allowing passing only a fraction of neutron pulses, avoiding superposition of neutrons from successive pulses.

Geometry 2 is similar to Debye-Scherer camera using photographic film. The scintillation detectors are mounted on parallel circles on a cylinder that can be translated along its axis. As a principle a single ring of detectors is enough, in practice a large number of rings makes the measurement time much shorter. The monochromatic beam incident on sample is produced by a double bent single crystal, the two curvature radii being different one from another (because diffraction geometry has not a cylindrical symmetry). This geometry has an important peculiarity: both, resolution and luminosity are dependent of the Bragg angle, then requiring performing corresponding correction for diffracted intensities.

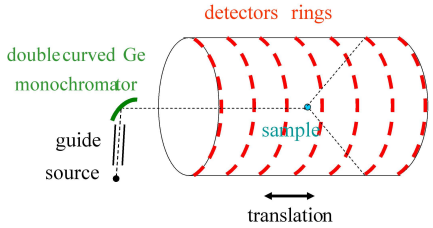

5.6.8 Dual-range Instrumentation for Wide Applicability Neutron Techniques

D Aranghel[1], M.O. Dima[1]
[1] *IFIN-HH, Bucharest, Romania*

Based on the proposal for a brilliant pulsed neutron source with wavelengths in the range of 0.1-100 angstrom at ELI we propose fostering the organisation of an Application Users Community centered on dual-range (thermal and cold) neutron characterisation equipment.Given the work of the group leader (Dr. Aranghel) on neutron scattering experiments in Berlin, Saclay and Julich (TOF and SANS experiments), this proposal will expand on those techniques to encompass both thermal and cold neutron applications. A brief view at the properties and suitability of the two energy ranges is indicated below.

- Thermal neutrons: (Wavelenght 1-3 angstrom Energy 10-100 meV) Investigations Atomic scale structures; Fast dynamics; Low energy resolution;
- Cold neutrons: (Wavelenght 3 - 300 angstrom Energy 0.3 μeV-10 meV) Nano-scale structures; Slow dynamics; High energy resolution;

The group proposes therefore starting with known applications, for which there is in-group experience, and fostering the attraction of the broader scientific community in the areas below. This is in line with the community-oriented goal of the ELI project itself:

- Bio-proteins / molecules: neutrons are an excellent hydrogen probe, with high H/D contrast. Applications are: function of protons in enzyme mechanisms (shuttling, transfer),D-labeled proteins in complex systems, proton-labels in deuterated systems, protein rigidity to D, protein interaction and clustering, structures (membranes, single-lipid monolayers, bio-mat interfaces, etc), protein-folding mechanisms and dynamics, etc.Micron level beam-focusing envisaged at ELI is particularly attractive for this field.
- Nano-composites/porousites and Soft-matter: surfactants are of extreme importance in modern technology. Examples are (nano-particle) wetting of heat-transfer pipes in nuclear reactors, oil extraction from porousites (above 2/3 of world oil is in porousites), oil adhesion in engines, etchants in microtechnology photolithography, special paints for the naval industry, detergents, adhesives, emulsifiers, de/foamers, firefighting, ferro-fluids, dipalmitoylphosphati-dylcholine prevents alveoli from collapsing(atelectasis), etc. Although seemingly trivial in nature and functions, it cannot be stressed enough how important these substances are. Self-Assembled Monolayers (SAM-s) can be used as nano-templates for nano-patterning in alignment of single wall carbon nanotubes, dip-pen nanolithography, smart-surface functionalisation of biosensors (selective, hydrophobicity based, protein affinity). SAM-s also have enormous potential in coatings as wetting control, chemical resistance layers, bio-compatibility, molecular recognition and cell attachment, electrodes, bio-electronics, control of electron transfer, selective attachment nano-particle coatings (i.e. bio-compatible magnetic nano-particle blood disinfectation of fungus with magnetic filtering). This enormous pool of applications stands on surface-interaction physics, or neutron probing in the range of q = 0.01 - 1 angstrom. Nano-porousites in turn are of interest for low-k materials in micro/nano-technology, for aerogels and xerogels in optics and printing industry (q range: 0.01-0.1 ang.$^{-1}$).
- Fullerenes, graphene: this is a class of materials still in the molecular structure studies stage (q range: 0.1-1 ang.$^{-1}$, thermal neutrons), however super-molecular compounds are appearing (such as single-molecule electronics, thiole-connected), which cannot withstand large energy-kicks and require ultra-cold neutrons for in-situ dynamics investigations.
- Magnetic nano-materials: magnetic grains can be structurally and dynamics wise very well understood with polarised neutrons (q = 0.01-0.1 ang.$^{-1}$). Magnetic and domain rotation, spin-torque in ultra-thin film sandwiches occur in the 100 nm skin layer that can be investigated with very-cold neutrons in back-scattering configuration (similar to the dedicated Brillouin Light Scattering method, with the advantage of not probing and integrating all the magnetic layers).

- Hydrogen fuel cells: being the perfect proton-tracer, neutrons are useful in H-location (2% sensitivity with diffraction), H-bonding (0.1% with vibrational spectroscopy), Hdiffusion(0.1% with quasi-elastic scattering), H nano-structuring (0.01% with SANS), H density profiles (2% with reflectometry), etc.

As mentioned in the beginning, there would be a minimal start-up dual-range equipment, with the possibility of further add-ons (or replacements) function of the community response or demands:
1. Cold Neutron Spectrometer - this instrument would have variable resolution and would cover a broad range both in energy and momentum transfer. Its resolution and ample energy-momentum range allow it to address a broad variety of scientific problems in biomaterials, polymer dynamics, bio-gels, interface physics, cements, nano-materials, rock characterisation, magnetic systems, quantum liquids, rotational tunneling spectroscopy, water dynamics, etc.
2. Time-of-flight / Small-Angle Neutron Scattering Spectrometer - this instrument would examine size, shape, internal structure and spatial aranjament of soft matter, coloidal systems, biological macromolecules, pharmaceuticals, food science, respectively on a length nano and bio materials scale. It would follow a design similar to Sans2d (ISIS), or SASI (Argonne).

References

[1] Scientific Case for ELI Nuclear Physics http://www.eli-np.ro/executive-comittee-meeting-april-12-13.php;

[2] P. Boni, NIM A586, 1-8 (2008);

[3] ANL-05/42, Work-Shop Proc., Intense Pulsed Neutron Source Division Argonne Nat. Labs (2005).

5.6.9 An Intense BRIlliant Positron-Source produced via the (γ, e^+e^-) Reaction (BRIP)

D. Habs[1], M. Gross[1], P. G. Thirolf[1], K. Schreckenbach[2], C. Hugenschmidt[2] and G. Dollinger[3]
[1] *Ludwig-Maximilians University, Munich, Germany*
[2] *Physik-Department E21, Technische Universität München, D-85747 Garching, Germany*
[3] *University of the Bundeswehr, Munich (Germany)*

Using an intense γ beam of 10^{13} photons/s with (2.5±0.5) MeV we propose to realize an intense moderated positron beam of about 10^7e$^+$/s via the (γ,e^+e^-) reaction. Using a Ne moderator we expect an about tenfold increased moderation efficiency compared to W or Pt moderators [1]. The intensity of this novel source is significantly weaker the presently most intense moderated positron source NEPOMUC at the Munich neutron source FRM 2 with about $9 \cdot 10^8$e$^+$/s [2], where about $10^{16}\gamma$/s from neutron capture hit the inner converter volume. Due to the small diameter and well-directed γ beam we expect for the new source a brilliance of $10^7 e^+$/[s(mm mrad)^2 0.1%BW], which is about 4 orders of magnitude more brilliant than the NEPOMUC source. Using fully polarized γ beams for the first time we will obtain an intense, fully polarized positron beam, which can be transported through beamlines via solenoidal fields to different detector systems [3]. Presently, we have a pulsed source with 120 Hz repetition rate and a peak intensity for the 200 ns long pulses of $5 \cdot 10^{11}$/s. These macropulses consist of 100 micropulses each with 2 ns spacing and 2 ps duration. Frequently pulsed positron beams are requested and one can improve the energy resolution of the positron beam by using a time dependent acceleration field. It is clear that significant improvements of the positron source are expected, when the γ is upgraded in a second phase to $10^{15}\gamma's$/s ans much higher repetition rate. Also presently the brilliance of the positron beam can be improved by remoderation by a factor of 10^3, while at the same time the intensity is reduced by a factor of 10–15 [4]. Low-energy positron beams are used in fundamental physics studies of the properties of positronium (Ps), Ps$^-$ or more complex electron-positron systems. In applied physics studies with positron beams of Fermi-surfaces, defects, interfaces etc. offer excellent diagnostics tools. The new brilliant source is best suited for micro-positron beams, e.g. in positron microscopy. Polarized positron beams open up a totally unexplored research area, where polarized electrons in e.g. magnetic structures can be studied.

References

[1] A. P. Mills and E. M. Gullikson, Appl. Phys. Lett. **49**, 1121 (1986).

[2] C. Hugenschmidt et al., NIM**A 593**, 616 (2008).

[3] C. Hugenschmidt et al., NIM **A 554**, 384 (2005).

[4] C. Piochacz et al., Appl. Surf. Sci. **255**, 98 (2008).

5.6.10 Intense BRIlliant Positron-Source: Positrons in Applied Physics

F. Constantin[1], P.M. Racolţa[1], I. Vâţă̆[1], E. Ivanov[1]
[1] *IFIN-HH, Bucharest, Romania*

Using the BRIlliant Positron-Source, a part of the produced positrons will be diverted into a Positron Gun facility which will enable high sensitivity measurements in applications of positron annihilation spectroscopy. The moderated positrons will be reaccelerated in the range of 0.8–50 keV and then focused on the target under study [1].
The beam line will have to steer the mono-energetic positrons far away in order to eliminate the noise of random gamma radiation. A typical coincidence setup, under high vacuum, will permit the studies of various materials, concerning defects (crystals), free volumes (polymers) and also to perform a deep profiling analysis. Experimental setups and results have already been realized in IFIN-HH using a ^{22}Na positron source, 10μCi, deposited on thin aluminized Mylar. The positron source is sandwiched

between the targets on the study and the coincidence gammas are recorded by two HPGE detectors; the acquisition system is a VME CAEN and the software is custom developed in our laboratory. Studies have been conducted on Aluminum and polymers [2].
On the another hand using high intensity positron bursts, thin film of porous silica will be implanted and Ps and Ps_2 will be created on the internal pore surfaces; the molecule formation occurs much more efficiently in the confined pore geometry. The Ps_2 molecule will lead the way for further multi-positronium work and Positronium chemistry. Using a more intense positron source, we expect to increase the Ps density to the point where many thousands of polarised Ps atoms will interact and undergo a phase transition to form a Bose Einstein condensate. The time evolution of dense Ps system interacting with the pores or different molecules will be measured the time distribution of o-Ps annihilation togheter the o-Ps polarization being the main physical parameters characterising the system. The o-Ps polarization and the interaction of the o-P atoms with different kinds of molecules can be measured by a conventional Time Differential Perturbed Angular Correlation applied to observe the anisotropy oscillation in the 3-gamma annihilation decay of polarised Psoitronium [3] and other PAS methods.

References

[1] A. Vasilescu, L. Craciun, I. A. Ghita, O. Constantinescu, F. Constantin, C. Chiojdeanu, C. N. Zoita, A. Kiss, D. Bojin and P.M. Racolta Status of an R&D project of a Positron Gun at Horia Hulubei NIPNE Bucharest Applied Surface Science 255 (2008) 46–49

[2] F. Constantin, L. S. Craciun, O. Constantinescu, I. A. Ghita, C. Ionescu, P. M. Racolta, M. Straticiuc, A. Vasilescu, V. Braic, C. Zoita, A. Kiss, D. Bojin Status and Perspectives for a Slow Positron Beam Facility at the HH—NIPNE Bucharest AIP Conf. Proc. – March 10, 2009 – Volume 1099, pp. 960-964

[3]] E. Ivanov, I. Vata, D. Dudu, I.Rusen and N. Stefan, Quantum beats in the 3-gamma annihilation decay of Positronium observed by perturbed angular distribution. Appliedf Surface Science 255(2008) 179-182

5.6.11 Positron-excited Auger Electron Spectroscopy (PAES)

C.M. Teodorescu[1], A.M. Vlaicu[1],C. Ghica[1] and D. Macovei[1]
[1] *National Institute of Materials Physics, Bucharest-Magurele (Romania)*

The principle of PAES has been demonstrated in 1988 [1]. Low energy positrons (10 eV) create core holes (3p in Ni or Cu) with a probability as high as 0.04, which yields a considerable signal / background ratio for Auger electrons, unlike the conventional Auger electron spectroscopy (AES). Additionally, the achievement of a convenient signal in conventional AES requires the use of an electron beam of considerable intensity, which may induce defects, enhanced surface reactivity, degrades organic compounds, etc. The PAES basic process is the following: low-energy positrons implanted into the sample are scattered towards the sample surface and trapped either in surface defects or in surface states, then they annihilate either with valence or core electrons. Around 10^{-3} electrons are emitted for an annihilated positron. PAES may be obtained with the same statistics as AES with the decrease of the energy deposited in the sample by three orders of magnitude. The initial experiment [1] was carried out with a flux of 10^4 positron/sec; nowadays, the available sources provide intensities of several orders of magnitude higher. In 1990, the extreme surface sensitivity of PAES was demonstrated by the dramatic reduction (by a factor of 4) of the Cu $M_{2,3}VV$ electrons induced by the adsorption of 0.5 ML S/Cu(001) [2]. This effect is determined by two factors: (i) the positive charge nature of the positrons; (ii) the spatial displacement of the positron surface states away from the copper single crystal surface, induced by the adlayer. The detection of the Auger electrons in this experiment was carried in coincidence with the photons generated by annihilation. The origin of this signal damping was confirmed by positron wavefunction calculation. A few time later, a complete model of "corrugated mirror" [1] was proposed to calculate the positron states and their annihilation rates

with core electrons. Metal surfaces of Al, Ni, Cu, and Au gave values of 1-5 % for these annihilation rates. For low Miller index surfaces, around 80 % of the positrons are annihilated with electrons from the topmost layer. The PAES decrease in intensity in the case of overlayer adsorption is strongly dependent on the impurity localization on the surface or in subsurface states. The simulations show that most elements exhibit detectable PAES signals, if the corresponding binding energy (BE) of the level from which the electron becomes annihilated is lower than 100 eV. The annihilation probability with a core electron has a dependence approximated as BE_{-1}, with a probability of about 1 % for BE = 100 eV and 0.05 % for BE = 500 eV [3]. The only comparable surface sensitive technique is low energy ion scattering (LEIS). But LEIS also may lead to sample degradation or sputtering. In turn, PAES is non-destructive. One of the limitations of PAES is that it cannot operate at high temperatures, since the positron is formed, which escapes from the surface, as evidenced by γ-ray spectroscopy [4]. One might expect that the remarkable intensity of positron beams that may be achieved at ELI-NP allows PAES investigations of Auger electrons involving deeper levels, such as O KLL (510 eV), C KLL (275 eV), N KLL (389 eV); this, together with the dramatic reduction in sample degradation and with the extreme surface sensitivity opens new analysis possibilities for all organic compounds, adsorbates, *in situ* assessment of surface and interfaces processes in catalytic processes, etc.

Other phenomena already evidenced are: the extreme sensitivity (0.02 ML) for the transition between the positron localization in the neighbourhood of the Cu(001) surface or pushed away by adsorbed atoms for Cs/Cu(001), a phenomenon which takes place for about 0.7 ML adsorbed [5]. In some cases, the positron localization prior to their annihilation shows an extremely high chemical selectivity, as in Au/Cu(001), where a noticeable signal ($\sim$ 40 % from the signal corresponding to one ML of Au) is provided by a low quantity (0.07 ML of Au adsorbed at the surface) [6]. The complete theory of positron localization in solids, in the vicinity of defects, surfaces or interfaces, shows, also, a pronounced chemical sensitivity [7]. These facts promoted, after some years, the setting up of a facility dedicated to low-energy positron production and of associated techniques NEPOMUC near Munich which provides nearly 109 positrons/sec. at 1 keV [8], whereas the first experiments implying the study of semiconductor surfaces [Si(001)] and of first ultrathin metallic layers on semiconductors [Cu/Si(001)] were immediately reported [9]. Perhaps not surprisingly, the first real experiments of surface and interface physics ever conducted in Romania concentrated on similar systems: metals deposited on Si(001), such as Fe/Si(001) [10].

In the framework of the ELI-NP project, we intend to develop the PAES technique by using positrons yielded by ELI [11]. In addition to the methods described above, in the actual case the positron flux should exceed by several orders of magnitude the fluxes obtained with the actual sources. Thus, the PAES technique will be further developed. We intend to study also positron annihilation Auger electron diffraction (PAED), by analyzing the angular distribution of the Auger electrons (angle resolved PAES, ARPAES). This method, coupled to the extreme high surface sensitivity of PAES, should allow accurate determinations of the geometry of adsorbates and of intimate details of reconstructed surface and interface geometries [12].

Another advantage provided by ELI-NP is the possibility of working with positron pulses of ultralow duration (ps), which makes it possible the achievement of coincidence experiments positron/electron, positron/ etc.

A modern surface and interface physics facility dedicated to positron annihilation related techniques will be implemented (Fig. 50), comprising:

- ultrahigh vacuum (UHV) chamber with pumping system, ports, sample manipulator with polar and azimuthal motion, load-lock, storage chamber, etc.;
- hemispherical electron energy analyzer, low angular acceptance, high brilliance;
- angle-integrated electron energy analyzer, high intensity, cylindrical mirror analyzer (CMA);
- electron time-of-flight analysis system;
- an electron gun for simultaneous achievement of AES experiments;
- a γ spectroscopy detector system, together with the required measurement chain for coincidence measurements (positron/γ, positron/electron, positron/electron/γ);
- 4 evaporators;
- one magnetron sputtering source;
- one plasma discharge source;

- ion gun for sample sputtering;
- quadrupole mass spectrometer for residual gas analysis, adsorption/desorption experiments.

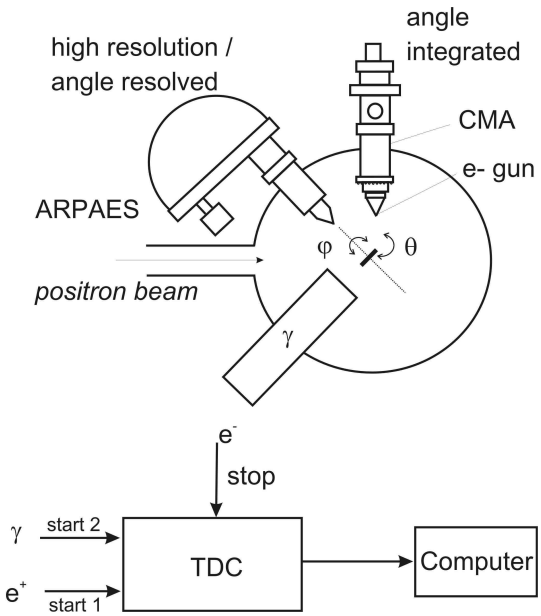

Figure 50: Experimental setup for PAES and ARPAES, together with a schematics of the multi-coincidence technique.

The detection methods or stipulated analyses will be:
- positron annihilation Auger electron spectroscopy (PAES);
- angle-resolved PAES (ARPAES);
- (AR)PAES obtained with coincidences γ - electron;
- (AR)PAES obtained with coincidences positron-electron;
- multi-coincidence methods positron - γ - electron, where for instance binding energies of positron surface states may be obtained etc.
- conventional Auger electron spectroscopy (AES); however, its integration in the proposed facility will allow a direct comparison of AES and PAES.

References

[1] A. Weiss, R. Mayer, M. Jibaly, C. Lei, D. Mehl, K.G. Lynn, *Phys. Rev. Lett.* **61**, 2246 (1988).

[2] D. Mehl, A.R. Koymen, K.O. Jensen, F. Gotwald, A. Weiss, *Phys. Rev. B* **41**, 799 (1990).

[3] K.O. Jensen, A. Weiss, *Phys. Rev. B* **41**, 3928 (1990).

[4] R. Mayer, A. Schwab, A. Weiss, *Phys. Rev. B* **42**, 1881 (1990) ; E. Soininen, A. Schwab, K.G. Lynn, *Phys. Rev. B* **43**, 10051 (1991).

[5] A.R. Koymen, K.H. Lee, D. Mehl, A. Weiss, K.O. Jensen, *Phys. Rev. Lett.* **68**, 2378 (1992).

[6] K.H. Lee, G. Yang, A.R. Koymen, K.O. Jensen, A. Weiss, *Phys. Rev. Lett.* **72**, 1866 (1994).

[7] M.J. Puska, R.M. Nieminen, *Rev. Mod. Phys.* **66**, 841 (1994).

[8] C. Hugenschmidt, K. Schreckenbach, M. Stadlbauer, B. Strasser, *Nucl. Instrum. Meth. Phys. Res. A* **554**, 384 (2005) ; ibid *Phys. Rev. B***252**, 3098 (2006).

[9] C. Hugenschmidt, J Mayer, K. Schreckenbach, *Surf. Sci.* **554**, 2459 (2007).

[10] N.G. Gheorghe, G.A. Lungu, M.A. Husanu, *Rom. Rep. Phys.* , submitted (2010) ; N.G. Gheorghe, M.A. Husanu, G.A. Lungu, R.M. Costescu, D. Macovei, C.M. Teodorescu, *Nanotech 2010 Technical Abstracts*, accepted.

[11] ELI Scientific case, Secs. B V.6 and C II.2.

[12] A. Mascaraque, J. Avila, C.M. Teodorescu, M.C. Asensio, E.G. Michel, *Phys. Rev. B.* **55**, R7315 (1997) ; J. Avila, A. Mascaraque, C.M. Teodorescu, E.G. Michel, M.C. Asensio, *Surf. Sci.* **377-379**, 856 (1997) ; M.G. Martin, J. Avila, M. Gruyters, C.M. Teodorescu, P. Dumas, Y.J. Chabal, M.C. Asensio, *Appl. Surf. Sci.* **123-124**, 156 (1998).

5.6.12 Positron Annihilation Spectroscopy (PAS)

C.M. Teodorescu[1], A.M. Vlaicu[1],C. Ghica[1] and D. Macovei[1]
[1] *National Institute of Materials Physics, Bucharest-Magurele (Romania)*

Positron Annihilation Spectroscopy (PAS) represents a non-destructive method to characterize electron structures, nature and concentration of defects (point defects and extended defects) in metals, alloys, semiconductors, ionic crystals, amorphous materials. The method relies on the positron-electron annihilation with the emission of two γ quanta of 0.511 MeV each propagating in opposite directions. There are two ways of generating positrons and, therefore, two types of positron sources:

i. Radioactive isotope based source (^{22}Na, ^{64}Cu, ^{58}Co and ^{68}Ge) showing β^+ decay (e.g. $^{22}\mathrm{Na} \rightarrow {}^{22}\mathrm{Ne} + \mathrm{e}^+ + \nu_e + \gamma_{(1.27MeV)}$)

ii. Sources based on e^- - e^+ pair generation, involving interaction energies $\geq$ 1.022 MeV. Such sources may use the bremsstrahlung of a decelerated beam of MeV-electrons of a LINAC onto a target (EPOS in Rossendorf, Germany; KEK in Tsukuba, Japan; AIST in Tsukuba, Japan; ANL in Argonne, USA; etc.), the γ radiation from a nuclear fission reactor (Delft, Holland) or the γ radiation from a nuclear reaction of the kind ^{113}Cd(n,γ)^{114}Cd resulting in three gamma photons with a total energy of 9.041 MeV which are used for the pair generation (Garching, Germany).

The positron lifetime in a solid depends on the local concentration of electrons. The lifetime of a positron captured in around an atomic vacancy is significantly longer than the lifetime of positrons in a matrix without structural defects. Based on this principle, one can detect and quantify the presence of structural defects. In a crystalline material, such detectable defects may be atom vacancies, dislocations, planar defects. In amorphous materials, such as polymers, the detectable defects are the free spaces between the polymeric chains.
The γ photons emitted by the annihilation process are detected and analyzed using three different spectroscopic techniques:

1. Positron Lifetime Spectroscopy - PALS. The technique currently applies in experimental set-ups using ^{22}Na sources where a 1.27 MeV γ photon is emitted in the same time with the e^+. The positron lifetime is measured with respect to the β^+ decay occurring with the emission of the 1.27 MeV photon. The technique allows determining the concentration of defects such as single vacancies, di-vacancies, clusters of vacancies or porosity in mesoporous materials. In the case of a pulsed positron beam (LINAC based sources) the positron lifetime is measured as the time difference between the 0.511-MeV photon and the machine pulse from timing system. Characteristic positron lifetimes in various materials vary from 0.1-0.5 ns in metals and semiconductors, to 0.5-5 ns in polymers and 1-100 ns in mesoporous materials, etc.

2. Angular Correlation of Annihilation Radiation - ACAR. The angle $\Theta_{x,y}$ between the γ photons emitted in opposite directions is in general different from 180o and it depends on the transversal components p_x and p_y of the electron momentum $\mathbf{p}$ with respect to the emitted γ photons ($\Theta_{x,y} = \mathrm{p}_{x,y}/\mathrm{m}_0\mathrm{c}$). The technique allows e.g. mapping of the Fermi surface in single crystals.

3. Doppler Broadening Spectroscopy - DBS. The energy of the emitted γ photons is slightly different from 0.511 MeV and it depends on the longitudinal component p_z of the electron momentum p with respect to the emitted γ photons (0.511 MeV $\pm$ ΔE, with $\Delta E = p_z c/2$). Samples with high defects content induce a narrowing of the 0.511 MeV spectral line. The technique allows getting information on the electron momentum in the sample. By analyzing the line profile, two parameters are determined, S and W, corresponding to annihilation processes with valence electrons and core electrons, respectively. For a better signal/background ratio, especially on the wings of the spectral line (W parameter), the set-up with two detectors operated in coincidence mode is used - Coincidence Doppler Broadening Spectroscopy (CDBS).

The energy spectrum of the emitted positrons is generally wide, reaching several hundreds of keV (e.g. ^{22}Na delivers e^+ with energies up to 540 keV). Before annihilation, positrons arrived inside the sample are thermalized in a layer with a thickness of the order 10^2 μm. Therefore, the extracted structural information results from a material layer with a thickness of only a few hundreds of μm next to the surface. In cases where information from the whole sample volume is of interest (thickness of the order of cm), another experimental variant is used, known as Gamma-induced Positron Spectroscopy (GIPS). In this configuration, a γ beam is directed towards the sample, generating e^--e^+ pairs right inside the sample (EPOS facility, Germany). The type of positron spectroscopy to be developed depends on the characteristics of the positron source. In the case of the lifetime spectroscopy (PALS), the time between two consecutive positrons must be much longer than the maximum lifetime to be detected. This condition limits upwards the activity of a positron source based on radioactive isotopes. Thus, in order to be able to measure lifetimes of the order of 0.5 ns (semiconductors), the source activity should not surpass 9x10^5 Bq (1 Bq = 1 disintegration/sec), which is equivalent to a repetition rate of 0.9 MHz. For lifetimes of the order of 10^2 ns, the source activity should be less than 2x10^5 Bq, the equivalent of repetition rates less than 0.2 MHz in the case of a pulsed source. On the other hand, there are a series of disadvantages when using low frequency pulsed sources (LINAC), such as low counting rate, low signal/noise ratio.

There are several constructive solutions of the positron annihilation spectrometers adopted worldwide:
• NEPOMUC at FRM-II in Garching (Munchen), Germany
- γ source = nuclear reactor; 5 beamlines: Lifetime; CDBS; PAES; positron microscope
- 5x10^8 e^+/s - the highest positron flow at the moment
• Argonne Project APosS, USA
- γ source = Linac, 15.5 MeV, 0.1 mA, 60 Hz
- under construction, estimated flow 3x10^9 e^+/s
• SOPHI Project in Saclay, France
- γ source = Mini LINAC: 6 MeV, 300 Hz, 0.2 mA; 10 kW
- under construction, estimated flow 10^8 e^+/s
• Positron Beam at IHEP Beijing, China
- under construction; PALS, AMOC, CDBS
- γ source = radioactive isotopes and LINAC
• EPOS: ELBE Positron Source @ Research Centre Dresden Rossendorf, Germany
- 40 MeV, 1 mA, 26 MHz repetition rate in cw mode; PALS, CDBS and AMOC with slow positrons
- Gamma-induced Positron Spectroscopy for bulk samples

In our case, **using the γ source** of high-brilliance and high-energy represents a **strong argument in favour of developing positron spectroscopy at ELI-NP**. The γ-ray beam could be used either to form a positron beam or to generate e^+-e^- pairs inside the sample (GIPS variant). Although a final decision has not been taken as to what LINAC solution would be adopted at ELI-NP, in case that the parameters of the LINAC facility to be constructed in the ELI-NP are at least of the same order of magnitude as the accelerator used at Argonne National Laboratory (APosS project), this will still allow to develop the PALS and DBS positron spectroscopy at ELI-NP as it is previewed at Argonne National Laboratory.
The utility of developing such spectroscopic techniques at ELI-NP consist in the first place in being

able to perform **on-site characterization and diagnosis of materials and components involved in the construction of the ELI-NP project itself**. This method could be used in conjunction with the other materials characterization techniques described as support tools for ELI-NP, the advantage of PAS consisting in the fact that it is a non-destructive method and it allows for investigations on bulk samples.

References

[1] **Defects in silicon after B+ implantation: A study using a positron-beam technique, Rutherford backscattering, secondary neutral mass spectroscopy, and infrared absorption spectroscopy**, S. Eichler, J. Gebauer, F. Borner, A. Polity, R. Krause-Rehberg, E. Wendler, B. Weber, W. Wesch, H. Borner, *Phys. Rev. B* **56**, 1393-1403 (1997).

[2] R. Krause-Rehberg, H. S. Leipner, ***Positron annihilation in Semiconductors***, Springer-Verlag, New York, (1998).

[3] P. Coleman, ***Positron Beams and their applications***, World Scientific, (2000).

[4] M. Charlton, J.W. Humbertson, ***Positron Physics***, World Scientific, (2001).

[5] **Positron annihilation spectroscopy in materials structure studies**, V. I. Grafutin, E. P. Prokopiev, *Physics - Uspekhi* **45**, 59 - 74 (2002).

[6] **Ortho-positronium lifetime measurement - positron source activity and statistics**, S. Thraenert, E.M. Hassan, R. Krause-Rehberg, *Nuclear Instruments and Methods in Physics Research B* **248**, 336-339 (2006).

[7] **Progress of the EPOS project:Gamma-induced Positron Spectroscopy (GiPS)**, R. Krause-Rehberg, W. Anwand, G. Brauer, M. Butterling, T. Cowan, A. Hartmann, M. Jungmann, A. Krille, R. Schwengner, A. Wagner, *Phys. Status Solidi C* **6**, 2451-2455 (2009).

[8] **Experimental elucidation of vacancy complexes associated with hydrogen ion-induced splitting of bulk GaN**, O. Moutanabbir, R. Scholz, U. Gosele, A. Guittoum, M. Jungmann, M. Butterling, R. Krause-Rehberg, W. Anwand, W. Egger, P. Sperr, *Phys. Rev. B* **81**, 115205 (2010).

5.6.13 AGPAS technique with high energy gamma beams

Gh. Cata-Danil[1], A.M. Popovici[1]
[1] *University POLITEHNICA of Bucharest (Romania)*

Accelerator-based Gamma-induced Positron Annihilation Spectroscopy (AG-PAS) [1, 2] is a new experimental technique that employ positron annihilation spectroscopy by using MeV gamma-rays to generate positrons instead of using radioactive or neutron-induced positron sources. This method open the possibility of probing residual stress in thick materials by Doppler broadening measurements [3] reflected in the line shape parameters of the 511 keV annihilation peak.The range of keV positrons in materials are in the order of few hundred micrometers and hence the depths in materials that can be investigated by positrons are limited to this range. Therefore, standard positron annihilation techniques are not appropiate to study defects in thick materials. With the new technique, the first measurements of AG-PAS were conducted by using bremsstrahlung radiation from an electron Linac to perform Doppler spectroscopy of positron annihilation. In those measurements residual stresses in thick materials are reflected in the narrowing of the Doppler broadening of the 511 keV peak and in an increase of the annihilation fraction with valence electrons. Since positron lifetime spectroscopy is a usefull instrument to study in details different types of defects, such as dislocations and vacancy clusters [3], it is extremly important to adapt enable positron lifetime measurements in AG-PAS. In references [1–3] Idaho group developed AG-PAS by using proton beams from accelerator to generate gamma rays used both for coincidence measurement and to generate positrons inside thick materials. At ELI-NP high briliance gamma source appears a natural technical environment to apply AG-PAS method. The laser pulse used for Compton backscattering could provides a start signal for the positron lifetime spectrometer and the stop signal is given by the detection of one of the two 511 keV photons. The recorded positron lifetime spectrum depends on the electron densities and hence provides information about the size of open volume defects. The method enables positron lifetime measurements in thick engineering materials up to tens of gm/cm2, a thickness not accessible by conventional positron lifetime spectroscopy.A strong point of the positron annihilation techniques is their unique ability to distinguish between different kinds of open volume defects and identify the defect size and its concentration in a single measurement. ELI-NP facility by its gamma source tunable in energy will allow to develop precise measurements in large volume samples, by recording data for the same sample at different gamma energies.

References

[1] F. A. Selim et al., Stress Analysis Using Bremsstrahlung Radiation, accepted to be published in Advances in X-ray Analysis, Vol. 46, proceedings of the 51 Denver Xray Conference, 2002

[2] F.A. Selim et al., Nucl. Inst. and Meth. B 192 (2002), p. 197

[3] F. A. Selim, D. P. Wells, J. F. Harmon, J . Kwofie, A. K. Roy, Applications of Electron Linacs in Stress and Defect Measurements, accepted to be published in proceedings of ANS meeting in Accelerators Applications in Nuclear Renaissance, 2003

5.6.14 Testing of radiation effects on commercial optical fibers

B Constantinescu[1]

[1] *IFIN-HH, Bucharest, Romania*

Radiation effects on commercial optical fibers must be characterize at all telecommunication windows because their behaviors are very important for space, military and civil agencies. Optical fibers are also good candidates for use in harsh environments like those encountered in Laser Megajoule or International Thermonuclear Experimental Reactor (ITER) facilities. Various types of optical fibers have very different behaviors when expose to pulsed X-rays, neutrons or gamma rays, the same main macroscopic changes being responsible for transmitted signal degradation: the radiation-induced attenuation (RIA) and the radiation-induced luminescence (RIL). The generation of point defects in the silica-glass matrix (pure or doped) is at the origin of RIA and RIL. The optical properties, concentrations and the stability of the induced defects govern the RIA and RIL levels and recovery kinetics. Using IR-UV spectrometers, pulsed X-rays (or synergetic X + neutrons) irradiations allow such studies especially focused on defects recovery kinetics in the internal between pulses.

References

[1] S.Girard, D.L. Griscom, J. Baggio, B. Brichard, F. Berghmans, Journal of Non-Crystalline Solids 352, 2637 (2006)

[2] S.Girard, Y. Querdane, A. Boukenter, J.-P. Meunier, Journal of Applied Physics 99, 023104 (2006).

[3] D. Sporea, Adelina Sporea, B. Constantinescu, Fusion Engineering and Design 74, 763 (2005).

[4] B. Constantinescu, R. Bugoi, E.R. Hodgson, R. Vila, P. Ioan, Journal of Nuclear Materials 367-370, 1048 (2007).

5.6.15 Materials research in high intensity radiation fields

C.M. Teodorescu[1], A.M. Vlaicu[1],C. Ghica[1] and D. Macovei[1]
[1] *National Institute of Materials Physics, Bucharest-Magurele (Romania)*

Interaction of the high power (> PW) laser radiation with the solid state matter produces specific effects, not completely known, on the structure and composition of the irradiated materials. The detailed knowledge of these effects has a fundamental interest for understanding the material behaviour in extreme conditions of irradiation. On the other hand, study of the irradiation effects significantly helps to optimization of the materials and components operating in the laser beam. This kind of research will have a novelty character at ELI-NP, in conditions of extremely high power and intensity of the laser radiation.

Tens of fs PW laser pulses can generate local ultrahigh pressures, of tens Mbar up to Gbar, inside the irradiated materials. Such mechanical shocks cause structural defects, compositional inhomogeneities, local melting and fast recrystallization, phase transitions etc. The structural and compositional changes under the laser radiation, or other types of radiation resulting from the laser-target interaction, are main reasons of the material degradation during the use in the laser beam. Investigation of the damage effects of the optical components, target support, secondary targets, radiation detectors or walls of the reaction chambers will allow the improvement of their performances and the extension of their lifetime in conditions of severe irradiation. The research results could be very helpful for the design of other classes of materials, more resistant when working in extreme conditions. It is worth mentioning that NIMP has a long collaboration with CERN (RD48 and Rd50) in improving the radiation hardness of Si detectors used in LHC experiments. All the structural defects induced by irradiation with various radiation beams (gamma, electrons, positrons, protons, neutrons, etc.) can affect the electronic properties of the materials, with direct impact on the macroscopic characteristics of the various micro/optoelectronic components used in the experiments.

Structure and chemistry of the bulk or surface of the irradiated materials can be approached by suitable techniques, like high-resolution transmission electron microscopy (HRTEM), scanning transmission electron microscopy (STEM), X-ray diffraction (XRD), x-ray photoemission spectroscopy (XPS), electron paramagnetic resonance (EPR) etc. These techniques are currently applied at the National Institute of Materials Physics (NIMP), at Bucharest-Magurele, with modern equipments and research teams with a long experience in the material characterization. The research of the irradiation effects could be therefore carried out at NIMP-Magurele, which would avoid additional investments within the ELI-NP Project for the corresponding equipment and space. The foreseen techniques for this kind of studies and the main capabilities of the NIMP equipments are briefly reviewed in the following.

High resolution transmission electron microscopy (HRTEM)
Currently, the high resolution transmission electron microscope (HRTEM) equipped with analysis accessories of high spatial and spectral sensibility and resolution (Energy Dispersive X-ray Spectroscopy - EDS, Electron Energy Loss Spectroscopy - EELS) represents a particularly powerful instrument for morphological, structural and compositional characterization of materials. At this time, NIMP owns an analytical transmission electron microscope used for morphological and structural studies based on diffraction contrast, as well as compositional determinations through EDS. Until the beginning of 2011, NIMP expects to acquire and begin operating a high-resolution analytical electron microscope able to provide information with sub 1 Å resolution both at structural and compositional level. The microscope, which will be equipped with an spherical aberration correcting device for S-TEM (Scanning Transmission Electron Microscopy), will operate both in TEM and in STEM mode. The presence of this correction device allows the formation of a 1 Å diameter electron probe, reaching a spatial resolution of $\leqslant 0.08$ nm in STEM mode. Among the major equipment that will be installed on the microscope column, we mention the EDS unit, which allows a compositional analysis with spatial resolution of $\leqslant 1$ nm and the EELS unit with an energy resolution of approximately 0.1 eV, which provides both compositional analysis and the visualization of the spatial distribution of the analyzed chemical elements, going up to atomic spatial resolution using the EFTEM (Energy Filtered Transmission Electron Microscopy) technique. Obtaining this information requires specialized preparation techniques for the samples to be investigated. Many of these sample preparation techniques already exist at NIMP, and will be supplemented with the acquisition of a dual FIB-SEM system until the beginning of 2011.
The transmission electron microscopy systems and the preparation techniques mentioned can be used as part all three types of contributions by NIMP to the running of the ELI project given in the introduction. The current performances of high spatial and energetic resolution electron microscopes allow up to atomic precision for the determination and characterization of extended structural defects (dislocations, plane defects) and the associated deformation field [1–3] or compositional defects [4–6] resulting from radiation-solid type interactions in the experiments conducted at ELI. These investigations will also be necessary for characterizing the thin film targets that will be irradiated with the high power laser beam. In addition, the electron microscopy sample preparation techniques, based on processing with ion beams (classical ion thinning, the FIB technique), can be taken into consideration for the purpose of preparing targets that consist of thin sheets of nanometer thickness.

X-Ray Diffraction (XRD)
The structural properties of the materials exposed to extreme radiation fields can be further investigated - before and after irradiation - by X-ray diffraction. Considering the specificity of various X-ray diffraction techniques and the fact that the analysed samples can be provided in various states, shapes, and amounts, one should consider several setups for the X-ray diffractometers, or a multipurpose diffractometer which can support several setups. Powder samples in large amounts require a standard configuration, where the properties of the beam from a standard X-ray generator are tailored only by divergence slits. As the quantity of the sample of interest could decrease to small selected amounts after the irradiation, enhancements in the detection system for parallel acquisition are required, such as the use of stripe array detectors, X-ray CCD cameras, stacked detector, imaging plates etc.. In many cases however, the sample does not come in the form of powder which can be spread on a flat sample holder, but is attached to a substrate of various shapes. In such cases, the use

of incident monochromatic and parallel X-ray beam is required. X-ray multilayer focussing mirrors can be additionally used to increase the incident beam intensity. The goniometer should allow sample investigation at fixed incident grazing angle while scanning only the detector, and sample stages with multiple orientation axes capabilities (Euler cradles). This setup which is adequate for large area samples can be also used for reflectometry measurements in the case of large area flat samples. However, when the sample of interest decreases to very small areas, or when the mapping of a certain area is required, the setup for X-ray diffraction require further beam tailoring in order to obtain point focus by capillary X-ray optics, and the detection system needs to record at once a solid angle of the diffracted beam by using X-ray CCD cameras or imaging plates. In such cases the standard X-ray generator is replaced by rotating anode X-ray generators, and the costs of the setup and exploitation costs increase considerably. This setup can also allow in-plane diffraction and reciprocal space mapping measurements. Recent X-ray diffractometers allow the reconfiguration of several setups on a single X-ray diffractometer unit, reducing the cost with respect to that of individual diffractometer units. Given the variety of the required setups, it is usually difficult - financially and logistically - to gather in one place all the required diffractometer setups.
However, considering the availability of several setups of X-ray diffractometers in the close vicinity of the ELI-NP facility – National Institute for Materials Physics (NIMP), National Institute for Laser, Plasma and Radiation Physics (NILPRP), Horia Hulubei National Institute of Physics and Nuclear Engineering (IFIN-HH), Institute for Microtechnology (IMT) – one can approach the X-ray diffraction investigations at these institutes.

X-ray photoelectron spectroscopy (XPS)
X-ray photoelectron spectroscopy (XPS) is one of the most powerful methods of investigating the chemical states and composition of surfaces. This method is based on exciting a sample by a monochromatic X-ray beam obtained from a conventional X-ray source and analyzing the resulting photoelectrons as a function of their kinetic energy. This gives a distribution of electrons as a function of their binding energy for the initial levels. The main features of this techniques are: (a) compositional sensitivity, with a precision for determining compositions of the order of 0.1 %; (b) surface sensitivity due to the photoelectron mean free paths of 0.5-1.5 nm; (c) chemical sensitivity through analysis of chemical shifts, which are of the order of 1-3 eV for most compounds; the resolution of current systems being approximately 0.35 eV; (d) the possibility of conducting composition and/or chemical state depth profiling, by combining XPS with controlled sample cleaning by ion (Ar^+) bombardment; (e) for monocrystalline samples, angle-resolved XPS can determine structural characteristics with reasonable precision through X-ray photoelectron diffraction (XPD); (f) for very small binding energies, the corresponding photoemission (ultraviolet photoelectron spectroscopy, UPS) allows the determination of valence band state densities; (g) for monocrystals, angle-resolved UPS allows the determination of dispersion laws in the valence band $E(\boldsymbol{k})$.
XPS spectroscopy and its associated techniques are very suitable for the study of surface modifications as a result of the interaction with a high intensity laser beam. It is possible to analyze contamination, etching, surface alloying, layer removing. We intend to make available to the ELI community the photoelectron spectroscopy expertise at NIMP, consisting of 3 systems, of which two are state-of-the-art, and a number of 11 specialists in this technique. The expertise mentioned is the most important nationally, corresponding to approximately 50 % of the total national expertise for a single institution (NIMP).

Electron paramagnetic resonance (EPR)
Electron paramagnetic resonance (EPR) spectroscopy represents a group of methods and experimental techniques that are used to detect species with unpaired electrons such as free radicals, transition metal ions or point defects in materials, including colour centers or defects produced by irradiation. These are based on observing the absorption of microwaves ($f > 1$ GHz), which induce transitions between energy levels in a magnetic field of non-zero spin electron systems in atoms/ions and molecules in either free or solid state, as well as those of systems associated with point (atomic) defects in the crystal lattices of solid materials.
The following type of information is obtainable by EPR techniques: the nature, valence state, structure

and symmetry of the detected paramagnetic species, the potential presence of neighbouring defects, the concentration, and the production mechanisms and their stability. Using such paramagnetic species as probes can also provide information about the host material, such as structure, local symmetry, lattice dynamics, and structural phase transition mechanisms.

References

[1] **Strain mapping around dislocations in diamond and cBN**, B. Willems, L.C. Nistor, C. Ghica, G. Van Tendeloo, *Phys. Status Solidi A-Appl. Mat.* **202**, 2224 (2005).

[2] **Characterization of** {111} **planar defects induced in silicon by hydrogen plasma treatments**, C. Ghica, L.C. Nistor, H. Bender, O. Richard, G. Van Tendeloo, A. Ulyashin, *Philos. Mag.* **86**, 5137 (2006).

[3] **TEM characterization of extended defects induced in Si wafers by H plasma treatment**, C. Ghica, L.C. Nistor, H. Bender, O. Richard, G. Van Tendeloo, A. Ulyashin, *J. Phys. D-Appl. Phys.* **40**, 395 (2007).

[4] **Atomic-scale study of electric dipoles near charged and uncharged domain walls in ferroelectric films**, C.-L. Jia, S.-B. Mi, K. Urban, I. Vrejoiu, M. Alexe, D. Hesse, *Nat. Mater.* **7**, 57 (2008).

[5] **An Introduction to High-resolution EELS in Transmission Electron Microscopy**, W. Grogger, F. Hofer, G. Kothleitner, B. Schaffer, *Top. Catal.* **50**, 200 (2008).

[6] **Column-by-column compositional mapping by Z-contrast imaging**, S.I. Molina, D.L. Sales, P.L. Galindo, D. Fuster, Y. Gonzalez, B. Alen, L. Gonzalez, M. Varela, S.J. Pennycook, *Ultramicroscopy* **109**, 172 (2009).